JUSTUS-LIEBIG-
UNIVERSITÄT
GIESSEN

Structure of a specific nuclear mRNP and the role of Hpr1 in mRNP assembly

Dissertation

zur Erlangung des Doktorgrades der Naturwissenschaften

(Dr. rer. nat.)

am Fachbereich 08 für Biologie und Chemie

der Justus-Liebig-Universität Gießen

Vorgelegt von

Nataliia Stefanyshena

Gießen, 2024

Die vorliegende Arbeit wurde am Institut für Biochemie (Fachbereich 08) der Justus-Liebig-Universität Gießen, unter Leitung von Prof. Dr. Katja Sträßer, erstellt.

Dissertation eingereicht am: 23.04.2024

Erstgutachter: Prof. Dr. Katja Sträßer
Fachbereich 08: Biologie und Chemie
Institut für Biochemie
Justus-Liebig-Universität Gießen

Zweitgutachter: Apl. Prof. Dr. Elena Evguenieva-Hackenberg
Fachbereich 08: Biologie und Chemie
Institut für Mikrobiologie und Molekularbiologie
Justus-Liebig-Universität Gießen

List of contents

1. Zusammenfassung

In Eukaryoten werden synthetisierte prä-mRNAs von zahlreichen RNA-bindenden Proteinen (RBPs) prozessiert und im Zellkern in Boten-Ribonukleoprotein-Partikel (mRNPs) verpackt. Reife mRNPs werden für die Translation in Proteine in das Zytoplasma exportiert. Der TREX-Komplex spielt eine wichtige Rolle bei der Verknüpfung von Transkription und mRNA-Export. In *S. cerevisiae* besteht er aus dem pentameren THO-Komplex (Hpr1, Tho2, Mft1, Thp2 und Tex1), der Helikase Sub2 und dem mRNA-Exportadaptor Yra1 sowie den SR-ähnlichen Proteinen Gbp2 und Hrb1. Die Deletion der THO-Komponente *HPR1* hat weitreichende Folgen für die Zelle, darunter eine erhöhte genomische Instabilität, Hyperrekombination sowie die Akkumulation von *R-Loops* und einen Defekt des mRNA-Exports. Der THO-Komplex interagiert mit Sub2, welches Yra1 auf das mRNP lädt, um anschließend den mRNA-Exportfaktor Mex67-Mtr2 zu rekrutieren. Mex67 kann durch verschiedene Adaptorproteine - Yra1, Nab2, Npl3 und Hpr1 – zu dem mRNP rekrutiert werden. Der mRNA-Exportfaktor Mex67-Mtr2 vermittelt den Export des mRNP durch den Kern-Poren-Komplex (NPC).

Das erste Ziel dieser Studie war die Untersuchung der Struktur von transkript-spezifischen mRNPs im Zellkern. Die Isolierung eines spezifischen mRNP wurde durch eine zweistufige Affinitätsreinigung erreicht. Im ersten Schritt wurde der gesamte Pool der nukleären mRNPs über Cbc2, eine Untereinheit des *cap-binding complex,* angereichert. Im zweiten Schritt wurden RNA-basierte Verfahren eingesetzt, um spezifisch die *CCW12*-mRNA mit den gebundenen Proteinen aufzureinigen. Die Isolierung von *CCW12*-mRNA über verschiedene Arten von Antisense-Oligonukleotiden und RNA-Aptameren wurde getestet und optimiert, um die technischen Herausforderungen der mRNP-Reinigung zu bewältigen. Die Aptamere MS2 und Mango ermöglichten eine spezifische und effiziente Reinigung des *CCW12* mRNP. Isolierte Partikel, die über diesen Aptameren aufgereinigt worden sind, wurden mit Hilfe der Elektronenmikroskopie visualisiert. Spezifische mRNPs konnten in einer guten Ausbeute für die weitere Strukturanalyse mit fortgeschrittenen Elektronenmikroskopietechniken angereichert werden.

Ein weiteres Ziel dieser Doktorarbeit war die Untersuchung der Rolle von Hpr1 bei der Bildung von mRNPs. Diese Arbeit zeigt, dass die Deletion von *HPR1* zu einer

erhöhten Menge der RBPs Nab2, Yra1 und Mex67 in der mRNP-Komposition führt. Dies steht im Einklang damit, dass diese Proteine in einem Δ*hpr1*-Stamm mehr mRNAs binden. Die Anwesenheit von Nab2 und Yra1 an den transkribierten Genen ist in Δ*hpr1*-Zellen erhöht, aber nicht bei Mex67. Die Proteine Nab2, Yra1 und Npl3 wurden in einem Δ*hpr1*-Stamm überexprimiert, da sie ebenfalls mRNA-Exportadaptoren sind. Defekt des nuklearen mRNA-Exports von Δ*hpr1*-Zellen wird durch Überexpression von Nab2 oder Yra1 supprimiert. Der wiederhergestellte mRNA-Export ist in beiden Fällen mit ähnlichen Veränderungen der mRNP-Komposition assoziiert: Einem weiteren Anstieg der Menge von Nab2 und einer Verringerung der Mex67-Menge zum Wildtyp (WT)-Niveau. Im Falle einer Überexpression von Yra1 in Δ*hpr1*-Zellen behält oder rekrutiert Yra1 mehr Nab2 zu den transkribierten Genen. Zusammengefasst könnte Yra1 in Abwesenheit eines funktionsfähigen THO-Komplexes als Assistent fungieren, um das Beladen von Nab2 auf die mRNPs zu unterstützen; hohe Nab2-Menge können den mRNA-Export stimulieren; die Menge von Mex67 kann die nukleäre mRNA-Retention und den Export regulieren. Die Deletion einer anderen wichtigen Komponente des mRNA-Exportwegs, des Nukleoporins *NUP60*, führt zu einer Veränderung der mRNPs, ähnlich wie bei einem Δ*hpr1*-Stamm: Erhöhte Menge von Nab2, Yra1 und Mex67. Die Hypothese lautet daher, dass erhöhte Mengen dieser Proteine Kennzeichen der mRNP-Retention sind, die durch die Unterbrechung des mRNA-Exportweges verursacht wird.

2. Summary

In eukaryotes, pre-mRNAs are processed and packaged by numerous RNA-binding proteins (RBPs) into messenger ribonucleoprotein particles (mRNPs) in the nucleus. Mature mRNPs are exported to the cytoplasm for the translation into proteins. The TREX complex plays an important role in coupling transcription and mRNA export. In *S. cerevisiae*, it consists of the pentameric THO complex (Hpr1, Tho2, Mft1, Thp2 and Tex1), the helicase Sub2, the mRNA export adaptor Yra1, and the SR-like proteins Gbp2 and Hrb1. Deletion of THO component *HPR1* results in vast consequences for the cell, such as increased genomic instability, hyperrecombination, accumulation of R-loops and an mRNA export defect. The THO complex interacts with Sub2, which loads Yra1 onto the mRNP for further recruitment of general mRNA exporter Mex67-Mtr2. Mex67 can be recruited to the mRNP through different adaptor proteins - Yra1, Nab2, Npl3 and Hpr1. The mRNA exporter Mex67-Mtr2 mediates the export of the mRNP through the nuclear-pore complex (NPC).

The first aim of this study was to determine the structure of nuclear transcript-specific mRNPs. Isolation of a specific mRNPs was accomplished by a two-step affinity purification. In the first step, nuclear mRNPs were enriched via Cbc2, a subunit of the cap-binding complex. In the second step, RNA-based approaches using different types of antisense oligonucleotides and RNA aptamers were implemented to specifically purify *CCW12* mRNA with its associated proteins. MS2 and Mango aptamers provided specific purification of the *CCW12* mRNP in sufficient yield. Particles isolated via these aptamers were visualised by electron microscopy. This study demonstrates that specific mRNPs can be enriched in a good yield for further structural analysis using advanced electron microscopic techniques.

Another aim of this study was to investigate the role of Hpr1 in mRNP assembly. It shows that deletion of *HPR1* leads to an increased level of Nab2, Yra1 and Mex67 in nuclear mRNPs. It is consistent with these proteins binding more mRNAs in Δ*hpr1* strain. The occupancy of Nab2 and Yra1 at the transcribed genes is increased in Δ*hpr1* cells, but not for Mex67. To investigate mRNA export in the absence of Hpr1, other mRNA export adaptors, such as Nab2, Yra1 and Npl3, were overexpressed in Δ*hpr1* cells. The mRNA export defect of Δ*hpr1* cells is suppressed by overexpression

of Nab2 or Yra1. In both cases, restored mRNA export is associated with similar changes in mRNP composition: further increase of Nab2 and reduction of Mex67 to the WT level. In case of Yra1 overexpression in Δ*hpr1* cells, Yra1 recruits or retains more Nab2 at transcribed genes. Taken together, in cells lacking a functional THO complex, Yra1 can act as assistant to facilitate the loading of Nab2 onto mRNPs; high levels of Nab2 can promote mRNA export; increase of Mex67 amount is associated with nuclear mRNA retention, while reduction of Mex67 to the WT level is related to restored mRNA export. Deletion of another important component of mRNA export pathway, nucleoporin *NUP60*, leads to changes in nuclear mRNPs similar to a Δ*hpr1* strain: increased levels of Nab2, Yra1 and Mex67. Therefore, it is hypothesized that increased levels of these proteins are hallmarks of mRNP retention caused by disruption of the mRNA export pathway.

3. Introduction

3.1. Gene expression

Gene expression is a fundamental and an essential process in the life of the cell. It consists of transcription, mRNA processing, nuclear mRNA export, translation and mRNA decay processes (Komili & Silver, 2008) (Fig. 1). In eukaryotic cells, the genetic information encoded in DNA is located in the nucleus, where it is transcribed into pre-mRNA by the RNA polymerase II (RNAPII). Newly synthesized primary transcripts undergo processing, such as 5’ capping, splicing, 3’ cleavage and polyadenylation.

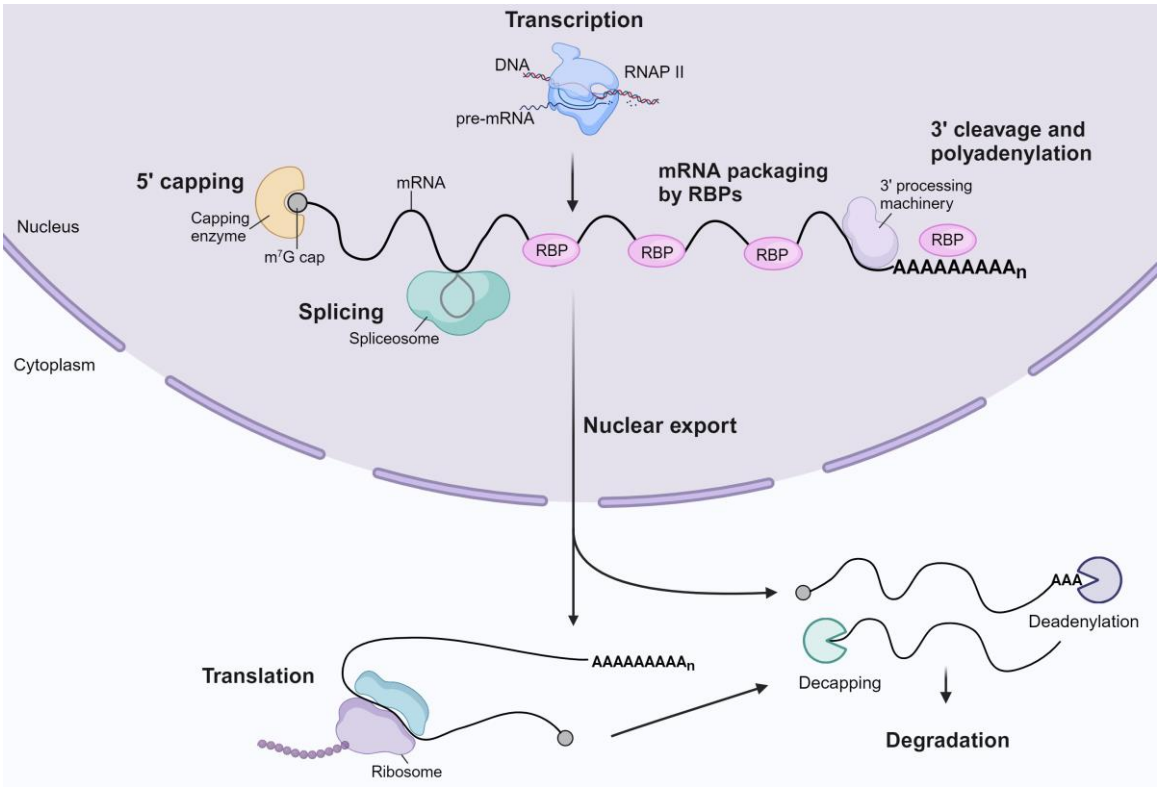

Figure 1. Scheme of the gene expression process. In the nucleus RNA polymerase II (RNAPII) transcribes protein-coding genes synthesizing a nascent transcript. The pre-mRNA is processed: the 5’ end is capped, introns are spliced out, and the 3’ end is cleaved and polyadenylated. The mRNA is packaged by RNA-binding proteins (RBPs) into an mRNP. The mature mRNP is exported through the nuclear-pore complex to the cytoplasm, where the mRNA is translated into the encoded protein. Deadenylation/decapping of mRNA initiates its degradation by exosome or 5’-3’ nucleases. Modified with BioRender after (Meinel & Sträßer, 2015; Passmore & Coller, 2022).

Simultaneously, mRNA is bound by RNA-binding proteins (RBPs) to assemble an mRNA ribonucleoprotein particle (mRNP). Correctly processed mRNAs within mRNPs are exported to the cytoplasm for translation into functional proteins and subsequent degradation (Passmore & Coller, 2022).

3.2. mRNP biogenesis

3.2.1. Transcription by RNAPII

Transcription is the first step of gene expression. In eukaryotic cells, transcription is carried out in the nucleus, where DNA is transcribed into mRNA by RNA polymerase II (RNAPII). The RNAPII is a 12 subunit complex. The prominent feature of the largest subunit of RNAPII, Rpb1, is an unstructured C-terminal domain (CTD). The CTD consists of the repetitive heptapeptide sequence Tyr1-Ser2-Pro3-Thr4-Ser5-Pro6-Ser7 – 26 repeats in yeast and 52 in human. Phosphorylation and dephosphorylation of five out of the seven residues play regulatory roles during the different transcription steps (Eick & Geyer, 2013; Singh et al., 2022).

Transcription consists of initiation, elongation and termination phases (Fig. 2B) (Greber & Nogales, 2019; Lyons et al., 2020). Initiation starts when RNAPII and general transcription factors (GTFs) TFIIA, TFIIB, TFIID, TFIIE, TFIIF and TFIIH form the pre-initiator complex (PIC) on the gene promoter. Cryo-EM, in combination with cross-linking and mass spectrometry, revealed the architecture of the PIC. The DNA promoter is directly bound by GTFs, whereas RNAPII is associated with GTFs but is not in contact with the promoter (Murakami et al., 2015). For the PIC assembly, TFIID, composed of TATA-box binding protein (TBP) and TBP associated factors, binds to the core promoter and induce a bend in the DNA. RNAPII and other GTFs localize to this bend. TFIIA and TFIIB flank and stabilize the bound TBP and DNA. Subsequent recruitment of RNAPII with pre-bound TFIIF leads to the formation of a “closed” complex, and addition of TFIIH and THIIE leads to an “open” PIC complex (Hantsche & Cramer, 2017). To change from the “closed” to the “open” conformation, TFIIH factor uses its helicase activity. The ATP-depended DNA helicase activity of TFIIH unwinds the DNA to start the synthesis of a short primary transcript. Then the Ser5 phosphorylation, mediated by the kinase activity of TFIIH, leads to promoter escape and switching from initiation to transcription elongation. The CTD loses its interaction with the GTFs, and RNAPII continues mRNA elongation (Sainsbury et al.,

2015). Additionally, the assembly of the PIC is enhanced by mediator. The mediator is a multi-protein complex, that consists of 25 subunits in yeast, has an elongated shape and is organized into head, middle, tail and Cdk8 kinase modules (Plaschka et al., 2015). The head and middle part interact with RNAPII. The tail interacts with specific transcription activator factors, which are bound to enhancer elements upstream of the promoter (Ansari & Morse, 2012; Soutourina et al., 2011). The mediator links enhancers and promoter and undergoes a conformational change with disassociation of the kinase domain to be able to interact with RNAPII (Petrenko, 2021).

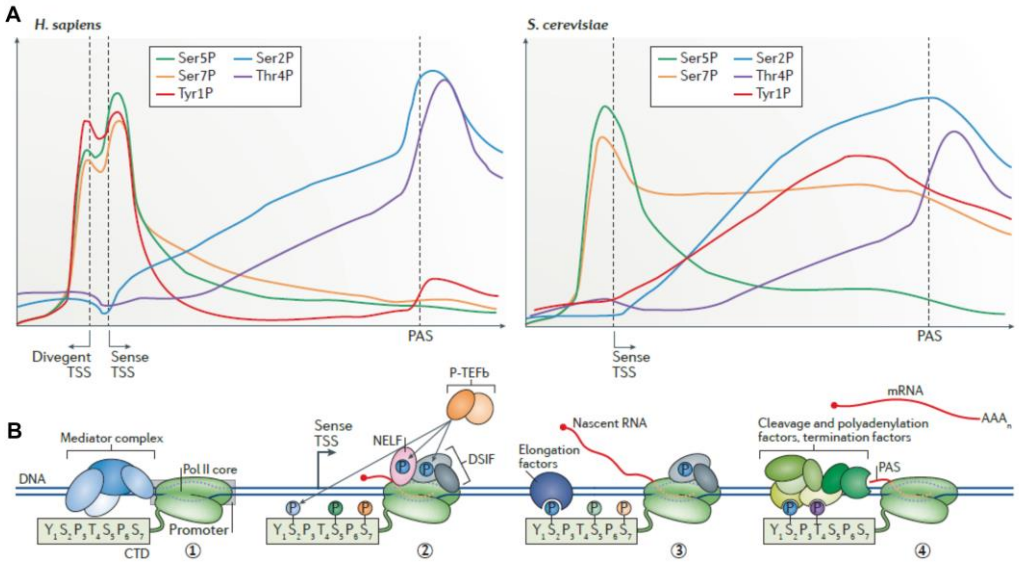

Figure 2. Regulation of transcription by RNAPII CTD phosphorylation. (A) Pattern of phosphorylation of the CTD of RNAPII during the transcription steps in human and yeast. The phosphorylation profiles are similar, except of the level of Tyr1P, which is in human higher in the promoter region, and for yeast it is increasing during transcription elongation. TSS – transcription start site, PAS – polyadenylation site. **(B)** Simplified overview of the stages of transcription. The RNAPII with unphosphorylated CTD and bound mediator complex is recruited to the promoter of the gene (step 1). Upon phosphorylation of Ser5, the affinity to the mediator complex is lost and RNAPII escapes the promoter. In metazoan, RNAPII has a promoter-proximal pausing, which is absent in yeast (step 2). In this step RNAPII is bound by the proteins NELF and DSIF. Factor TEFb phosphorylates them, as well as Ser2 of CTD. This leads to release of the factors and RNAPII is entering the active elongation phase. Increased Ser2P level leads to a recruitment of elongation factors during transcription elongation (step 3). High Ser2 and Thr4 phosphorylation are associated with recruitment of cleavage and polyadenylation factors and transcription termination (step 4) (Harlen & Churchman, 2017).

Transcription initiation is associated with a high level of phosphorylation (P) of Ser5 and Ser7. Ser5P mediates the recruitment of capping enzymes (McCracken et al., 1997; Schwer & Shuman, 2011). The CTD phosphorylation profiles of yeast and metazoan are very similar, but in metazoan the level of Tyr1P is high at the promoter region, whereas in yeast it increases during the elongation (Fig. 2A). In metazoan, Tyr1P is associated with a promoter-proximal RNAPII pausing 30 - 50 base pairs (bp) downstream of the transcription start site. Interestingly, budding yeast *Saccharomyces cerevisiae* lacks this pausing under normal conditions, but could gain two stall sites at the 5' end of most genes under peroxide stress (Badjatia et al., 2021). In yeast, transcription elongation is characterized by a decrease of Ser5P and an increase of Ser2P and Tyr1P, although level of Tyr1P decreases before the polyadenylation site (PAS) and level of Ser2P downstream of it (Harlen & Churchman, 2017; Singh et al., 2022; Xie et al., 2021). Ser2P is associated with recruitment of elongation and mRNA processing factors. Transcription termination is characterized by a peak of Ser2P and Thr4P, which promote the recruitment of termination, cleavage and polyadenylation factors (Mayer, Heidemann, et al., 2012). Therefore, pre-mRNA becomes largely co-transcriptionally processed: the 5' cap is added, introns are spliced out and the 3' end is cleaved and polyadenylated.

3.2.2. mRNA processing

3.2.2.1. 5' capping

After the first 20 - 30 nucleotides of the new transcript are synthesized, a cap structure is added to the 5' end of the pre-mRNA. The 5' cap provides the stabilization and protection of the mRNA from degradation by 5' - 3' exonucleases. The capping process consists of three steps. The first step is removal of the γ-phosphate from the triphosphate of the first nucleotide by RNA triphosphatase Cet1. On the second step, guanylyltransferase Seg1 transfers a guanosine monophosphate (GMP) from GTP to the 5' end. The result of such a transfer is the formation of an unusual linkage between 5' phosphate of GMP and 5' β-phosphate of the first nucleotide of the pre-mRNA. In yeast, triphosphatase and guanylyltransferase activities are provided by two distinct proteins, while in metazoan, one bifunctional protein Mce1 has an N-terminal triphosphatase and a C-terminal guanylyltransferase domain (Changela et al., 2001). The third step of capping is the methylation of the attached GMP in its N7 position by the

methyltransferase Abd1 with formation of 7-methylguanosine (m7G) cap, or so called the cap 0 structure. In addition, 2'-O position of ribose of the first transcribed nucleotide is methylated by 2′-O-methyltransferase to form the cap 1 structure. Some mRNA are additionally 2'-O-methylated on the second transcribed nucleotide (cap 2 structure) (Ramanathan et al., 2016).

Capping occurs in coordination with transcription. Phosphorylation of Ser5 within the heptapeptides of CTD of RNAPII during transcription initiation leads to recruitment of guanylyltransferase Seg1 and methyltransferase Abd1. Additionally, Seg1 has dual specificity and also interacts with phosphorylated Ser7 of the CTD (Bharati et al., 2016). Triphosphatase Cet1 is not directly associated with RNAPII CTD, but bound to Seg1 (Gu et al., 2010; Takase et al., 2000). The cryo-EM structure of RNAPII and capping enzymes revealed that Seg1-Cet1 span the RNA exit tunnel of RNAPII in a way that the emerging mRNA can be quickly and efficiently capped to ensure the protection of the transcript (Martinez-Rucobo et al., 2015). Phosphorylation of Ser2 within the CTD leads to the dissociation of capping enzymes Cet1 and Seg1. The methyltransferase Abd1 stays associated with RNAPII during transcription elongation (Schroeder et al., 2000).

In yeast cells, the cap is recognized by the cap-binding complex (CBC), consisting of the proteins Cbc1 and Cbc2. CBC remains associated with the mRNA until the mRNA is exported to the cytoplasm, where the complex is replaced by the translation initiation factor eIF4E (Jeong et al., 2019). Furthermore, CBC is involved in splicing of the first intron, as well as in promoting 3' end processing and nuclear mRNA export (Flaherty et al., 1997; Görnemann et al., 2005; Sen et al., 2019).

3.2.2.2. Splicing

Splicing is the removal of introns from the pre-mRNA. This process occurs as two consequent transesterification reactions with changing one phosphodiester bond to another (Kastner et al., 2019). Introns contain three conserved sequences – 5' splice site (SS), branch point (BP) and 3' SS. In the first transesterification reaction – the branching – the phosphate of the 5' SS is attacked by the 2'-OH group of adenosine (A) of the branch point (BP) (Fig. 3A). As a result the bond between the intron and the exon 1 is lost and lariat intron-exon 2 structure is formed.

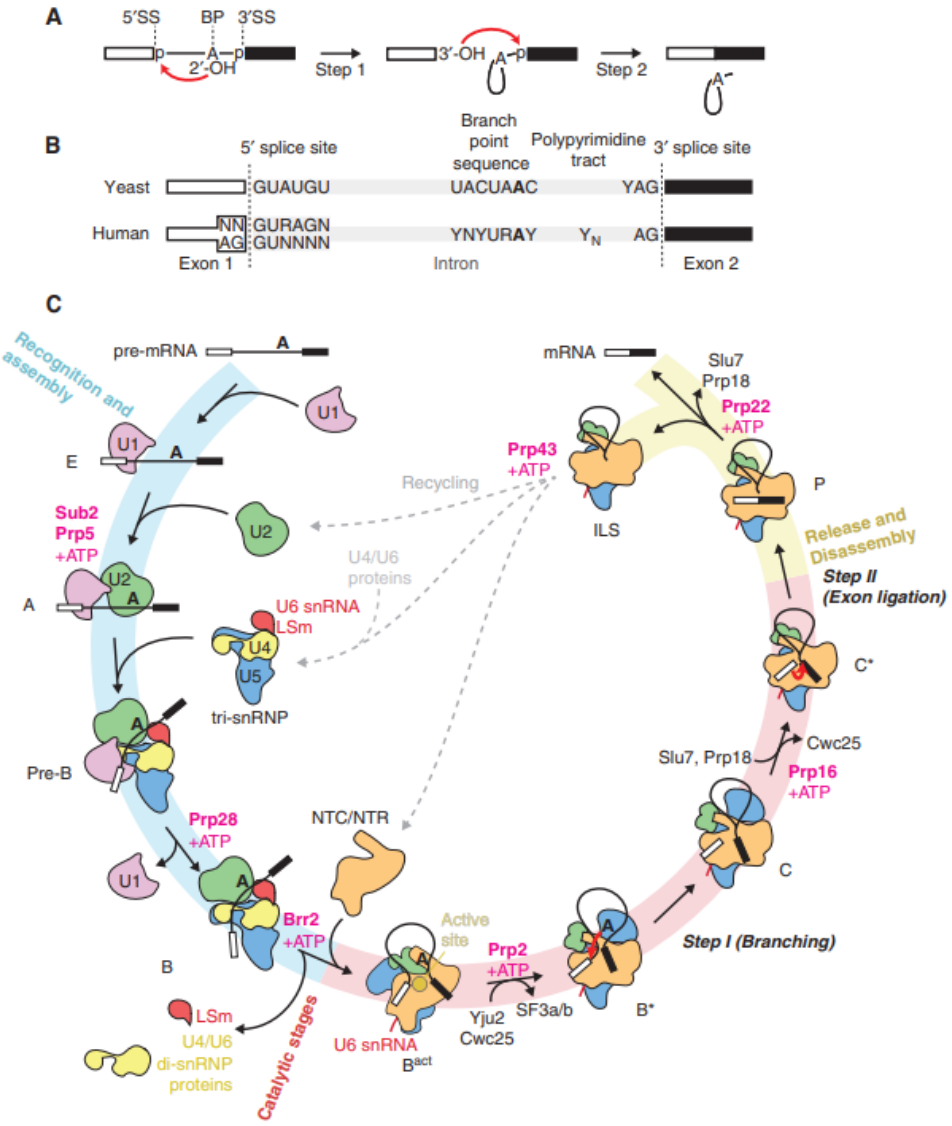

Figure 3. Schematic representation of the splicing process. (A) Schematic representation of the two transesterification reactions of splicing (ss – splicing site; BP – branchpoint). **(B)** Comparison of the conserved sequences within human and yeast introns. **(C)** Scheme of the splicing cycle. Recognition and assembly of spliceosome (blue part of the cycle) with stepwise recruitment of U1 snRNP (E-complex), U2 snRNP (A-complex) and tri-snRNP U4/U5-U6 (pre-B complex). The following remodeling by Prp28 displaces U1 (B-complex). Recruitment of Brr2 disassociates U4 snRNA together with U4/U6 and LSm proteins. The catalytical stage (red part) starts, when U6 snRNA folds and associates with U2 snRNA to form an active site. The NTC/NTR is recruited to stabilize the active site (B act complex). The remodeling by Prp2 leads to the release of proteins SF3a and b and recruitment of branching factors Yju2 and Cwc25 (B* complex). The first reaction of branching occurs (complex C). The helicase Prp16 dissociates with branching factors, while Slu7 and Prp18 proteins are recruited to the second transesterification reaction (complex C*). After the catalytical stage, ligated exons and the intron lariat are in the P-complex. Helicase activity of Prp22 leads to displacement of Slu7 and Prp18 and release of spliced mRNA. Intron lariat remains associated with spliceosome (ILS, intron lariat spliceosome) until Prp43 disassociate to be reused for another round of splicing (Plaschka et al., 2019).

During the second step, the OH group of the 3’ end of the first exon attacks phosphodiester bond of the 3’ SS to break it. This leads to ligation of two exons (Fig. 3A).

Both splicing reactions are accomplished by the spliceosome. This large molecular machinery is formed by 5 small nuclear RNAs (snRNAs) (U1, U2, U4, U5, U6) and around 100 proteins in yeast or 300 in human (Chen & Moore, 2015). The snRNAs and proteins form complexes, called small nuclear ribonucleoprotein particles (snRNPs). Some proteins are not assembled into snRNPs, but nevertheless take part in splicing, e.g. helicases or splicing factors.

Splicing is a complex process (reviewed in Plaschka et al., 2019; Wilkinson et al., 2020; Yan et al., 2019). Extensive structural studies revealed details about spliceosome remodeling during splicing (Fig. 3C). The 5’ SS of introns is recognized and bound by U1 snRNP. In yeast, the BP interacts with branch point binding protein (BBP) Msl5 in heterodimer form with Mud2 (metazoan U2AF65). In mammalian, the BBP SF1 binds the BP, while U2AF35-U2AF65 interacts with the 3’ SS (Berglund et al., 1997; Wang et al., 2008). This early spliceosome is known as E complex or commitment complex. Recruitment of DEAD-box helicases Prp5 and Sub2 leads to a substitution of BBP and U2AF by U2 snRNP and formation of a pre-spliceosome, also known as A complex (Plaschka et al., 2018; Wang et al., 2008). The pre-spliceosome associates with the pre-assembled tri-snRNP U4/U5-U6 and forms the pre-catalytic B complex. Despite the fact that the pre-B complex contains all needed factors to perform branching, U4 functions as chaperon to keep U6 in its inactive conformation and the 5’ SS is covered by bound U1 (Charenton et al., 2019). Recruitment of Prp28 displaces U1 and U5 binds the 5’ exon to tether it in place (B complex) (Boesler et al., 2016). Brr2 displaces U4, which leads to remodeling, where U6 and U2 form a catalytic site, but in a conformation, that inhibits the branching (B act complex). In the B act complex, U6 binds the 5’ SS, and U2 interacts with the BP sequence. The complex also interacts with Prp19-associated and Prp19-related complexes (NTC and NTR, respectively), required for spliceosome stabilization (Chan & Cheng, 2005). The next remodeling by DEAH-box ATPase Prp2 brings the 5’ SS and the BP together to the active site (B* complex) and it eventually results in the branching reaction with formation of the complex C (Fabrizio et al., 2009; Wan et al., 2019). In yeast, introns typically have a highly conserved YAG nucleotide sequence in the end (AG in human) (Fig. 3B). The G pairs with the G of the 5’ SS

and A – with A in the BP by non-Watson-Crick base-pairing. The 5' SS and BP are covalently bound with formation of a branching lariat structure (Galej et al., 2016). The C-complex is remodeled by Prp16 ATPase, that results in formation of the C* complex. The 3' SS is docked into the active site of the C* complex (Wilkinson et al., 2017). The complex undergoes an exon ligation reaction by exon ligation factors (Slu7, Prp17, Prp18). It leads to formation of a post-catalytic spliceosome, also called P complex (Bai et al., 2017). Spliced mRNA is released upon the Prp22-remodeling activity, the lariat structure remains associated with spliceosome (ILS, intron lariat spliceosome) (Company et al., 1991; Wan et al., 2017). Helicase Prp43, upon activation by splicing factor Ntr1, disassociates lariat and snRNAs (Tanaka et al., 2007).

Contrary to the human genome with introns in 95% of the genes, only 5% of the yeast protein-coding genes contain introns. Remarkably, due their high expression, 30% of total mRNAs contain introns in yeast (Ares et al., 1999). One-third of these introns are not essential, 20% have minor impact on the growth phenotype and only three are essential (Parenteau et al., 2008). Furthermore, human RNAs undergo alternative splicing and produce different isoforms of the same gene. For yeast, majority of the intron-containing RNAs are not alternatively spliced, with very few exceptions (Grund et al., 2008; Juneau et al., 2009).

Another distinct trait of metazoan mRNAs is the exon junction complex (EJC), which is bound 20 - 24 nucleotides upstream of each exon junction. The EJC is proposed to be involved in mRNA export by interaction with transcription-export complex TREX via the protein ALYREF (Pacheco-Fiallos et al., 2023).

In yeast splicing is coupled to mRNA export. For instance, RBP protein Npl3, as well as the ATP helicase Sub2 of the TREX complex are involved in both, splicing and mRNA export (Kress et al., 2008; Libri et al., 2001).

3.2.2.3. 3' end processing

3' end processing of mRNA consists of recognition of a polyadenylation signal (PAS), cleavage and the addition of a poly(A) tail (Kumar et al., 2019; Rodríguez-Molina & Turtola, 2023). In *S. cerevisiae*, these processes are performed by highly conserved 1 MDa cleavage and polyadenylation factor CPF and accessory cleavage factors CFIA and CFIB. The proteins of the CPF complex are organized in three modules

with different enzymatic activities – endonuclease, polymerase and phosphatase (Casañal et al., 2017).

In *S. cerevisiae*, the PAS consists of multiple cis-elements: UA-rich efficiency element, A-rich positioning element and U-rich elements up- and downstream the cleavage site (Fig. 4). Proteins of CPF recognize the PAS, and the endonuclease Yhs1 cleaves the pre-mRNA 10 - 30 nucleotides downstream of it (usually preceded by the nucleotides CA) (Chan et al., 2011). The cleavage results in formation of 5' and 3' products. The 5' product is polyadenylated by poly(A) polymerase Pap1, while the 3' product is degraded by torpedo exonuclease Rat1 to trigger transcription termination (Kim, et al., 2004). The phosphatase Glc7 dephosphorylates the CPF complex to switch from cleavage to polyadenylation (He & Moore, 2005). Another phosphatase of the CPF complex, Ssu72, is involved in transcription (by dephosphorylation Ser5 of the CTD of RNAPII) and in 3' end processing (independently of its catalytic activity) (Krishnamurthy et al., 2004). Reconstitution of the recombinant complex revealed that the protein Fip1 is bridging the poly(A) polymerase Pap1 to CPF via its interaction with the endonuclease Yth1 (Kumar et al., 2021). For the polyadenylation, the 3' end of pre-mRNA is enclosed in cleft of U-shaped Pap1. The binding of Pap1 to RNA substrate and Mg-ATP leads to a closed conformation of Pap1 to enable poly(A) synthesis (Balbo & Bohm, 2007). The stable association of Pap1 with CPF via Fip1 results in fast poly(A) synthesis.

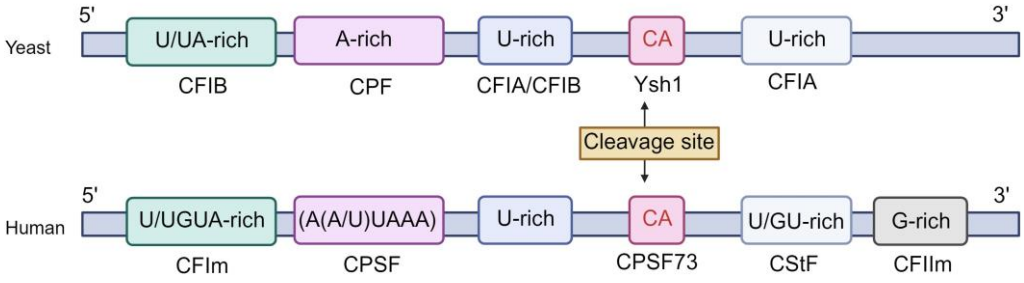

Figure 4. Cis-elements required for 3' end processing of yeast and human pre-mRNA. Specific cis-elements of pre-mRNA are organized in boxes. The protein complexes of the 3' end processing machinery are labeled below the cis-elements, which they recognize. The cleavage site is indicated with an arrow. Created with BioRender based on (Boreikaitė & Passmore, 2023; Chan et al., 2011).

The average poly(A) tail length in yeast is around 60 nucleotides. According to *in vitro* studies, yeast may have a three-layered regulation of poly(A) tail length (Turtola et al., 2021). After the addition of 60 nucleotides, the poly(A)-binding protein Nab2 binds to the tail, inhibits the activity of Pap1 and terminates polyadenylation. In case of Nab2 depletion, another poly(A)-binding protein, Pab1, terminates polyadenylation and produce 90 nucleotide long tails. Notably, Pab1 is mostly cytoplasmic, but can shuttle to the nucleus and contribute to poly(A) tail length regulation via its interaction with CFIA (Amrani et al., 1997; Dunn et al., 2005; Minvielle-Sebastia et al., 1997). The third layer of poly(A) tail length regulation, when both Nab2 and Pab1 are absent, is CPF itself. The CPF complex can terminate polyadenylation after 100 - 200 adenosines. This intrinsic regulation depends on CFIA and CFIB (Turtola et al., 2021).

Although the 3' end processing machinery is conserved among eukaryotic species, the polyadenylation mechanisms of yeast and mammals have distinctive features. In mammals, canonical PAS consists of an (A(A/U)UAAA) sequence 10 - 30 nucleotides upstream and U/GU-rich region 30 nucleotides downstream of the cleavage site (Millevoi, 2010). The cleavage and polyadenylation specific factor CPSF recognizes the PAS. Synthesis of the first 10 - 12 nucleotides is slow due to weak association of CPSF with poly(A) polymerase PAP. However, binding of poly(A)-binding protein PABPN1 stabilizes this interaction and leads to the rapid synthesis of the poly(A) tail. PABPN1 covers the 250 nucleotide long poly(A) tail with 15 - 20 molecules of the protein. Due to steric reasons, more molecules of PABN1 cannot be associated with the poly(A) tail. This leads to the loss of interaction between CPSF and PAP and termination of polyadenylation (Kühn et al., 2009).

Polyadenylation is tightly connected to transcription termination. For instance, depletion of Pcf11 or endonuclease Ysh1 leads to global transcription readthrough (Baejen et al., 2017). However, transcription termination occurs 200 (for yeast) or up to 1500 nucleotides (for human) downstream the PAS, where RNAPII disassociates from the template (Mischo & Proudfoot, 2013). There are two main models of transcription termination. According to the allosteric model, transcribing the PAS leads to conformational changes of RNAPII, its slowing down and promoting the termination. Based on another, so called torpedo model, 5'-3' exonuclease Rat1 degrades 3' cleavage product until it reaches and displaces RNAPII (Rodríguez-Molina et al., 2023).

Noteworthy, pre-mRNA can have multiple non-canonical poly(A) sites. Depending on the PAS recognition and cleavage, this can result in an alternative polyadenylation and thus mRNA isoforms with different length of the 3' UTR. Interestingly, in yeast alternative polyadenylation was observed as a response to environmental changes, e.g. DNA damage (Graber et al., 2013) or nutrient deprivation (Geisberg et al., 2020).

The processing of mRNA is closely interconnected with its nuclear export. For instance, multiple RBPs within mRNPs are reported to function in 3' end processing as well as in mRNP export (described below in 3.2.3.2 and 3.2.3.3).

3.2.3. Nuclear mRNP assembly and export

3.2.3.1. Recruitment of RNA-binding proteins

Co-transcriptionally, pre-mRNA is bound by RNA-binding proteins (RBPs). RBPs can be recruited in several ways: co-transcriptionally via CTD of RNAPII, via the C-terminal region (CTR) of elongation factor Spt5 or by mRNA itself. Furthermore, it has been proposed, that these three recruitment platforms are forming a so called a "molecular mRNP packaging station" to efficiently orchestrate the complex process of mRNP assembly (Meinel & Sträßer, 2015). Such an orchestration is largely regulated by distinct phosphorylation pattern of the CTD of RNAPII during the transcription cycle, as mentioned above (3.2.1). In addition to the capping, splicing and 3' end processing factors, CTD of RNAPII also interacts with proteins that form the mRNP. For instance, SR-like protein Npl3 binds to the phosphorylated Ser2 of the CTD of RNAPII (Dermody et al., 2008). Furthermore, the THO subcomplex of TREX directly interacts with CTD of RNAPII phosphorylated at serines S2 and S5 (Meinel et al., 2013).

Another recruitment platform is provided by the elongation factor Spt5. Spt5 interacts with the subunits Rpb4/7, Rpb1 and Rpb2 of RNAPII (Li et al., 2014) and binds ssRNA in a sequence-specific manner (Blythe et al., 2016). Spt5 has C-terminal region (CTR), consisting of 15 hexapeptide repeats that are phosphorylated at its residues. The CTR, phosphorylated by the kinase Bur1, recruits the polymerase associated factor 1 (PAF1) complex, which is involved in transcription elongation (Liu et al., 2009; Squazzo et al., 2002; Wier et al., 2013). Furthermore, the CTR of Spt5 has been reported to be involved in the recruitment of the mRNA capping enzymes

(Lidschreiber et al., 2013) and the 3' end cleavage factor CFI (Mayer, Schreieck, et al., 2012).

In addition, mRNA itself can serve as a recruitment platform for RBPs. RBPs have different RNA recognition domains, such as an RNA-recognition motif (RRM), zinc fingers (ZnF), K homology domain (KH) or others (Lunde et al., 2007). Interestingly, some RBPs bind to specific RNA sequences, while other do not have sequence specificity. For instance, Nab2 binds to a polyadenosine sequence via its seven tandem ZnF domains (Kelly et al., 2007), but also has specificity to a 7 nucleotide sequence stretch of A followed by G (Guisbert et al., 2005) or a GUAG motif (Baejen et al., 2014). Another RBP, Npl3, has specific binding to G/U-rich RNAs by its RRM domains, and non-sequence-specific binding outside its RRMs (Deka et al., 2008). In addition to their direct binding to mRNA, RBPs are recruited to mRNA via adaptor proteins.

3.2.3.2. TREX/THO complex and its subunit Hpr1

TREX is a highly conserved protein complex that plays a key role in coupling transcription and mRNA export. In yeast, this 470 kDa complex consists of the pentameric THO subcomplex (**Hpr1,** Tho2, Mft1, Tex1 and Thp2), the SR-like proteins Hrb1 and Gbp2, the helicase Sub2 and the mRNA export adaptor protein Yra1.

The TREX complex is involved in transcription (Rondón et al., 2003). It binds to nascent RNA and travels along the transcribed gene with RNAPII (Sträßer et al., 2002). The THO subcomplex directly interacts with the CTD of RNAPII phosphorylated at S2 and S5 (Meinel et al., 2013). The SR (serine-arginine)-like proteins Hrb1 and Gbp2 interact with the Ctk1 kinase, which phosphorylates the CTD of RNAPII during transcription elongation (Hurt et al., 2004). The TREX complex is recruited to all protein-coding genes, but preferentially to long GC-rich genes or genes with multiple internal tandem repeats (Chávez et al., 2001; Voynov et al., 2006). The TREX does not distribute evenly along the genes, but with gradual increase towards the 3' end (Gómez-González et al., 2011; Meinel et al., 2013). TREX dissociates downstream of the polyadenylation site (Kim et al., 2004). Interestingly, while the recruitment of the yeast TREX complex is directly

transcription-coupled, human TREX is recruited to mRNA during splicing (Masuda et al., 2005).

TREX is also involved in mRNA export. THO directly interacts with Sub2 via its Tho2 protein (Xie, Clarke, et al., 2021). Sub2 loads Yra1 onto the mRNP, followed by binding of the mRNA exporter Mex67-Mtr2 to Yra1 (Sträßer & Hurt, 2001).

Recent cryo-electron microscopy studies revealed that the yeast THO complex forms a dimeric assembly. Tho2 and Hpr1 create a dimeric platform in an antiparallel fashion. Mft1 and Thp2 of each monomer form “arms” towards each other and provide a vast homodimerization interface. Another smaller dimerization interface is comprised by the N-terminal helices of two Tex1 proteins (Schuller et al., 2020; Xie, Clarke, et al., 2021). In human, the seven subunits of one THO complex form a 28-subunit tetramer. It was suggested that the tetramer may bind few mRNA regions or associated proteins simultaneously (Pühringer et al., 2020). A recent study shows that in human three TREX tetramers binds to the same mRNP via its UAP56 (Sub2) subunits (Pacheco-Fiallos et al., 2023).

Hpr1 is a subunit of the THO/TREX complex, involved in various cellular processes. Deletion of *HPR1* leads to an increase of transcription-dependent recombination (hyperrecombination) and genome instability (Chávez et al., 2000). It is associated with defects in DNA replication and stalling of the replication fork (Wellinger et al., 2006).

The absence of *HPR1* is associated with accumulation of harmful R-loops, composed of DNA-RNA hybrids and displaced single stranded DNA (Luna et al., 2019; San Martin-Alonso et al., 2021). These structures impair transcription elongation, which leads to chromosomal instability in ∆*hpr1* cells (Huertas & Aguilera, 2003; Mishra et al., 2021). In addition to R-loop-mediated transcription defects, mutations in *HPR1* are also associated with R-loop independent transcription impairment (Gómez-González & Aguilera, 2009). Hpr1 interacts with RNAPII (Chang et al., 1999; Y. Li et al., 2005). As mentioned above, Hpr1 within the TREX complex travels along the genes with RNAPII, and loss of *HPR1* results in decreased processivity and occupancy of RNAPII at the genes (Mason & Struhl, 2005).

Moreover, *Δhpr1* cells (as well as other THO null mutants) exhibit mRNA export defects with accumulation of poly(A)$^+$ RNA in the nucleus (Sträßer et al., 2002). Deletion of *HPR1* leads to decreased co-transcriptional recruitment of RBPs Sub2

and Yra1 (Zenklusen et al., 2002). Additionally, Hpr1 may function as adaptor of mRNA exporter Mex67. The C-terminal end of Hpr1 directly interacts with the ubiquitin-associated (UBA)-domain of Mex67. Deletion of this UBA domain leads to a decreased gene occupancy of both, Hpr1 and Mex67. Moreover, ubiquitination of Hpr1 is required for the recruitment of Mex67 to the genes (Gwizdek et al., 2006).

Hpr1 is also involved in 3' end processing of mRNA. For instance, Δ*hpr1* cells exhibits 3' end processing defect of the *CYC1* precursor RNA *in vitro* (Saguez et al., 2008). Furthermore, the occupancy of processing factor Pcf11 is increased for some genes in Δ*hpr1* strain, however, in the "heavy" chromatin fraction. This fraction is pelleted during standard chromatin preparation and might represent stalled intermediates of mRNP biogenesis (Rougemaille et al., 2008).

3.2.3.3. mRNP assembly by mRNA-binding proteins

Co-transcriptionally, mRNA is bound by numerous RBPs. Many of them are identified and known (Klass et al., 2013; Mitchell et al., 2013). Some of the RBPs remain associated with mRNA and package it into export-competent mRNA ribonucleoprotein particles (mRNPs). Proteins that are known to be part of nuclear mRNPs in *S. cerevisiae* are described below.

In the nucleus, 5' end of mRNA is bound by the cap binding complex (CBC), consisting of proteins **Cbc1** and **Cbc2**. CBC promotes mRNA export by recruitment of the RBPs Yra1 and Npl3 to chromatin in a THO- and Sub2-independent manner (Sen et al., 2019). CBC is exported with mRNP to the cytoplasm, where it becomes replaced by eIF4E, a translation initiation factor (Fortes et al., 2000).

The SR-like proteins **Hrb1** and **Gbp2** are components of the TREX complex. They are loaded onto the mRNP. These shuttling proteins play a role in quality control of spliced mRNA in yeast. Deletion of *HRB1* and *GBP2* results in the leakage of unspliced pre-mRNA to the cytoplasm (Hackmann et al., 2014; Lu & Krebber, 2021).

The ATP-depended DEAD-box RNA helicase **Sub2** is involved in splicing (Libri et al., 2001; M. Zhang & Green, 2001). Additionally, as a part of the TREX complex, Sub2 plays a role in mRNA export (Saguez et al., 2013; Sträßer et al., 2002). The mRNA export adaptor Yra1 binds Sub2 and the mRNA exporter Mex67-Mtr2 via the same N- and C-terminal domains (Sträßer & Hurt, 2001). It has been suggested that Sub2 recruits Yra1 to load it onto the mRNA, and then Sub2 gets replaced by Mex67-Mtr2

before mRNA export. The THO complex and a C-terminal fragment of Yra1 stimulate the ATPase activity of Sub2 (Ren et al., 2017). This might be a mechanism of mRNP remodeling and loading of Yra1 onto the mRNP by Sub2.

Yra1 is an RBP with RNA annealing activity (Portman et al., 1997). It directly binds RNA and acts as an export adaptor protein to recruit mRNA exporter Mex67 to the mRNP (Sträßer & Hurt, 2000; Zenklusen et al., 2001). Yra1 does not leave the nucleus and disassociates from the mRNP before the mRNA gets exported (Lund & Guthrie, 2005). This disassociation is mediated by ubiquitination of Yra1 by the E3 ligase Tom1 (Iglesias et al., 2010). Yra1 couples 3' end processing and mRNA export by direct binding to the Pcf11 subunit of the yeast cleavage factor CFIA. Interaction of Yra1 with Pcf11 or Sub2 is mutually exclusive. Moreover, recruitment of Yra1 to actively transcribed genes is independent of Sub2, but dependent on Pcf11 (Johnson et al., 2009). This suggests an model of mRNP assembly, where Pcf11 first binds Yra1 and then Yra1 is transferred to Sub2.

Tho1 is an RBP, that binds to chromatin in a THO- and RNA-dependent manner (Jimeno et al., 2006). Overexpression of Tho1 suppresses the growth and mRNA export defect, as well as the hyperrecombination phenotype in Δ*hpr1* cells (Jimeno et al., 2002). Tho1 exhibits a novel annealing activity enhanced by Sub2, and multicopy *THO1* reduces the level of R-loops in Δ*hpr1* strain (Miosga, 2022). According to a recent crystal structure, a C-terminal domain of Tho1 interacts with two Sub2 molecules to form multimers on RNA. Moreover, Sub2 has overlapping binding regions to interact either with the THO complex or Tho1, which suggests that these interactions are occurring at different time points (Xie et al., 2023).

Npl3 is a shuttling SR-like protein. It directly interacts with the CTD of RNAPII (Dermody et al., 2008; Lei et al., 2001). Npl3 is involved in transcription elongation, termination and 3' end processing. Loss of Npl3 leads to transcriptome-wide termination readthrough (Holmes et al., 2015). It has been suggested that Npl3 is involved in 3' end processing of pre-mRNA by competing with cleavage factor CFI for binding to poly(A) signals (PAS). In such a way, Npl3 mask cryptic PAS to ensure the recognition of proper PAS by cleavage factors (Bucheli et al., 2007). Furthermore, Npl3 is involved in splicing by co-transcriptional recruitment of splicing factors (Kress et al., 2008). Phosphorylated Npl3 activates the ATPase Prp28, needed for spliceosome remodeling (Yeh et al., 2021). Npl3 is involved in mRNP assembly by

co-transcriptional recruitment of some RBPs to the genes and by loading other RBPs onto the mRNP (Keil et al., 2023). Moreover, Npl3 is involved in mRNA export and functions as another adaptor of Mex67-Mtr2 exporter to the mRNA (Gilbert & Guthrie, 2004; Lee et al., 1996).

The nuclear polyadenylated RBP **Nab2** is an essential shuttling RBP. Nab2 binds to poly(A) tails and regulates their length. Depletion of Nab2 is associated with hyperadenylation, as well as accumulation of poly(A)$^+$ RNA in the nucleus (Hector et al., 2002). In addition to the crucial function of Nab2 in poly(A) tail length control, it is not only recruited to the 3' end, but bound along the genes, which are actively transcribed by RNAPII and RNAPIII (González-Aguilera et al., 2011; Reuter et al., 2015). Furthermore, Nab2 is co-precipitated with mRNAs of different length and associates with most of yeast transcripts (Batisse et al., 2009). The N-terminal PWI-domain of Nab2 is important for nuclear export of RNA and Nab2, while its RGG (Arg-Gly-Gly) domain is required for nuclear import of Nab2. Its seven CCCH Zinc fingers (ZnF) are crucial for binding to the poly(A) tail (Kelly et al., 2007; Marfatia et al., 2003). Binding of Nab2 to RNA induces dimerization of its ZnF 5 - 7 and leads to compaction of the mRNA within the mRNP (Aibara et al., 2017). Nab2 functions in mRNA export as an adaptor protein for Mex67. It directly interacts with Mex67, and Yra1 enhances this interaction (Iglesias et al., 2010). The N-terminal domain of Nab2 binds to Mlp1 protein, which is associated with the nucleoplasmic side of the nuclear pore complex (NPC) (Fasken et al., 2008). Likely, in this way Nab2 targets the mRNA to the NPC. Notably, Nab2 is also involved in transcription termination. Loss of Nab2 leads to a defect in transcription termination with transcriptome-wide transcriptional readthrough (Alpert et al., 2020).

Interestingly, the new yet uncharacterized protein **Yhs7** was co-purified as a component of nuclear mRNPs. In cross-linking mass spectrometry experiment it showed to have multiple interaction sites with Yra1 (Bonneau et al., 2023).

The packaging of mRNA by mentioned RBPs is accompanied by recruitment of **Mex67-Mtr2**. This mRNA exporter mediates the nuclear export of mature mRNPs through the NPC to the cytoplasm.

3.2.3.4. Nuclear export of mRNP

Transcription and translation are spatially separated in eukaryotic cells. The connection between them is established through the NPC. Transport of proteins and non-coding RNAs (e.g., tRNA, miRNA, snRNA, rRNA) via the NPC to the cytoplasm is mediated by exportins, proteins of the karyopherin family. The direction of this transport is mediated by the GTPase Ran. In the nucleus Ran is bound to GTP, and in cytoplasm to GDP. The GTP-GDP gradient is regulated by RanGEF (GDF exchange factor) in the nucleus and RanGAP (GTPase activating protein) in the cytoplasm. Exportins bind a nuclear cargo together with RanGTP, then move through the NPC and release the cargo in the cytoplasm upon RanGTP hydrolysis (Köhler & Hurt, 2007).

However, export of mRNPs is not depended on exportins and GTP hydrolysis. On the contrary, it requires the exporter **Mex67-Mtr2** in yeast and NFX1-NXT1 (Tap–p15) in metazoans (Fig. 5A). Mex67 binds RNA without any sequence specificity for certain RNA motifs (Baejen et al., 2014; Santos-Rosa et al., 1998). Mex67 has rather low affinity to mRNA and is recruited to mRNA via its adaptor proteins, such as Yra1, Npl3, Nab2 and Hpr1 (Gilbert & Guthrie, 2004; Gwizdek et al., 2006; Iglesias et al., 2010; Sträßer et al., 2000). Export-competent mRNP with bound Mex67-Mtr2 is targeted to and transported through the NPC.

According to the “gene gating” model, actively transcribed genes are located in close proximity to NPCs to ensure that assembled mRNP can be quickly exported to the cytoplasm (Bensidoun et al., 2021; Blobel, 1985). Two conserved multiprotein complexes – SAGA and TREX-2 – are involved in “gene gating”. SAGA (Spt-Ada-Gcn5 acetyltransferase) is a chromatin modifying complex, which binds to promoters of the genes upon transcription activation. SAGA recruits the TREX-2 complex composed of the proteins Sus1, Thp1, Sac3, Sem1 and Cdc31. TREX-2 is bound to the nuclear side of the NPC. It functions as a tether for transcribing genes and promotes efficient mRNP export (García-Oliver et al., 2012). Associated with mRNP, Mex67 interacts with TREX-2 through the N-terminal domain of Sac3, which contains phenylalanine-glycine (FG) repeats (Dimitrova et al., 2015). Sac3 together with Cdc31 and two Sus1, in turn, interact with Nup1, a nucleoporin of the NPC (Jani et al., 2014).

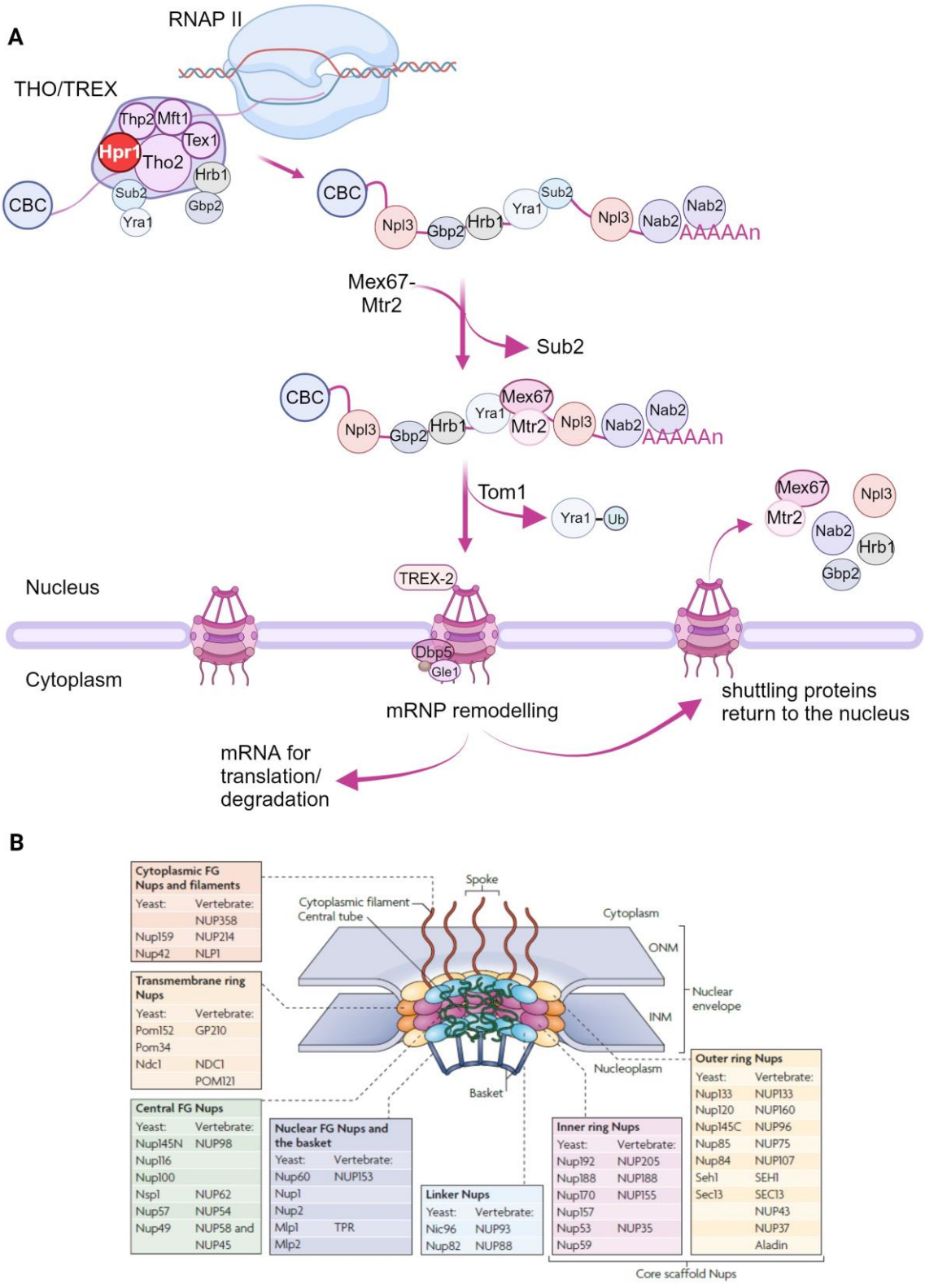

Figure 5. Nuclear mRNA export. (A) The TREX complex couples transcription and mRNA export. It binds to the nascent RNA and travels with RNAP II along the gene. Co-transcriptionally, pre-mRNA is packaged by RBPs into mRNPs. TREX component Sub2 loads Yra1 onto the mRNP. Yra1 uses the same domain for interaction with Sub2 and general exporter Mex67. Sub2 is displaced as a result of binding of Yra1 to Mex67. In this way, Mex67 together with its cofactor Mtr2 is loaded onto the mRNP. The mature mRNP is targeted for the export through the nuclear pore complex (NPC). Yra1 remains in

the nucleus as a result of ubiquitination by ubiquitin-ligase Tom1. Mex67 interacts with the TREX-2 complex, tethered to the nuclear side of the NPC, via interactions with its nucleoporins. Mex67 binds Phe-Gly FG-repeats of the nucleoporins of the central channel of the NPC to enable the translocation of mRNPs through the NPC to the cytoplasm. In the cytoplasm, the mRNP is remodeled by the RNA-helicase Dbp5 with its co-factor Gle1 and the small molecule inositol hexakisphosphate (IP6) (brown circle). The mRNA is entering the translation/degradation process, while shuttling proteins are exported back to the nucleus for the next round of export. **(B)** The structure of nuclear pore complex (NPC) in yeast and human with labeled nucleoporins (Nups). For nuclear mRNA export the most important are the FG-Nups on the nuclear side of the NPC, as well as in central channel and cytoplasmic filaments. ONM – outernuclear membrane, INM – inner nuclear membrane. Figure (A) is created with BioRender; figure (B) is from (Strambio-De-Castillia et al., 2010).

NPCs are large macromolecular machineries perforating the nuclear envelope (Fig. 5B). They have a size of around 50 MDa in yeast and 120 MDa in metazoan. The yeast NPC consists of about 30 different nucleoporins presented in multiple copies - 500 copies in total (Kim et al., 2014; Rajoo et al., 2018). The central channel of the NPC is formed by FG-nucleoporins, which contain extensive FG-repeats (Terry & Wente, 2009). Mex67-Mtr2 binds to FG-repeats via its UBA and NFT2-like domains (Fribourg et al., 2001; Grant et al., 2002; Sträßer et al., 2000). The interaction between Mex67-Mtr2 and the FG-repeats of the central channel has a weak nature to ensure the translocation through the NPC (Xie & Ren, 2019).

On the cytoplasmic side of the NPC, FG-repeats of Nup159 and Nup42 bind Mex67-Mtr2 to position mRNPs for remodeling by the DEAD-box ATPase Dbp5 and its cofactor activator Gle1 with the small molecule inositol hexakisphosphate (IP6) (Adams et al., 2014). Mex67-Mtr2 is displaced by Dbp5 to prevent the return of exported mRNP back to the nucleus (Lund & Guthrie, 2005). According to the current mRNA export model, Mex67 and other shuttling RNA-binding proteins return to the nucleus where they can be a part of the mRNA export pathway again. However, another advanced fluorescence microscopy study suggests, that Mex67 may function as “mobile nucleoporin” and interacts with the NPC independently of the mRNA and ATPase activity of Dbp5. According to this model, export-competent mRNP is loaded on Mex67 at the NPC, and Mex67 does not shuttle between nucleus and cytoplasm to provide mRNA export (Derrer et al., 2019).

3.3. Purification of transcript-specific nuclear mRNPs

Although the protein components of nuclear mRNPs have been identified, little is known about their stoichiometry and structure of mRNPs, how different mRNPs may vary dependent on mRNA length or different species. Lack of this knowledge caused by the technical challenges of mRNP purification. To date, it is considered that a nuclear mRNP is composed of one transcript-specific mRNA and a set of the RBPs. Therefore, protein- or RNA-centric approaches are used to pull down the mRNPs (McHugh et al., 2014). The protein approach is based on purification of a tagged protein component of the mRNP. As different mRNPs consist of the same RBPs, a pool of all mRNPs is enriched with this method. Indeed, in *S. cerevisiae*, purification of mRNPs via protein Nab2 enriches elongated particles various in size (15 - 35 nm in length, 5 - 7 nm in width) (Batisse et al., 2009). In human, mRNPs form non-uniform compact globules with an average size of around 45 nm, covered on their surface with multiple TREX complexes (Pacheco-Fiallos et al., 2023). However, there are only few studies about nuclear mRNP structure and, furthermore, no available structure of a specific mRNP. To purify transcript-specific mRNPs, RNA-centric methods, based on antisense oligonucleotides or aptamers, can be implemented (Gerber, 2021).

3.3.1. Antisense oligonucleotides approach

Antisense oligonucleotides (ASOs) are short single-stranded RNA or DNA oligonucleotides designed to specifically hybridize to the RNA of interest. The ASOs are chemically modified to prevent their degradation by nucleases. The chemistry of the ASOs determines its operating principle: to decay the target, or to bind it without causing degradation. Based on modification type, ASOs are divided into three generation groups (Quemener et al., 2020).

ASOs of the first generation include modifications in the phosphate backbone at the phosphodiester bond, where oxygen is substituted by a sulfur, amine or methyl group (Fig. 6). Phosphorothioates (PS) ASOs with sulfur modification are the most common. They have increased half-life and the ability to recruit the RNase H enzyme, that degrades RNA within DNA-RNA hybrids (Zhang et al., 2021). Thereby, binding of the PS ASO to the specific mRNA target leads to its degradation by RNase H and thus prevents protein synthesis. The PS ASOs have promising properties for

scientific research and targeted medicine, but they also have been shown to bind proteins non-specifically (Liang et al., 2014).

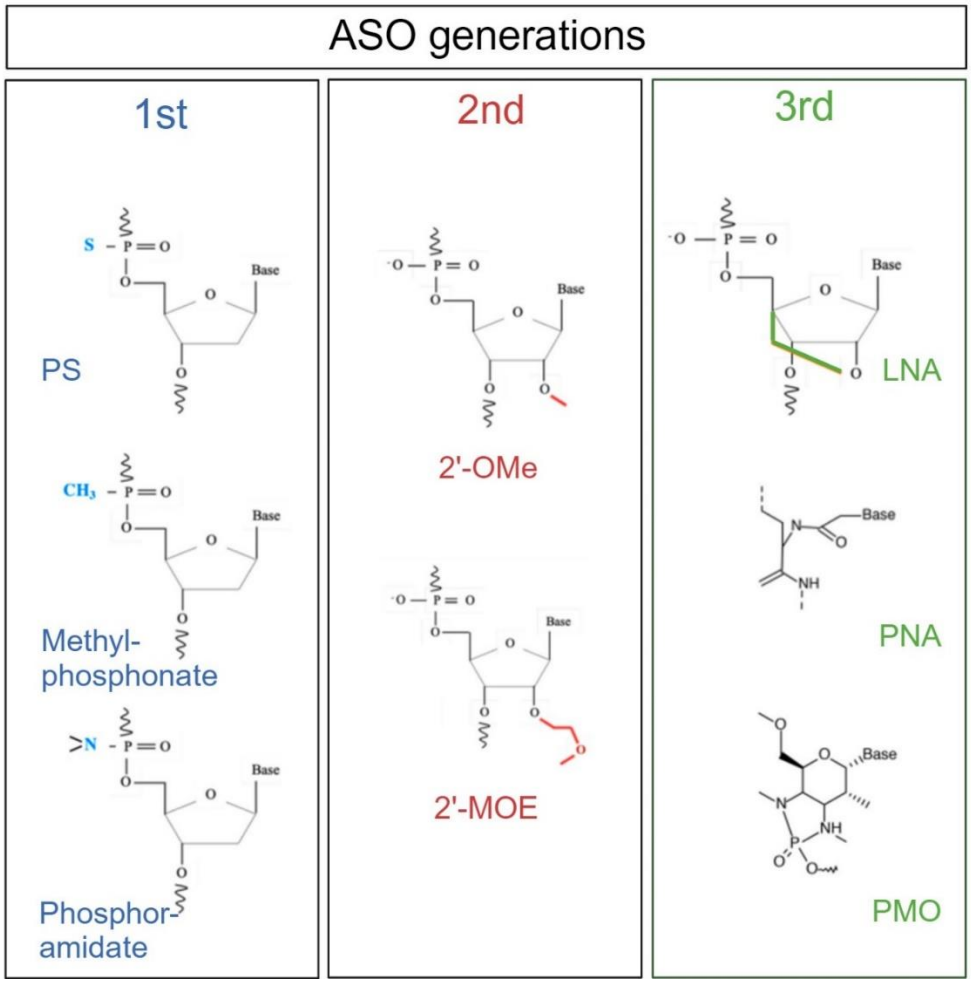

Figure 6. Three generations of ASOs. Structures of the common ASO representatives. ASOs - antisense oligonucleotides; PS – phosphorothioates; 2'-OMe - 2'-O-methyl; 2'-MOE - 2'-O-methoxyethyl; LNA - locked nucleic acids; PNA - peptide nucleic acid; PMO - phosphorodiamidate morpholino oligomers. Figure is modified after (Quemener et al., 2020).

To increase ASOs specificity, the modifications 2'-O-methyl (2'-OMe) and 2'-O-methoxyethyl (2'-MOE) were introduced at the 2' position of ribose (Fig. 6). These ASOs belong to the second generation. They show a higher stability against nucleases and higher affinity to the target. Moreover, the second generation ASOs are unable to recruit RNase H for RNA degradation (Juliano, 2016; Karaki et al., 2019). It makes them a powerful tool in assays, where RNA has to be captured with high affinity and specificity, but not degraded. To benefit from the higher affinity of 2'-

OMe and 2'-MOE ASOs, but also to make them capable to recruit RNase H, chimeric "gapmer" ASOs were designed. In the gapmer ASO, the central "gap" part is composed of 8 - 10 unmodified DNA nucleotides, which are flanked by 2' modified RNA nucleotides on both sides of the "gap" (Maranon & Wilusz, 2020). Thus, the central gap mediates RNase H recruitment, whereas the 2' modified nucleotides protect the ASO from nuclease degradation and provide high affinity and specificity (Pollak et al., 2020).

The third generation ASOs include very diverse modifications to further improve the affinity to the target RNAs. The most common representatives of the modifications are locked nucleic acids (LNAs), peptide nucleic acid (PNAs) and phosphorodiamidate morpholino oligomers (PMOs) (Fig. 6). Binding of these ASOs do not trigger RNase H activation, but they may potentially form very stable hybrids with the target RNA and function as steric blockers to impair translation (Dhuri et al., 2020; Tallet-Lopez et al., 2003).

ASOs have been used in different applications to purify specific RNA or RNA-protein complexes. Among the advantages of ASOs are high affinity and direct interaction with the target RNA. This method does not require the introduction of specific RNA tags that may interfere with the RNA structure. For purifications, mainly 2'-OMe ASOs or LNA ASOs are used, as their binding does not lead to RNase H-induced RNA degradation. To enable the pulldown of an ASO and its bound target, ASOs are biotinylated and captured with streptavidin-coupled beads (Smith et al., 2017).

ASOs were successfully used for the purification of viral RNA (Knoener et al., 2017; Phillips et al., 2016; Upadhyay et al., 2013) and lncRNA Xist (Chu, Zhang, Teixeira Da Rocha, et al., 2015; Mchugh et al., 2015) to identify their binding proteins by mass spectrometry. There are also examples for the purification of mRNA with interacting proteins and miRNAs in human cell lines (Hassan et al., 2013) and *C. elegans* (Theil et al., 2019). ASOs also have been used to capture mRNP complexes, for instance, in the tandem RNA isolation procedure (TRIP). TRIP is a two-step purification of endogenously formed cross-linked mRNP complexes. In the first step, all poly(A) RNAs are bound using oligo(dT) beads, and in the second step, specifically designed and biotinylated 2'-OMe ASO binds to the target mRNA and to the streptavidin beads (Iadevaia et al., 2018; Matia-González et al., 2017). Alternatively, LNA/DNA mixmers

were implemented to capture specific RNPs *in vitro* in *Drosophila* embryo and human HeLa cell extracts (Rogell et al., 2017).

Mentioned examples of RNA-protein purifications suggest new possibilities for an investigation of specific mRNPs. However, this method still has major limitations, such as low yield of purified RNA or unspecific interactions. For instance, even partial hybridization of the ASO with non-target RNA may lead to cross-hybridization and enrichment of non-specific mRNA (Iadevaia et al., 2018).

3.3.2. Aptamer-based affinity capture

RNA aptamers are short and folded single-stranded RNA sequences that bind a specific ligand – small molecule or protein – with high affinity and specificity. Identification of potential aptamers and their substrates is achieved by systematic evolution of ligands by exponential enrichment (SELEX) (Mallikaratchy, 2017). This method provides a library of potential RNA aptamers and their ligands. After the determination of their binding affinity, the best candidates are used to tag RNA of interest. Introducing the aptamer may interfere with RNA structure and affect its interactions with RBPs. To avoid this, aptamers are typically inserted in the 3' or 5' UTR of RNA (Gemmill et al., 2019).

RNA aptamers are widely used to purify RNA-protein complexes. These aptamers and their properties are listed in the Table 1. The most common of them are described in more details below.

S1 streptavidin binding aptamer was cloned into *RPR1* RNA subunit of RNase P to isolate this RNP complex in *S. cerevisiae* (Srisawat, 2001). This is a one-step purification, in which the S1 aptamer can directly bind to streptavidin-coupled beads and be natively eluted with biotin. However, S1 aptamer provides low yield of target RNP (Srisawat, 2002).

To improve its properties, the original S1 aptamer was modified (**S1m**) by extending its stem part. Modified S1m exhibited higher affinity to streptavidin when used in four repeats (**4xS1m**). The 4xS1m aptamer was applied for *in vitro* isolation of mRNPs. Despite of high efficiency of binding *in vitro*, the aptamer failed to capture endogenous mRNP complexes *in vivo* (Leppek, 2013).

Table 1. List of RNA aptamers used to purify RNA-protein complexes. General properties, such as size of the aptamers (nt, nucleotides), their ligands and binding affinity (Kd, dissociation constant; n/d – non-determined) are specified.

Aptamer	Size, nt	Ligand	Kd	Ref.
Tobramycin-binding	40	Tobramycin	9 - 12 nM	(Jiang & Patel, 1998)
Streptomycin-binding	46	Streptomycin	1 μM	(Wallace et al., 1998; Windbichler et al., 2006)
PP7	25	PP7 coat protein	1 nM	(Lim et al., 2001)
D8	33	Dextran B512	n/d	(Srisawat et al., 2001)
S1	44	Streptavidin	70 nM	(Srisawat & Engelke, 2002)
4xS1m	47 (4 repeats)	Streptavidin	29 nM	(Leppek & Stoecklin, 2014)
MS2	19 (up to 24 repeats)	MS2 coat protein	0.6 - 2.7 nM	(Tutucci et al., 2018)
Mango	23 core	Thiazole orange (TO)	3.2 nM	(Dolgosheina et al., 2014)
Csy4	20	Csy4 nuclease	50 pM	(Lee et al., 2013)

MS2 – another commonly used aptamer – is derived from the MS2 bacteriophage. Ligand of the MS2 loop is the bacteriophage MS2 coat protein (MCP). The MS2-MCP system is among the most prevalent for RNA capture. This system went through many modifications, such as different amount of MS2 repeats or nucleotide substitution in the loop for higher affinity (Tutucci et al., 2018). The MS2 loop has been used to purify spliceosome complexes via maltose binding protein (MBP) fused to MCP (Deckert et al., 2006; Zhou et al., 2002). Moreover, spliced AdML and β-globin mRNAs were isolated via MS2 loop from HeLa nuclear extracts *in vitro* (Merz et al., 2007). To enable affinity capture and visualization of mRNA, the RNA binding protein purification and identification (RaPID) method was developed. It is based on the interaction of fluorescent reporter MS2-MCP-GFP and streptavidin-binding protein tag (SBP). Using RaPID, specific mRNAs *ASH1*, *OXA1*, or *SRO7* were isolated. Interestingly, these mRNAs were co-precipitated with some other

transcripts, which might suggest presence of few mRNAs within one mRNP (Slobodin, 2010). Yet another application of MS2 aptamer is MS2-tagged RNA affinity purification (MS2-TRAP), for which MCP is fused to GST for affinity pull down (Yoon, 2016). For example, mRNA *fbl* and its associated proteins were purified using the MS2-TRAP approach from *Drosophila* (Huang et al., 2022).

Mango aptamer is a short RNA aptamer with a complex structure. It consists of a 23 nucleotides core, flanked by complementary “arms”, forming a double-stranded stem. Mango binds its ligand – fluorophore thiazole orange (TO) derivates – with high affinity (Dolgosheina et al., 2014). A crystal structure revealed that the aptamer core binds to TO1 fluorophore molecule, but also to biotin and even a polyethylenglycol linker between TO1 and biotin (Trachman III et al., 2017). Fluorogenic properties of Mango resulted in developing the brighter variants Mango II, III and IV. They were used to visualize non-coding RNAs (5S rRNA, U6 snRNA and small Cajal body-specific RNA scaRNA) and β-actin mRNA in mammalian cells (Autour et al., 2018; Cawte et al., 2020). Coupling TO1 with biotin allows to implement the Mango aptamer system for both, visualization and purification of specific RNP complexes. For instance, the Mango aptamer was used to purify U1 snRNP from *S. cerevisiae* and S6 RNP from *E. coli* via TO1-desthiobiotin immobilized on streptavidin beads (Panchapakesan et al., 2017).

Another example for the purification of RNA-protein complexes is a **Csy4**-based approach. CRISPR endoribonuclease Csy4 specifically binds 16 nt hairpin sequence, which can be integrated into the RNA of interest (Haurwitz et al., 2010). Addition of imidazole activates Csy4 to cleave the hairpin and release a native transcript with associated proteins. Biotinylated Csy4 was used to purify hairpin tagged human pre-miRNAs *in vitro* and identify its interacting proteins (Lee et al., 2013).

Along with ASOs, RNA aptamers are another powerful tool for mRNP purification. However, their application is limited due to low yield and usage predominantly for *in vitro* systems.

3.4. Aim of this study

Assembly and export of nuclear mRNPs is an essential part of gene expression. In *Saccharomyces cerevisiae* the RBPs composing nuclear mRNPs are known, as well as the importance of the TREX complex in coupling transcription and mRNA export (Klass et al., 2013; Mitchell et al., 2013; Sträßer et al., 2002). What still remains enigmatic, is the mRNP structure and stoichiometry. This lack of knowledge is explained by technical challenges to purify the low-abundant, multi-component and dynamic mRNPs. While the first steps in purification of all nuclear mRNPs have been taken, the niche of purification of transcript-specific mRNPs is still empty (Batisse et al., 2009; Bonneau et al., 2023). Possibility to purify a specific mRNP could answer the questions about its structure, as well as mRNPs' differences within one organism or between the species. The **first aim** of this study is to develop an effective method to purify specific nuclear mRNPs from *Saccharomyces cerevisiae* under native conditions and determine its structure by electron microscopy. To accomplish this goal, this study will establish a two-step affinity purification. For the first step, an isolation of the cap-bound mRNPs will be optimized to obtain a high yield of total nuclear mRNPs. For the second step, the RNA-centric approaches will be implemented to isolate only transcript-specific mRNPs. For this, different ASOs that specifically hybridize to the mRNA of interest, will be tested. As an alternative method, the mRNA of interest will be tagged with various RNA aptamers. After the selection of the most promising ASO/aptamer candidates, the purification conditions will be modified and optimized to obtain high specificity and yield of the mRNP of interest. The improved methods will be used to examine the structure of the natively isolated endogenous particles with electron microscopy.

In addition to this structural project, the **second aim** of this study is to investigate the role of Hpr1, a subunit of the TREX/THO complex, in mRNP assembly. Hpr1 is involved in transcription and mRNA export (Chávez et al., 2000; Huertas & Aguilera, 2003; Sträßer et al., 2002). However, how Hpr1 affects mRNP assembly is not known. Hpr1 is a component of the mRNP export pathway, in which mRNA export adaptor Yra1 recruits general mRNA exporter Mex67-Mtr2 to the mature mRNP for its export (Sträßer & Hurt, 2001; Zenklusen et al., 2001). The possibility of alternative mRNA export pathways is discussed since not only Yra1, but Nab2, Npl3, and Hpr1 itself were reported to be adaptors of Mex67 (Gilbert & Guthrie, 2004; Gwizdek et al., 2006; Iglesias et al., 2010). Therefore, another goal is to investigate how mRNA

export works in absence of Hpr1 and which potential alternative mechanisms of the export can take place. To address these questions, changes in nuclear mRNP composition will be assessed upon depletion or deletion of *HPR1*. RNA binding and co-transcriptional recruitment of RBPs will be evaluated. Furthermore, the possibilities and mechanisms of alternative mRNA export pathways will be explored by elucidating the role of other mRNA export adaptor proteins, such as Nab2, Yra1 or Npl3 in Δ*hpr1* cells.

Taken together, this study will contribute to the complex and technical challenge of purification of transcript-specific mRNP and elucidating its structure. Furthermore, it will bring new insights into the role of TREX component Hpr1 in the essential processes of mRNP assembly and export.

4. Materials

4.1. Chemicals and consumables

Table 2. Chemicals and consumables.

Name	Supplier
2-mercaptoethanol	Merck
2-Propanol	Carl Roth
3-Indolacetic acid (auxin)	Sigma-Aldrich
Acetic acid	VWR Chemicals
Acrylamide (29:1) 40%	AppliChem GmbH
Adenine hemisulfate salt	Sigma-Aldrich
Agar Bacteriology grade	Applichem GmbH
Agarose	Applichem GmbH
Amylose magnetic beads	New England Biolab (NEB)
Ammonium persulfate (APS)	VWR Chemicals
Ampicillin	Applichem GmbH
ATP	NEB
Bacto™ Peptone	BD Biosciences
Bacto™ Yeast extract	BD Biosciences
Benzamidine HCl	MP Biomedicals
Boric acid	Merck
Bovine serum albumin (BSA)	Carl Roth
Bromophenol blue	Applichem
Clarity™ Western ECL Substrate	Bio-Rad Laboratories
Coomassie Brilliant Blue R-250	AppliChem
D-Glucose Monohydrate	Sigma-Aldrich
Diethyl pyrocarbonate (DEPC)	Carl Roth
DEPC-treated water	Carl Roth
Dimethyl sulfoxide (DMSO)	Sigma-Aldrich
Dipotassium phosphate (K2HPO4)	Grüssing GmbH
Disodium phosphate (Na2HPO4)	Carl Roth
Dithiothreitol (DTT)	Sigma-Aldrich
dNTPs (dATP, dTTP, dCTP, dGTP)	Thermo Fisher Scientific

D-Sorbitol	Carl Roth
Dynabeads™ M-280 Tosylactivated	Invitrogen
Dynabeads™ Protein G	Invitrogen
Dynabeads™ M-280 Streptavidin	Invitrogen
Ethanol	Fisher Chemical
Ethylenediaminetetraacetic acid (EDTA)	Sigma-Aldrich
Ficoll® 400	Carl Roth
Formaldehyde	ORG Laborchemie
Gel loading dye, purple (6x)	NEB
Genetecin (G418)	ThermoFisher (Gibco)
Glycerol	Carl Roth
Glycine	Labochem international
HDGreen™ DNA stain	Intas
HEPES	Carl Roth
Herring sperm DNA	Invitrogen
Hydrochloric acid (HCl)	Carl Roth
IGEPAL CA-630	Sigma-Aldrich
IgG Sepharose 6 Fast Flow	GE Healthcare
L-Arginine-HCl	Biomol GmbH
L-Aspartic acid	Sigma-Aldrich
Leupeptin (Hemisulfate)	Carl Roth
L-Histidine	Sigma-Aldrich
L-Isoleucine	Sigma-Aldrich
Lithium chloride (LiCl)	Merck
L-Leucine	Sigma-Aldrich
L-Lysine Monohydrochloride	Sigma-Aldrich
L-Methionine	Sigma-Aldrich
L-Phenylalanine	Sigma-Aldrich
L-Threonine	Sigma-Aldrich
L-Tryptophan	Sigma-Aldrich
L-Tyrosine	Sigma-Aldrich
L-Valine	Biomol GmbH
Liquid nitrogen	Linde
Magnesium chloride (MgCl2)	Merck

Magnesium sulfate (MgSO4)	Merck
Methanol	Merck-Millipore
Monopotassium phosphate (KH2PO4)	Carl Roth
Monosodium phosphate (NaH2PO4)	Merck
Nicotinamide adenine dinucleotide (NAD)	Sigma-Aldrich
Pepstatin A	AppliChem
Pierce™ High Capacity Streptavidin Agarose	Thermo Scientific
Polyethylene glycol (PEG) 3800/4000	Carl Roth
Polylysine	Sigma-Aldrich
Polysorbate 20 (Tween 20)	Merck
Polyvinylpyrrolidone (PVP)	Sigma-Aldrich
Ponceau S	Serva
Potassium chloride (KCl)	ORG Laborchemie
Potassium hydroxide (KOH)	Merck
Powdered milk, fat free, blotting grade	Carl Roth
Rothi®-Mount FluorCare DAPI	Carl Roth
Roti®-Aqua-Phenol	Carl Roth
Salmon sperm DNA (ssDNA)	Applichem
Sodium acetate (NaOAc)	Merck
Sodium citrate	Merck
Sodium chloride (NaCl)	Merck
Sodium deoxycholate	Sigma-Aldrich
Sodium dodecyl sulfate (SDS)	AppliChem
Sodium hydroxide (NaOH)	Merck
SuperSignal™ West Dura Extended Duration Substrate	Thermo Scientific
Tetramethylethylendiamin (TEMED)	Carl Roth
TO1-3PEG-Desthiobiotin Fluorophore	Applied Biological Materials (ABM)
Trichloroacetic acid (TCA)	Merck
TRIS	Carl Roth
Triton X-100	AppliChem
TRIzol™ Reagent	Invitrogen
tRNA from *E. coli* MRE600	Roche diagnostics
Tryptone BioChemica	AppliChem

Uracil	Sigma-Aldrich
Urea	AppliChem
Yeast nitrogen base, w/o amino acids	Formedium

4.2. Equipment and devices

Table 3. Equipment and devices.

Name	Supplier
70 Ti rotor	Beckman Coulter
AM100, micro scale	Mettler-Toledo
Apollo®, liquid nitrogen container	Cryotherm
Avanti JXN-26 Centrifuge	Beckman Coulter
Bioruptor UCD-200, Sonication System	Diagenode
ChemoCam Imager ECL HR 16-3200	Intas
Duomax 1030, Platform shakers, rocking	Heidolph Instruments
FastPrep-24TM 5G	MP Biomedicals
Freezer/Mill® 6870D	Spex®SamplePrep
Gel iX20, Transilluminator/gel docu	Intas
Hera safe, laminar flow cabinet	Thermo Fisher Scientific
HeraFreeze HFU T Series	Thermo Scientific
HT Multitron Pro shaking incubator	Infors
IKA® KS 4000 ic control, shaking incubator	IKA Labortechnik
IKAMAG® RCT, magnetic stirrer	IKA Labortechnik
Incubator with HT Labotron, shaker	Aqua Lytic / Infors
Incubators	Memmert
Innova®44 shaking incubator	Eppendorf / New Brunswick
JLA-8.1, JA-10 rotors	Beckman Coulter
Lab phenomenal pH 1000L, pH meter	VWR
LED blue light transilluminator	Nippon genetics
Megafuge 40R	Thermo Scientific, Heraeus
Milli-Q® integral water purification system	Merck
Mini-Protean® Tetra Electrophoresis Cell	Bio-Rad Laboratories

ND-1000, Spectrophotometer	NanoDrop
Optima XPN-80 Ultracentrifuge	Beckman Coulter
PeqStar XS Thermocycler	Peqlab
PM2000, scale	Mettler-Toledo
RCT basic, magnetic stirrer	IKA Labortechnik
Research Pipettes 2, 10, 20, 100, 200, 1000, 5000 µl	Gilson
Rotator	neoLab
SBH130D, block heater	Stuart®
SW22, shaking waterbath	Julabo
T3 Thermocycler	Biometra
Tabletop Centrifuge 5424, 5424R	Eppendorf
Tabletop Centrifuge 5430, 5430R	Eppendorf
Thermomixer 5436	Eppendorf
Trans-Blot® Turbo Transfer System	Bio-Rad Laboratories
Typhoon FLA 9500	GE Healthcare
Vakulan CVC 3000	Vacuubrand
VF2, vortex mixer	IKA Labortechnik
VX-150, autoclave	Systec

4.3. Media, buffers and solutions

4.3.1. Water

Water for buffers and solutions was purified with the Milli-Q-synthesis System (Millipore) and autoclaved. Heat-sensitive solutions were sterile filtrated through 0.22 µm filter. Buffers for RNA-based methods were prepared with DEPC-treated (RNase-free) water to reduce a risk of RNA degradation. For self-made DEPC-treated water diethylpyrocarbonate (DEPC) was stirred in water (0.1% final concentration) overnight. To remove DEPC, the water was autoclaved twice.

4.3.2. Media

Lysogeny broth (LB)	SOC media
1 % peptone	2 % tryptone
0.5 % yeast extract	0.5 % yeast extract
0.5 % NaCl	10 mM NaCl

pH 7.2

(15 g agar / 1 l for plates)

0.5 mM KCl

10 mM MgCl2

10 mM MgSO4

pH 7.0

Synthetic dropout medium (SDC) for 1 l

6.75 g yeast nitrogen base (w/o aa)

0.6 g complete synthetic amino acid mix (SCM)

20 g glucose

10 mL of each 100x aa stock except one for the selection

pH 5.5

Yeast complete medium (YPD)

1 % yeast extract

2 % peptone

2 % glucose

pH 5.5

(15 g agar / 1 l for plates)

4.3.3. Buffers and solutions

Cloning

Gibson assembly master mix

1 × Isothermal (ISO) reaction buffer

4 U/µl T5 exonuclease

4 U/µl Taq DNA ligase

25 U/ml Phusion DNA polymerase

5x Isothermal (ISO) reaction buffer

500 mM TRIS-HCl pH 7.5

50 mM MgCl2

50 mM DTT

1 mM of each dNTPs

5 mM NAD

25 % PEG-8000

50x TAE buffer

2 M TRIS

1 M NaOAc

50 mM EDTA

pH 8.0

Transformation of *Saccharomyces cerevisiae*

Solution I

1x TE

100 mM LiOAc

Solution II

1x TE

100 mM LiOAc

40 % PEG 3800 or 4000)

10x TE
100 mM TRIS pH 7.5
10 mM EDTA

Yeast whole cell extract preparation

Pre-treatment solution
1.85 M NaOH
7.5 % 2-mercaptoethanol

Tandem Affinity Purification (TAP)

TAP lysis buffer
50 mM HEPES-KOH pH 7.5
100 mM KCl
1.5 mM MgCl2
0.15 % NP-40
1 mM DTT
1x protease inhibitor (PI)

TAP wash buffer
50 mM HEPES-KOH pH 7.5
200 mM KCl
1.5 mM MgCl2
0.15 % NP-40
0.5 mM DTT

100x protease inhibitor (PI)
6.85 mg pepstatin A
1.42 mg leupeptin hemisulfate
850 mg PMSF
1.65 g benzamide HCl
Up to 50 mL EtOH

10x PBS
1.4 M NaCl
27 mM KCl
43 mM Na2HPO4
18 mM KH2PO4

Purification of specific nuclear mRNP

TAP wash buffer
50 mM HEPES-KOH pH 7.5
100 mM KCl
1.5 mM MgCl2
0.15 % NP-40
0.5 mM DTT

ASO-wash buffer
10 mM HEPES-KOH pH 7.5
150 mM KCl
0.5 mM EDTA
0.05 % Tween 20

ASO-elution buffer
50 mM HEPES-KOH pH 7.5
150 mM KCl
16 mM biotin

Mango-wash buffer
15 mM HEPES-KOH pH 7.5
150 mM KCl
0.05 % Tween 20

Mango-elution buffer
15 mM HEPES-KOH pH 7.5
100 mM KCl
0.05 % Tween 20
20 mM biotin

Maltose elution buffer
10 mM HEPES-KOH pH 7.5
100 mM NaCl
15 mM maltose

SDS polyacrylamide gel electrophoresis

4x Separating buffer
1.5 M TRIS pH 8.8
8 mM EDTA
0.6 % SDS

Separating gel (10 %)
3 mL acrylamide (40 %; 29:1)
3 mL 4x separating buffer
6 mL H2O
100 µL 10 % APS
20 µL TEMED

4x Stacking buffer
0.5 M TRIS pH 6.8
8 mM EDTA
0.6 % SDS

Stacking gel (4 %)
400 µL acrylamid (40 %; 29:1)
1 mL 4x stacking buffer
2.6 mL H2O
30 µL 10 % APS
10 µL TEMED

4x SDS loading dye
0.25 M TRIS-HCl
0.1 M DTT
9 % SDS
0.2 % Bromophenol blue
40 % Glycerol

Coomassie staining solution
0.5 % Coomassie R250
25 % isopropanol
10 % acetic acid

5x SDS Running buffer

125 mM TRIS

1 M Glycine

20 mM EDTA

0.5 % SDS

Western blot

10x TRIS buffered saline + Tween 20 (TBST)

500 mM TRIS pH 7.5

1.5 M NaCl

1 % Tween 20

Semi-dry Western blot buffer

25 mM TRIS

192 mM Glycin

20 % Methanol

Chromatin Immunoprecipitation (ChIP)

Low-salt buffer

50 mM HEPES (pH 7.5)

150 mM NaCl

1 mM EDTA

1 % Triton-X 100

0.1 % SDS

0.1 % sodium deoxycholate

High-salt buffer

50 mM HEPES (pH 7.5)

500 mM NaCl

1 mM EDTA

1 % Triton-X 100

0.1 % SDS

0.1 % sodium deoxycholate

TLEND

10 mM TRIS (pH 8.0)

0.25 M LiCl

1 mM EDTA

0.5 % NP-40

0.5 % sodium deoxycholate

10x TE

100 mM TRIS

10 mM EDTA

pH 7.5

Elution buffer

50 mM TRIS (pH 7.5)

10 mM EDTA

1 % SDS

10x PBS

1.4 M NaCl

27 mM KCl

43 mM Na2HPO4

14 mM KH2PO4

RNA Immunoprecipitation (RIP)

RNA IP-buffer
25 mM TRIS (pH 7.5)
150 mM NaCl
2 mM MgCl2
0.2 % Triton X 100
0.5 mM DTT

Fluorescence *In Situ* Hybridization (FISH)

Wash buffer
1.2 M sorbitol
100 mM KPO4 (pH 6.4)

20 x SSC (pH 7.0)
3 M NaCl
300 mM sodium citrate

Prehybridization buffer
50 % formamide
10 % dextran sulfate
125 µg/mL tRNA from *E. coli* MRE600
500 µg/mL herring sperm DNA
4 x SSC
1 x Denhardt's solution

50x Denhardt's solution
1 % polyvinylpyrrolidone (PVP)
1 % bovine serum albumin (BSA)
1 % Ficoll® 400

Poly(A) tail length assay

20% PAA – 8 M Urea PAGE
4.8 g Urea
1 ml 10x TBE
5 ml 40 % acrylamide (29:1)
100 µl 10 % APS
10 µl TEMED
(total volume 10 mL)

10x TBE
1 M boric acid
1 M Tris
25 mM EDTA
pH 8.3

4.4. Organisms

4.4.1. *E. coli* strains

Table 4. *E. coli* strains.

Strain	Genotype	Reference
DH5α	F– endA1 glnV44 thi-1 recA1 relA1 gyrA96 deoR nupG purB20 φ80dlacZΔM15 Δ(lacZYA-argF)U169, hsdR17(rK–mK+), λ–	(Taylor et al., 1993)

4.4.2. Yeast strains

Table 5. *S. cerevisiae* strains.

Strain	Genotype	Reference
RS453	MATa, ade2-1, his3-11,15, ura3-52, leu2-3,112, trp1-1, can1-100, GAL+	(Sträßer & Hurt, 2000)
Δ*ccw12*	MATa; ade2-1, his3-11,15, ura3-52, leu2-3,112, trp1-1, can1-100, GAL+; YLR110c::kanMX4	This study
Δ*ccw12 CBC2-TAP*	MATa, ade2-1, his3-11,15, ura3-52, leu2-3,112, trp1-1, can1-100, GAL+; YLR110c::kanMX4; CBC2-CBP-TEV-protA::TRP1	This study
CBC2-TAP	MATa; ade2-1; his3-11,15; ura3-52; leu2-3,112;trp1-1 can1-100; GAL+; CBC2-CBP-TEV-protA::TRP1	B. Keil
Δ*ccw12 MBP-MCP*	MATa; ade2-1; his3-11,15; ura3-52; leu2-3,112;trp1-1 can1-100; GAL+; Δccw12::kanMX; MBP-MCP::Leu	J. Seidler
W303	MATa, ura3-1, trp1-1, his3-11,15, leu2-3,112, ade2-1, can1-100, GAL+	(Thomas &Rothstein, 1989)
Δ*hpr1*	Mata; ura3-1; ade2-1; his3-11,5; trp1-1; leu2-3,112; can1-100; hpr1::HIS3	R. Rothstein
CBC2-TAP	CBP20-CBP-TEV-protA::TRP1; Mata; ura3-1; trp1-1; his3-11,15; leu2-3,112; ade2-1; can1-100; GAL+	This study
Δ*hpr1 CBC2-TAP*	MATa; ura3-1; trp1-1; his3-11,15; leu2-3,112; ade2-1; can1-100; GAL+; CBC2-CBP-TEV-protA::TRP1; hpr1::HIS3	This study
CBC2-TAP MEX67-6xHA	MATa; ura3-1; trp1-1; his3-11,15; leu2-3,112; ade2-1; can1-100; GAL+; CBC2-CBP-TEV-protA::TRP1; MEX67-HA::kanMX	This study
Δ*hpr1 CBC2-TAP*	MATa; ura3-1; trp1-1; his3-11,15; leu2-3,112; ade2-1; can1-100; GAL+; hpr1::HIS3; CBC2-	This study

MEX67-6xHA	CBP-TEV-protA::TRP1; MEX67-HA::kanMX	
osTIR	MATa; ura3-1; trp1-1; his3-11,15; leu2-3,112; ade2-1; can1-100; GAL+; URA3:::osTIR	K. Hühn
HPR1-AID-6xHA	MATa; ura3-1; trp1-1; his3-11,15; leu2-3,112; ade2-1; can1-100; GAL+; URA3:::osTIR Hpr1-AID-6HA::Hyg	This study
HPR1-AID CBC2-TAP	MATa; ura3-1; trp1-1; his3-11,15; leu2-3,112; ade2-1; can1-100; GAL+; URA3:::osTIR Hpr1-AID-6HA::Hyg; CBC2-CBP-TEV-protA::TRP1	This study
HPR1-AID CBC2-TAP MEX67-6xHA	MATa; ura3-1; trp1-1; his3-11,15; leu2-3,112; ade2-1; can1-100; GAL+; URA3:::osTIR Hpr1-AID-6HA::Hyg; CBC2-CBP-TEV-protA::TRP1; Mex67-6HA::KanMX4	This study
NAB2-TAP	MATa; ura3-1; trp1-1; his3-11,15; leu2-3,112; ade2-1; can1-100; GAL+; Nab2-CBP-TEV-protA::TRP1	This study
Δ*hpr1 NAB2-TAP*	MATa; ura3-1; trp1-1; his3-11,15; leu2-3,112; ade2-1; can1-100; GAL+; Nab2-CBP-TEV-protA::TRP1; hpr1::HIS3	This study
HPR1-AID NAB2-TAP	URA3:::osTIR Hpr1-AID-6HA (plasmid 2352)::Hyg; Nab2-CBP-TEV-protA::TRP1	This study
MEX67-TAP	MATa; ura3-1; trp1-1; his3-11,15; leu2-3,112; ade2-1; can1-100; GAL+; Mex67-CBP-TEV-protA::TRP	This study
Δ*hpr1 MEX67-TAP*	MATa; ura3-1; trp1-1; his3-11,15; leu2-3,112; ade2-1; can1-100; GAL+; Tho2-9myc::KanMX4; hpr1::HIS3; Mex67-CBP-TEV-protA::TRP	This study
YRA1-TAP	MATa; ura3-1; trp1-1; his3-11,15; leu2-3,112; ade2-1; can1-100; GAL+; Yra1-CBP-TEV-protA::TRP	This study
Δ*hpr1 YRA1-TAP*	MATa; ura3-1; trp1-1; his3-11,15; leu2-3,112; ade2-1; can1-100; GAL+; Tho2-9myc::KanMX4; hpr1::HIS3; Yra1-CBP-TEV-protA::TRP	This study
THO2-9myc TEX1-6HA MFT1-3myc HPR1-6HA	MATa; ura3-1; trp1-1; his3-11,15; leu2-3,112; ade2-1; can1-100; GAL+; Tho2-9myc::KanMX4; Tex1-6HA::Leu; Mft1-3myc::Trp; Hpr1-6HA::His	This study
THO2-9myc TEX1-6HA MFT1-3myc HPR1-6HA THP2-TAP	MATa; ura3-1; trp1-1; his3-11,15; leu2-3,112; ade2-1; can1-100; GAL+; Tho2-9myc::KanMX4; Tex1-6HA::Leu; Mft1-3myc::Trp; Hpr1-6HA::His; Thp2-TAP::Ura	This study
Δ*hpr1 THO2-9myc TEX1-6HA MFT1-3myc HPR1-6HA THP2-TAP*	MATa; ura3-1; trp1-1; his3-11,15; leu2-3,112; ade2-1; can1-100; GAL+; Tho2-9myc::KanMX4; hpr1::HIS3; Tex1-6HA::Leu; Mft1-3myc::Trp; Thp2-TAP::Ura	This study

HPR1-AID THO2-9myc TEX1-6HA MFT1-9myc THP2-TAP	URA3:::osTIR Hpr1-AID-6HA::Hyg; Tho2-9myc::KanMX4; Tex1-6HA::Leu; Mft1-9myc::His Thp2-Trp	This study

4.5. Oligonucleotides

Table 6. Oligonucleotides used for cloning.

Name	Sequence (5'→3')
CCW12-Mango I vector fwr	GAAGGGACGGTGCGGAGAGGAGAGAATGTATAAATTTTTTATAAACTTTTTTGGCATTTAACAAATATATAACA
CCW12-Mango I, II, III, IV vector rev	GAAGCCATACCAAACGACGAGCGT
CCW12-Mango I, II, III, IV fragment fwr	ACGCTCGTCGTTTGGTATGGCTTC
CCW12-Mango I fragment rev	TACATTCTCTCCTCTCCGCACCGTCCCTTCGAATGTATAAATAATAATAAACTAAG
CCW12-Mango II vector fwr	GAAGGAGAGGAGAGGAAGAGGAGAGAATGTATAAATTTTTTATAAACTTTTTTGGCATTTAACAAATATA
CCW12-Mango II fragment rev	TACATTCTCTCCTCTTCCTCTCCTCTCCTTCGAATGTATAAATAATAATAAACT
CCW12-Mango III vector fwr	GGAAGGAGGAGGGAAGAATGTATAAATTTTTTATAAACTTTTTTGGCATTTAACA
CCW12-Mango III fragment rev	TACATTCTTCCCTCCTCCTTCCGAATGTATAAATAATAATAAAC
CCW12-Mango IV vector fwr	CGAGGGAGGGGAGGAGAGGCGAGAATGTATAAATTTTTTATAAACTTTTTTGGCATTTAACAAATATAT
CCW12-Mango IV fragment rev	TACATTCTCGCCTCTCCTCCCCTCCCTCGGAATGTATAAATAATAATAAAC
OE Nab2 vector fwr	AAAATTATTTAATGGTTGATGAATTCCTGCAGCCCGG
OE Nab2 vector rev	TGTAATGAACCACACGATCGGATATCAAGCTTATCGATACCGTCG
OE Nab2 fragment fwr	GTATCGATAAGCTTGATATCCGATCGTGTGGTTCATTACA
OE Nab2 fragment rev	CCCCCGGGCTGCAGGAATTCATCAACCATTAAATAATTTTGTACACTTATAATAACAC
OE Yra1 vector fwr	TCATAATAGTTTTTTGAATTCCTGCAGCCCGGG
OE Yra1 vector rev	CGGGGAAATCCAATTGATATCAAGCTTATCGATACCGTCGAC
OE Yra1 fragment	GATAAGCTTGATATCAATTGGATTTCCCCGAACAGC

fwr	
OE Yra1 fragment rev	GGGCTGCAGGAATTCAAAAAACTATTATGATAACCTTGCTCAAGTCAAAC
OE Mex67 vector fwr	CTTGGACCGTAAAACTGCCTGCAGCCCGGGGGATCCACT
OE Mex67 vector rev	AAAATTTGGAGGACGAATTCGATATCAAGCTTATCGATACCGT
OE Mex67 fragment fwr	GCTTGATATCGAATTCGTCCTCCAAATTTTGCACCTC
OE Mex67 fragment rev	GATCCCCCGGGCTGCAGGCAGTTTTACGGTCCAAGCGG
Mex67-HA vector fwr	CTCGAATTCATCGATTAATGATATTGTTCCCTGTTTCAGCCG
Mex67-HA vector rev	GACCTGCAGCGTACGGAACTGCACAAATGCTTCTCTAGG
Mex67-HA fragment fwr	TAAACTGTATATTTTTTGTGATACTGTGCGGCTGAAACAGGGAACAATATCATTAATCGATGAATTCGAGCTCG
Mex67- HA fragment rev	AAAGGGTTTTCAGAGTAGCATGAATGGCATCCCTAGAGAAGCATTTGTGCAGTTCCGTACGCTGCAGGTCGAC

Table 7. Oligonucleotides used for genome tagging.

Name	**Sequence (5'→3')**
CBC2-TAP fw	AGACCAGGTTTCGATGAAGAAAGAGAAGATGATAACTACGTACCTCAGTCCATGGAAAAGAGAAG
CBC2-TAP rev	TATATATATCTGTGTGTAGAATCTTTCTCAGATATAAATTGATTGATTCTATACGACTCACTATAGGG
HPR1-HA frw	GCTACTTCGAACATTTCTAATGGTTCATCTACCCAAGATATGAAACGTACGCTGCAGGTCGAC
HPR1-HA rev	ATGAATTTCTTATCAGTTTAAAATTTCTATTAAGAGGATAATTTAATCGATGAATTCGAGCTCG
MEX67-HA fwr	AAAGGGTTTTCAGAGTAGCATGAATGGCATCCCTAGAGAAGCATTTGTGCAGTTCCGTACGCTGCAGGTCGAC
MEX67-HA rev	TAAACTGTATATTTTTTGTGATACTGTGCGGCTGAAACAGGGAACAATATCATTA ATCGATGAATTCGAGCTCG
MEX67-TAP fwd	CAGAGTAGCATGAATGGCATCCCTAGAGAAGCATTTGTGCAGTTCTCCATGGAAAAGAGAAG
MEX67-TAP rev	TATATTTTTTGTGATACTGTGCGGCTGAAACAGGGAACAATATCATCATACGACTCACTATAGGG
HPR1-AID fwr	GCAGCTACTTCGAACATTTCTAATGGTTCATCTACCCAAGATATGAAACCTAAAGATCCAGCCAAAC

HPR1-AID rev	TGCATGAATTTCTTATCAGTTTAAAATTTCTATTAAGAGG ATAATTTACTGATATCATCGATGAATTC
NAB2-TAP fwr	CCGCAAACCAGTTTTACGCACCAAGAACAAGATACGGA AATGAAC TCCATGGAAAAGAGAAG
NAB2-TAP rev	AAGGGTCACAGGAACATGAATTTCGTTCCGTGATTTTAA TAGTAATCATACGACTCACTATAGGG
YRA1-TAP fwr	CTTGAAGATCTGGACAAGGAAATGGCGGACTATTTCGA AAAGAAA TCCATGGAAAAGAGAAG
YRA1-TAP rev	AATTTAATAAAACCAAATTAAATCAAACAAAAAATTGACA ATTAATTATACGACTCACTATAGGG
THO2-myc fwr	TCAGGCGCTTCCGCAAGGTCCCAAGGGTGGGAATTAC GTCAGTAGGTACCAGAGGCGTACGCTGCAGGTCGAC
THO2-myc rev	AACTATCAAAGTACACGTTAAAATTCAGCTCGGGTATGT TAAGTACTAGTAATTA ATCGATGAATTCGAGCTCG
TEX1-HA fwr	TAAGAATACTGATAGGATTGGCAAGGATAGGCCGAGTA GATTCAACTCAAAAAAACGTACGCTGCAGGTCGAC
TEX1-HA rev	AATGAAAGAAAAAGAATGTGCATTTTCTACCGCATTCCT TCCATCAGGTAACTTA ATCGATGAATTCGAGCTCG
MFT1-myc fwr	ACTTGGAGGCACTACAAGCGATTTTAGTGCGTCTTCCT CTGTTGAAGAAGTAAAACGTACGCTGCAGGTCGAC
MFT1-myc rev	CTATGTGTCTATATGCCTTTTCTATTTAGTAAGAGCTATG CATTATACGTGGTCA ATCGATGAATTCGAGCTCG
THP2-TAP fwr	TCGGAAAGCTATCCTGTAGATAAAGAAGGTGACATAGTT TTAGAATCCATGGAAAAGAGAAG
THP2-TAP rev	GTATAACTCTATCTAACTTGTGCAGGCTGGTTAAATAAA ATGTGCTTATACGACTCACTATAGGG

Table 8. Antisense oligonucleotides (ASOs) used for specific binding to *CCW12* mRNA.

Name	**Sequence (5'→3')**
ASO1	GTGTTTAAGCGAATGACAGA
ASO2	TAGCAGTGGTAACGTTAGCA
ASO3	AAAGCTGGGGAGACAGTTTC
ASO4	TTGGGGCTTCAGTGGTCAAT
ASO5	GACAGAGTGAGTTGGAGCAG
ASO6	TACAACAACAAAGCAGCGGC
ASO7	TAAAAAATTTAGAATGTATAAATAATAATAAAC
ASO8	GTTAAATGCCAAAAAAGTTTATAAAAAATT
LNA1	+GTG+TTT+A+AG+CGAATGACAGA

LNA2	GTG+TTTA+AGCGA+ATGACAGA
LNA3	GTG+TTT+A+AGCGAAT
LNA4	GTG+TTT+A+AGCGAATGA

"+" in front of nucleotide marks modification with locked nucleic acid (LNA)

Table 9. Oligonucleotides used for qPCR.

Name	**Sequence (5'→3')**
CCW12 5' fwd	ACTGTCGCTTCTATCGCCGC
CCW12 5' rev	TTGGCTGACAGTAGCAGTGG
PGK1 5' fwd	TTGCCAACCATCAAGTACGTTT
PGK1 5' rev	CCCAAGTGAGAAGCCAAGACA
NTR fwd (Mayer et al., 2010)	TGCGTACAAAAAGTGTCAAGAGATT
NTR rev (Mayer et al., 2010)	ATGCGCAAGAAGGTGCCTAT
PMA1 3' fwd	CAGAGCTGCTGGTCCATTCTG
PMA1 3' rev	GAAGACGGCACCAGCCAAT
CCW12 3' fwd	TGAAGCTCCAAAGAACACCACC
CCW12 3' rev	AGCAGCAGCACCAGTGTAAG
YEF3 3' fwd	TCTGGTCACAACTGGGTTAGTG
YEF3 3' rev	GCAATCTTGTTACCCATAGCATCGA
ILV5 3' fwd	TGGTACCCAATCTTCAAGAATGC
ILV5 3' rev	ACCGTTCTTGGTAGATTCGTACA
RPL9B 3' fwd	AGGACGAAATCGTCTTATCTGGT
RPL9B 3' rev	CAGATTTGTTGCAAGTCAGCGG
DBP2 3' fwd	CTTCACCGAACAAAACAAAGGTT
DBP2 3' rev	TCGGGAGGAATATTTTGATTAGCT
ACT1 3' fwd	ATCATGAAGTGTGATGTCGATGTC
ACT1 3' rev	ATGGTGGTACCACCGGACATAA
RPS14B 3' fwd	AAGACCCCAGGACCAGGTG
RPS14B 3' rev	GATACGGCCAATCCTCAAACCAG
PRL28 3' fwd	TGGAAGCCAGTCTTGAACTTGG
PRL28 3' rev	TTGGTCTCTCTTGTCTTCTGGGA
RNAseH ASO1 fwr	CTTCTGTCATTCGCTTAAAC
RNAseH ASO1 rev	AGAAGCGACAGTAGAAAATT
RNAseH ASO2 fwr	TACTGTCGCTTCTATCGCCGCT
RNAseH ASO2 rev	CGTGGTCTTCACAAGAAGTGATGG

RNAseH ASO3 fwr	TGTCGCCGCTGTCGCTTCTG
RNAseH ASO3 rev	TCGACGGTGACGGTAGCGG
RNAseH ASO4 fwr	CCGTCACCGTCGATGACGTTATC
RNAseH ASO4 rev	ACTGGAGCAGCAGTAGAAGTACCG
RNAseH ASO5 fwr	GCTCCAAAGAACACCACCTC
RNAseH ASO5 rev	CAGCAGCACCAGTGTAAGAG
RNAseH ASO6 ASO7 fwr	TGTCACCTCTTACACTGGT
RNAseH ASO6 ASO7 rev	GAATTTCTACTAAATCCCAATTGT
RNAseH ASO8 fwr	GCTGCTTTGTTGTTGTAAACT
RNAseH ASO8 rev	AAAAACATTATATGCGTTTCGAAC

Table 10. Oligonucleotides used for extension poly(A) test (ePAT).

Name	**Sequence (5'→3')**
Anchor primer (Jänicke et al., 2012a)	GCGAGCTCCGCGGCCGCGTTTTTTTTTTTT
TVN primer	GCGAGCTCCGCGGCCGCGTTTTTTTTTTTTGC
PGK1 fwr	GAATTGAATTGAAATCGATAGATC
SED1 fwr	GATGTTTCTTACGCGTTGCGTG
PMA1 fwr	GAGCACAATTCACAACACGCAC
YEF3 fwr	GGGTGATGCTTACGTTTCTTCTG

4.6. Aptamer sequences

Mango aptamer sequences consist of core sequence (in bold), left arm, right arm as a reverse complement of the left arm. Left and right arms form an RNA stem. Core sequence can be inserted in pre-existing or an arbitrary RNA stem.

Table 11. Aptamer sequences.

Aptamer	Sequence	Reference
Mango I	TACATTC**GAAGGGACGGUGCGGAGAGGAGA**GAATGTA	(Autour et al., 2018; Panchapakesan et al., 2017)
Mango II	TACATTC**GAAGGAGAGGAGAGGAAGAGGAGA**GAATGTA	
Mango III	TACATTC**GGAAGGAUUUGGUAUGUGGUAUA**GAATGTA	
Mango IV	TACATTC**CGAGGGAGUGGUGAGGAUGAGGCGA**G	

	AATGTA	
12x MS2	On plasmid pET251-pUC 12xMS2V6 Loxp KANr Loxp (addgene)	(Tutucci et al., 2018)

4.7. Plasmids

Table 12. Plasmids.

Name	Description	Reference
pRS314	pBlueScript based yeast centromere vector with TRP marker	(Sikorski & Hieter, 1989)
pRS315	pBlueScript based yeast centromere vector with LEU2 marker	(Sikorski & Hieter, 1989)
pRS316	pBlueScript based yeast centromere vector with URA marker	(Sikorski & Hieter, 1989)
pRS314-*CCW12*	ORF + 500 bp of 5' and 500 bp of 3' UTR of CCW12 was cloned into pRS315	This study
pRS316-*CCW12*	ORF + 500 bp of 5' and 300 bp of 3' UTR of CCW12 was cloned into pRS316	This study
pRS314-*CCW12-Mango I*	Mango I aptamer sequence integrated in 3' UTR of *CCW12* cloned into pRS314	This study
pRS315-*CCW12-Mango I*	Mango I aptamer sequence integrated in 3' UTR of *CCW12* cloned into pRS315	This study
pRS314-*CCW12-Mango II*	Mango II aptamer sequence integrated in 3' UTR of *CCW12* cloned into pRS314	This study
pRS314-*CCW12-Mango III*	Mango III aptamer sequence integrated in 3' UTR of *CCW12* cloned into pRS314	This study
pRS314-*CCW12-Mango IV*	Mango IV aptamer sequence integrated in 3' UTR of *CCW12* cloned into pRS314	This study
pRS316-*CCW12-12xMS2V6*	MS2 aptamer sequence integrated in 3' UTR of *CCW12* cloned into pRS316	Johanna Seidler
pBS1479	For genomic C-terminal TAP-tagging (CBP-TEV-2x protein A), TRP1-KL	(Puig et al., 2001)
pBS1539	For genomic C-terminal TAP-tagging, URA3 marker	(Puig et al., 2001)
pRS424	High copy plasmid for overexpression, Trp	(Sikorski &

	marker	Hieter, 1989)
pRS425	High copy plasmid for overexpression, Leu marker	(Sikorski & Hieter, 1989)
pRS424-*YRA1*	ORF + 500 bp of 5' and 500 bp of 3' UTR of *YRA1* was cloned into pRS424	This study
pRS425-*YRA1*	ORF + 500 bp of 5' and 500 bp of 3' UTR of *YRA1* was cloned into pRS425	This study
pRS425-*MEX67*	ORF + 500 bp of 5' and 500 bp of 3' UTR of *MEX67* was cloned into pRS425	This study
pRS425-*MEX67-6HA*	ORF of *MEX67* was C-terminal tagged with 6HA; + 500 bp of 5' and 500 bp of 3' UTR	This study
pRS424-*NAB2*	ORF + 500 bp of 5' and 500 bp of 3' UTR of *NAB2* was cloned into pRS424	This study
pRS425-*NAB2*	ORF + 500 bp of 5' and 500 bp of 3' UTR of *NAB2* was cloned into pRS425	This study
pRS425-*NPL3*	ORF + 500 bp of 5' and 500 bp of 3' UTR of *NPL3* was cloned into pRS425	Philipp Keil

4.8. Markers

Table 13. Markers.

Name	Supplier
1 kb DNA Ladder	NEB
1 kb Plus DNA Ladder	NEB
100 bp DNA Ladder	NEB
Color Prestained Protein Standard, Broad Range	NEB
Low Range ssRNA Ladder	NEB
RiboReady™ Color Micro RNA Ladder	VWR

4.9. Enzymes

Table 14. Enzymes.

Name	Supplier
DNase I	Thermo Fisher Scientific
Dpn I	NEB
Klenow Fragment, exo-	NEB
M-MuLV Reverse Transcriptase	NEB
Phusion® High-Fidelity DNA Polymerase	NEB

Proteinase K	Sigma-Aldrich
Restriction Enzymes	NEB
RNase A	Thermo Fisher Scientific
RNase H	NEB
RNase T1	Thermo Fisher Scientific
SuperScript™ II Reverse Transcriptase	Thermo Fisher Scientific
SuperScript™ III Reverse Transcriptase	Thermo Fisher Scientific
T4 DNA Ligase	NEB
T4 RNA Ligase	NEB
T5 Exconuclease	NEB
Taq DNA Ligase	NEB
Taq DNA Polymerase	Self-made
Tobacco Etch Virus (TEV) protease	Self-made
Zymolyase 20T	Carl Roth
Zymolyase 100T	Carl Roth

4.10. Antibodies

Table 15. Antibodies.

Name	Source	Dilution	Supplier
anti-Cbc1	rabbit	1:20000	Görlich lab
anti-HA tag	rabbit	1:1000	Sigma-Aldrich
anti-Mex67	rabbit	1:5000	(Sträßer et al., 2000)
anti-Myc tag	rabbit	1:500	Merck Millipore
anti-Nab2	mouse	1:5000	Swanson lab
anti-Npl3	rabbit	1:5000	Guthrie lab
anti-Pgk1	mouse, monoclonal	1:10000	Abcam
anti-RNA Pol II (8WG16)	mouse	1:250	Covance
anti-Sub2	rabbit	1:10000	(Sträßer et al., 2002)
anti-Tho1	rabbit	1:5000	Pineda lab
anti-Tubulin	rat, monoclonal	1:1000	Abcam
anti-Yra1	rabbit	1:2000	(Sträßer & Hurt, 2000)
ChromPure rabbit IgG (for ChIP, RIP)	rabbit		Jackson IR Laboratories

Peroxidase anti-Peroxidase (PAP)	rabbit, monoclonal	1:5000	Sigma-Aldrich
anti-rabbit-HRP	goat, monoclonal	1:3000	Bio-Rad Laboratories
anti-mouse-HRP	goat, monoclonal	1:3000	Bio-Rad Laboratories
anti-rat-HRP	goat, monoclonal	1:5000	Sigma

4.11. Software

Table 16. Software.

Name	Application
ImageJ, FIJI	Quantitative analysis (Western blot), FISH
ImageQuantTL	Gel analysis
Microsoft Excel	Quantitative analysis (e.g., ChIP, RIP)
RNAfold web server (ViennaRNA Package 2.0)	RNA secondary structure prediction
SnapGene	Cloning, primer design
QuantStudio™ Design & Analysis Software	qPCR analysis

5. Methods

5.1. Cloning

5.1.1. Polymerase chain reaction (PCR)

For the applications such as plasmid cloning and yeast genome integrations, High-Fidelity DNA Polymerase was used to amplify DNA of interest from template (plasmid or genomic DNA) using specific primers. The components of PCR reaction and thermal conditions are listed in Table 17. Annealing temperature was calculated based on primer properties using NEB Tm calculator web-tool. Extension time was determined according to the length of expected PCR product. The length of PCR products were checked on 1% agarose-TAE gel with addition of Intas HDGreen™ to visualize products with UV light.

Table 17. Standard PCR reaction: components and thermal conditions.

Component	**1 reaction (50 µL)**	**Final concentration**
Nuclease-free water	To 50 µL	
5x Phusion HF Buffer	10 µL	1x
2.5 mM dNTPs	4 µL	200 µM
10 µM primer forward	2.5 µL	0.5 µM
10 µM primer reverse	2.5 µL	0.5 µM
Template DNA	variable	10 ng of plasmid DNA or 100 ng gDNA/reaction
Phusion DNA Polymerase	0.5 µL	1.0 U/reaction

Step	**Temperature**	**Time**
Denaturation	98°C	30 sec
Amplification	98°C	10 sec
(35 cycles)	45 - 72°C	30 sec
	72°C	30 sec/kb
Final extension	72°C	10 min
Hold	4°C	

5.1.2. Gibson assembly

Gibson assembly for a plasmid cloning was modified after the original protocol (Gibson et al., 2009). Primers for a cloning were designed with SnapGene software as two pairs: to amplify vector or fragment in PCRs. Primers were designed to have an overlap of 30 - 40 nt. Obtained PCR products for vector and fragment DNA were cleaned up using NucleoSpin® Gel and PCR Clean-up-kit (Macherey-Nagel). PCR products were treated with DpnI enzyme to digest traces of plasmid template for 30 min at 37°C with next enzyme inactivation step for 20 min at 80°C. Concentration of vector and fragment were measured with NanoDrop and converted in pmol amounts using the formula: *pmol = (concentration in ng) x 1000 / (length in base pairs x 650 daltons)*. For Gibson assembly 1:3 vector to fragment pmol ratio was used (50 - 100 ng of vector in pmol, and respectively calculated amount of fragment). Vector and fragment were added to 15 µL of Gibson Master Mix in 20 µL of total reaction volume and incubated at 50°C for 1 hour. 2 µL of Gibson assembly product was used to transform *E. coli* competent cells.

5.1.3. *E. coli* transformation

To transform *E. coli*, competent cells were prepared according to manufacturer's manual (Mix & Go *E. coli* Transformation Kit, Zymo Research) and stored at -80°C until needed. 50 µL cell aliquot was thawed on ice, then 2 µL of Gibson assembly product or 1 µL of plasmid (25 - 100 ng) was added and incubated on ice for 30 min. The mixture was placed at 42°C for 1 min for the heat shock, then directly transferred for 1 min on ice. Then 450 µL of SOC media were added to the cells and incubated for 1 h at 37°C and 180 rpm for recovery. 150 µL of cell suspension was spread on LB-agar selective plates with ampicillin and incubated at 37°C overnight.

5.1.4. Colony PCR for *E. coli* and plasmid isolation

To test if formed after the transformation colonies are positive for the plasmid of interest, colony PCR was performed. Small amount of the cells was scraped into PCR reaction volume. The components and thermal conditions of the colony PCR are listed in Table 18. Products of the PCR were separated on 1% agarose-TAE gel with addition of Intas HDGreen™ for visualization with UV light. Colonies, positive for expected PCR product, were used for plasmid isolation with NucleoSpin® Plasmid (NoLid)-kit (Macherey-Nagel) according to manufacturer's manual. Isolated plasmids were confirmed by sequencing (Microsynth).

Table 18. *E. coli* colony PCR: components and thermal conditions.

Components	1 reaction (10 µL)	Final concentration
Water	To 10 µL	
10x Taq buffer	1 µL	1x
2.5 mM dNTPs	0.8 µL	200 µM
10 µM primer forward	0.2 µL	0.2 µM
10 µM primer reverse	0.2 µL	0.2 µM
Template (cells)		
Taq DNA polymerase	0.5 µL	

Step	Temperature	Time
Initial denaturation	96°C	7 min
Amplification	96°C	30 sec
(30 cycles)	45-68°C	45 sec
	68°C	1 min/kb
Final extension	68°C	5 min
Hold	4°C	

5.2. Transformation of *Saccharomyces cerevisiae*

To transform yeast cells with plasmid of interest, overnight preculture was diluted in 50 mL of medium to OD_{600} 0.2. Yeast cell culture was grown at 30°C 180 rpm until mid-log phase OD_{600} 0.6 - 0.8, then spun down (3 min 3600 rpm), washed once with 10 mL H2O and once with 500 µL solution I. Cell pellet was resuspended in 250 µL solution I and used for transformation. For each transformation reaction 50 µL cells were mixed with 5 µL carrier single-stranded DNA (2 mg/mL), 100 ng plasmid DNA and 300 µL solution II. Then cells were incubated for 30 min on the turning wheel at RT, placed for 10 min at 42 °C and then for 3 min on ice. Cells were washed once with 1 mL of water, resuspended in 100 µL of water and plated on selective agar plates.

For genomic integration, 150 µL of PCR product (ca. 5 µg DNA) was precipitated with 0.1 volume of 3 M sodium acetate pH 5.2 and 2.5 - 3 volumes of ice cold 100% ethanol overnight. DNA was spun down for 20 min 13000 rpm at 4°C, washed with 80% ethanol, dried and resuspended in 15 µL of 1x TE buffer. This DNA was used

for transformation reaction instead of plasmid DNA as described above, but with an extra recovery step in 1 mL of YPD for 2 - 6 hours at 30°C and 180 rpm. After the recovery time, cells were spun down and spread on selective media agar. Cells were incubated for 2 - 4 days at 30°C until colonies were formed. Strains were verified with yeast colony PCR or Western blot.

5.3. Yeast colony PCR

Small amount of yeast cells was resuspended in 15 µL solution of Zymolase T20 (2.5 mg/ml Zymolaze in sodium phosphate buffer pH 7.5) and incubated for 20 min at RT, 5 min at 37°C and 5 min at 95°C. Then 60 µL of water was added and 5 µL of this suspension was used as a template for PCR reaction with Taq DNA polymerase (components and conditions are listed in the Table 18).

5.4. Dot spot assay

To estimate the growth of yeast cells, a spotting assay was performed. Freshly streaked yeast cells were resuspended in 2 mL water. The suspensions for each tested strain were diluted to the same OD_{600} 0.09 (first spot). Then 10-fold serial dilution was made for three more spots (1:10, 1:100, 1:1000). 5 µL of each dilution were spotted on selective media agar plates, air-dried and placed at 25, 30 and 37°C for 2 days and at 16°C for up to 6 days.

5.5. Yeast whole cell extract preparation

To evaluate a total level of the protein in cells, whole cell extracts were prepared as described in (Knop et al., 1996). Briefly, 10 mL of the yeast culture were harvested at OD_{600} of 0.6, resuspended in 500 µL water and 150 µL of pre-treatment solution and incubated on ice for 20 min. Then 82.5 µL of 100% TCA was added and incubated for 20 min on ice, vortex every 5 min. Samples were spun for 20 min 13000 rpm 4°C and supernatant was discarded completely. Each pellet was resuspended in 85 µL of 1x SDS loading dye and 15 µL of TRIS-base to neutralize the acid. Sample were boiled for 5 min 95°C, spun 3 min 13000 rpm and loaded on SDS-PAGE for the following Western blot with antibodies against of proteins of interest. Protein levels were quantified using Image J.

To verify genomic tagging of proteins, fast preparation of the cell extract was performed. For this, small amount of the cells was scraped in 85 µL of 1x SDS loading dye and small amount of the glass beads was added. The cells were lysed with FastPrep-24 5G device (45 sec 6 m/s setting) twice, boiled for 5 min 95°C, spun 3 min 13000 rpm and loaded on SDS-PAGE for further Western blot.

5.6. Tandem Affinity Purification (TAP)

To purify the protein of interest together with its interacting partners, Tandem Affinity Purification (TAP) was used according to (Puig et al., 2001). For the purification, protein of interest was tagged at the C-terminal end with TAP tag. TAP tag consists of few modules: protein A for binding to IgG-coupled beads, TEV protease cleavage site to elute purified proteins from IgG beads and calmodulin binding peptide CBP for the second purification step to improve the purity of the sample. To purify nuclear mRNPs, first purification step was used with next TEV cleavage to elute purified complexes. To prepare cell extracts, 2 L of yeast culture were grown in appropriate medium at 30°C 110 rpm till OD_{600} 3.5. The cells were harvested 5 min 5000 rpm, resuspended in 2 mL of 1x PBS and flash-frozen by pipetting cell suspension into the liquid nitrogen. To prevent a degradation of protein-RNA complexes, cells were lysed by cryomilling in liquid nitrogen and stored at -80°C until use. For purification, cell grindates were thawed in 10 mL of TAP lysis buffer supplemented with 1 mM DTT and 1x protease inhibitor. Samples were pre-cleared by spinning down the cell debris at 4000 rpm for 12 min at 4°C. Supernatants were spun in an ultracentrifuge at 40000 rpm for 1 hour 4°C. Separated fatty phase was removed using vacuum pump, and supernatant was transferred to the new tube, avoiding transferring parts of the pellet. Then 500 µL of pre-washed IgG Sepharose beads was added to the cleared lysate and incubated for 1.5 h at 4°C on a turning wheel. After the binding step, beads with bound proteins were spun down at 1800 rpm 3 min 4°C. Supernatant was removed, 10 mL of the TAP wash buffer was added to the beads, spun again and discarded. The beads were transferred to Mobicol and washed with 15 mL of the TAP wash buffer at 4 °C. After the washing step, beads were resuspended in 145 µL of the TAP wash buffer and 5 µL TEV protease (4.2 mg/ml) and incubated for 1 h at 16 °C on the turning wheel. After the TEV cleavage, eluates were collected by spinning Mobicol for 3 min 2000 rpm at 4°C. For the protein analysis of purified target protein and its

interacting partners, TEV eluate was mixed with 4x SDS loading dye, boiled for 7 min 95 °C, spun down 13 000 rpm 3 min and loaded on SDS-PAGE for further Western blot analysis.

5.7. Purification of a specific nuclear mRNP

Purification of a specific nuclear mRNP was performed in two affinity steps. In the first step, TAP purification was done to purify all nuclear mRNP pool. It was performed via TAP-tagged Cbc2 protein as described in 5.6 with few modifications: ultracentrifugation at 40000 x g for 16 min at 4°C; IgG beads binding step for 1 h at 4°C; and TAP wash buffer had 100 mM KCl instead of 150 mM KCl. The second step was done to purify only transcript-specific mRNPs from whole pool of nuclear mRNPs. This second step is based on the affinity of the specific ligand to the target mRNA. In this work, two different RNA-based approaches were used: antisense oligonucleotides (ASOs), designed to hybridize to the target mRNA, and RNA aptamer-based approach with integrating RNA aptamer sequence into the 3' UTR of target mRNA and using ligand that specifically binds the aptamer.

5.7.1. Antisense oligonucleotides approach

ASO design and RNAse H assay

Antisense oligonucleotides (ASOs) for *CCW12* target mRNA were designed by (Wierschem, 2020) according to the published recommendations (Iadevaia et al., 2018). Designed ASOs were tested for their RNA-binding affinity using RNAse H assay. This assay is based on the capability of RNAse H to recognize and digest RNA in the DNA-RNA hybrids (Zhang et al., 2021). For the RNAse H cleavage assay TEV eluate (200 µL) after purification from the 2 L culture was adjusted to a volume of 1 mL with 1x RNAse H buffer and 60 mM NaCl. 500 µL of the sample was taken for a negative control (no ASO) and 500 µL for test ASO (add 100 pmol DNA ASO). Samples were incubated for 2 h at 4°C on the turning wheel for ASO binding, then treated with 2.5 µL of RNase H (5 U/µL) for 20 min at 37°C. RNA extraction, DNAse I digest and qPCR were performed to check level of the target mRNA *CCW12* for tested ASOs. As RNase H digests RNA in RNA-DNA hybrids, tested DNA ASOs with good hybridization to *CCW12* have no detectable *CCW12* after RNase H treatment in comparison to the untreated sample. If tested ASO does not bind to the target mRNA and does not form the DNA-RNA hybrid, the mRNA is not recognized and not

digested by RNAse H. It leads to the same *CCW12* level for treated and untreated with RNAse H samples.

Antisense oligonucleotides (ASO) purification

The first step of purification was performed as described in 5.7 to enrich nuclear mRNPs. ASO-based purification was optimized after (Wierschem, 2020). Obtained TEV eluates were incubated with 100 pmol of respective ASO (2'-OMe RNA or LNA), which was labeled at the 3' end with biotin or desthiobiotin. The ASO binding was done for 15 min at RT on the turning wheel. Then 100 µL of pre-washed M-280 Streptavidin magnetic beads were added and incubated for 30 min at 25°C 950 rpm. Beads were washed 5 times with 750 µL ASO-wash buffer for 2 min on the turning wheel at RT and collected with magnetic-particle collector. For experiments with native elution, desthiobiotin-labeled ASOs were used. They were displaced by incubation of the beads with 100 µL ASO-elution buffer (16 mM biotin) for 30 min at RT on the turning wheel. 20 µL of the eluate was taken for RNA analysis with RT-qPCR, and 80 µL for protein analysis with Western blot. For denatured elution, directly after washing the beads were resuspended in 100 µL wash buffer and divided for 20 µL and 80 µL for RNA and protein analysis, respectively. For negative staining and electron microscopy imaging, native eluates were used.

5.7.2. Mango aptamer purification

To purify nuclear transcript-specific mRNP, Mango aptamer-based approach was optimized after (Panchapakesan et al., 2017). The principle of the method is based on specific binding of RNA Mango aptamer with its ligand – thiazole orange desthiobiotin (TO1-Dtb). As the ligand is coupled with desthiobiotin, it can be pulled down using streptavidin-coupled beads and eluted with biotin under native conditions. For this purification plasmid was cloned, bearing the DNA sequence of the target mRNA *CCW12* with Mango aptamer sequence integrated into the 3' UTR region of *CCW12*. As a negative control was used a plasmid encoding *CCW12* without Mango aptamer insertion. The plasmids were transformed into *Δccw12* Cbc2-TAP strain. The first TAP step, described above, enriched the pool of nuclear mRNPs in the TEV eluate. All next steps were performed in the dark as TO1-Dtb is light-sensitive fluorophore. For the second, TEV eluate was incubated with 1 µL TO1-Dtb (0.5 mg/mL) for 1 hour at 4°C. Then 100 µL of pre-washed High Capacity Streptavidin agarose beads were added and incubated for 15 min on the turning

wheel at RT. Beads were washed with 1 mL Mango-wash buffer 5 times for 2 min on the turning wheel at RT and centrifuged at 20 x g for 1 min. For native elution beads were incubated with 100 µL Mango-elution buffer (20 mM biotin) for 30 min at RT on the turning wheel. For RNA analysis 20 µL of eluate were used for TRIzol RNA extraction followed by RT-qPCR. For protein analysis, 80 µL were used for Western blot. For denatured elution beads were resuspended in 100 µL BB buffer directly after washing and divided on 20 µL for RNA and 80 µL for protein analysis. Native eluates were used for negative staining and electron microscopy of samples.

5.7.3. MS2-MCP system for mRNP purification

An alternative aptamer-based approach to purify specific mRNP via MS2 aptamer and its ligand MS2 coat protein (MCP) was implemented (Zhou et al., 2002). Plasmid, encoding *CCW12* with 12xMS2 aptamer integrated into its 3' UTR, was used for the purification. Plasmid encoding *CCW12* without aptamer was used as negative control. The plasmids were transformed into *Δccw12* strain with Cbc2-TAP (for the first step of purification) and MCP-MBP protein (for the second step). The target mRNA with integrated MS2 aptamer binds MCP-MBP protein, which can be pulled down via binding of MBP to amylose beads. For this approach, TEV eluate was incubated with 25 µL of pre-washed magnetic amylose beads for 1 hour at 4°C on the turning wheel. Beads were washed 5 times with 1 mL TAP wash buffer for 2 min each on the turning wheel at 4°C. After the last wash, beads were incubated with 100 µL elution buffer (15 mM maltose) for 30 min on the turning wheel at 4°C. 20 µL of native eluate was taken for RNA and 80 µL for protein analysis. Native eluates were used for negative staining transmission electron microscopy of purified mRNPs.

5.8. SDS polyacrylamide gel electrophoresis

To separate protein according to their size, sodium dodecylsulfate polyacrylamide gel electrophoresis (SDS-PAGE) was used (Laemmli, 1970). Protein samples were mixed with SDS loading dye, boiled for 7 min at 95°C, spun for 3 min 13000 rpm. The samples were loaded on 10% or 12% SDS-PAGE. The gel run at 200 V until front dye run out of the gel. The gel with separated proteins was used for transferring onto membrane for subsequent Western blot or stained according to modified Coomassie staining technique (Wong et al., 2000). For the staining, gel was covered with Coomassie staining solution, heated up in microwave and incubated on the rocket

shaker for 15 min or longer. To remove excessive stain, gel was heated up with 10% acetic acid and incubated for 15 min on the shaker. This step was repeated until background was cleared.

5.9. Western blot

After the protein separation on SDS-PAGE, proteins were transferred onto nitrocellulose membrane according to semi-dry Western blot approach (Towbin et al., 1979). The membrane was blocked for 1 h in 5% milk-TBST at RT on rocket shaker. Then membrane was incubated with primary antibody against the protein of interest overnight at 4°C on the rocket shaker. Next day membrane was washed 3 times with 1x TBST for 10 min, incubated with horse radish peroxidase (HRP)-coupled secondary antibody for 1 h at RT on the rocket shaker. Then the membrane was washed again 3 times with 1x TBST for 10 min. Protein signal was detected with chemiluminescence reagents CheLuminate-HPR ECL solution (Applichem), imaged with ChemoCam Imager (Intas) and quantified with Image J.

5.10. RNA extraction

Total RNA was extracted with TRIzol reagent according to manufacturer's manual. Briefly, 1 mL of TRIzol was added to the sample, incubated for 5 min at RT to dissociate nucleoproteins complexes. For samples with low RNA content, hot TRIzol was used: instead of 5 min at RT, samples were placed for 7 min at 60°C and 750 rpm. Then 200 µL of chloroform was added, vortexed, incubated for 3 min at RT and spun down for 15 min 12000 x g at 4°C. Upper phase was transferred to a new tube, equal volume of ice-cold isopropanol was added, shortly vortexed and incubated for 10 min. Samples were spun down at 12000 x g for 10 min at 4°C. RNA formed white pellets. Supernatant was discarded and 1 mL of 75% ethanol (in DEPC-treated water) was added, spun down for 5 min at 7500 x g 4°C. Supernatant was discarded completely and RNA was air-dried for 10 min to remove residual ethanol. RNA was resuspended in 50 µL of DEPC-treated water. If DNase digest was not implemented in the upstream protocol, samples were treated with 7 Units of DNase I for 30 min at 37°C and the digest was stopped by addition of 5 mM EDTA and incubation for 10 min at 65°C. Concentration of RNA was determined using NanoDrop and RNA was used for downstream applications. For large sample volume (e.g., 500 µL in RNAse

H assay), RNA was mixed with equal volume of PCI mix (Phenol:Chloroform:Isoamyl Alcohol), vortex, spun for 10 min 14000 rpm at RT. Upper phase was transferred to a fresh tube, mixed with 500 µL of chloroform, vortex, spun again. The upper phase was transferred into a new tube and precipitated with 0.1 volume of 3 M sodium acetate pH 5.2 and 3 volumes of 100% ethanol overnight at -20°C. On the next day samples were spun down for 20 min 13000 rpm at 4°C. Precipitated RNA pellets were washed with 80% ethanol, air-dried and resuspended in 50 µL of DEPC-treated water for subsequent applications.

5.11. Reverse transcription

Reverse transcription was performed to synthesize cDNA from RNA templates. M-MuLV or SuperScript reverse transcriptase enzymes were used according to manufacturer's recommendations. For each reaction 100 ng of RNA template were used and reverse transcription was performed for 1 h at 42°C. Synthesized cDNA was precipitated with 1/10 of its volume of 3 M NaOAc pH 5.2 and 3 volumes of 100% ethanol at -20°C overnight. Then samples were spun for 20 min 15000 rpm at 4°C, washed with 80% ethanol and spun 15 min 15000 rpm at 4°C. Supernatant was discarded completely, cDNA was dried in the vacuum evaporator and dissolved in water to perform qPCR.

5.12. qPCR

To assess level of RNA after mRNP purification and RNA immunoprecipitation (RIP), or level of DNA after chromatin immunoprecipitation (ChIP), respective cDNA or purified DNA were used in quantitative real-time PCR. The components and thermal conditions of qPCR are listed in Table 19. Standard curves were used to determine efficiency of the qPCR primers. Melting curve analysis was perform to check specificity of primers. Samples were diluted in water before pipetting qPCR reactions (1:10 dilutions for samples for mRNP purification; 1:20 for ChIP experiment; 1:5 for RIP). To run qPCR reactions QuantStudio 3 cycler (Applied biosystem) was used. Cycle threshold (Ct) values of the samples were determined by QuantStudio™ Design & Analysis Software.

Table 19. qPCR: components and thermal conditions.

Components	1 reaction (10 µL)	Final concentration
Water	2.3 µL	100 pmol/µL
100 µM primer forward	0.1 µL	0.2 µM
100 µM primer reverse	0.1 µL	0.2 µM
2x PowerUp™ SYBR Green® Mastermix	5 µL	1x
Template (DNA or cDNA sample)	2.5 µL	

Temperature	Time
95°C	10 min
95°C	15 sec
60°C	60 sec
68°C	1 min/kb
Melting curve	
95°C	15 sec
60°C	60 sec
95°C	15 sec

5.13. Negative staining transmission electron microscopy

To visualize purified specific nuclear mRNPs by electron microscopy, negative staining was used (Lusetti et al., 2003; Scarff et al., 2018). The staining procedure included conditioning of a grid surface, absorption of particles on the grid, washing and staining. For conditioning of the grid surface, to make it hydrophilic and “sticky” for the particles, 30 µL of 1% alcian blue was placed on the grid for 1 min and washed with 7 droplets of water using “Grid-On-Drop” method by putting grid on droplet. The absorption step was done by putting the grid on 10 µL of sample droplet to absorb purified mRNP particles for 10 min. Then the grid was washed on 3 droplets of water by a brief contact of the grid with droplet. After the last wash the excess of water was removed with filter paper. Grid was stained on the 30 µL droplet of 1% uranyl acetate by a brief contact with the droplet. The grid with stained sample was used for electron microscopy (Zeiss EM900).

5.14. Chromatin Immunoprecipitation (ChIP)

To investigate protein-DNA interactions, antibody-based Chromatin Immunoprecipitation (ChIP) was performed according to (Fan et al., 2008; Mayer et al., 2010). Strains with TAP tagged proteins of interest were used. 100 mL of cell culture were grown in YPD to OD_{600} 0.8 and cross-linked with 1% formaldehyde for 20 min at RT with gentle shaking. Cross-linking was quenched with 12.5 mL of 3 M Glycin for 10 min. Spun cells (3600 rpm 3 min 4°C) were washed twice with 25 mL of ice-cold 1x PBS, resuspended in 1 mL of ice-cold low-salt buffer, centrifuged. Obtained pellets were frozen in liquid nitrogen and stored in -80°C until needed. For procedure, cells were thawed on ice, resuspended in 800 µL low-salt buffer, supplemented with 1x protease inhibitor PI, and transferred to 300 µL glass beads. Cell lysis was carried with FastPrep-24 5G device (45 sec 6 m/s setting) twice with 2 min break on ice in between. Lysed cells were released in TPX-tubes with 512 µL low-salt buffer by centrifugation at 500 rpm 2 min 4°C. For chromatin fragmentation, lysates were sonicated with Bioruptor UCD-200 (Diagenode) three times for 15 min (30s ON/30 s OFF; "HIGH" mode) with 5 min breaks in between for cooling the device with ice. Fragmented chromatin was spun first for 5 min 14000 rpm 4°C and then for 10 min 14000 rpm 4°C. Concentration of DNA in supernatants was measured by NanoDrop and all samples were adjusted to the same amount of DNA. 10 µL of adjusted samples were taken as input samples. For TAP-ChIP 15 µL of pre-washed IgG-Dynabeads were added to the sample and incubated 2.5 h on turning wheel at RT. For RNAPII ChIP adjusted samples were first incubated with 4 µL α-RPB1 antibody (1 mg/mL) for 1.5 hour and then with 15 µL Protein G beads for 1 hour. After immunoprecipitation, magnetic beads were collected with magnetic-particle collector and washed with 800 µL of buffer (2x low-salt buffer, 3x high-salt buffer, 3x TLEND and 2x with 1x TE pH 8.0) – each time for 2 min at RT on the turning wheel. Washed beads were resuspended in 130 µL elution buffer and incubated in for 25 min at 65°C 1000 rpm. Eluates were collected and mixed with 80 µL 1x TE and 10 µL Proteinase K. Input samples from before were mixed with 80 µL 1x TE, 80 µL elution buffer and 10 µL Proteinase K. Samples were incubated in thermo-cycler for 2 min at 37°C for Proteinase K treatment and 14 hours at 65°C for reversal cross-linking. DNA cleanup of samples was made with PCR NucleoSpin® Gel and PCR Clean-up-kit (Macherey-Nagel) according to manufacturer's manual and the DNA was eluted with 140 µL 1x TE. The eluates were diluted in water (1:20)

and used for qPCR. To determine the efficiency (*E*) of qPCR primers, standard curves were used. As a negative control, non-transcribed region (NTR) on chromosome V (174131–174200) was used. The occupancy of the target protein was calculated as its enrichment for particular gene relative to NTR, using 2^(−ΔΔCt) method (Livak & Schmittgen, 2001). Formula used for the quantification: *(E^(Ct IP – Ct Input)NTR)/(E^(Ct IP – Ct Input)Gene)*.

5.15. RNA Immunoprecipitation (RIP)

To investigate protein-RNA interactions, RNA immunoprecipitation method was applied according to (Selth et al., 2009). Strains with TAP-tagged proteins of interest were used. 400 mL yeast cell culture were grown in YPD at 30°C until OD_{600} of 0.8. Cells were centrifuged at 6000 rpm 3 min 4°C, washed once with cold 1x PBS, spun again, and cell pellets were frozen in liquid nitrogen and stored at -80°C for further use. For the experiment, cells were resuspended in 1 mL RNA IP-buffer with 20 µL protease inhibitor. Cell suspension was divided on two equal parts: each of the parts was lysed with 500 µL glass beads with FastPrep machine 3 times 20 sec (6m/s setting) with 1 min break on ice in between. Lysates were released into 15 mL tube by punching the hole in the bottom and in the top of lyse tube and spinning for 1 min 500 rpm. Lysates were centrifuged 5 min 13000 rpm at 4°C. Supernatant was transferred to a new tube and spun for 10 min 13000 rpm at 4 °C. 900 µL of supernatant was treated with DNAse I (660 units) for 30 min on ice. After the digest, 10 µL of samples were taken for RNA extraction (input). After this, 35 µL of pre-washed IgG beads were added to 900 µL of lysate and incubated for 3 hours on the turning wheel at 4°C. After the binding, beads were washed at 4°C for 8 times with 1 mL RNA-IA buffer, each wash step for 2 min on the turning wheel. After the last wash, buffer was discarded and 1 mL of TRIzol was added directly to the beads. Then RNA was isolated and reverse transcribed into cDNA for the next analysis by qPCR. As negative control (nc), RIP was also performed with non-tagged protein strain. To determine the efficiency (E) of PCRs, standard curves were used. Obtained Ct values were used to calculate enrichment over non-tagged negative control sample according to the formula: *(E^(Ct IP – Ct Input)nc)/(E^(Ct IP- Ct Input)).*

5.16. Fluorescence *In Situ* Hybridization (FISH)

To determine localization of mRNA in yeast cells, oligo(dT)50-Cy3 fluorescent probes against poly(A)+ RNA were used. *In situ* hybridization was done according to (Amberg et al., 1992). Briefly, cells were grown to OD_{600} of 0.8 at 30°C. 8.75 mL of cell culture was removed and fixed with 1.25 mL of 37% formaldehyde for 90 min at RT on the turning wheel. The rest of the cell culture was shifted to 37°C on water bath for 1 hour. 8.75 mL aliquot of these cells were fixed with 1.25 mL of 37% formaldehyde 15 min at 37°C in the water bath and then for 75 min at RT on the turning wheel. Cross-linked cells were spun for 5 min 3000 rpm and washed once with 5 mL 0.1 M KPO4 pH 6.4. Then cells were resuspended in 1 mL wash buffer (0.1 M KPO4 pH 6.4, 1.2 M Sorbitol), pelleted for 3 min 3600 rpm, treated with 100 µg 100T zymolase in 200 µL wash buffer for 30 min at 30°C. Obtained spheroplasts were centrifuged for 4 min 2000 rpm, washed once with 1 mL washing buffer and gently resuspended in 800 µL of the wash buffer. 100 µL of suspension were pipetted on poly-lysine covered coverslip. After 5 min, non-adherent cells were removed by aspiration. Coverslips with adherent cells were air-dried for 8 min, incubated for 10 min in 200 µL 2x SSC buffer. After aspirating 2x SSC buffer from the cells, 12 µL of prehybridization buffer was added to the cells and coverslips were incubated for 1 h at 37°C in humid chamber. After this incubation, 0.75 µL of 1 pmol/µL oligo(dT)50-Cy3 probe was added and coverslips were placed at 37°C overnight in the humid chamber. This and the following steps were performed in the dark to protect fluorescent probe from light. After hybridization cells were washed with 3 mL 0.5x SSC for 30 min at RT on rocket shaker. Coverslips with cells were air-dried for 5 hours. For DNA detection, 6 µL of ROTI®Mount FluorCare DAPI mounting media was pipetted on microscope slide and dried coverslip with cells were flipped on the slide. Coverslips were fixed to the microscope slide with nail polish. Cells were imaged with microscope connected to CCD camera.

5.17. Poly(A) tail length assay

5.17.1. Bulk poly(A) tail assay

To assess the length of poly(A) tails, radioactive 3' end labeling with [32P]-pCp was performed as described in (Minvielle-Sebastia et al., 1991). Cells were grown till OD_{600} of 0.8 at 30°C or shifted for 1 h to 37°C. Total RNA was extracted using TRIzol

reagent according to manufacturer's manual. To label the 3' end of RNA, 1 µg of extracted RNA, 1 mM ATP, 10% DMSO, 0.25 µM [32P]-pCp and 10 U T4 RNA ligase were incubated in 30 µL reaction volume overnight at 4°C. After the labelling, everything but poly(A) tails were digested for 2 h at 37°C in 80 µL reaction volume by using 80U RNAse T1, 4 µg RNAse A, 10 mM Tris-HCl pH 7.5, 300 mM NaCl. Then RNA was again extracted with TRIzol, resuspended in 10 µL of DEPC-treated water, mixed with RNA loading dye, boiled for 5 min at 95°C and placed on ice. 20% PAA – 8M Urea PAGE was pre-run for 30 min at 180 V. Samples were loaded on the gel and run till front dye reached the lower part of the gel. Gel was wrapped in the plastic film and phosphoscreen was placed onto the gel overnight. Signal was measured by using phosphor imaging (Typhoon FLA 9500).

5.17.2. Extension poly(A) test (ePAT)

To assess poly(A) tail length of individual transcripts, extension Poly(A) Test (ePAT) was implemented according to (Jänicke et al., 2012). For the test, 25 mL of respective yeast strains were harvested at OD_{600} of 0.8 and total RNA was extracted using TRIzol as described before. The 1 µg of total RNA was mixed with 1 µL of PAT anchor primer in 11 µL reaction volume and incubated for 5 min at 80°C. Then reaction was cooled down to 37°C and 8 µL of master mix with Klenow polymerase was added (4 µL 5x SSIII buffer, 1 µL 0.1 mM DTT, 1 µL 10mM dNTPs, 1 µL Ribolock, 1 µL Klenow exo-). This step was followed by 30 min incubation at 37°C for polymerase activity and 10 min at 80°C for its deactivation. The reaction was cooled down to 55°C and 1 µL of reverse transcriptase SSIII was added directly to the reaction on the thermoblock to prevent internal priming of PAT anchor primer associated with temperature drop. Reverse transcription was performed for 30 min at 55°C with 10 min enzyme deactivation at 80°C. Obtained cDNA was diluted in water (1:6) and 10 µL of it was used as a template for PCR with Phusion polymerase. Additionally, reverse transcription for size control was done using TVN primer. TVN (also known as T12VN) is similar to anchor primers, but has two additional bases at the 3' end (V – A, G or C; N – any base). These bases lock primer to the 3' poly(A) junction and first 12 adenosines of poly(A) tail (Beilharz & Preiss, 2009). For T12VN sample, mixture of extracted RNA from different samples in total amount of 1 µg was mixed with TVN primer, and transcribed into cDNA by reverse transcriptase SSIII. No extension by Klenow polymerase was implemented. Obtained cDNA was diluted in water (1:11) and 10 µL was used for PCR. For the PCR, universal PAT anchor primer

was used as reverse primer, and forward primer was designed in the 3' UTR of the transcript of interest. The 10 µL of the PCR product was mixed with DNA loading dye and separated on 2.5% agarose-TAE gel containing Intas HDGreen™ for detection with UV light. Alternatively, PCR products were also checked on non-denaturing native 8% PAGE-TBE gel.

5.18. R-loop assay

To assess the level of R-loops, an assay with using S9.6 antibody against DNA-RNA hybrid was performed. The 10 mL of yeast cell cultures was grown to OD_{600} of 0.5, spun down for 3 min 3600 rpm, washed once with 10 mL of water, spun again. To extract gDNA, cell pellets were resuspended in 500 µL H2O, 200 µL TSNTE, 200 µL glass beads and 300 µL PCI mixture (Phenol:Chloroform:Isoamyl alcohol), vortexed for 5 min and spun down for 10 min 14000 rpm. Transferred upper phase was extracted with equal volume of chloroform, spun again. After that, next upper phase was taken and precipitated with 1.2 ml of 100% ethanol overnight at -20°C. Samples were spun for 30 min 13000 rpm 4 °C and washed once with 80% ethanol. Precipitated DNA was dried in vacuum evaporator for 10 min at 42 °C and resuspended in 100 µL H2O. 10 µg of gDNA was mixed with RNase 3 (5 U) and RNase T1 (500 U) in total reaction volume of 100 µL. The 100 µL were divided on 2 samples per 50 µL, one of them was treated with RNase H (10 U). Both samples were incubated at 37 °C for 2 hours. Then 2x serial dilution in SSC buffer was made (1 µg DNA in first dot). 40 µL of each dilution was applied onto positively charged nylon membrane in Dot Blot apparatus. After filtration in Dot Blot apparatus, membrane was UV-crosslinked, blocked for 1 h in 5% milk-PBST and incubated with primary antibody against DNA-RNA hybrid or dsDNA (loading control) overnight at 4 °C. Next day membrane was washed 3 times per 10 min with PBST and incubated with secondary antibody for 1 h at RT. Then membrane was washed 3 times per 10 min with PBST and signal was detected with chemiluminescent reagents.

6. Results

This study diverges in two directions - structural and functional. The first chapter is dedicated to the purification of a specific nuclear mRNP and elucidating its structure by electron microscopy. In the second chapter, the role of the protein Hpr1, a component of the TREX complex, in mRNP assembly is investigated.

6.1. Structure of a transcript-specific nuclear mRNP

Tremendous scientific progress led to identification of numerous RNA-binding proteins (RBPs) in *S. cerevisiae* and human cells (Castello et al., 2012; Mitchell et al., 2013). However, the structure of nuclear mRNPs is still largely enigmatic.

To determine the first known structure of a nuclear mRNP, this study aimed to enrich nuclear transcript-specific mRNPs in a two-step affinity purification under native conditions from *S. cerevisiae*. Since yield is a critical point of mRNP isolation, highly transcribed *CCW12* mRNA was chosen as a target for the purification. In the first step, all nuclear mRNPs were purified, in the second step only mRNPs containing the *CCW12* mRNA were specifically enriched. Morphology of the population of purified *CCW12* mRNPs was visualized by negative stain and electron microscopy.

6.1.1. Purification of nuclear mRNPs

The first step of purification was aiming to enrich the whole pool of nuclear mRNPs. For this purpose, TAP-tagged component of cap-binding complex (CBC) Cbc2-TAP was used to pull down nuclear mRNPs with IgG-coupled beads followed by its elution by TEV protease cleavage.

To preserve the native structure of mRNPs, the goal was to minimize the time of the purification, in particular because this first step has to be followed by an extra round of RNA-specific pull down. For this purpose, TAP purification protocol was adapted after (Wierschem, 2021). Usual TAP-binding step using IgG Sepharose beads for 2 h was compared with 1 h binding. It has been suggested before, that magnetic non-porous beads might have better binding properties in shorter time, than large porous IgG Sepharose (Bonneau et al., 2023; Oeffinger et al., 2007). Therefore, an

additional sample was included, where IgG-coupled M280-magnetic beads were incubated for 30 min with the lysate. Obtained TEV eluates of nuclear mRNPs were tested for protein and RNA level. On the Coomassie stained SDS-PAGE (Fig. 7A, top), protein levels for 2 h and 1 h binding with IgG Sepharose look similar (line 6 and 7). On the respective Western blot (Fig. 7A, bottom), the detected proteins (mRNP components) show similar protein levels for 2 h and 1 h binding with IgG Sepharose. Not detected cytoplasmic protein Pgk1 proves the purity of isolated nuclear mRNPs. Incubation for 30 min with magnetic beads is not sufficient to provide a yield as good as with Sepharose beads (Fig. 7A, line 8 cf. line 6 and 7). Remarkably, decreasing the binding time from 2 h to 1 hour for Sepharose beads results in reduced protein background of represented RBPs in the non-tagged WT control (Fig. 7A, bottom, line 3 cf. line 2). In accordance with the protein level, target *CCW12* mRNA shows no enrichment for the sample with magnetic beads (Fig. 7B). In case of Sepharose, the *CCW12* mRNA has higher enrichment during 1 h incubation in comparison with 2 h binding time. Such a shortening of TAP binding step does not only minimize purification time, but also results in higher protein and RNA yield as well as lower background.

Another approach to minimize the purification time and increase its yield was an adjustment of the centrifugation of lysates. In contrast to previously used centrifugation at 27900 rpm for 1 hour (Wierschem, 2022), 15 min at 20000 rpm was applied. The shorter centrifugation on lower speed leads to more starting material to purify from, as there is more protein in the lysate after the centrifugation (Fig. 7C, line 3 cf. 1, line 7 cf. 5). This also results in more protein in the TEV eluate (Fig. 7C, line 8 cf. 6). Importantly, such a reduction of centrifugation speed and time does not compromise the purity of the purification – protein background in non-tagged WT sample remains similar (Fig. 7C, line 2 and 4). In addition, it does not lead to contamination of the purified nuclear mRNPs by cytoplasmic protein Pgk1, which was used as a control (Fig. 7C, bottom). In accordance to the protein level, target *CCW12* mRNA also shows an increased level in TEV eluate for samples with a centrifugation for 15 min at 20000 rpm (Fig. 7D).

Mentioned optimizations result in a higher yield of nuclear mRNPs as well as in shorter procedure time, important for mRNP stability and integrity.

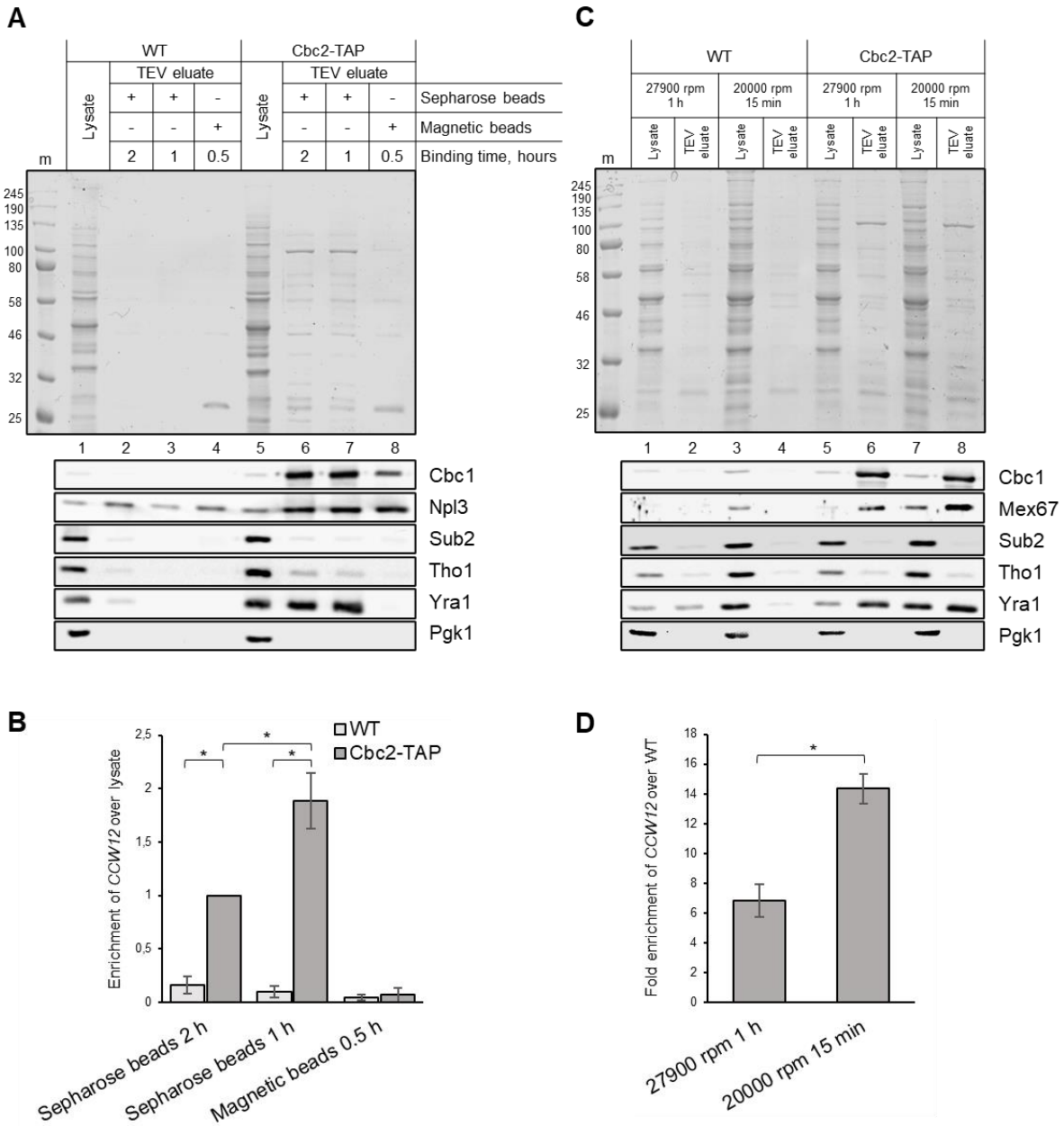

Figure 7. Optimization of nuclear mRNP purification. Purification of nuclear mRNPs via Cbc2-TAP. WT cells (RS453) with non-tagged Cbc2 were used as a negative control. **(A, B)** Optimizing the binding time and beads type: **(A)** Coomassie stained SDS-PAGE of lysates and purified TEV eluates (top) ("m" – protein marker with noted sizes, kDa). Western blotting (bottom) with antibodies against RNA-binding proteins, components of mRNPs. Cytosolic protein Pgk1 was used to assess the purity of the sample. **(B)** The level of *CCW12* mRNA in TEV eluate determined by RT-qPCR. Fold enrichment of *CCW12* is calculated over its level in lysate and set to 1 for one of compared conditions (Cbc2-TAP, Sepharose beads 2 h) (bars represent mean ± SD; Student's t-test, * p≤0.05). **(C, D)** Optimization of centrifugation step: **(C)** Coomassie stained SDS-PAGE of lysates and purified TEV eluates (top). Western blotting (bottom) with antibodies against represented proteins. **(D)** The level of *CCW12* mRNA in TEV eluates determined by RT-qPCR. Fold enrichment of *CCW12* in Cbc2-TAP TEV eluate is calculated over non-tagged WT control (bars represent mean ± SD; Student's t-test, * p≤0.05).

Additional attempts to minimize the purification time led to decreased purification yield. For instance, binding time reduction from 1 h to 40 or 20 min caused reduced level of protein and RNA in TEV eluate (Appendix Fig. 1).

After optimization of the first purification step, obtained TEV eluates enriched in nuclear mRNPs were used for the subsequent isolation of transcript-specific mRNPs.

6.1.2. Purification of transcript-specific nuclear mRNPs

To purify a transcript-specific mRNP of interest, RNA-centric methods based on antisense oligonucleotides (ASOs) or RNA aptamers (Mango and MS2 aptamer) were implemented. These approaches were optimized to isolate the transcript-specific mRNP *CCW12* in high amount and purity. Morphology of the purified transcript-specific mRNP was visualized with electron microscopy.

6.1.2.1. Antisense oligonucleotide-based mRNP purification

ASO hybridization to the target mRNA

Antisense oligonucleotides (ASOs) are short DNA or RNA oligonucleotides that are complementary to the target mRNA. The ASOs for *CCW12* mRNA were designed previously by Wierschem, 2021. Since mRNA is packaged with RBPs, it means that some of the predicted binding sites might not be accessible for ASO hybridization. To assess this, an RNase H assay was performed. TEV eluates, obtained after Cbc2-TAP purification, were incubated with DNA-ASOs against target mRNA *CCW12* (Fig. 8A). After the binding of the DNA-ASOs to *CCW12* mRNA, samples were treated with RNase H. RNase H recognizes DNA-RNA hybrids and degrades the RNA strand. Following RT-qPCR with primers flanking the predicted hybridization site was performed. In case of the well accessible site on mRNA, DNA-ASO hybridizes to it, RNase H recognizes the hybrid and degrades the mRNA. Therefore, mRNA level would be lower than in the control samples without ASO. On the contrary, if the binding site is not accessible, DNA-ASO cannot hybridize, RNase H cannot digest mRNA and mRNA levels remains the same as in the control sample (Fig. 8B).

Decreased amounts of *CCW12* in comparison to “no ASO” control indicates that all tested DNA-ASOs bind to the target mRNA (Fig. 8C). However, for ASO2 and ASO5 *CCW12* levels are higher, hence, they have the lowest binding among the

represented ASOs. Likely, their binding sites on *CCW12* are not well accessible and covered by mRNP components. The lowest amount, which represents the highest hybridization efficiency, is observed for ASO1 and ASO8. Interestingly, their binding sites are in the 5' UTR and 3' UTR, respectively. This fits into the concept of mRNA being tightly covered by RBPs and more compact in its coding region, while 5' and 3' UTR being more "open" and accessible.

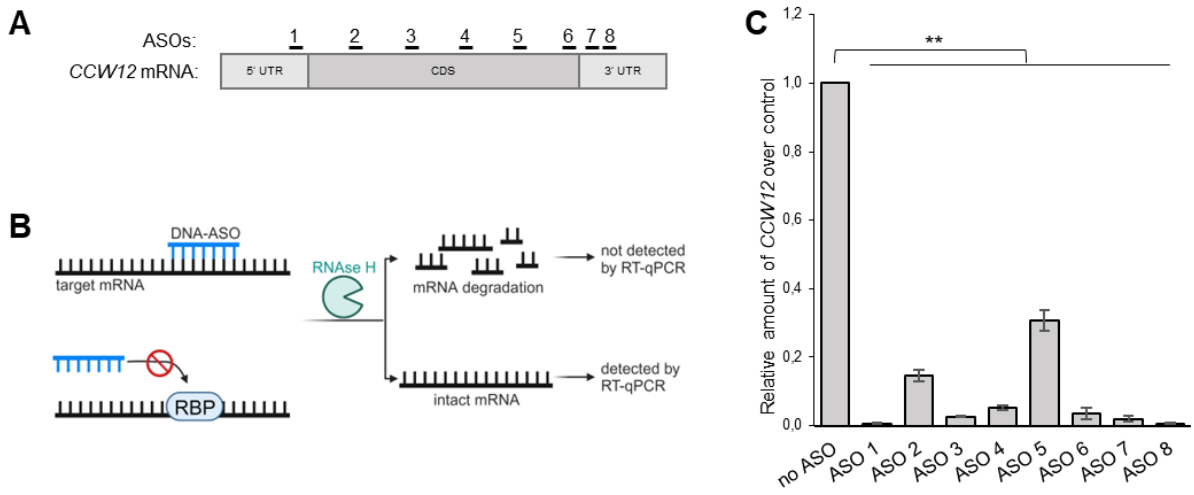

Figure 8. Hybridization of ASOs to *CCW12* mRNA. (A) Schematic representation of ASO binding sites on *CCW12* mRNA. **(B)** Scheme of the RNase H assay. DNA-ASO binds to target mRNA. RNase H recognizes DNA-RNA hybrid and degrades mRNA. If the binding site is occupied by an RNA-binding protein (RBP), mRNA remains intact. Changes in mRNA level is assessed by RT-qPCR. Scheme is created with BioRender. **(C)** Relative amount of *CCW12* mRNA over control (no ASO) after RNase H digest. Lower amount displays higher hybridization level (bars represent mean ± SD; Student's t-test, ** p≤0.01).

Selection of ASO candidates to purify *CCW12*-containing mRNPs

The designed ASOs indeed bind target *CCW12* mRNA, however differently. To select the best candidate for purification of *CCW12* mRNP, all 8 ASOs were tested in comparison. This pre-selection revealed that ASOs 1 - 4 provide higher enrichment of purified *CCW12* mRNA (Appendix Fig. 2). Therefore, the ASOs 1 - 4 were tested again, but with a Δ*ccw12* strain as negative control. The 2'-OMe modified RNA ASOs with biotin label at their 3' end were used. ASO-bound complexes were pull down with streptavidin-coupled beads and analyzed for their RNA and protein content (Fig. 9A). All of these four ASOs shows specific enrichment of *CCW12* mRNA over the

control (unrelated mRNA *PGK1*), but ASO1 provides the highest enrichment of *CCW12* (Fig. 9B). However, protein level does not coincide with RNA amounts. If there is more RNA enriched with ASO1, more of co-purified proteins would be expected. But the highest protein level is obtained with ASO3 (Fig. 9C). Such a disparity can be explained by non-specific binding of ASOs. Presence of proteins in Δ*ccw12* control confirms the non-specific binding of ASOs to RBPs (Fig. 9C).

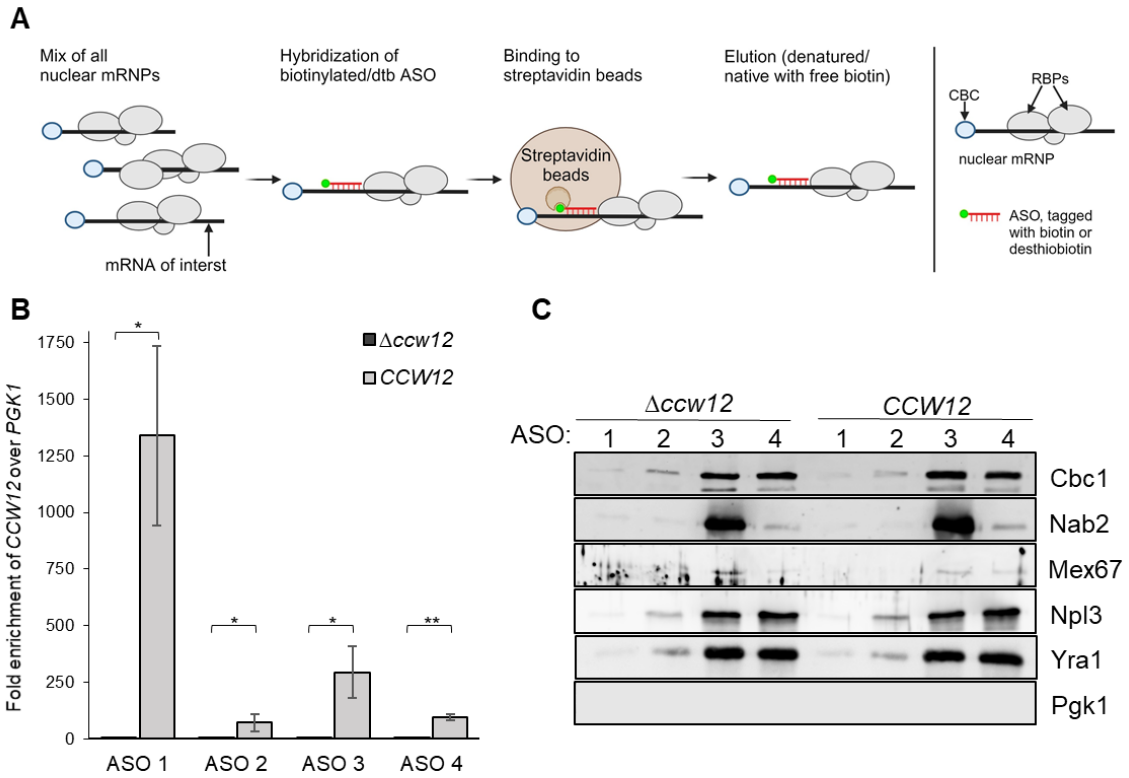

Figure 9. Purification of *CCW12* mRNP using ASO 1 - 4. (A) Scheme of ASO-based purification. TEV eluate, enriched in nuclear mRNPs, is incubated with 2'-OMe ASO, labelled with biotin/desthiobiotin on its 3' end. Via this tag, ASO binds to streptavidin magnetic beads. Purified target mRNA and its associated proteins can be eluted by denatured elution or by native elution with free biotin. Created with BioRender. **(B)** Fold enrichment of purified *CCW12* mRNA over unrelated *PGK1* was determined by RT-qPCR (bars represent mean ± SD; Student's t-test, ** p≤0,01). **(C)** Co-purified RBPs, detected with respective antibodies by Western blot. The Δ*ccw12* is used as negative control.

While the mRNA level purified via ASOs is specific, the protein level is not. This rise the question if ASOs bind both, target mRNP and single RBPs. If so, it does not interfere with electron microscopy and the mRNPs can be distinguished from single-

protein background. To increase purity and yield of the purification, ASO1 and ASO3 were chosen for further experiments.

Optimization of ASO-based purification of mRNP

For electron microscopy of transcript-specific mRNPs, yield and purity are critical parameters. To improve it, series of experiments were performed. The most crucial of them are described below, others are summarized in Appendix table 1.

Different amounts of 2'-OMe-RNA ASO were tested for *CCW12* purification. The titration shows that the amount of ASO is critical for enrichment of *CCW12* mRNA. The highest yield of *CCW12* is observed when 100 pmol ASO are used for purification. Lower ASO amount (50 pmol) is not enough for effective hybridization to the target mRNA and leads to lower *CCW12* enrichment. Higher ASO quantities (200, 300, 600, 1200 pmol) results in gradual decrease of enrichment of purified mRNA (Fig. 10A). Proteins, co-purified with *CCW12*, shows a non-specific signal, as there is no difference to Δ*ccw12* control (Fig. 10B).

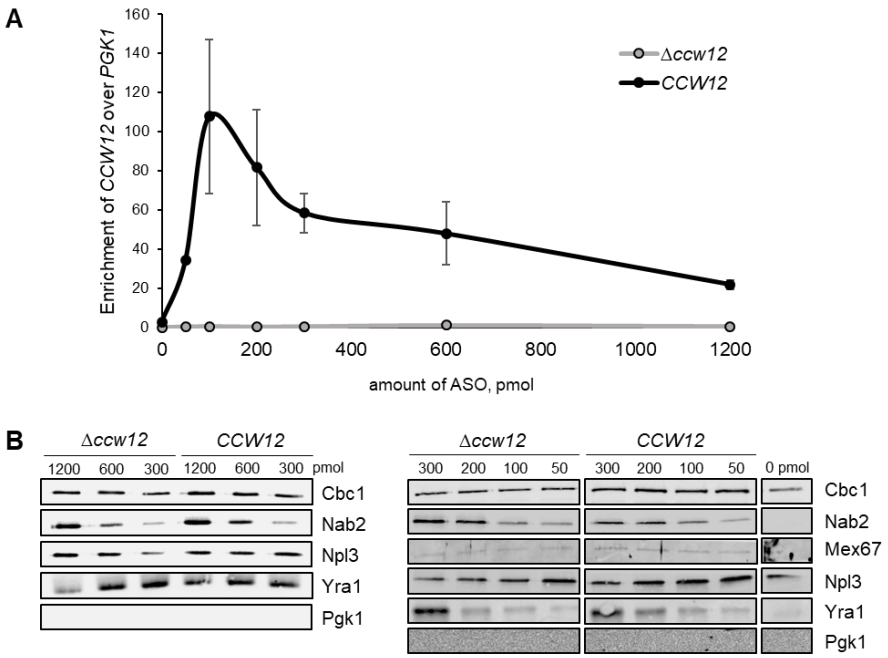

Figure 10. Amount of ASO is critical for mRNA purification yield. (A) Titration of 2'-OMe-ASO3 amount (0 - 1200 pmol) for mRNP purification. Enrichment of *CCW12* over unrelated *PGK1* was determined by RT-qPCR. Graph represents mean ± SD. **(B)** Co-purified RBPs determined by Western blot for represented titration amounts of ASO. The Δ*ccw12* strain was used as negative control.

For some proteins, higher ASO quantity corresponds to more protein in both *CCW12* sample and Δ*ccw12* control. This is contradicting to the impact of the amount of ASO on mRNA yield, where increase of ASO over 100 pmol leads to lower *CCW12* enrichment. Thus, more ASO binds more of RBPs instead of binding the target *CCW12* mRNA.

To estimate if other ASO types can overcome non-specific protein binding or increase purification yield, 2'-OMe-RNA ASO was compared with locked nucleic acid (LNA) modified RNA ASOs and with DNA ASO (Fig. 11A). The 2'-OMe-ASO1 and respective LNA ASO with locked nucleic modifications in several different nucleobases (LNA1 - 4) were used for purification. The 2'-OMe-ASO1 provides the highest enrichment of *CCW12* mRNA (Fig. 11B). On protein level, 2'-OMe-ASO1 and LNA4 have the highest signal (Fig. 11C). However, 2'-OMe-ASO1, as well as all tested LNAs demonstrates non-specific protein binding in Δ*ccw12* strain (Fig. 11D). Introduction of LNA modifications increases melting temperature of ASOs. In contrast to 2'-OMe-ASOs, LNA ASOs require higher temperature for hybridization to the target. Likely, binding of LNA ASOs to *CCW12* is not efficient enough under native conditions and, therefore, leads to decreased amount of purified *CCW12*. In turn, DNA-ASO was not able to specifically purify *CCW12* mRNA (Fig. 11E). Presumably, detected proteins in this case represents proteins non-specifically bound to the beads or DNA-ASO (Fig. 11F).

Since non-specific protein binding is an acute problem of ASO-based purification, competitive binding was implemented to reduce protein background. To decrease non-specific protein binding to the beads, they were incubated with BSA prior to ASO binding. Such a treatment does not influence the level of purified *CCW12* mRNA (Appendix Fig. 3A). On protein level, it leads to non-specific changes of copurified proteins. While protein background in Δ*ccw12* strain and "no ASO" sample is reduced after pre-incubation of the beads with 5% or 10% BSA, the same decrease is observed for proteins co-purified with *CCW12* (Appendix Fig. 3B).

To decrease non-specific binding of ASOs to RBPs, tRNA was added as a competitor during ASO binding. The addition of tRNA does not affect enrichment of *CCW12* (Appendix Fig. 3C), as well as it does not result in specific decrease of protein background (Appendix Fig. 3D).

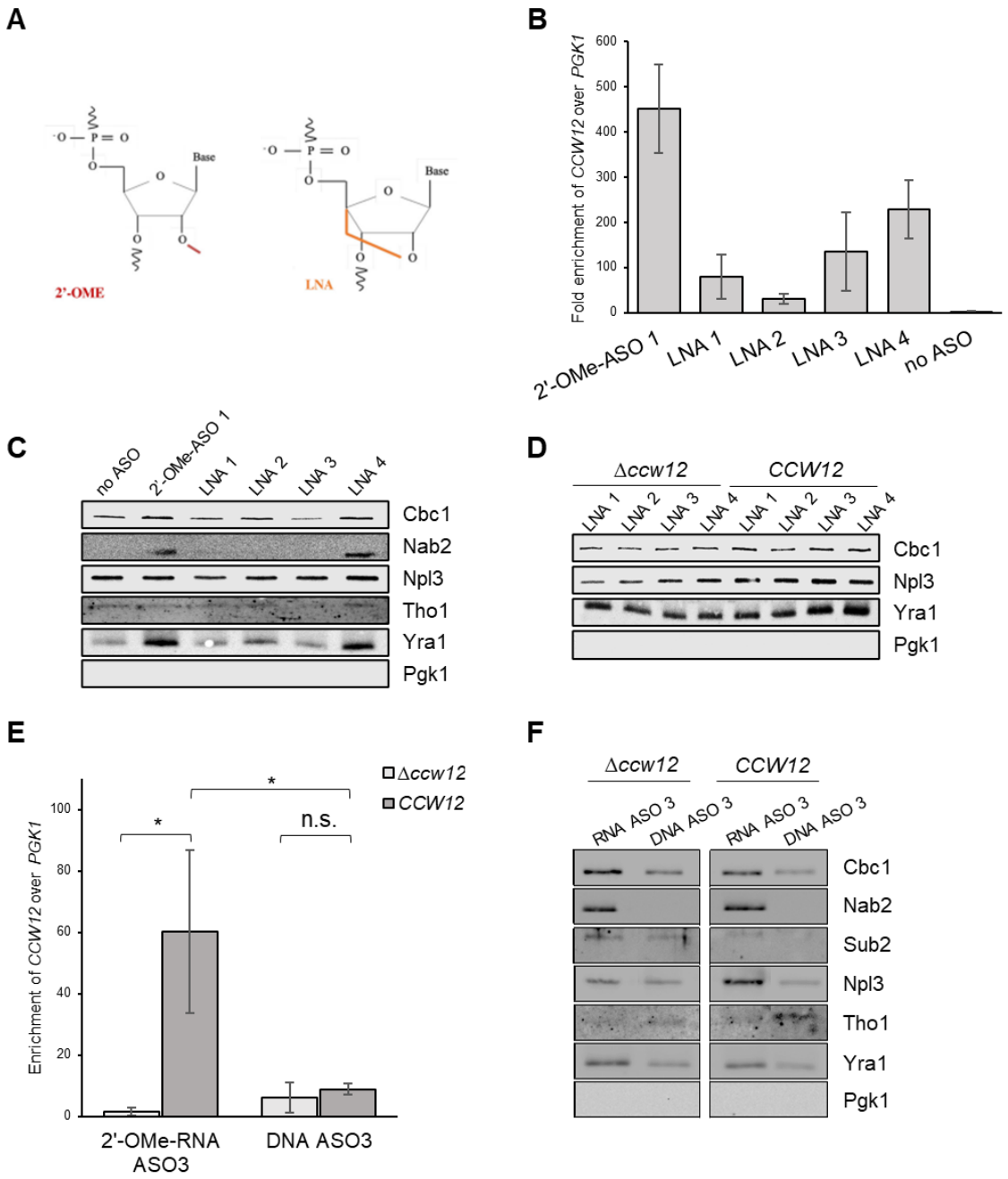

Figure 11. ASO type affects yield of purified *CCW12*. (A) Structure of 2'-OMe ASO and locked nucleic acid ASO (LNA) (Quemener et al., 2020). **(B)** Purification of *CCW12* mRNA via 2'-OMe ASO1 or respective LNA ASOs with LNA modifications in different nucleobases (LNA 1 - 4). The *CCW12* RNA level was determined by RT-qPCR and calculated as fold enrichment over unrelated *PGK1*. Bars represent mean ± SD. **(C)** RBPs, co-purified via 2'-OMe ASO or LNA ASOs. Protein level was determined by Western blot against represented RBPs. **(D)** Non-specific binding of RBPs by LNA ASOs in control Δ*ccw12* strain visualized by Western blot. **(E)** Comparative purification of *CCW12* via 2'-OMe RNA ASO3 or respective DNA ASO3. mRNA level was determined by RT-qPCR and calculated as fold enrichment over *PGK1*. Bars represents mean ± SD; Student's t-test, * p≤0.05, n.s. – not significant. **(F)** RBPs, co-purified via RNA ASO3 (2'-OMe) or DNA ASO3 and determined by Western blot.

As shown above, *CCW12* mRNA is specifically enriched via ASO, while proteins are not. Possibly, the amount of co-purified proteins is very low and, therefore, the difference between *CCW12* and Δ*ccw12* protein samples is not detectable by Western blot. To increase the yield of ASO-based purification, mixture of two or six ASOs were compared to the purification via a single ASO1. While the amount of *CCW12* was slightly increased, the background level of *PGK1* mRNA had risen considerably, especially when a mix of six ASOs was used (Appendix Fig. 4B). Therefore, using the mix of two or six ASOs results in decreased enrichment of *CCW12* mRNA over unrelated *PGK1* mRNA (Appendix Fig. 4A). On protein level, using the mixtures of ASOs leads to increased non-specific protein binding (Appendix Fig. 4C).

Microscopy of *CCW12* purified via ASO does not detect mRNP particles

To further increase the yield of *CCW12*, ASO-based purification was upscaled from 2 L of culture (1x) to 24 L (12x). Amounts of ASOs or beads and washing step were tested and adapted for 24 L culture samples. However, larger amount of culture does not result in higher enrichment of *CCW12* over unrelated *PGK1* (Fig. 12A).

For some of the RBPs (Cbc1 and Yra1), 12x upscale leads to more protein, for another (Nab2 and Npl3) the protein level is even lower than in the 1x sample. Moreover, there are no specific changes for all tested proteins: Δ*ccw12* control looks similar to *CCW12* sample for both, 1x sample and upscaled 12x sample (Fig. 12B).

Electron microscopy of the native biotin eluates failed to detect mRNP particles (Fig. 12C). Instead of expected compact particles, there are some elongated structures which are either debris or parts of disrupted particles. Specific enrichment of *CCW12* mRNA suggests that ASOs are the good tool to purify an RNA of interest alone, but not the native mRNPs. One of the possible explanation is that ASOs interfere with mRNP structure and disrupt it.

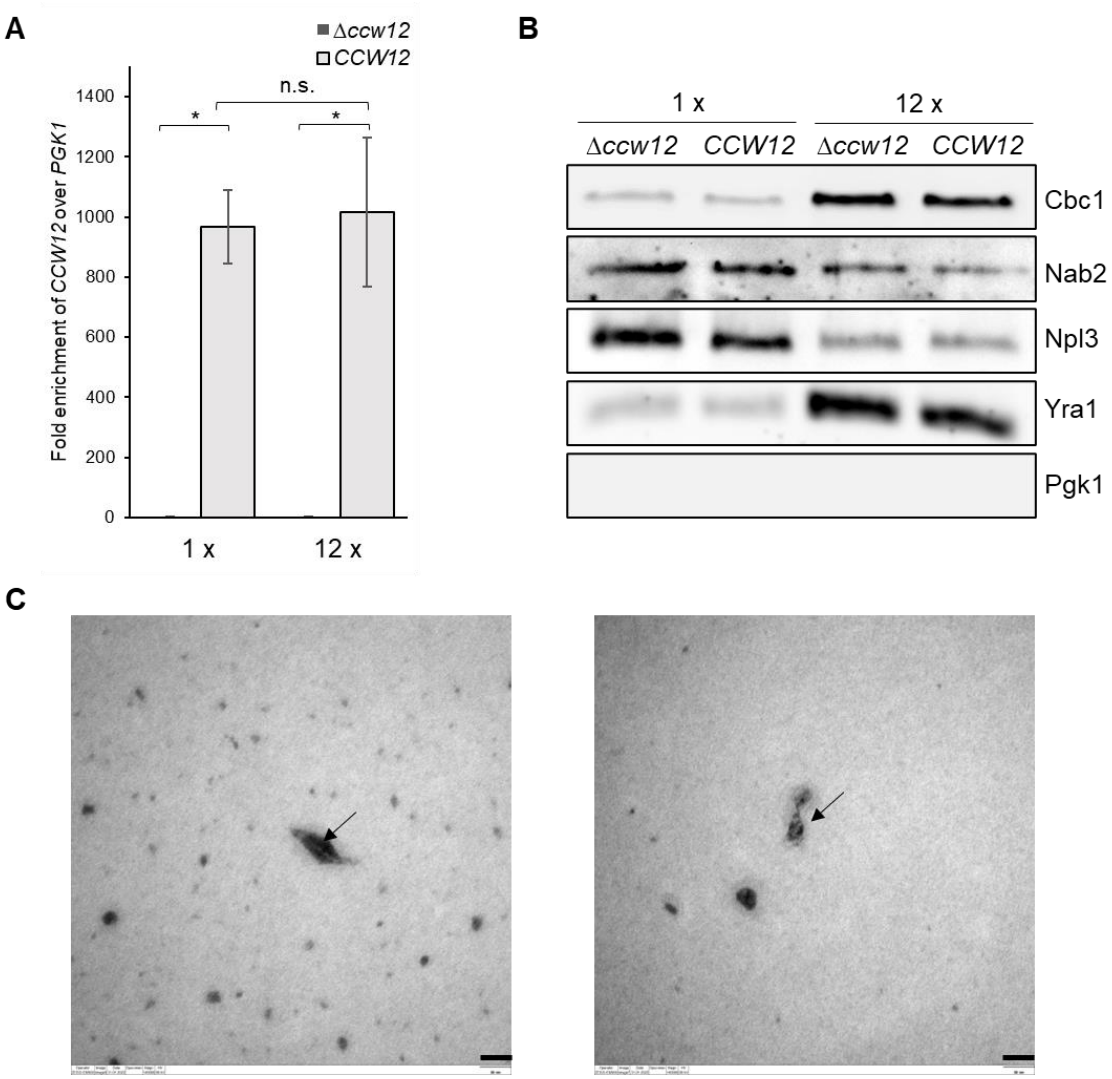

Figure 12. Microscopy of *CCW12* purified via ASO does not visualize mRNP particles. (A) Fold enrichment of *CCW12* mRNA over unrelated *PGK1* for 2 L (1x) or 24 L (12x) of the yeast culture (bars represent mean ± SD; Student's t-test, * p≤0.05, n.s. – non-significant). **(B)** Co-purified RBPs detected by Western blot. **(C)** Negative staining of native eluates visualized by electron microscopy. Arrows indicate debris or disrupted particles. No compact mRNPs were detected (magnification 140000x, scale bars 50 nm). Negative staining and electron microscopy were done by Dr. Ulrich Gärtner (Institute for Anatomy and Cell Biology, JLU Giessen) and Johanna Seidler.

6.1.2.2. Purification of specific mRNP via Mango aptamer

Tagging *CCW12* with Mango aptamer

As an alternative to ASO, aptamer-based approach was implemented. The target *CCW12* mRNA was fused to a Mango I aptamer sequence. To exclude potential interference of the aptamer with mRNA structure, sequence was cloned into 3' UTR of *CCW12*. Three different insertion positions (P1, P2 and P3) within the 3' UTR were

chosen to select the best candidate for further purification (Fig. 13A). Plasmids encoding *CCW12-Mango I* or *CCW12* without aptamer were obtained and transformed into a Δ*ccw12* strain. To investigate, if Mango I integration has a destabilization effect on *CCW12*, mRNA levels were assessed by RT-qPCR. In comparison to the WT *CCW12* level, integration of Mango I aptamer in all three positions does not destabilize *CCW12*. It shows a tendency to a slight increase of mRNA level, but this change is not statistically significant (Fig. 13B). It also does not impair growth of the cells at 30°C and does not display heat-sensitive phenotype at 37°C (Fig. 13C). At 16°C and 25°C Δ*ccw12* strain has slower growth and complementing this strain with *CCW12-Mango* I restored the cell growth for all three constructs (P1, P2 and P3). It is worth to mention, that the background strain, used for these experiments (WT RS453), was observed to have a cold-sensitive phenotype. Remarkably, at 16°C cells with Mango I aptamer grow even better than the WT. Taken together, it shows that integration of Mango I aptamer at three different positions does not have negative impact on mRNA level or cell growth. However, the accessibility of the Mango aptamer for the ligand might be dependent on its position within the mRNA.

The aim was to determine which one of the three insertion position provides the highest efficiency for the mRNP purification. Mango aptamer integrated into *CCW12* binds its ligand thiasole orange coupled to desthiobiotin (TO1-Dtb). Subsequently, TO1-Dtb binds to streptavidin beads and can be denatured or natively eluted with free biotin (Fig. 13D). *CCW12* with Mango I aptamer in first position (P1) showed the highest mRNA yield among the three tested constructs, and it was significantly different from RS453 control (Fig. 13E, left). On protein level, position P1 also showed higher amount of co-purified proteins (Fig. 13E, right). Therefore, *CCW12-Mango I* construct with aptamer insertion in the first position (P1) was selected for further optimizations and tests. As part of the selection process, different types of Mango aptamers were tested. Except of the mentioned above Mango I, there are also Mango II, III and IV with a modified sequence of the aptamer core (Appendix Fig. 5). Therefore, all four aptamer types, integrated in position P1, were tested for purification of *CCW12* mRNP. Mango I aptamer provides the best RNA and protein yield in mRNP purification (Appendix fig. 5B). For the simplicity, from now on *CCW12-Mango I* with insertion in position 1 (P1) will be named *CCW12-Mango*.

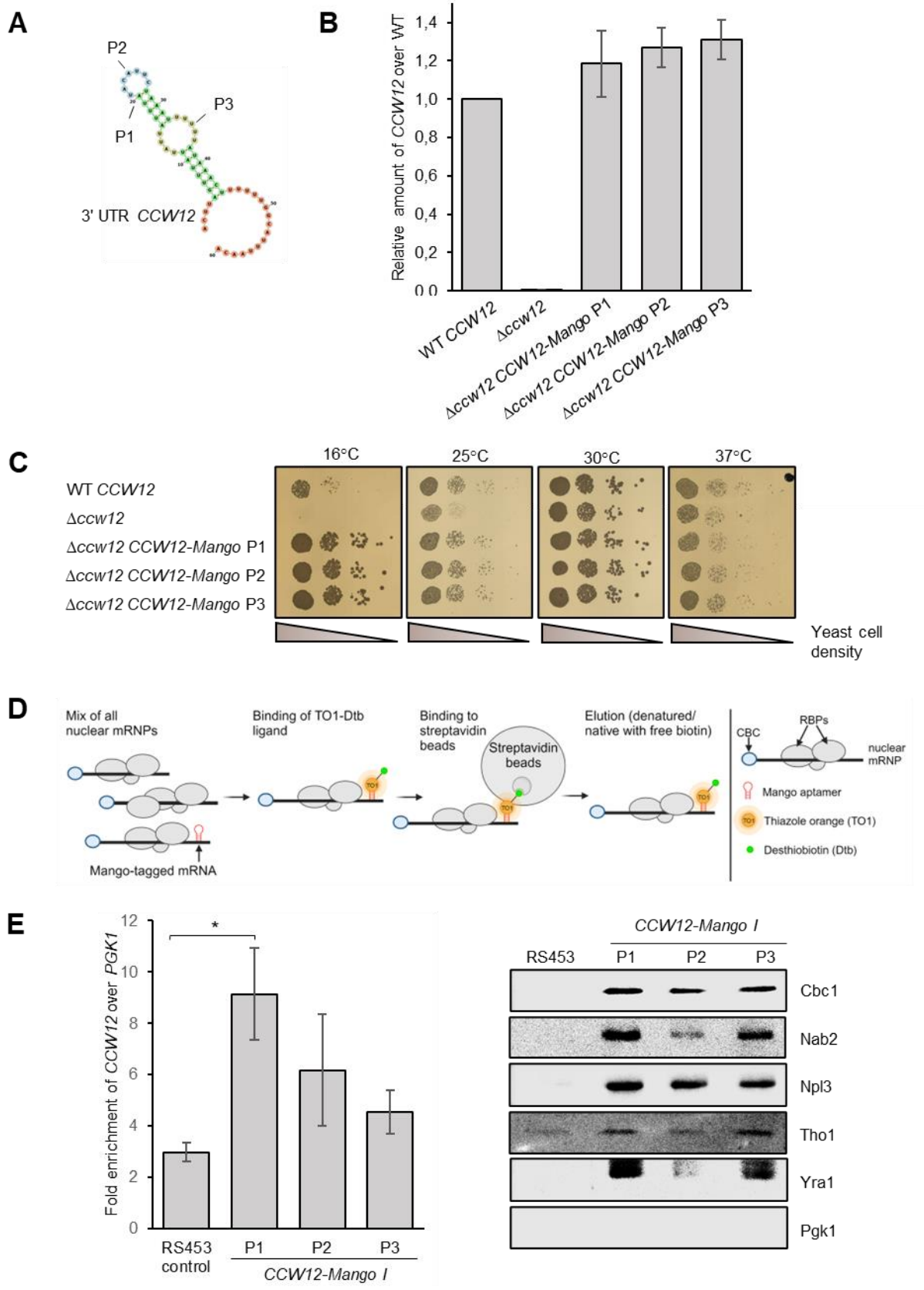

Figure 13. Integration of Mango aptamer does not have destabilization effect on *CCW12* mRNA level or cell growth and can be used for mRNP purification. (A) 3' UTR of *CCW12* and three positions (P1, P2, P3) of Mango aptamer insertion. Secondary structure prediction of 3' UTR of

CCW12 was done with RNAfold web server. **(B)** Integration of Mango aptamer does not destabilize *CCW12* mRNA level. The mRNA level in strains with *CCW12-Mango* constructs with different positions of aptamer integration (P1, P2, P3) was assessed by RT-qPCR and quantified as *CCW12* fold change over WT. Values for WT cells were set to 1. **(C**) Integration of Mango aptamer does not have negative effect on cell growth. Cell growth was assessed by Dot spot assay of strains with Mango aptamer in three different positions of *CCW12* 3' UTR. Cells were spotted in 10-fold serial dilutions on the plates and grown for 2 days at 25, 30 and 37°C or 6 days at 16°C. **(D)** Scheme of Mango-based purification of mRNPs. Mango-tagged RNA binds its ligand thiazole orange (TO1) coupled with desthiobiotin (Dtb). Desthiobiotin then binds to streptavidin beads and pulled complexes can be natively eluted with free biotin or denatured. Created with BioRender. **(E)** Nuclear mRNP purification via different *CCW12-Mango* constructs. Left: mRNA level in final eluate. RNA was extracted and analyzed by RT-qPCR. Fold enrichment of *CCW12* was calculated over unrelated *PGK1* mRNA. Bars represent mean ± SD, * p≤0.05. Right: protein level detected by western blot with antibodies against RNA-binding proteins of mRNPs.

Notably, the ligand of Mango aptamers is the fluorophore thiasole orange (TO1). Its fluorescence properties can be used to check functionality of Mango aptamer by detection of TO1 fluorescence upon aptamer binding. Indeed, in accordance with published data (Dolgosheina et al., 2014), fluorescence of TO1-Dtb can be detected upon its binding to RNA oligonucleotide with the Mango aptamer sequence *in vitro* (Appendix Fig. 6A). Moreover, it was possible to detect fluorescence of TO1-Dtb bound to *CCW12-Mango* mRNA *in vivo* in *S. cerevisiae* cells (Appendix Fig. 6B).

Optimization of the Mango aptamer-based purification of *CCW12* mRNP

After the selection of Mango aptamer type and its insertion position in the 3' UTR of *CCW12* mRNA, purification conditions were tested and optimized. Despite the fact that non-porous magnetic beads are recommended for mRNP purification (Oeffinger et al., 2007), for Mango-based purification high-capacity streptavidin agarose beads were a better choice. While magnetic beads failed to enrich target *CCW12* and had non-specific protein binding in the control RS453 strain, the agarose beads showed specific purification of *CCW12* and no protein background in the RS453 control (Fig. 14 A and B).

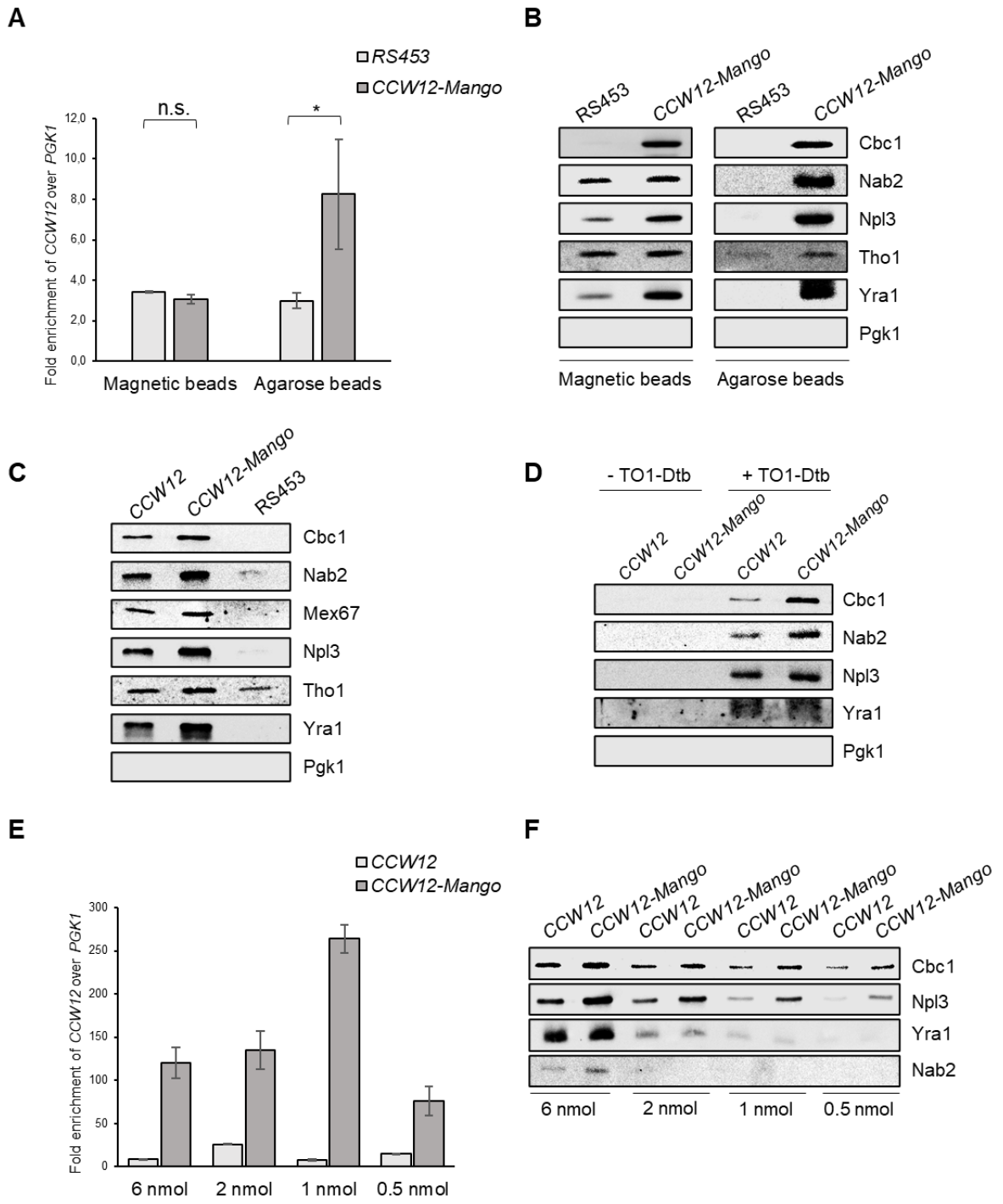

Figure 14. Type of beads and amount of TO1-Dtb ligand are important for mRNP purification via Mango aptamer. (A - B) Streptavidin-coupled agarose beads provide better purification of *CCW12-Mango* mRNPs than magnetic beads. The mRNA yield (A) and co-purified RBPs (B). Bars represent mean ± SD, * p≤0.05, n.s. non-significant. **(C)** Non-specific binding of TO1-Dtb to RBPs is illustrated by presence of RBPs in *CCW12* control. **(D)** Non-specific protein binding is due to the binding to the TO1-Dtb ("+ TO1-Dtb"), but not to the beads ("- TO1-Dtb"). Protein levels were determined by Western blot against the represented proteins. **(E - F)** Titration of ligand TO1-Dtb. Enriched mRNA level was calculated over unrelated *PGK1* (E). Co-purified proteins are detected by Western blot (F).

As mentioned before, the purification has two steps: Cbc2-TAP to enrich all nuclear mRNPs, and a transcript-specific step that targets the mRNA of interest. The RS453 control, used on the first steps of optimization process, does not have Cbc2-TAP, and represents the absence of non-specific binding to the beads. Using as a control the Cbc2-TAP strain with non-tagged *CCW12* detected RNA-binding proteins (Fig. 14C). This indicates non-specific protein binding to the TO1-Dtb ligand, but not to the beads (Fig. 14D). In contrast to the ASO-based purification, for Mango aptamer the protein level in *CCW12* control was lower than in *CCW12-Mango* sample. Therefore, further optimizations were performed to further decrease the protein background in the control strain.

Thus, it was decided to determine what amount of TO1-Dtb ligand is sufficient to effectively bind the *CCW12-Mango* RNA. Decrease of TO1-Dtb concentration by 6 times (to 1 nmol) leads to the highest enrichment of *CCW12-Mango* mRNA (Fig. 14E). However, going even lower to 0.5 nmol results in a significant reduction of *CCW12-Mango* enrichment. On protein level, for 1 nmol TO1-Dtb there are still some non-specific protein binding in the *CCW12* control (Fig. 14F). Remarkably, for 1 nmol TO1-Dtb sample, protein level is much lower than for 6 nmol. This supports the idea, that the unbound TO1-Dtb binds to the single RBPs. That would explain the disproportion for 6 nmol samples, where the strongest protein signal did not match with lower RNA levels.

Further tests were carried out to improve the yield and purity of the Mango-based purification. The optimization conditions and their conclusions are summarized in the Appendix table 2.

Morphology of *CCW12-Mango* mRNP

Despite of all optimization and improvements of *CCW12-Mango* purification, yield continued to be a critical point for visualization of the particles by electron microscopy. To increase the number of purified particles, purification from usual 2 L yeast culture sample (1x) was upscaled and optimized for 24 L culture (12x). Indeed, this upscaling significantly increased the mRNA yield of target *CCW12-Mango* without compromising the purity of mRNA (Fig. 15A). On protein level, upscaling resulted in more Cbc1, Nab2 and Yra1, and difference between control *CCW12* and target *CCW12-Mango* was clear. But Npl3 protein showed high non-specific binding

in the control sample (Fig. 15B). Upscaling of the sample resulted in sufficient number of particles for visualization with electron microscopy (Fig. 15C). Since mRNA level is very specific and protein level is enriched in comparison to the control, the observed particles are likely *CCW12-Mango*. However, observed particles do not look uniform and have different shapes. Perhaps, mRNPs lose their integrity during sample preparation procedure and need to be stabilized with mild crosslinking before visualization with negative staining.

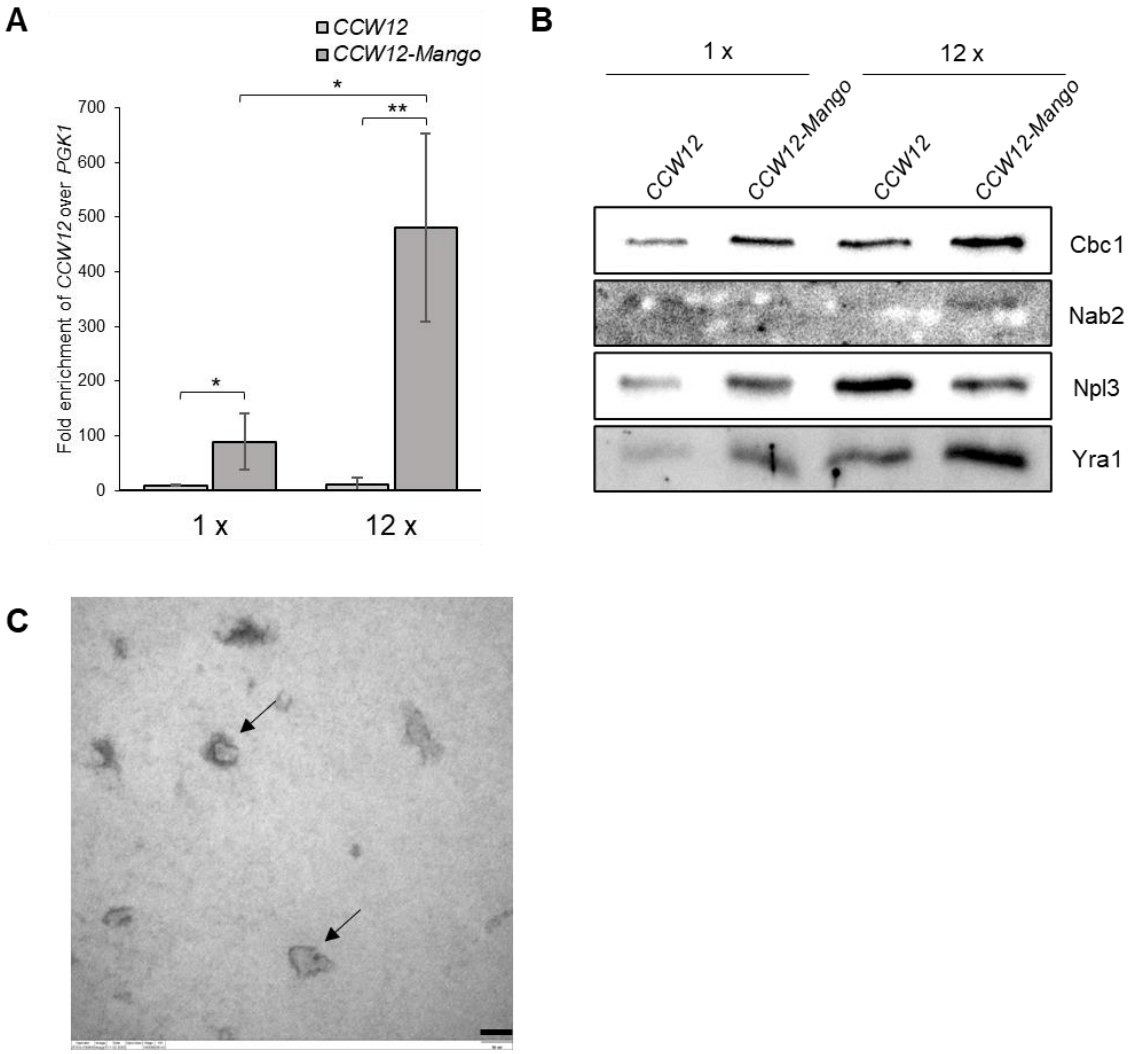

Figure 15. Microscopy of *CCW12*-Mango mRNP visualizes particles. (A) Fold enrichment of *CCW12* over *PGK1* for 1x (2 L) and 12x (24 L) purification, determined by RT-qPCR. Bars represent mean ± SD, * p≤0.05, ** p≤0.01. **(B)** Co-purified proteins detected with respective antibodies by Western blot. **(C)** Negative staining of obtained particles (indicated with arrows) in a native eluate, detected by electron microscopy (magnification 140000x, scale bar 50 nm). Negative staining and electron microscopy was done by Dr. Ulrich Gärtner (Institute for Anatomy and Cell Biology, JLU Giessen) and Johanna Seidler.

6.1.2.3. MS2-MCP system to purify specific mRNP

Another alternative approach to purify specific *CCW12* mRNP is via MS2 aptamer and its ligand MS2-coat protein (MCP). Purification protocol of *CCW12-MS2* from 2 L of yeast culture was established and optimized by Johanna Seidler (unpublished).

For this study, the protocol for 2 L culture purification (1x) was adapted for a 24 L upscaled purification (12x) to increase the yield of mRNP particles for visualization by electron microscopy. For the purification, the strain Δ*ccw12* Cbc2-TAP, expressing the MS2-coat protein (MCP) tagged with maltose-binding protein (MBP) was transformed with plasmid encoding *CCW12-MS2* or *CCW12* as a control. In the cells MCP-MBP binds the MS2 loop of target mRNA, and via MBP it can be bound to amylose beads with subsequent native elution with maltose (Fig. 16A).

The 12x upscaling results in specifically increased enrichment of *CCW12-MS2* mRNA (Fig. 16B). Remarkably, amount of proteins, co-purified with *CCW12-MS2*, is greatly increased in 12x sample in comparison to 1x sample. Furthermore, there is a clear difference in protein level between control *CCW12* and *CCW12-MS2* for upscaled samples (Fig. 16C). In the electron microscopy it was possible to detect particles. Similar to the observed *CCW12-Mango* particles, the *CCW12-MS2* particles have different shapes (Fig. 16E). In comparison, in the TEV eluate enriched with all nuclear mRNPs, the particles are very compact (Fig. 16D). Extending the purification with MS2 isolation step of specific mRNP seems to lead to the loss of this compact structure. Perhaps, alike for Mango-based purification, to stabilize the particles, *CCW12-MS2* might need cross-linking in native eluate before imaging, or even in the TEV eluate where particles are still compact.

Overall, the described purifications of transcript-specific nuclear mRNP *CCW12* via Mango or MS2 aptamer results in detectable particles of a size of around 28 nm. Further improvement are required to obtain more stable uniform particles which can be used for further studying of mRNP structure and stoichiometry, for instance by cryo-electron microscopy and cross-linking mass spectrometry. Certainly, these aptamer-based methods can be adapted to enrich different transcript-specific mRNPs within different species to compare their structure and composition.

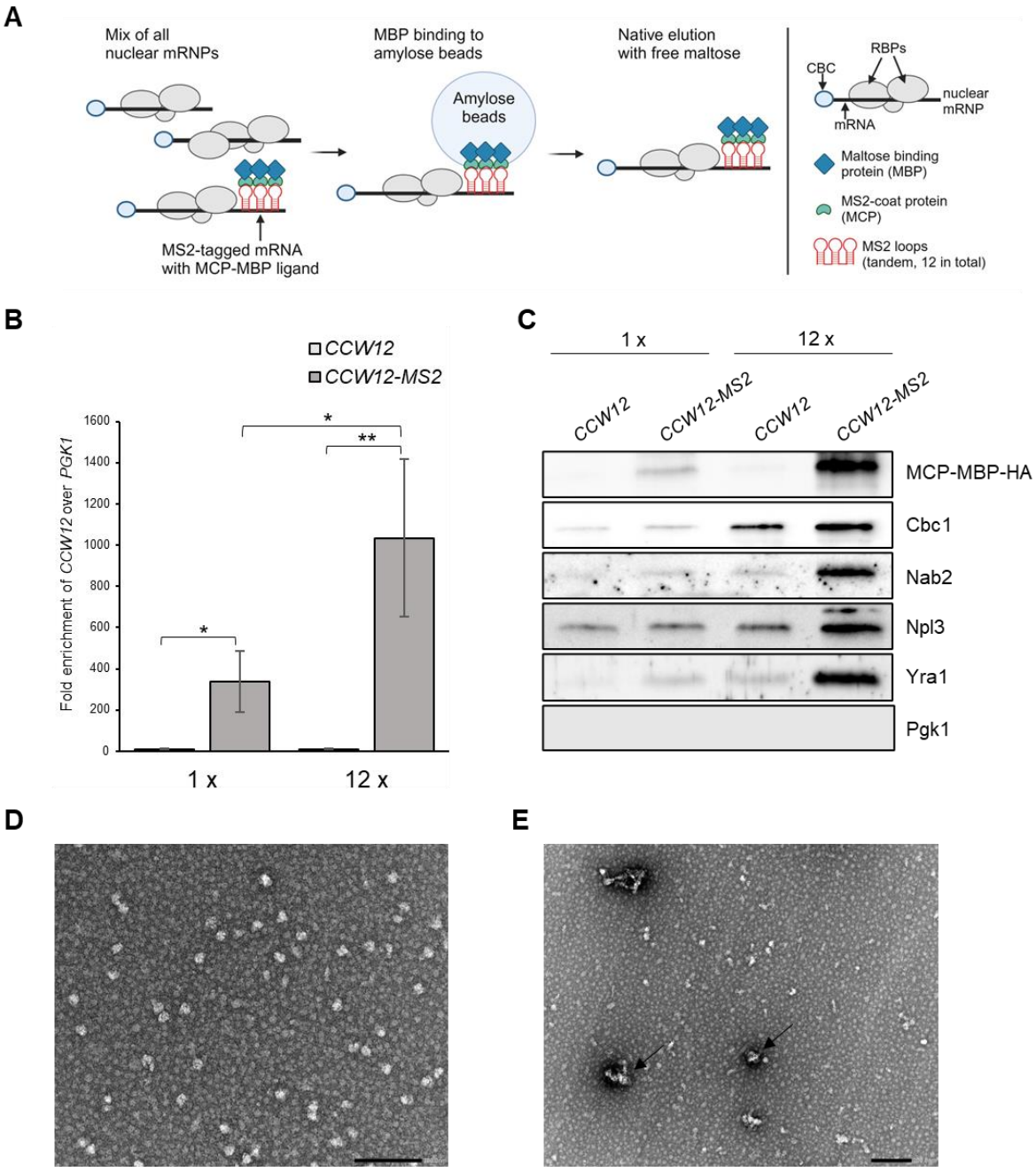

Figure 16. Upscaling the *CCW12*-MS2 purification results in detectable particles. (A) Scheme of mRNP purification via MS2-MCP system. MS2-tagged mRNA binds its MCP ligand, tagged with MBP tag. The MBP binds to amylose beads. Particles are released by native elution with maltose. **(B)** The mRNA level of *CCW12* purified from 1x (2 L) or 12x (24 L) culture, calculated as fold enrichment over unrelated *PGK1*. Bars represent mean ± SD, * p≤0.05, ** p≤0.01. **(C)** Co-purified proteins detected by Western blot with respective antibodies. **(D)** Negative staining of nuclear mRNPs in TEV eluate (1st step of purification) (magnification 50000x, scale bar 200 nm). **(E)** Negative staining of the native eluate enriched with *CCW12-MS2* mRNPs (indicated with arrows) (2nd step of purification) (magnification 30000x, scale bar 200 nm). Negative staining and electron microscopy of 12x upscaled eluates were done by Janett Piesker (Max Plank Institute for Heart and Lung Research) and Johanna Seidler.

6.2. Role of THO/TREX component Hpr1 in mRNP assembly

Hpr1 is a protein of the pentameric subcomplex THO, which is part of the TREX complex. Hpr1 is involved in transcription and mRNA export. In addition, its deletion is associated with increased genomic instability and hyperrecombination (Chávez et al., 2001; Sträßer et al., 2002; Wellinger et al., 2006). The aim of this study was to elucidate the role of Hpr1 in mRNP assembly and export for better understanding of the molecular mechanisms of mRNA export in *Saccharomyces cerevisiae*.

6.2.1. Depletion of Hpr1 with the auxin-inducible degron system

Hpr1 is a non-essential protein, therefore deletion of *HPR1* is not lethal for the cells. However, gene deletion causes long-term changes in phenotype, which may be associated with the accumulation of secondary effects. In order to estimate the first changes in the cell in the absence of Hpr1, auxin-inducible degron (AID) system was implemented to deplete Hpr1. The AID system provides rapid depletion of the protein of interest upon addition of the plant hormone auxin to the growth media. Natural (indole-3-acetic acid, IAA) or synthetic (1-naphtaleneacetic acid, NAA) auxin triggers a pathway of proteasome degradation of AID-tagged protein (Fig. 17A).

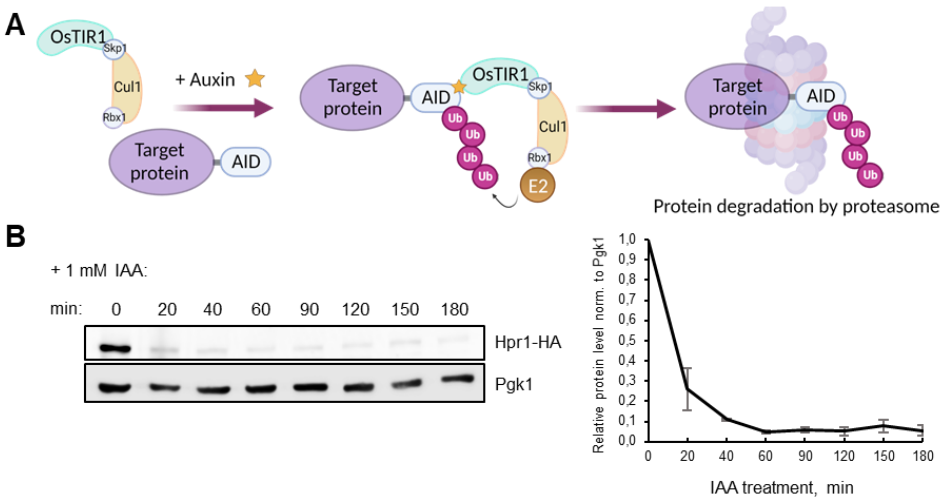

Figure 17. Rapid depletion of Hpr1 upon addition of auxin. (A) Scheme of AID system modified after (Nishimura et al., 2009). Addition of auxin promotes the interaction of OsTIR1 and AID-tag of the target protein. It leads to the recruitment of E2 ligase, that ubiquitinates AID and targets the protein for degradation by the proteasome. **(B)** Protein level of Hpr1 at different time points of incubation with 1mM auxin (IAA). Western blot of the whole cell extracts with respective antibodies. Pgk1 was used as a loading control. Hpr1 level was quantified with ImageJ and normalized to Pgk1. Data represents mean ± standard deviation (SD).

For depletion, *HPR1* was tagged at the C-terminal end with AID tag. Addition of 1 mM IAA resulted in rapid depletion of Hpr1 (Fig. 17B). Already after 20 min of auxin treatment the level of Hpr1 in the cells was drastically decreased. The lowest Hpr1 level was observed after 1 hour of incubation with auxin. Longer time points did not bring further changes in the protein level. Therefore, for the next depletion experiments 1 h of auxin treatment was applied.

6.2.2. Growth defects in the absence of Hpr1

To assess how the depletion of Hpr1 affects cell growth, dot spot assay was performed. Without auxin treatment (- IAA), *HPR1-AID* strain grows like wild-type at tested temperatures. However, presence of auxin (+ IAA) causes the depletion of Hpr1 and leads to growth defects of *HPR1-AID* in comparison to WT (W303), especially at 16, 25 and 37°C. At 30°C, the temperature optimal for yeast, the growth is slightly impaired (Fig. 18A). In comparison, growth of Δ*hpr1* cells slows down more than for the depletion. The Δ*hpr1* cell growth is notably impaired already at 25 and 30°C. In accordance to the published data (Betz et al., 2002), Δ*hpr1* strain shows major cold- and heat-sensitive phenotypes at 16 and 37°C (Fig. 18B). Such growth defects can be associated with various altered processes in the cell, one of them is mRNA export.

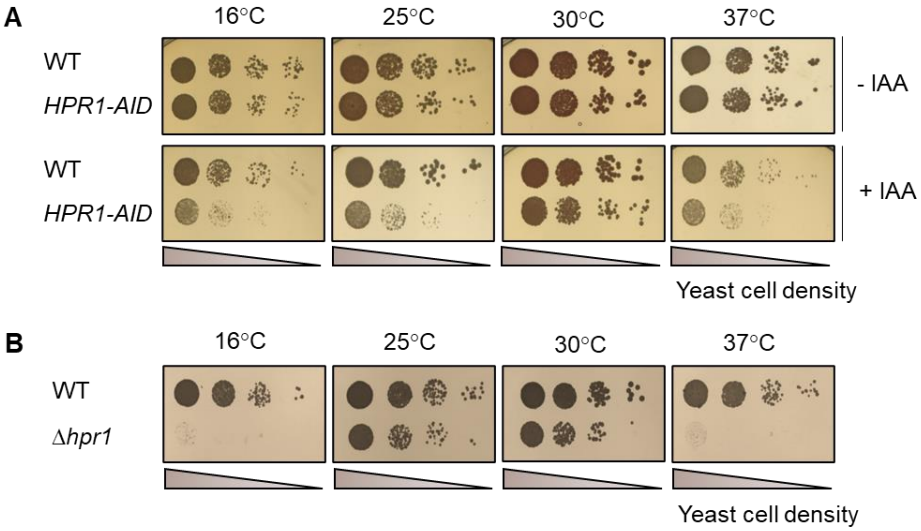

Figure 18. Depletion of Hpr1 and deletion of HPR1 leads to temperature sensitive growth phenotypes. (A) Dot spot growth assay of WT and *HPR1-AID* cells. Serial dilutions of cells were spotted onto control plates without auxin (- IAA; YPD) or auxin-containing plates (+ IAA; YPD) for Hpr1 depletion. **(B)** Dot spot growth assay of WT and *Δhpr1* strains on YPD plates. Cells were grown for 2 days at 25°C, 30°C and 37°C or for 6 days at 16°C.

6.2.3. mRNA export defect in the absence of Hpr1

Hpr1, as a part of TREX complex, is involved in mRNA export. It was observed before that Δ*hpr1* cells accumulate poly(A)+ RNA in the nucleus at 30°C and after 2 h shift to 37°C (Sträßer et al., 2002). Indeed, at the optimal 30°C some cells of the Δ*hpr1* strain display mild mRNA export defect, which is enhanced by an 1 h shift of the cells to 37°C (Fig. 19).

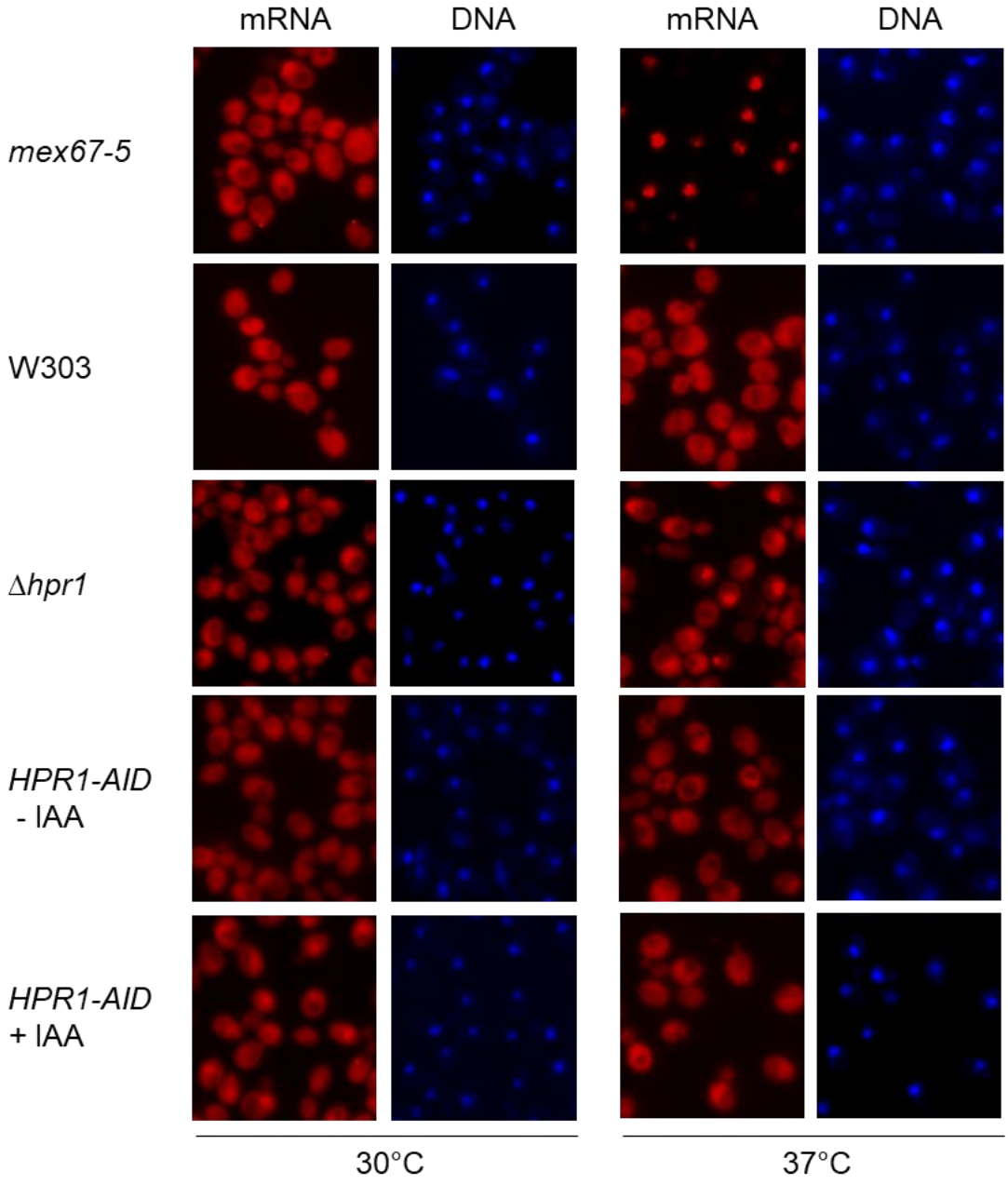

Figure 19. Nuclear mRNA export is impaired in the absence of Hpr1. mRNA export was analyzed by fluorescence *in situ* hybridization (FISH) at 30 and 37°C. *mex67-5* strain, known for strong export defect at 37°C, was used as a positive control. *WT* W303 and *HPR1-AID* (-IAA) were compared with deletion of *HPR1* (Δ*hpr1*) or depletion of Hpr1 (*HPR1-AID* + IAA). Poly(A)$^+$ RNA was visualized with oligo(dT)50-Cy3, DNA was stained with DAPI.

Furthermore, rapid depletion of *HPR1-AID* upon auxin addition (+ IAA) also resulted in accumulation of mRNA in the nucleus. Interestingly, in case of Hpr1 depletion more cells accumulate mRNA at 30°C than at 37°C. As a positive control strain *mex67-5* was used. It has a very strong mRNA export block when shifted to 37°C. Noticeably, mRNA export defect in the absence of *HPR1* was not as strong, as for *mex67-5*. Since *HPR1* is not essential, cells are either trying to compensate its absence by some alternative mechanisms of mRNA export, or only export of certain RNAs is affected upon deletion/depletion of *HPR1*.

6.2.4. Nuclear mRNP composition is changed upon depletion/deletion of *HPR1*

To assess the role of Hpr1 in mRNP assembly, nuclear mRNP purification was performed in a WT strain and strains with deleted/depleted *HPR1*. Nuclear mRNPs were enriched via Cbc2, a component of CBC, tagged at the C-terminus with a TAP-tag. Co-purified proteins in obtained TEV eluates were analyzed by Western blot for RBPs known to be a part of mRNPs.

Remarkably, short Hpr1 depletion for 20 min does not affect mRNP composition (Appendix fig. 7). Depletion of Hpr1 upon 1 h incubation with auxin leads to slight increase of poly(A)-binding protein Nab2 in lysates, as well as exhibits the first changes in the mRNP composition (Fig. 20A-B, Lysate). The first reaction on the absence of the Hpr1 is over 2-fold increase of Nab2 in nuclear mRNPs, while the rest of represented proteins remains unchanged (Fig. 20A-B, TEV eluate).

Deletion of *HPR1* leads to increased levels of Nab2 and Yra1 in lysates (Fig. 20C-D, Lysate). The Δ*hpr1* strain that displays long-term changes shows even higher increase of Nab2 level in nuclear mRNPs. Additionally, levels of mRNA export adaptor Yra1 and mRNA exporter Mex67 are increased in nuclear mRNPs (Fig. 20C-D, TEV eluate). Therefore, as a response to the absence of Hpr1, first Nab2 level increases, with a following increase of Mex67 and Yra1 in mRNP composition.

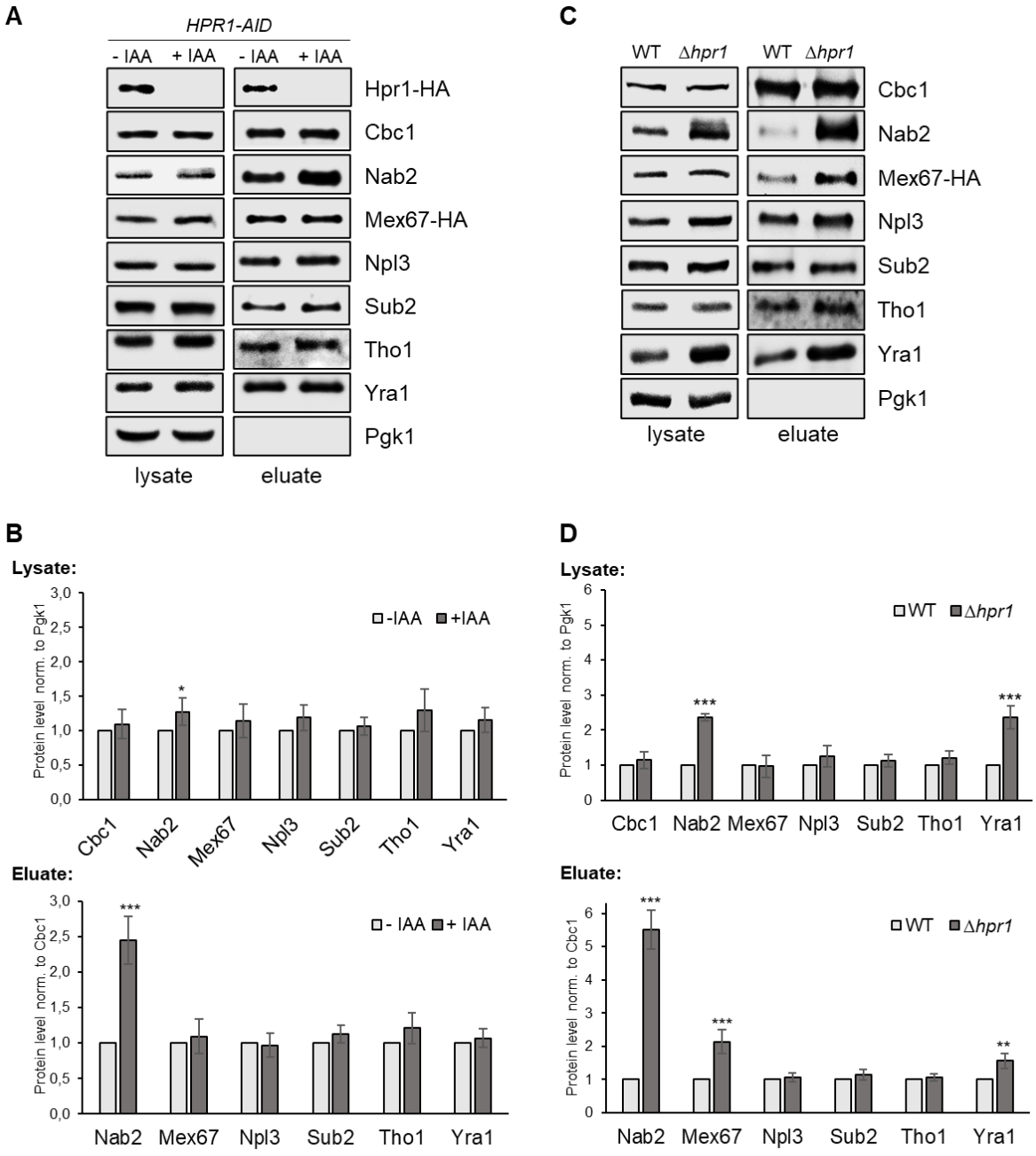

Figure 20. Nuclear mRNP composition specifically changes in the absence of Hpr1. (A) Cbc2-TAP purification of nuclear mRNPs from strain with WT Hpr1 (- IAA) or strain after 1 h Hpr1 depletion (+ IAA). **(B)** Quantification of the protein levels in lysates (upper panel) and TEV eluates (lower panel) for WT (-IAA) and Hpr1 depletion (+IAA). **(C)** Cbc2-TAP purification from WT and *Δhpr1* cells. **(D)** Quantification of the protein levels in lysates (upper panel) and TEV eluates (lower panel) for WT and *Δhpr1* cells. Proteins were detected by Western blot with antibodies against the indicated RBPs. Protein levels were quantified with ImageJ and normalized to the signal of Pgk1 for lysates and to the CBC subunit Cbc1 for TEV eluates. Protein levels for WT cells were set to 1 (bars represent mean ± SD; Student's t-test, **p<0.01; ***p<0.001).

It is worth noting that longer Hpr1 depletion for 6 h was characterized by changes in mRNP composition, similar to ones observed in Δ*hpr1* strain (Appendix fig. 7). Interestingly, depletion of Hpr1 for 3 h affected mRNP composition differently: in addition to increased level of Nab2, reduced level of other RBPs – Sub2 and Tho1 – was observed (Appendix fig. 7). This suggests the presence of intermediate states of mRNP composition between the first reaction upon Hpr1 depletion and long-term changes in Δ*hpr1* cells.

6.2.5. RNA binding of Nab2, Yra1 and Mex67 is increased in Δ*hpr1* strain

As depletion of Hpr1 leads to increase of Nab2 level and deletion of *HPR1* – to increased levels of Nab2, Mex67 and Yra1, the aim was to check RNA-binding properties of mentioned proteins by RNA immunoprecipitation. For this, proteins of interest were pulled down via TAP-tag and IgG antibodies and co-immunoprecipitated RNAs were analyzed by RT-qPCR. Highly transcribed intronless (*PMA1, CCW12, YEF3, ILV5, RPL9B*) and intron-containing (*DBP2, ACT1, RPS14B, RPL28*) transcripts were chosen for analysis.

Despite the fact that Hpr1 depletion led to increased Nab2 level in nuclear mRNPs (Fig. 20A-B), the RNA immunoprecipitation experiment showed no difference in RNA binding of Nab2 upon Hpr1 depletion (Fig. 21A). This might be an indicator, that observed 2-fold increase in the amount of Nab2 in nuclear mRNPs represents more molecules of Nab2 on the same mRNP, rather than recruitment of Nab2 to more transcripts.

In contrast to Hpr1 depletion, Δ*hpr1* cells showed increased RNA binding of Nab2 (Fig. 21B). Likely, in Δ*hpr1* cells there are more molecules of Nab2 on the same mRNP as well as increased recruitment of Nab2 to more transcripts. Proteins Yra1 and Mex67 also showed increased binding to all analyzed transcripts in Δ*hpr1* cells (Fig. 21B-D). Therefore, the general tendency shows that Nab2, Mex67 and Yra1 have increased RNA-binding properties and are recruited to more transcripts in Δ*hpr1* strain.

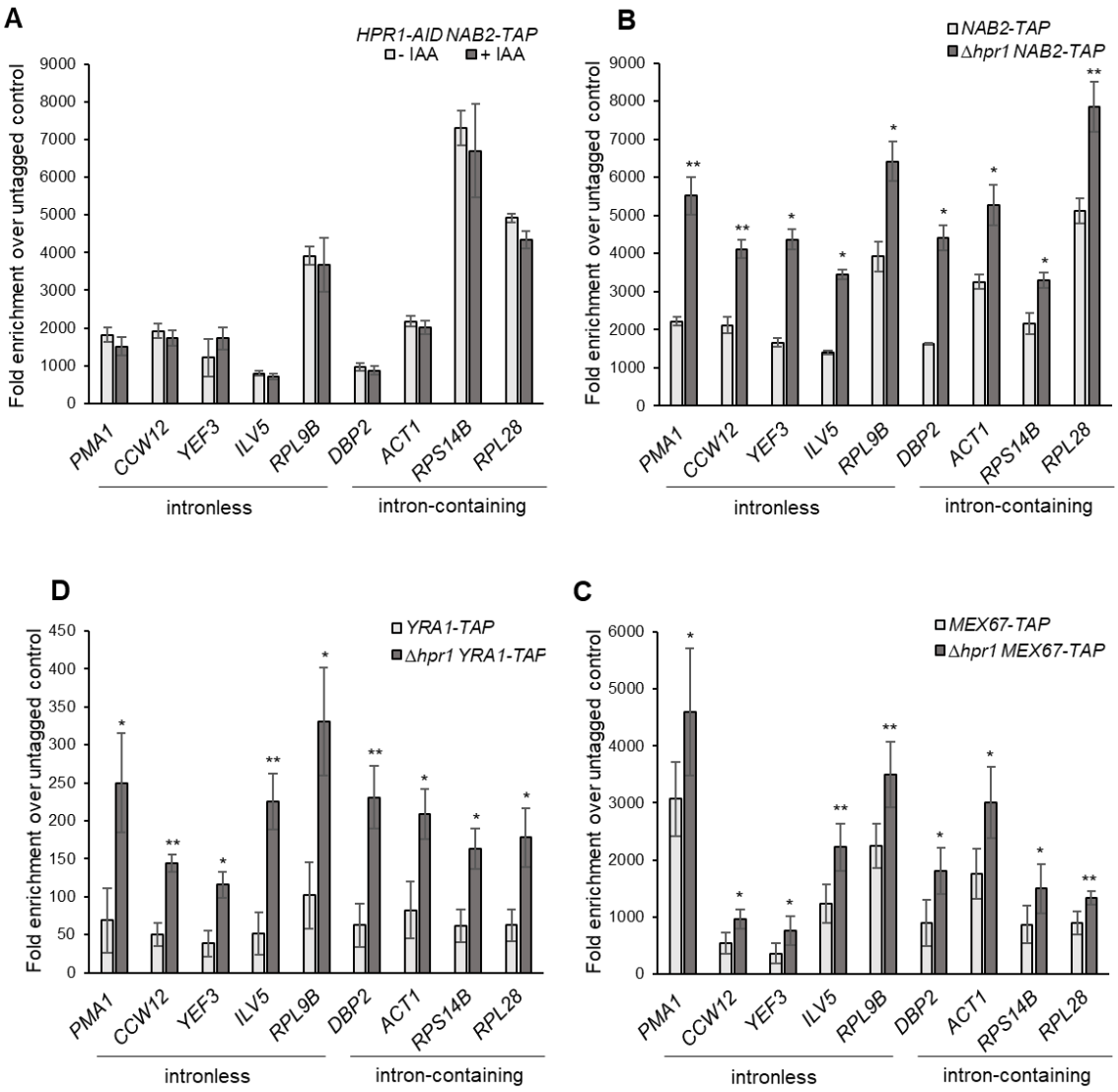

Figure 21. RNA binding of Nab2, Yra1 and Mex67 increases in Δ*hpr1* cells. (A) Binding of Nab2 to RNA upon depletion of Hpr1 (+ IAA). **(B, C, D)** Respectively, RNA binding of Nab2, Mex67 and Yra1 is increased in Δ*hpr1* cells. The level of mRNA was determined as enrichment over the level of a non-tagged control by RT-qPCR (bars represent mean ± SD; Student's t-test; *p<0.05; **p<0.01).

6.2.6. Occupancy of Nab2 and Yra1 at transcribed genes is increased in Δ*hpr1* strain

To determine whether more Nab2, Mex67 and Yra1 is already recruited co-transcriptionally, chromatin immunoprecipitation (ChIP) was performed. The protein of interest with TAP-tag was pulled down via IgG beads and analyzed for co-precipitated DNA by qPCR. As for RNA immunoprecipitation, highly transcribed intronless and intron-containing genes were analyzed. It was shown before that the

occupancy of RNAPII is decreased in Δ*hpr1* strain (Huertas et al., 2006; Mason & Struhl, 2005). Indeed, for tested highly transcribed genes around two-fold decrease of RNAPII occupancy was observed for Δ*hpr1* cells (Fig. 22A). Recruitment of RBPs is dependent on transcription level. To take into account changes in transcription in Δ*hpr1* cells, occupancies of proteins of interest were normalized to RNAPII occupancy.

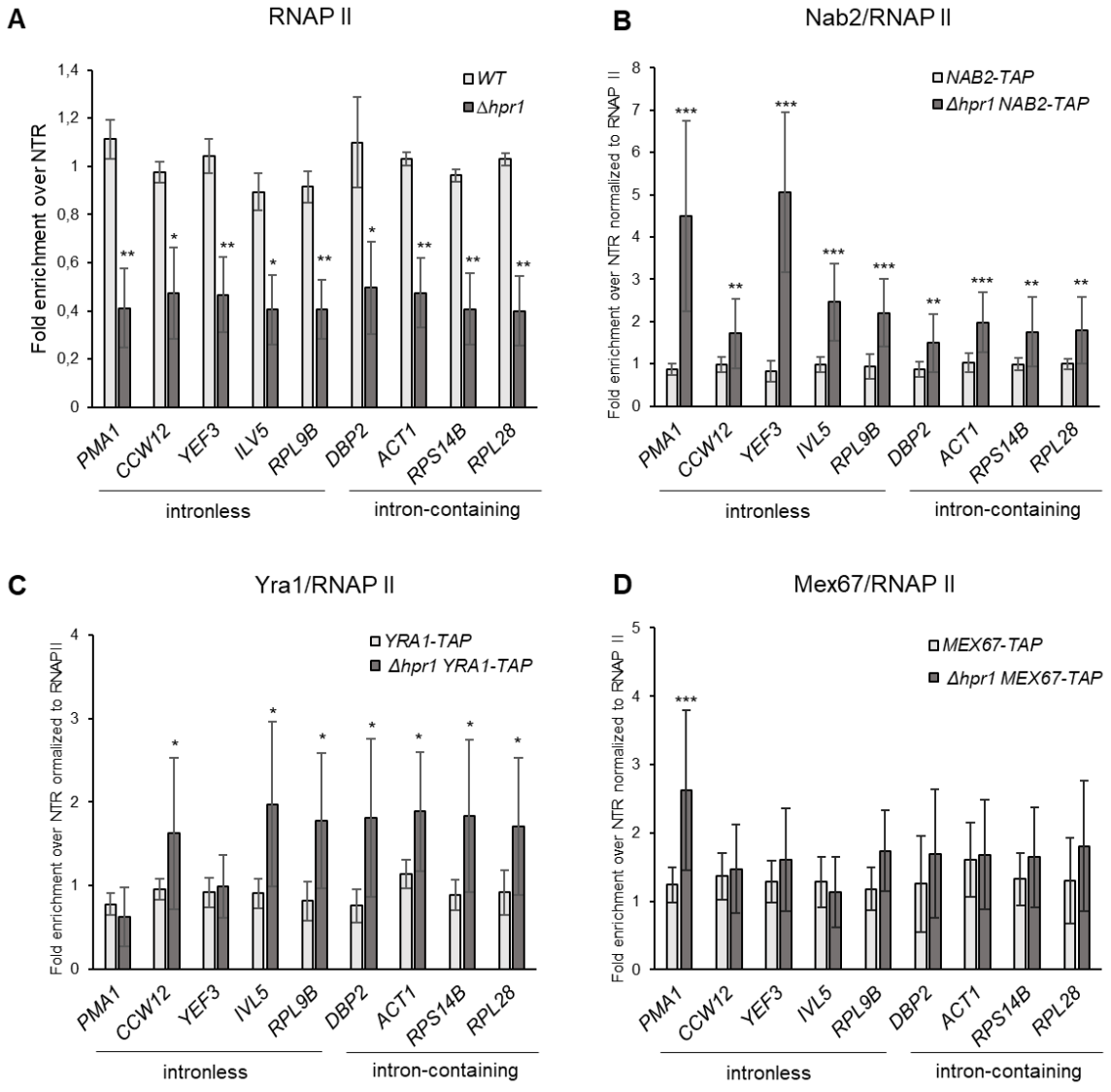

Figure 22. The occupancy at transcribed genes in Δ*hpr1* cells is increased for Nab2 and Yra1, but not changed for Mex67. (A) The occupancy of RNAPII is decreased in Δ*hpr1* strain. **(B, C)** The occupancies of Nab2 and Yra1 are increased in the absence of *HPR1*. **(D)** Mex67 occupancy for the most of the tested genes remains unchanged. The protein occupancy was assessed by chromatin immunoprecipitation (ChIP). Obtained enrichments were calculated over non-transcribed region (NTR, 174131–174200 on chr. V), normalized to RNAPII occupancy level and set to 1 for WT strain (bars represent mean ± SD; Student's t-test; *p<0.05; **p<0.01; *** p<0.001). Experiment was performed by Salome Barbakadze.

Occupancy of Nab2 was increased for all tested genes in a Δ*hpr1* strain (Fig. 22B). In a similar way, occupancy of Yra1 was increased for almost all tested genes (Fig. 22C). On the contrary, occupancy of Mex67 remained unchanged for nearly all tested genes (Fig. 22D).

Collectively, deletion of *HPR1* leads to increased co-transcriptional recruitment or retention of Nab2 and Yra1 to chromatin, perhaps for their further loading onto mRNP. Observed increase of Mex67 in nuclear mRNPs in Δ*hpr1* cells does not happen already co-transcriptionally, but it seems to be loaded onto mRNPs later in a post-transcriptional manner.

6.2.7. Overexpression of Nab2 or Yra1 suppresses the nuclear mRNA export defect of Δ*hpr1* cells

Mex67-Mtr2 is a general mRNA exporter. Mex67 binds to RNA with low affinity and requires adaptor proteins to be recruited to the mRNA to mediate the export. In a current model of mRNA export, Yra1 is an adaptor of Mex67. However, also other nuclear mRNP components such as Nab2 and Npl3, as well as Hpr1 itself, are suggested to be export adaptors of Mex67 (Gilbert & Guthrie, 2004; Iglesias et al., 2010). Interestingly, Mex67, Nab2 and Yra1 are increased in nuclear mRNPs in Δ*hpr1* strain, but Npl3 levels remain unchanged (Fig. 20C-D). Since nuclear mRNA export is impaired in Δ*hpr1* cells, potentially, cells are trying to bypass nuclear mRNA retention by increasing the level of Nab2, Yra1 and Mex67. To check this, Nab2, Yra1 and Mex67 were overexpressed in Δ*hpr1* cells using high-copy plasmids encoding the respective protein. Additionally, overexpression of Npl3, which did not show any changes in mRNP composition, but known to be another export adaptor of Mex67, was included. WT (W303) and Δ*hpr1* strains were transformed with an empty vector for comparison. Strikingly, overexpression of Nab2 or Yra1 suppresses nuclear mRNA export block of Δ*hpr1* cells for both, 30 and 37°C, and nuclear mRNA export becomes restored and comparable to the WT (Fig. 23).

Despite the fact that Mex67 is also increased in mRNPs in Δ*hpr1* cells, overexpression of this protein does not suppress mRNA export defect. The same is observed in case of Npl3 overexpression (Fig. 23). No changes for Npl3 overexpression can indicate that Npl3, as an export adaptor, is not involved in mRNA

export in Δ*hpr1* strain. On the contrary, mRNA export adaptors Nab2 and Yra1 can promote mRNA export in Δ*hpr1* cells.

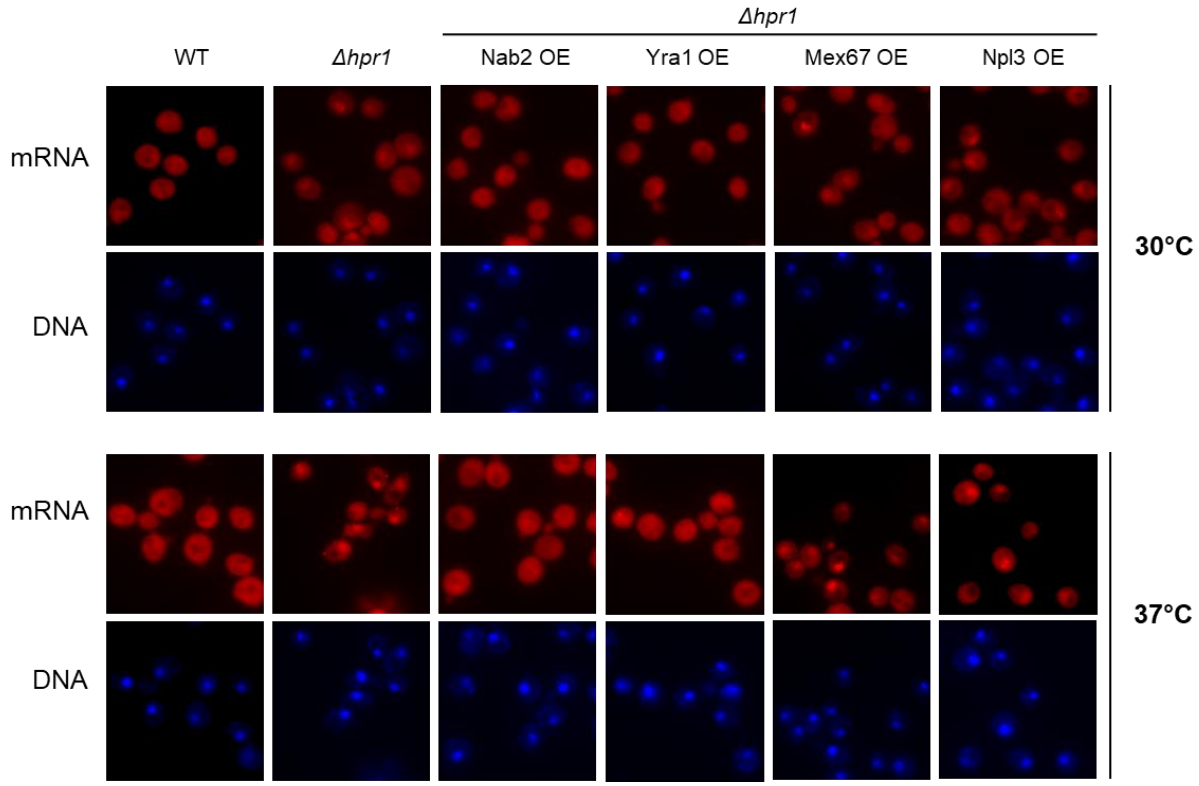

Figure 23. Nuclear mRNA export defect in *Δhpr1* cells is suppressed by overexpression (OE) of Nab2 or Yra1, but not Mex67 or Npl3. mRNA export is visualized via fluorescence *in situ* hybridization (FISH) at 30 and 37°C. mRNA was detected by oligo(dT)50 coupled to a Cy3-fluorecent dye. DNA was stained with DAPI.

6.2.8. Overexpression of Nab2 or Yra1 suppresses growth defect of Δ*hpr1* strain

Since overexpression of Nab2 or Yra1 suppress mRNA export defect in Δ*hpr1* strain, dot spot assay was performed to check if it also restores impaired growth. In accordance with mRNA export results, overexpression of Nab2 and Yra1 were able to suppress the heat-sensitive phenotype of Δ*hpr1* cells at 37°C, as well as its growth defect at 30°C (Fig. 24). Despite the fact that overexpression of Mex67 and Npl3 in Δ*hpr1* cells does not have an impact on mRNA export, these cells grow slightly better at 37°C than Δ*hpr1* cells without overexpression. Perhaps, this effect is not associated with mRNA export, but some other process in the cell. Interestingly, at 16°C overexpression of Yra1 suppresses cold-sensitive phenotype of Δ*hpr1*, while

overexpression of Nab2 has very subtle effect on growth. A similar effect is also observed for 25°C, where Δ*hpr1* cells overexpressing Yra1 grow faster than cells overexpressing Nab2. It can suggests different mechanism of suppression by Yra1 and Nab2 at 16°C and 25°C, or stronger influence of Yra1 overexpression on the cell growth.

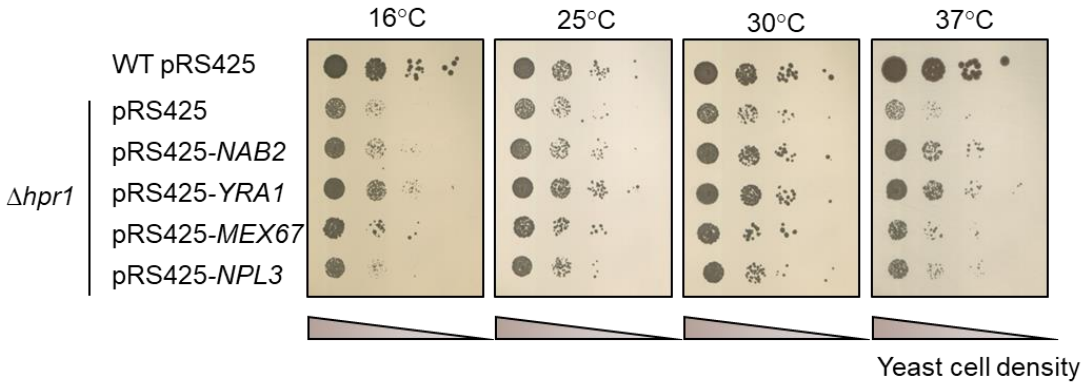

Figure 24. Growth defect of Δ*hpr1* cells is suppressed by overexpression of Nab2 or Yra1. Dot spot growth assay of WT, Δ*hpr1* cells and Δ*hpr1* cells overexpressing Nab2, Yra1, Mex67 and Npl3. Serial dilutions of cells were spotted onto SDS (-Leu) plates. Cells were grown for 2 days at 25°C, 30°C and 37°C or for 6 days at 16°C.

6.2.9. Overexpression of Nab2 or Yra1 leads to increase of Nab2 and decrease of Mex67 in nuclear mRNPs

To understand how overexpression of Nab2 and Yra1 suppresses the mRNA export defect of Δ*hpr1* cells, mRNP composition in these cells was assessed. Since Mex67 and Npl3 overexpression did not improve mRNA export defect in Δ*hpr1* strain, it was also important to investigate if they affect mRNP composition at all. As described before, nuclear mRNPs were enriched via Cbc2-TAP and levels of co-purified proteins were determined by Western blot (Fig. 25A). Interestingly, changes in protein level can be already observed in lysates (Fig. 25B, upper panel). In comparison to the WT, deletion of *HPR1* leads to increase of Nab2 and Yra1 in lysate. Overexpression of Nab2 in Δ*hpr1* cells leads to a further increase in the amount of Nab2 and Yra1 in the lysate. And *vice versa*, Yra1 overexpression in Δ*hpr1* cells results not only in increase of Yra1 levels, but also of Nab2 levels. These changes suggest a close interrelation between Nab2 and Yra1, particularly in the cells lacking *HPR1*.

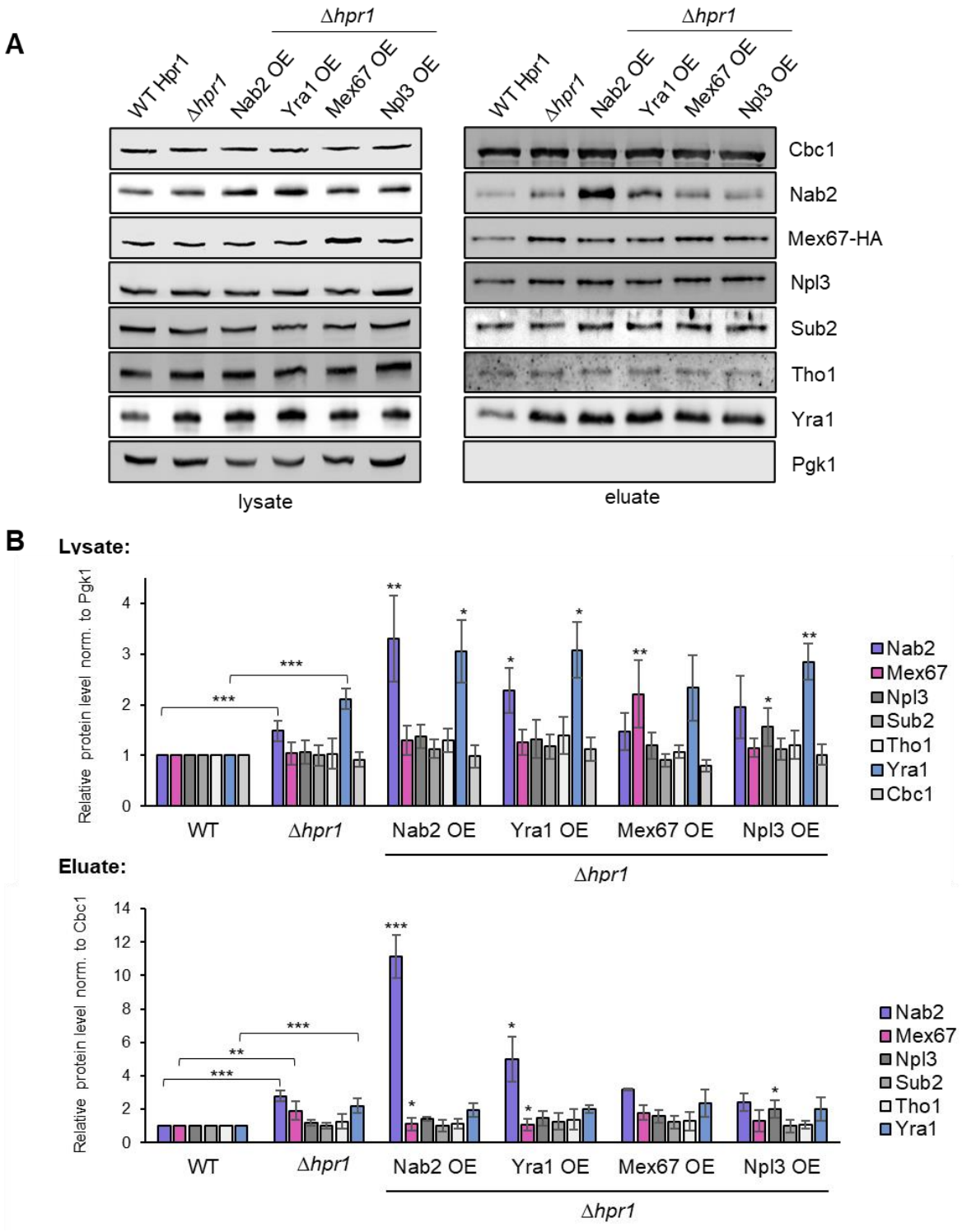

Figure 25. Overexpression of Nab2 or Yra1 in *Δhpr1* cells leads to increased amount of Nab2 and decreased amount of Mex67 in nuclear mRNPs. (A) Protein levels determined by Western blot with antibodies against respective protein in lysate (left) and TEV eluates (right). **(B)** Quantification of the protein levels in lysates (upper panel) and TEV eluates (lower panel). Protein levels were quantified with ImageJ and normalized to the signal of Pgk1 for lysates and to the CBC subunit Cbc1 for TEV eluates. Protein levels for WT cells were set to 1 (bars represent mean ± SD; Student's t-test, *** p≤0.001; ** p≤0.01; * p≤0.05; asterisks with brackets represent comparison between WT and *Δhpr1* cells, asterisks without brackets represent comparison to *Δhpr1* cells).

In comparison to the Δ*hpr1* strain itself, overexpression of Mex67 in Δ*hpr1* cells does not influence the amount of other tested RBPs in the lysate. Interestingly, overexpression of Npl3 in Δ*hpr1* cells also causes a slight increase of Yra1 in comparison to the lysate of Δ*hpr1* cells.

Analysis of TEV eluates, i.e. enriched nucear mRNPs, demonstrates specific changes in composition of nuclear mRNPs (Fig. 25B, lower panel). It was shown above that deletion of *HPR1* results in increased level of Nab2, Yra1 and Mex67, but not Npl3 in nuclear mRNPs (Fig. 20C-D). In case of overexpression of Nab2 in Δ*hpr1* cells, even more of Nab2 is incorporated into mRNPs, while Mex67 levels decrease (Fig. 25B, lower panel). Surprisingly, overexpression of Yra1 does not lead to incorporation of more Yra1 into mRNPs, but to increased amount of Nab2 and decreased level of Mex67. This is fascinating, because overexpression of Nab2 or Yra1 restores the nuclear mRNA export in Δ*hpr1* cells and causes similar changes in nuclear mRNPs. Moreover, the observed increase of Nab2 amount in nuclear mRNPs upon Yra1 overexpression might indicate that Yra1 recruits more Nab2 to the mRNPs. This Nab2 increase seems to be specific and, likely, it is not an artifact of the increase observed in lysate, since higher level of Yra1 in the lysate does not result in an increased abundance of Yra1 in nuclear mRNPs.

Mex67 overexpression in Δ*hpr1* cells does not change mRNP composition: even though there is more of Mex67 in the lysate, in TEV eluates levels of all tested RBPs remains the same as in Δ*hpr1* cells without overexpression (Fig. 25B). This could explain the absence of an effect of Mex67 overexpression on the impaired mRNA export in Δ*hpr1* cells (Fig. 23). This also illustrates, how exquisitely mRNA export is regulated – more of the mRNA exporter Mex67 does not mean improved mRNA export. On the contrary, Mex67 level is decreased to the WT level within mRNP upon Nab2 or Yra1 overexpression in Δ*hpr1* cells. It suggests that excess of Mex67 either leads to impaired mRNA export or it is a response on nuclear mRNA retention.

6.2.10. Yra1 overexpression in Δ*hpr1* cells leads to increased occupancy of Yra1 and Nab2 at transcribed genes

Since overexpression of Yra1 in Δ*hpr1* results in increased level of Nab2 composing the mRNP, it suggests that Yra1 recruits more of Nab2 to the mRNP. To check if this

recruitment takes place already co-transcriptionally, chromatin immunoprecipitation experiments were performed.

Upon Nab2 overexpression in Δ*hpr1* cells, its occupancy was not changed for almost all tested transcripts, and for two of them it even showed a decreased level (Fig. 26A). This suggests that the observed increase of Nab2 in nuclear mRNPs occurs post-transcriptionally with loading more of Nab2 onto the mRNP.

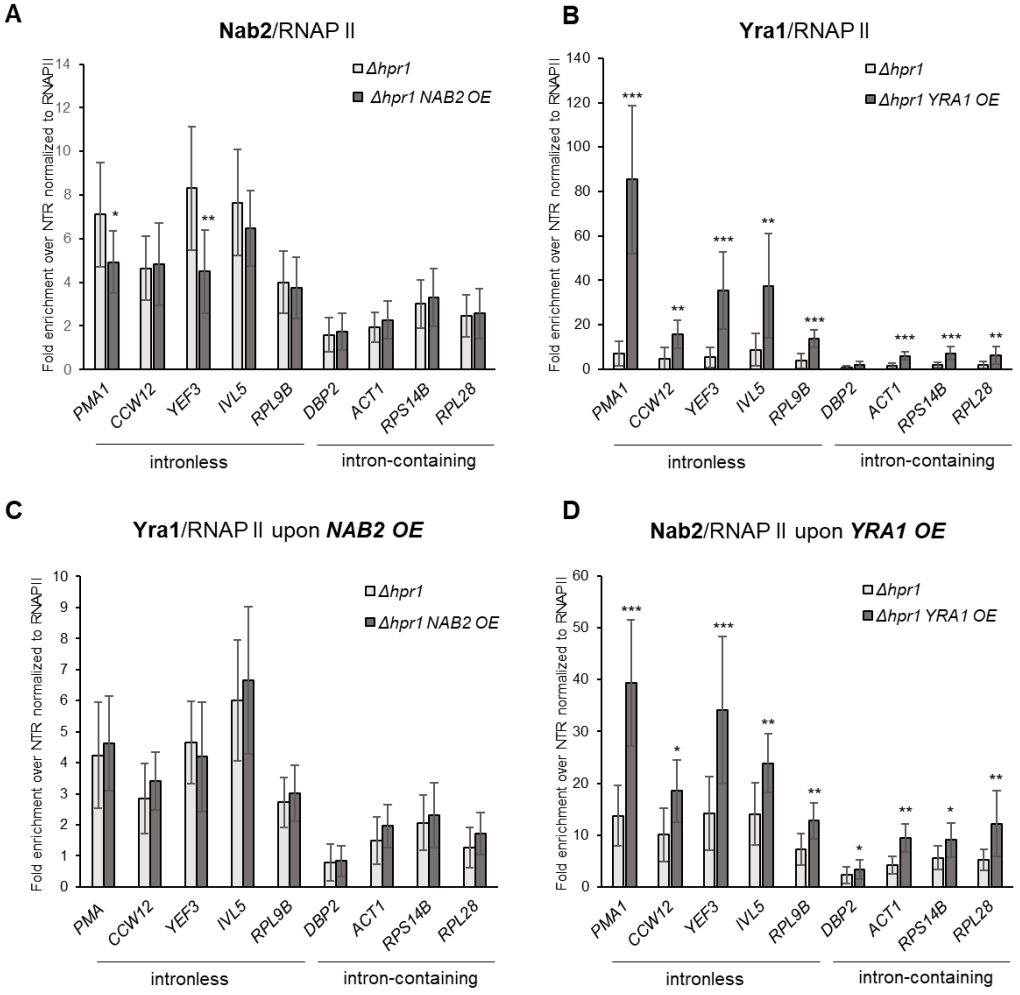

Figure 26. Overexpression of Yra1 in Δ*hpr1* cells results in increased occupancy of Yra1 and Nab2 at the genes. (A) Occupancy of Nab2 in Δ*hpr1* cells does not change upon Nab2 overexpression. **(B)** The occupancy of Yra1 in Δ*hpr1* cells increases upon Yra1 overexpression. **(C)** The occupancy of Yra1 in Δ*hpr1* cells remains unchanged upon Nab2 overexpression. **(D)** The occupancy of Nab2 in Δ*hpr1* cells increases upon Yra1 overexpression. The protein occupancy was assessed by ChIP. Obtained enrichments were calculated over non-transcribed region (NTR) and normalized to RNAPII occupancy level of the respective strains. Level of RNAPII was unchanged for compared samples (data not shown) (bars represent mean ± SD; Student's t-test; *p<0.05; **p<0.01; *** p<0.001). Experiments (A) - (C) were performed by Salome Barbakadze.

In case of Nab2 overexpression, Yra1 occupancy at represented genes also remained unchanged (Fig. 26C). Yra1 overexpression in Δ*hpr1* cells leads to increased occupancy of Yra1 at the genes (Fig. 26B). Interestingly, Nab2 occupancy is also increased by Yra1 overexpression in Δ*hpr1* cells (Fig. 26D). Perhaps, upon overexpression Yra1 recruits more Nab2 to the genes co-transcriptionally for its further loading onto nuclear mRNPs. Likely, in case of sufficient amount of Nab2 upon its overexpression, assistance of Yra1 for loading Nab2 onto mRNP is not needed.

6.2.11. Suppression of the mRNA export block or growth defect in Δ*hpr1* cells is not associated with polyadenylation of RNA

Based on the data above, impaired mRNA export and growth of Δ*hpr1* cells are restored, when more of Nab2 is incorporated into mRNPs. To find the mechanism in which excess of Nab2 can suppress the nuclear mRNA export defect, a number of potential hypotheses were tested. Nab2 is a protein especially important for regulation of poly(A) tail length (Hector et al., 2002). To check, if overexpression of Nab2 overcomes nuclear mRNA retention by regulating RNA polyadenylation, poly(A) tail lengths for bulk mRNA were assessed. The 3' ends of total RNAs, extracted from respective yeast strains, were radioactively labeled. Non-poly(A) RNAs were digested, and undigested poly(A) tails were separated by Urea PAGE (Fig. 27A). As a positive control, thermosensitive *mex67-5* cells were used, which display elongated poly(A) tails after shift to 37°C (Estruch et al., 2012). Indeed, for *mex67-5* control strain, poly(A) tails are noticeably longer after cells were shifted from 30°C to 37°C for 1 hour (Fig. 27B, lane 7 cf. 14). However, for the Δ*hpr1* strain and Δ*hpr1* with Nab2,Yra1, Mex67 or Npl3 overexpression there is no such prominent difference in the length of poly(A) tails as in *mex67-5* cells (Fig. 27B, lanes 1 - 6 for cells grown at 30°C, lanes 8 - 13 for 37°C). Potentially, there could be changes in poly(A) tail length, which were not visualized because of the limitation of the method. Furthermore, only some transcripts might have a different poly(A) tail length, but not bulk mRNA. To determine this, extension poly(A) test (ePAT) assay was applied (Jänicke et al., 2012). Here, the length of the poly(A) tails of individual transcripts is determined by using anchor primer for reverse transcription, followed by subsequent gene-specific PCR (Fig. 27C).

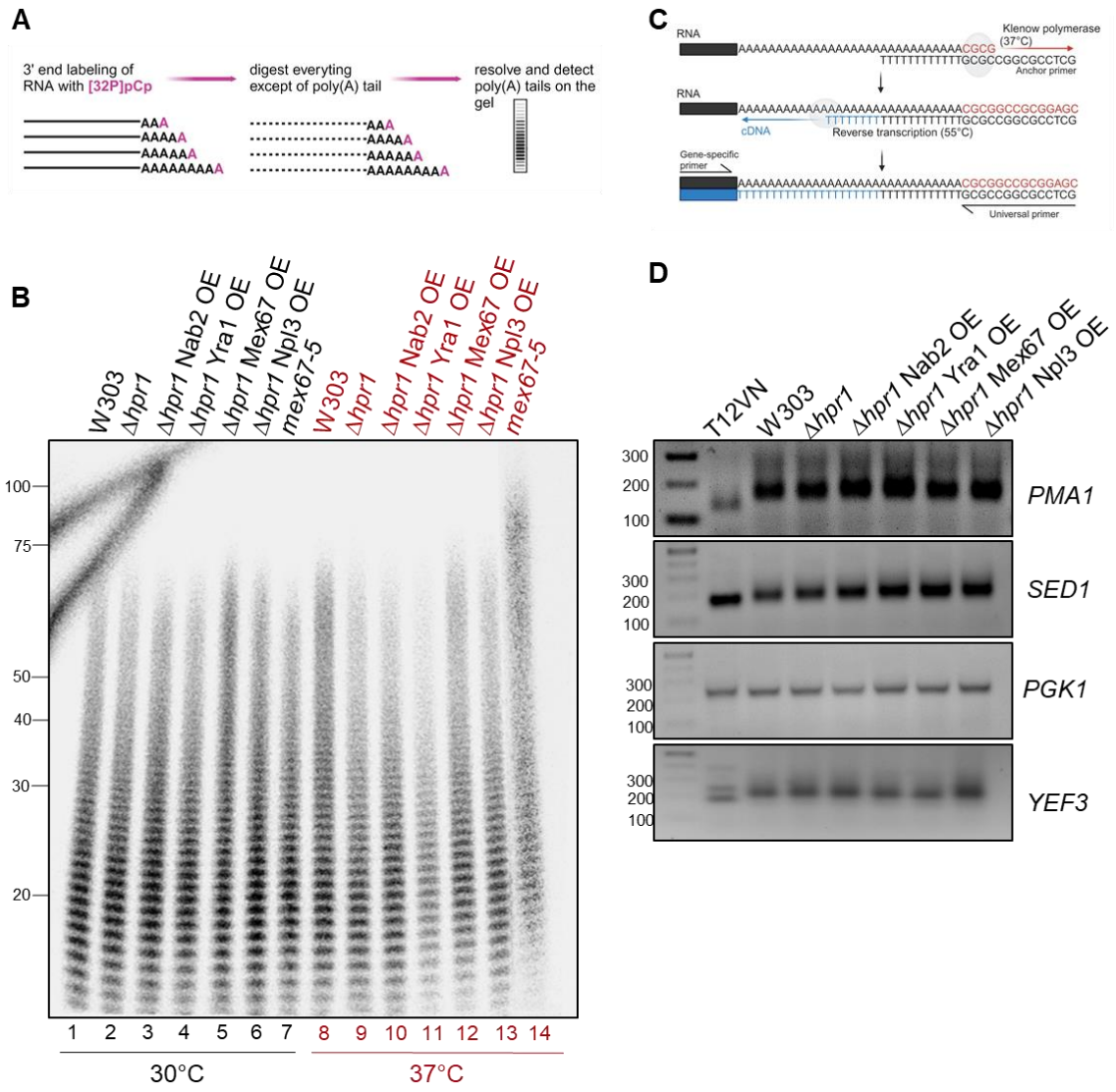

Figure 27. Length of poly(A) tails does not change in *Δhpr1* cells and in *Δhpr1* cells with overexpression of Nab2, Yra1, Mex67 or Npl3. (A) Scheme of poly(A) tail assay for bulk mRNA. Total RNA was extracted and labelled at the 3' end with [32P]pCp. The RNA was treated with an RNase mix to digest all RNA except of poly(A) tails. The poly(A) tails were separated by Urea PAGE and visualized by phosphor imaging. Scheme is modified after (Nousch et al., 2013). **(B)** Bulk poly(A) tail length of *Δhpr1* cells without and with overexpression (OE) of Nab2, Yra1, Mex67 or Npl3. Poly(A) tails from the respective strains grown at 30°C (black) or shifted for 1 h to 37°C (red), radioactively labeled and separated on 20% PAA Urea PAGE. RNA size is specified on the left side of the gel (20-100 nt). **(C)** Scheme of ePAT assay for individual transcript modified after (Jänicke et al., 2012). **(D)** Poly(A) tail length for individual transcripts. Total RNA was extracted, annealed with an anchor primer and extended with Klenow polymerase. RNA was reverse transcribed at 55°C to avoid internal priming. Obtained cDNA was amplified with transcript-specific primer. For T12VN size control, no extension by Klenow polymerase was done, but reverse transcription with T12VN primer, that was anchored to the poly(A) site. This results in a product with a 12-adenosine tail. Obtained PCR products were separated on 2.5% agarose-TBE gel. DNA ladder sizes (100-300 nt) are indicated on the left side of the gel.

As transcripts of interest, two highly transcribed transcripts, *PMA1* and *YEF3*, that have increased RNA-binding activity of Nab2 in RNA immunoprecipitation experiments in Δ*hpr1* cells (Fig. 21B) were chosen. Additionally, two other mRNAs, *SED1* and *PGK1*, that were reported to be hyperadenylated in the absence of Nab2 (Hector et al., 2002) were tested. The T12VN primer was used as a size control for the product with 12 adenosines tail. The 2 variable nucleotides VN (V is A, G, or C, and N is any base) tether this primer to the polyadenylation site (Beilharz & Preiss, 2009). Obtained PCR products were examined for the shift for longer or shorter poly(A) tail. However, a clear shift is not observed for Δ*hpr1* strain in comparison to the WT for all tested transcripts (Fig. 27D). Overexpression of Nab2 or Yra1 also does not affect poly(A) tail length of these four representative transcripts. Likely, overexpression of Nab2 or Yra1 suppresses the nuclear mRNA export defect in Δ*hpr1* strain using a mechanism that does not dependent on the poly(A) tail length of mRNAs.

6.2.12. Overexpression of Nab2 or Yra1 in Δ*hpr1* cells is unrelated to R-loops or transcription termination

Deletion of *HPR1* is associated with increased genomic instability and formation of harmful R-loops. R-loops are three-stranded structures that consist of a DNA-RNA hybrid and a displaced single-stranded DNA. They contribute to genetic instability by impairing transcription elongation (Huertas & Aguilera, 2003). Some RBPs resolve R-loops, for instance overexpression of Tho1 in Δ*hpr1* strain leads to decreased level of R-loops (Miosga, 2022). To test the hypothesis that effect of Nab2 or Yra1 on mRNA export in *Δhpr1* strain could be explained by R-loop resolution, an R-loop assay was performed with respective strains (Fig. 28). For Nab2, Yra1 and Mex67 overexpression in *Δhpr1* strain, no significant difference in comparison to *Δhpr1* cells was observed. Remarkably, overexpression of Npl3 was able to slightly decrease R-loop levels in *Δhpr1* strain (Fig. 28B). Interestingly, *Δnpl3* cells were reported to have R-loop mediated transcription-dependent instability (Santos-Pereira et al., 2013). This suggests that Npl3 is another RBP potentially involved in R-loop prevention. Overall, these results propose that mechanism of restored mRNA export by Nab2 or Yra1 overexpression in Δ*hpr1* cells is independent of R-loop resolution.

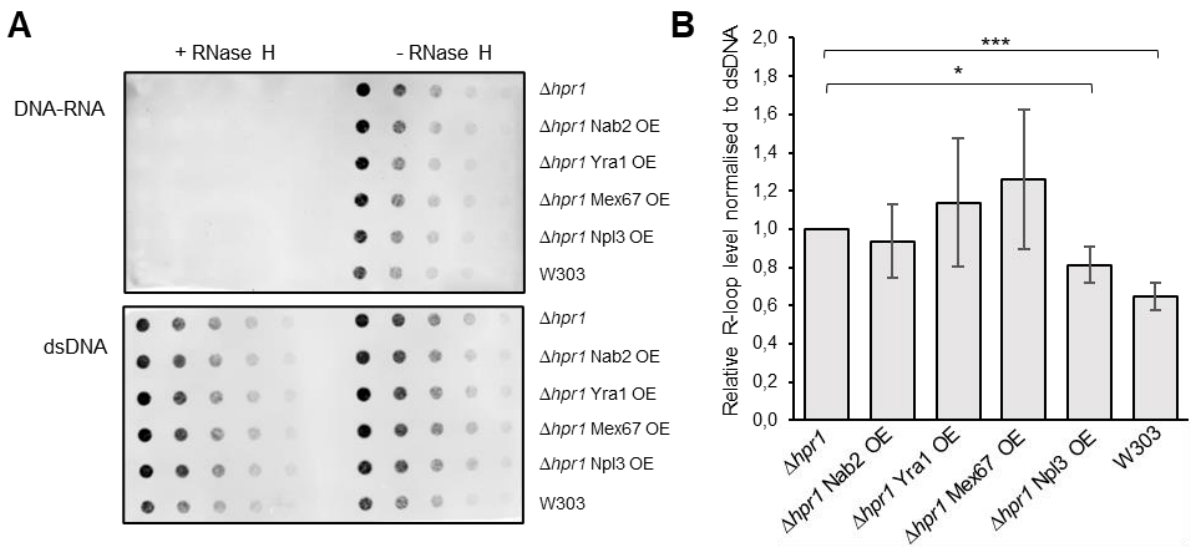

Figure 28. R-loop level in *Δhpr1* strain is not affected by overexpression of Nab2, Yra1 or Mex67, but Npl3. (A) Serial dilutions of genomic DNA from respective strains were spotted and UV-cross-linked to a positively charged membrane, followed by incubation either with an antibody S9.6 against DNA-RNA hybrid for R-loop visualization, or an antibody against dsDNA as a loading control. Specificity of the S9.6 antibody was confirmed by treatment of the samples with RNase H. **(B)** Level of R-loops was quantified with ImageJ and normalized to dsDNA. The R-loop level for *Δhpr1* cells was set to 1 (bars represent mean ± SD; Student's t-test, ** p≤0.01; * p≤0.05).

To check another potential mechanism of mRNA export block suppression, it was important to investigate transcription termination. Hpr1, as a part of the THO/TREX complex, is important for transcription elongation but also termination. Interestingly, it has been reported that Nab2 depletion leads to a genome-wide transcriptional readthrough (Alpert et al., 2020). To assess if deletion of *HPR1* causes transcriptional readthrough and if Nab2 overexpression can suppresses it, RT-qPCR was performed. The transcriptional readthroughs were determined using primers downstream the 3' UTR and normalized to the expression level of representative transcripts (Fig. 29A). Choice of target transcripts *UBC9*, *DTD1* and *RPL2A* was made based on transcripts with transcriptional readthrough caused by Nab2 depletion (Alpert et al., 2020). Transcript *VHR2* was included, since it exhibits transcription readthrough in *Δnpl3* cells (Holmes et al., 2015). Quantification of readthrough and its normalization to the gene body level revealed that *RPL2A* and *VHR2* have longer transcripts in *Δhpr1* cells, but this defect is not suppressed by overexpression of Nab2, Yra1, Mex67 or Npl3 (Fig. 29B).

Indeed, for some individual transcripts deletion of *HPR1* can lead to transcriptional readthrough and results in longer transcripts. However, this transcription termination defect is not a mechanism to suppress mRNA export defect in *Δhpr1* strain.

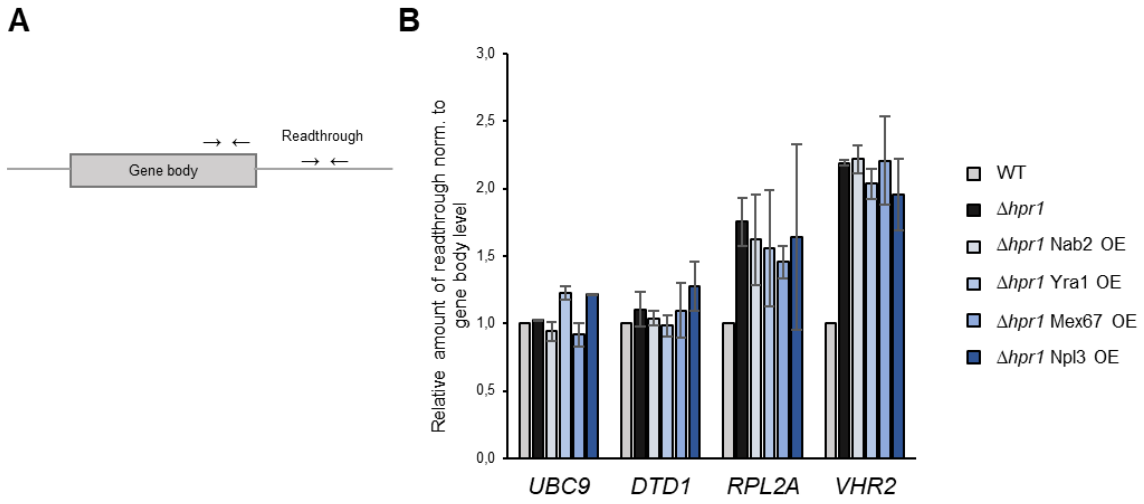

Figure 29. Transcriptional readthrough is observed for some transcripts in *Δhpr1* cells, but it is not suppressed by overexpression of Nab2, Yra1, Mex67 or Npl3. (A) Scheme of primer positions to detect readthrough and normalize it to the number of transcripts (primers in gene body). **(B)** Amount of longer transcripts with transcriptional readthrough was determined by RT-qPCR and normalized to the gene body level. WT level was set to 1 (bars represent mean ± SD).

6.2.13. Deletion of *NUP60* leads to the similar changes of mRNP composition as deletion of *HPR1*

As shown above, nuclear mRNPs have higher level of Mex67 in Δ*hpr1* cells with defective mRNA export, while decrease of Mex67 to the WT level upon Nab2 or Yra1 overexpression suppresses the mRNA export defect in Δ*hpr1* cells (Fig. 25B). Perhaps, the observed increase of Mex67 in Δ*hpr1* cells (Fig. 20C-D) is not a mechanism to compensate defective mRNA export, but a cause or consequence of mRNA retention in the nucleus.

To check if high levels of Mex67 can promote the mRNA export block, WT cells were transformed with plasmids overexpressing Mex67 and its cofactor Mtr2. However, overexpression of Mex67-Mtr2 does not lead to higher Mex67 levels in nuclear mRNP, and therefore it does not affect mRNA export (Appendix Fig. 8).

Since it was not possible to “force” Mex67-Mtr2 into mRNPs by overexpression, it was decided to check mRNP composition in other strains with defective mRNA export. If increased levels of Mex67 observed in Δ*hpr1* cells is a cause of the nuclear mRNA retention, then it might also be detected for other strains that show an mRNA export defect. To assess it, Cbc2-TAP purification of nuclear mRNPs in cells with deleted *NUP60* or *NUP1* was performed. Nup60 and Nup1 are FG-nucleoporins located on the nucleoplasmic side of the NPC. Deletion of *NUP60* or *NUP1* leads to accumulation of poly(A)+ RNA in the nucleus (Fischer et al., 2002). Deletion of *NUP1* has no effect on mRNP composition (Fig. 30). Therefore, it is important to verify if Δ*nup1* strain indeed has mRNA export defect as it was reported before.

Interestingly, deletion of *NUP60* leads to increased levels of Nab2, Yra1 and Mex67 in nuclear mRNPs (Fig. 30B, right panel). This is similar to the changes observed in Δ*hpr1* cells (Fig. 20C-D). Moreover, identically to the Δ*hpr1* cell lysate, Nab2 and Yra1 were also increased in Δ*nup60* cell lysate (Fig. 30B, left panel).

Overall, increased levels of Mex67, Nab2 and Yra1 might be a specific response to deletion of one of the components of the mRNA export pathway associated with nuclear mRNA retention. This would explain why deletion of *HPR1* (involved in early steps of mRNA export) results in similar mRNP composition as deletion of *NUP60* (later steps of mRNA export).

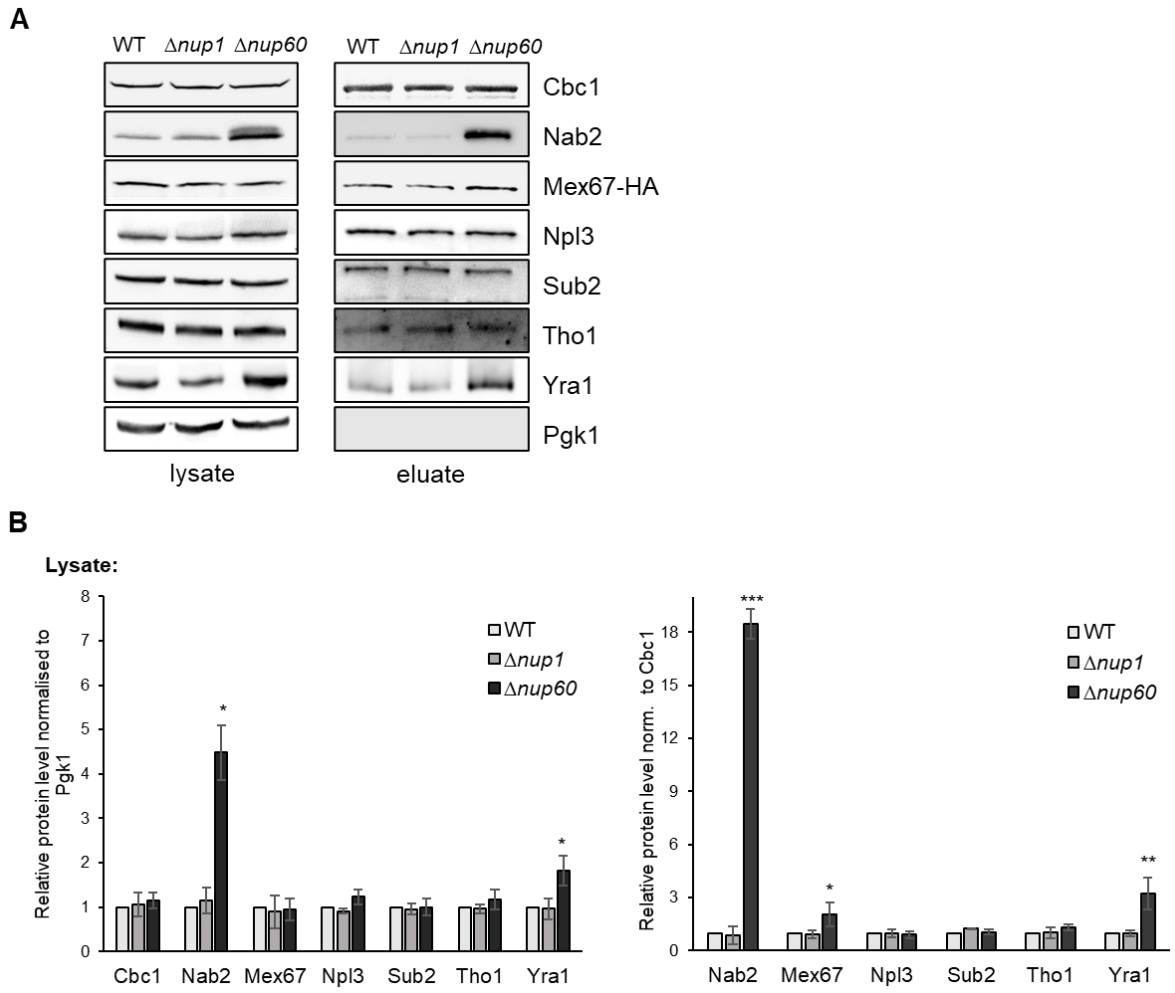

Figure 30. Deletion of *NUP60* leads to the similar mRNP composition changes as deletion of *HPR1*. (A) Representative RBPs in lysates and TEV eluates in WT, *Δnup1* and *Δnup60* strains. Proteins enriched in Cbc2-TAP purification were detected by Western blotting with antibodies against the indicated RBPs. **(B)** Protein levels in lysates (left panel) and TEV eluates (right panel) were quantified with ImageJ, normalized to the signal of Pgk1 (for lysates) or to the signal of the CBC subunit Cbc1 (for eluates) and set to 1 for WT cells (bars represent mean ± SD; Student's t-test, *p<0.05; **p<0.01; ***p<0.001).

7. Discussion

7.1. Structure of a transcript-specific nuclear mRNP

The first aim of this study was to purify a specific nuclear mRNP from *Saccharomyces cerevisiae* under native conditions and determine its structure by electron microscopy. Up to date, mRNP architecture is poorly investigated. Only few studies purified and visualized a pool of nuclear mRNPs (Batisse et al., 2009; Bonneau et al., 2023; Pacheco-Fiallos et al., 2023). Moreover, there are no reported structural studies of native transcript-specific mRNPs, which would be crucial for understanding the structure and stoichiometry of different mRNPs.

This study provides a comparison of RNA-centric approaches to isolate highly-transcribed nuclear mRNP of *CCW12* in two-step affinity purification. In the first step all nuclear mRNPs were enriched via Cbc2-TAP. Optimization of the first step of purification reduced the isolation time by 2 hours as well as increased yield of *CCW12* mRNPs. After Cbc2-TAP purification step, TEV eluates enriched with all nuclear mRNPs, were used for the second step of *CCW12* isolation via RNA-centric approaches. Purification protocols were established and optimized to improve purification yield and specificity as well as to preserve the structure of target mRNPs. Obtained results demonstrates that aptamer-based approaches using the MS2 or Mango system can be used to purify specific nuclear *CCW12* mRNPs in sufficient amount to visualize the particles by electron microscopy.

7.1.1. ASO-based purification specifically enriches *CCW12* RNA, but not native mRNPs

The ASO-based methods were used before to analyze the protein interactome of specific RNAs by mass spectroscopy or to isolate cross-linked protein-RNA complexes (Chu, Zhang, Da Rocha, et al., 2015; West et al., 2014; Yoon & Gorospe, 2016). This study aimed to purify endogenous mRNPs with ASOs under native conditions for detection by electron microscopy.

Important criterion for ASO-based purification was the type of ASO. First generation DNA ASOs have been reported for purification of c-Myc mRNA and its interacting proteins in a K562 human cell line (Spiniello et al., 2019). However, in our study,

DNA ASOs does not enrich the target *CCW12* (Fig. 11E). Either DNA ASO cannot affectively anneal to *CCW12* or its annealing leads to *CCW12* degradation by cellular RNase H.

The second generation 2'-OMe-RNA ASO provides specific purification of *CCW12* mRNA in higher yield than the third generation LNA ASOs (Fig. 11B). However, Δ*ccw12* negative control revealed non-specific protein binding of ASOs (Fig. 9C). Non-specific protein binding was reported before for the first generation phosphorothiolates ASO (Hyjek-Składanowska et al., 2023). However, second and third generations – 2'-OMe and LNA ASOs – also show non-specific protein binding in our study. This non-specific protein binding can be explained by electrostatic interaction between negatively charged ASOs and positively charged residues of proteins. Furthermore, RBPs might have predisposition to bind these RNA ASOs independently of sequence specificity. Applying competitor binders (BSA or tRNA) does not reduce the non-specific protein binding (Appendix fig. 3B, D). Moreover, using random RNA ASO as competitor also fails to decrease the non-specific protein binding (Johanna Seidler, unpublished).

A critical point for ASO-based purification was the amount of the oligonucleotides. The optimal 100 pmol ASO amount provides the highest mRNA yield. Increasing the amount to 200, 300, 600 and 1200 pmol leads to a gradual decrease of *CCW12* yield, but increase of protein signal for the most of represented RBPs (Fig. 10). Perhaps, unbound fraction of the ASO binds single RBPs.

Despite the optimization of ASO purification, non-specific protein binding remained to be its major pitfall. If ASOs would bind both, mRNP and single RBPs, it would not interfere with electron microscopy. In this case mRNPs can be distinguished from the single-protein background. It might be, that the protein enrichment is so low, that differences for Δ*ccw12* control and *CCW12* are not detectable by Western blot. However, for upscaled purification (from 2 L yeast culture to 24 L) protein signals remained unspecific (Fig. 12A, B). Examination of the native eluates with electron microscopy showed no detectable compact particles. Some elongated structures were observed (Fig. 12C). It could be either disassembled particles or some debris. Perhaps, ASO binding can lead to disruption of mRNPs. This coincide with the observation, that ASOs bind RNAs with high specificity, but fail to specifically co-enrich RBPs. It is also possible that ASOs do not disassemble the mRNPs, but the

sample preparation for electron microscopy affects the particle structure. According to (Bonneau et al., 2023), isolated nuclear mRNPs were not detected by cryo-EM. Instead, only the long fibers were visible, which could represent single RNAs. Only switching the visualization method to cryo-electron tomography (cryo-ET) resulted in detectable compact particles (Bonneau et al., 2023). While compacted yeast mRNP particles expected to be around 30 nm, the 1000 nt long linear RNA has a size of around 340 nm (Batisse et al., 2009). The mRNA of interest *CCW12* consists of 507 nucleotides. Therefore, structures about 120 nm in size, observed in the native eluates, are either unfolded RNAs disrupted by ASOs or some unrelated debris.

Taken together, it was demonstrated that ASOs can be used to specifically isolate RNA of interest, but is not suitable for purification of native mRNPs. However, its high hybridization potential can be used for isolation of mRNPs stabilized by crosslinking.

7.1.2. Purification of *CCW12* mRNP via Mango or MS2 aptamer results in detectable particles

As an alternative approach, aptamer-based purifications were used to isolate *CCW12* mRNP. First attempts of the purifications were done with streptavidin-binding 4xS1m aptamer integrated in the 3' UTR of *CCW12*. This aptamer showed promising results for *in vitro* purifications of RNA-protein complexes (Leppek & Stoecklin, 2014). However, in our purification of endogenous mRNPs, the yield of *CCW12-4xS1m* purification was very low (data not shown). Since the amount of particles is essential to obtain the mRNP structure, more efficient aptamer systems were required. Mango aptamer was originally developed to label and visualize RNA upon its binding with fluorophore ligand thiazole-orange (TO1) (Dolgosheina et al., 2014). Coupling TO1 with desthiobiotin (Dtb) enables the usage of this ligand for isolation of RNAs. While the ASO method does not require any manipulation of the mRNA, position of aptamer insertion can interfere with RNA structure and affect the purification. Insertion of Mango aptamer in 3' UTR of *CCW12* mRNA did not have any destabilization effect on *CCW12* mRNA level or cell growth (Fig. 13, B, C). It seems that in these cases the aptamer integration does not interfere with *CCW12* functions in the cells.

Purification via Mango aptamer provided specific enrichment of *CCW12* mRNA (Fig. 13E). Notably, some non-specific protein binding of TO1-Dtb was observed in a non-tagged *CCW12* control (Fig. 14D). On the contrary to the ASO-based method, a clear

difference in protein signal between *CCW12* control and *CCW12-Mango* was observed. Upscaling *CCW12-Mango* purification from 2 L to 24 L of yeast culture resulted in a 5-fold increase in enrichment of *CCW12-Mango* mRNA (Fig. 15A), as well as an increase in protein level for most of the represented proteins (Fig. 15B).

Using another aptamer MS2 and its ligand MS2-coat protein (MCP) was also successful for isolation of *CCW12-MS2* mRNPs. In this case, upscaling to 24 L led to an over 3 times increase in enrichment of *CCW12* mRNA (Fig. 16B). Furthermore, co-enriched protein level was specific and the best among the all implemented methods (Fig. 16C).

Purification yield is crucial for low abundant transcript-specific mRNP. The upscaling of *CCW12-MS2* and *CCW12-Mango* resulted in a significant 3 - 5 times increase of the particle count in the native eluates. For electron microscopy a certain amount of particles is required. The absolute values of *CCW12* were calculated using a defined amount of linearized *CCW12*-bearing plasmid for qPCR (Johanna Seidler, unpublished data). The quantification suggests, that the lysate from 2 L culture contained 2.44 pmol of *CCW12* (1471 x 10^9 copies), while the respective TEV eluate, enriched with nuclear mRNPs, had 0.28 pmol (170 x 10^9 copies). Hence, in the TEV eluate there are around 10% of lysate *CCW12*. Likely, most of *CCW12* in the lysate are cytoplasmic. The final native eluate enriched in transcript-specific mRNP from 2 L cultures had around 0.0002 pmol of *CCW12*. Upscaling of Mango or MS2-based purification to 24 L cultures increased it up to 0.001 pmol (0.57 x 10^9 copies) of specific mRNP in 100 µL of eluate. The amount of particles seems to be sufficient for detection. For instance, suggested limitation for electron microscopy of a 65 nm virus is 10^7 particles/mL (Blancett et al., 2017). Therefore, the 12x upscaling of the purifications is supposed to provide enough particles for the detection by electron microscopy.

Indeed, negative staining of native eluates resulted in detectable particles for both, *CCW12-Mango* (Fig. 15C) and *CCW12-MS2* (Fig. 16E) purifications. For comparison, the TEV eluate with the whole pool of nuclear mRNPs was visualized with electron microscopy. In the TEV eluate particles were compact and had around 28 nm in size (Fig. 16D). This coincides with the expected size of yeast mRNPs purified before via Nab2-TAP using GraFix method (Batisse et al., 2009). GraFix includes sucrose gradient centrifugation with glutaraldehyde cross-linking. Particles, obtained by

GraFix, had a size range of 15 - 35 nm and elongating shape. For our study, some of nuclear mRNPs in the TEV eluate were looking more globular, others were slightly elongated. Since it is a mix of different nuclear mRNPs, they can have more elongated shape in case of longer mRNA within a particle.

Since purified *CCW12* mRNA and its associated proteins were specifically enriched via Mango or MS2 aptamers, observed particles are expected to be *CCW12*-containing mRNPs. However, examination of the native eluates revealed that obtained particles does not look uniform (Fig. 15C, 16E). Differences in shape might indicate that RBPs dissociate and need to be stabilized with mild crosslinking before negative staining and microscopy. If it does not result in the expected uniformity, the particles need to be stabilized during the purification. For instance, they could be crosslinked in the TEV eluate, where particles were still very compact and uniform. To avoid a decrease of purification yield, only mild cross-linking has to be applied. The particle amount is a critical criterion for this study. This is the reason why the described GraFix method (Batisse et al., 2009) is not favorable for this research. Gradient centrifugation leads to a loss of material and cross-linking is associated with a decrease of purification yield.

To prove that purified particles are indeed the *CCW12* mRNPs, immunogold labeling can be used. For instance, immunogold-labeled antibody against MS2-coat protein (MCP) (ligand of MS2 aptamer) can be applied. Moreover, this labeling can visualize *CCW12-MS2* already in TEV eluates, where particles are desirably compact. However, the TEV eluate is a mixture of different nuclear mRNPs. To increase a chance to detect transcript-specific *CCW12*, it has to be overexpressed. Unfortunately, immunogold labeling cannot be exclusively used for *CCW12-Mango*, as its ligand is not a protein, but the small molecule TO1-Dtb. Therefore, only RBPs could be labeled, but they are considered to be the same for all mRNPs.

Our study focused on the isolation of transcript-specific mRNPs in *S. cerevisiae*. Another recent study reports the structure of human TREX complex together with compact globular mRNPs (Pacheco-Fiallos et al., 2023). These human mRNPs were larger (around 45 nm), had a globular uniform core and were covered on their surface with three TREX complexes. However, isolated yeast nuclear mRNPs did not have TREX complex on their surface (Bonneau et al., 2023). Observed differences between human and yeast mRNPs can be either species-determined or caused by

different sample preparations. For human TREX-mRNP isolation, cross-linking and treatment with nuclease was used to obtain separated particles on the grid (Pacheco-Fiallos et al., 2023). However, such manipulations could interfere with mRNP structure. Additionally, observed difference could reflect different biogenesis stages of mRNPs. Purification via THO/TREX components would represent earlier stages of mRNP formation, whereas TREX is thought to disassociate from mRNPs before they are directed to the export.

Taken together, this study shows that Mango and MS2 aptamer provides efficient purification of transcript-specific *CCW12* mRNP in sufficient amount for detection by electron microscopy. Visualized particles have an expected size of around 28 nm. Furthermore, observed particles will be stabilized by cross-linking and examined via cryo-EM or cryo-ET and cross-linking mass spectrometry. Advanced mRNP structure and stoichiometry still needs to be discovered, but the possibility to isolate transcript-specific mRNPs is a big step in this complex process. It can help to understand the differences between different transcript-specific mRNPs within one or different organisms at different stages of their biogenesis.

7.2. Role of THO/TREX component Hpr1 in mRNP assembly

The second aim of this study was to investigate the role of the protein Hpr1 in mRNP assembly. Hpr1 is a part of the TREX complex, important for coupling transcription and mRNA export (Sträßer et al., 2002). However, it remains unknown how Hpr1 affects the mRNP assembly. This study shows that deletion of *HPR1* leads to increase of mRNA export adaptor proteins Nab2 and Yra1 and mRNA exporter Mex67 in nuclear mRNPs. It reveals that overexpression of Nab2 or Yra1 bypasses mRNA export defect of Δ*hpr1* cells. This restored mRNA export associated with increase of Nab2 and decrease of Mex67 to the WT level in nuclear mRNPs. Moreover, deletion of nucleoporin *NUP60* results in similar changes in nuclear mRNPs as deletion of *HPR1*: increase of Nab2, Yra1 and Mex67.

7.2.1. Absence of Hpr1 is associated with growth and mRNA export defects

Deletion of *HPR1* is known to impair cell growth (Betz et al., 2002). Indeed, growth of Δ*hpr1* strain is drastically impaired at 37°C and 16°C, and slower than the WT at 25°C and 30°C (Fig. 18B). Hpr1 depletion also lead to impaired cell growth. However, the cells are more tolerant to the cold or heat at 16°C or 37°C than Δ*hpr1* strain (Fig. 18A). Defective growth reflects defective cellular processes.

Hpr1 is involved in mRNA export. It becomes essential when general mRNA exporter Mex67 is defective (Jimeno et al., 2002). In accordance to the published data, Δ*hpr1* strain has an mRNA export defect at 30°C, which is enhanced at 37°C (Fig. 19). The depletion of Hpr1 upon 1 h auxin addition also results in mRNA export defect (Fig. 19). Hence, it illustrates that the first response on the absence of Hpr1 affects the mRNA export.

It was shown that not only Δ*hpr1* strain, but others deletion mutants of THO proteins have a similar effect on mRNA export (Sträßer et al., 2002). Potentially, this mRNA export defect can be associated with the absence of a functional THO complex. Thp2-TAP co-precipitation showed, that upon *HPR1* deletion the THO complex is no longer formed (Appendix fig. 9A). Protein Thp2 remains associated with Mft1 (Appendix fig. 9A). This fits to the predicted structure of the yeast THO complex, where Thp2 and Mft1 form an interaction platform (Schuller et al., 2020). However, the interactions of Thp2 with Tho2 and Tex1 in Δ*hpr1* strain are lost. It remains unknown if Tho2 stays to be bound to Tex1. Co-precipitation of the largest Tho2 protein in Δ*hpr1* strain can answer this question. Overall, observed defects in Δ*hpr1* cells are consequences of non-functional THO complex.

7.2.2. mRNP assembly in the absence of Hpr1

Depletion of Hpr1-AID is associated with very first changes of mRNP composition, while Δ*hpr1* strain represents long-term changes. After 20 min of auxin treatment, when 75% of Hpr1 is depleted (Fig. 17B), no differences in mRNP composition was observed (Appendix fig. 7). Likely, the response on the shorter depletion time is not yet formed. Depletion of Hpr1 for 1 h, when the whole cell Hpr1 level drops to around 5% (Fig.17B), leads to a 2-fold increase of Nab2 in nuclear mRNPs (Fig. 20A-B). Remarkably, longer Hpr1 depletion for 3 h results in even higher level of Nab2, but

decrease of RBPs Sub2 and Tho1. This intermediate state is very distinct from other depletion points or deletion of *HPR1*. It speaks for dynamic changes of mRNPs during Hpr1 depletion. Depletion of Hpr1 for 6 h leads to further increase of Nab2 and Yra1 increase. This is similar to nuclear mRNPs in Δ*hpr1* cells.

In Δ*hpr1* cells, there is 5-fold increase of Nab2 level, as well as 2-fold increase of Yra1 and Mex67 in nuclear mRNPs (Fig.20C-D). Potentially, the increase of Nab2, Yra1 and Mex67 might be an attempt to bypass defective mRNA export in Δ*hpr1* cells. Interestingly, level of another Mex67 adaptor, the protein Npl3 remains unchanged upon *HPR1* deletion (Fig. 20C-D). It suggests the existence of different mRNA export pathways involving Yra1, Nab2 or Npl3 as adaptors of Mex67. Interestingly, reported RNA immunoprecipitation experiments suggests that Nab2 and Npl3 can be preferentially associated with different subset of RNAs. For instance, Npl3 was largely associated with transcripts of ribosomal proteins, while Nab2 was enriched for transcripts of proteins required for transcription (Guisbert et al., 2005). Another study showed that Nab2 preferentially associates with short and Yra1 with long transcripts (Baejen et al., 2014). However, yet another study reported that Nab2 is associated with large amount of mRNAs of different lengths without preferences for specific group of transcripts (Batisse et al., 2009). According to our study, adaptor proteins Nab2 and Yra1, but not Npl3, can modulate nuclear mRNA export in Δ*hpr1* cells. This supports the concept of Nab2-Yra1 or Npl3 being involved in different mRNA export pathways or having different unrelated roles in mRNA export.

Another difference between Nab2 and Npl3 is associated with ubiquitination, particularly, by ubiquitin ligase Tom1. *tom1* mutants accumulate Nab2 and mRNA in the nucleus near the NPCs, but do not affect Npl3 localization (Duncan et al., 2000). Interestingly, Tom1 also promotes disassociation of Yra1 from mRNPs before mRNP export (Iglesias et al., 2010). The RBPs Mex67 and Hpr1 are also ubiquitinated. UBA domain of Mex67 directly binds both, ubiquitin and Hpr1 (Gwizdek et al., 2006). It was proposed that Hpr1 binding leads to conformational changes and increased ubiquitination of UBA domain of Mex67 (Hobeika et al., 2007). Therefore, lack of Hpr1-Mex67 interaction and also impaired ubiquitination of Mex67 in Δ*hpr1* cells might affect mRNP assembly.

7.2.3. RNA binding of Nab2, Yra1 and Mex67 is increased in Δ*hpr1* cells

Despite the 2-fold increase of Nab2 in nuclear mRNPs upon Hpr1 depletion (Fig. 20A), RNA-binding properties of Nab2 remained unchanged (Fig. 21A). Perhaps, observed increase indicates that there are doubling of Nab2 on the same RNA, therefore the same amount of RNA is co-precipitated with Nab2. It has been shown that Nab2 can form dimers upon RNA binding (Aibara et al., 2017). In this way Nab2 might compact RNA within the mRNP. Potentially, removal of Hpr1 and the large THO complex could expose mRNA parts that become compacted by Nab2 dimers. In contrast to Hpr1 depletion, in Δ*hpr1* cells RNA binding of Nab2 was increased. While Nab2 had 5-fold increase in mRNP composition in Δ*hpr1* cells (Fig. 20B), its RNA binding shows 2-fold increase (Fig. 21B). Perhaps, Nab2 binds to more transcripts, as well as the amount of the Nab2 molecules on the same RNA can be increased.

In accordance with the observed increase in nuclear mRNP composition, Yra1 and Mex67 show 2-fold increase in RNA-binding ability in Δ*hpr1* cells (Fig. 21C, D). It suggests that Nab2, Yra1 and Mex67 binds to more transcripts in Δ*hpr1* strain than in the WT.

7.2.4. Occupancy of Nab2 and Yra1 at transcribed genes is increased in Δ*hpr1* strain

While RNA-binding properties of Nab2, Yra1 and Mex67 were increased in Δ*hpr1* strain, their co-transcriptional recruitment was different. Nab2 or Yra1 occupancies at tested highly-transcribed genes were increased (Fig. 22B, C). It suggests, that in Δ*hpr1* strain more Nab2 and Yra1 are co-transcriptionally recruited to the genes for subsequent loading onto the mRNP. In case of Mex67, its occupancy on chromatin remained unchanged (Fig. 22D). It suggests that increased amount of Mex67 in nuclear mRNPs in Δ*hpr1* cells is not recruited to the transcribed genes co-transcriptionally, but loaded onto mRNP later. It is worth to note, that there were no differences in protein occupancies between tested intronless or intron-containing transcripts. Hence, at least on the co-transcriptional recruitment level, these proteins seem to be not involved in splicing.

7.2.5. Overexpression of Nab2 or Yra1 supress growth defect and mRNA export defect in Δ*hpr1* cells

Increase of Nab2, Yra1 and Mex67 in nuclear mRNPs in Δ*hpr1* strain could be an attempt to bypass defective mRNA export. Remarkably, overexpression of Nab2 or Yra1 in Δ*hpr1* cells was able to restore mRNA export and suppress growth defect of Δ*hpr1* cells (Fig. 23-24). It suggests that Nab2 and Yra1 work together or have overlapping functions. This idea is supported by many cross-links found between Nab2 and Yra1 within mRNPs (Bonneau et al., 2023). Additionally, Nab2 overexpression was shown to supress some defects of *yra1* mutant (Vinciguerra et al., 2005). Interestingly, overexpression of Yra1 in WT cells has negative effect on genomic stability and replication (Gavaldá et al., 2016). However, in Δ*hpr1* strain with known genomic instability and impaired replication, it was able to restore cell growth and mRNA export (Fig. 23-24). It illustrates the importance of regulation of Yra1 level in the cells.

Interestingly, overexpression of general mRNA exporter Mex67 can circumvent lethal phenotype of Δ*yra1* cells (Iglesias et al., 2010), but have no effect on mRNA export defect in Δ*hpr1* strain (Fig. 23). Additionally, overexpression of another Mex67 adaptor, Npl3, fails to suppress mRNA export defect in Δ*hpr1* cells (Fig. 23). This indicates, that Nab2 and Npl3 as adaptors of Mex67 can be involved in distinct mRNA export pathways.

7.2.6. Overexpression of Nab2 or Yra1 in Δ*hpr1* cells leads to increase of Nab2 and decrease of Mex67 in nuclear mRNPs

In comparison to Δ*hpr1* strain, overexpression of Nab2 in Δ*hpr1* cells leads to a further increase of Nab2 in nuclear mRNPs, while Mex67 decreases to the WT level (Fig. 25B, Eluate). Remarkably, overexpression of Yra1 in Δ*hpr1* cells results in similar changes of mRNP composition: an increase of Nab2 and a decrease of Mex67 (Fig. 25B, Eluate). Hence, both of these cases of restored mRNA export are associated with similar mRNP composition. It again demonstrates the interconnection between Nab2 and Yra1 and their functions. Interestingly, the level of Yra1 itself remains unchanged in mRNPs (Fig.25B, Eluate). It means that Yra1 can recruit Nab2 to the mRNP. Remarkably, in the lysates, overexpression of Yra1 leads to an

increase of Nab2, while overexpression of Nab2 results in Yra1 increase (Fig. 25B, Lysate). Deletion of *HPR1* itself also shows increased levels of Yra1 and Nab2 in the lysate. Perhaps, levels of Yra1 and Nab2 can be co-regulated to provide either mRNA export or retention.

Importantly, Yra1 might be auxiliary, dispensable adaptor protein. Yra1 is associated with only 20% of transcripts and, furthermore, is dispensable for mRNA export in *Drosophila melanogaster* or *Caenorhabditis elegans* (Gatfield & Izaurralde, 2002; Hieronymus & Silver, 2003; Longman et al., 2003). Furthermore, in *S. cerevisiae* lethal phenotype of Δ*yra1* cells can be bypassed by overexpression of Nab2 or Mex67 (Iglesias, 2010).

Similar changes in mRNP composition upon Nab2 or Yra1 overexpression (Fig. 25B, Eluate) shows, that for efficient mRNA export in Δ*hpr1* cells more of Nab2, but less of Mex67 is needed. Since Nab2 is known to be involved in mRNA export as an adaptor of Mex67, its increase in nuclear mRNPs might facilitate mRNA export. However, the decrease of the mRNA exporter Mex67 to WT level is an unexpected change. It suggests that high Mex67 levels in mRNPs in Δ*hpr1* cells (Fig. 20C-D) might be not an attempt to compensate defective mRNA export, but a marker for nuclear mRNA retention. Mex67 is a general mRNA export factor, however nothing is known about its function for nuclear mRNA retention. The overexpression of Mex67 does not lead to any changes in mRNP composition (Fig. 25B, Eluate). It suggests that the amount of this protein within the mRNP is highly regulated. Therefore, for mRNA export Mex67 has to be on a specific WT-like level. Potentially, as a result of Nab2 overexpression, excessive Nab2 could compete with Mex67 for binding to mRNA. Since the affinity of Mex67 to RNA is rather low, excessive Nab2 could displace it. However, it seems unlikely, since both, Mex67 and its adaptor proteins are needed for mRNA export. The observed specific changes, likely, require more sophisticated regulation.

7.2.7. Overexpression of Yra1 results in increased occupancy of Yra1 and Nab2 at the transcribed genes in Δ*hpr1* cells

Yra1 overexpression in Δ*hpr1* cells results in more of Nab2 in nuclear mRNPs (Fig.25B, Eluate). It suggests that Yra1 either recruits Nab2 to the genes already co-

transcriptionally or facilitates its loading onto the mRNP later. Overexpression of Nab2 in Δ*hpr1* strain does not change Nab2 occupancy (Fig. 26A). In this case, Nab2 is loaded onto the mRNP later. On the contrary, overexpression of Yra1 in Δ*hpr1* strain leads to increased occupancy of both, Yra1 and Nab2 (Fig. 26B, D). Therefore, Yra1 either retains or recruits Nab2 to the gene for its subsequent loading onto the mRNP. This finding confirms that Yra1 facilitates Nab2 loading onto the mRNP. It was suggested before that Yra1 promotes and stabilizes the interaction between Nab2 and Mex67 *in vitro* (Iglesias et al., 2010). Perhaps, Yra1 might also stabilize the Nab2-Mex67 interaction within the mRNP.

7.2.8. Role of Nab2 in mRNA export in Δ*hpr1* cells is not coupled to polyadenylation, R-loop resolution or transcription termination

As shown before, the increase of Nab2 in nuclear mRNPs in Δ*hpr1* strain is able to suppress the growth defect and mRNA export defect. Nab2 is a poly(A) binding protein that regulates the length of poly(A) tails. The mRNA export block is often associated with hyperadenylation. Therefore, the theory that mRNAs in Δ*hpr1* strain have elongated poly(A)-tails, and an increased Nab2 level trimming it to the normal length could explain the restored mRNA export in Δ*hpr1* strain. However, the poly(A) tail length of bulk RNAs or individual transcripts showed no difference for Δ*hpr1* strain or Δ*hpr1* bearing respective multicopy plasmids for protein overexpression (Fig. 27). This indicates, that the function of Nab2 in mRNA export can be independent from its role in polyadenylation. While the occupancy of Nab2 is the highest on the 3’ end of RNA, it is not restricted to it and distributed along the genes and transcripts (Baejen et al., 2014; González-Aguilera et al., 2011). Therefore, Nab2 functions in poly(A) tail length control and mRNA export can be overlapping, but also can be uncoupled. Despite the unchanged polyadenylation level, the mechanism of restored mRNA export can be also connected to the 3’ end processing of mRNA. For instance, *in vitro* 3’ end processing assays showed impaired cleavage of pre-mRNA in Δ*hpr1* extracts (Saguez et al., 2008). Therefore, this possibility also can be explored.

The Δ*hpr1* cells have increased genomic instability and R-loop formation (Luna et al., 2019). While overexpression of another RBP, Tho1, was reported to resolve harmful R-loops (Miosga, 2022), it is not the case for Nab2. Therefore, overexpression of Nab2 does not restore mRNA export by reducing the level of R-loops in Δ*hpr1* cells

(Fig. 28). Interestingly, overexpression of another export adaptor, Npl3, in Δ*hpr1* strain leads to the decrease of R-loop levels (Fig. 28B). This ability of Npl3 could be another interesting point to investigate. Indirect hint for the role of Npl3 in R-loop regulation is that Δ*npl3* cells have R-loop dependent hyperrecombination (Santos-Pereira et al., 2013).

Hpr1 is also involved in transcription. Its deletion leads to decreased occupancy and processivity of RNAPII (Mason & Struhl, 2005). Overexpression of Nab2 or Yra1 in Δ*hpr1* strain did not affect RNAPII occupancy at the 3' end of transcribed genes (Salome Barbakadze, Master thesis). Therefore, there were no hints for potentially improved RNAPII processivity upon Nab2/Yra1 overexpression. The *HPR1* deletion could be also associated with transcription termination defects. Interestingly, Nab2 depletion was shown to result in global transcriptional readthrough (Alpert et al., 2020). While Δ*hpr1* cells indeed showed transcriptional readthrough for some of the tested transcripts, overexpression of Nab2 was not able to suppress this defect (Fig. 29).

Likely, in Δ*hpr1* cells the role of Nab2 in mRNA export is not related to improved transcription, decreased R-loop level or normalized polyadenylation. Potentially, restoration of mRNA export upon Nab2 overexpression exclusively reflects its function in mRNA export.

7.2.9. Disruption of different parts of mRNA export pathway results in similar mRNP composition changes

In Δ*hpr1* strain nuclear mRNA retention is associated with an increased level of Mex67 in mRNP composition (Fig. 19, Fig. 20B). Upon Nab2 or Yra1 overexpression in Δ*hpr1* cells mRNA export is restored (Fig.23). In these cases, Mex67 in mRNP composition reduces to the WT level (Fig. 25). Surprisingly, higher amounts of general mRNA exporter Mex67 does not improve mRNA export, but associates with mRNA retention in Δ*hpr1* cells. Perhaps, Mex67 level has to be precisely regulated to perform the mRNA export. Overexpression of Mex67 does not lead to its increase in mRNPs, and therefore it is not possible to see if its increase can cause mRNA export defect in WT cells (Appendix fig. 8). However, if increase of Mex67 is associated with

mRNA retention in the nucleus, it is supposed to be observed also for other mutants with defective mRNA export.

Nup60 is a nucleoporin located on the nucleoplasmic side of NPCs. Its deletion results in defective mRNA export (Fischer et al., 2002). Strikingly, our study showed that deletion of *NUP60* leads to similar changes as the deletion of *HPR1* – increased Nab2, Yra1 and Mex67 in nuclear mRNPs (Fig. 30). It suggests, that disruption of different parts of the mRNA export pathway, either Hpr1 closer to transcription site, or Nup60 at the NPC, results in the same mRNP composition. In this case, more of Nab2, Yra1 and Mex67 in mRNPs could be either a cause or a consequence of nuclear mRNA retention. If these mRNPs are aberrant, e.g. have inefficient mRNA processing or improperly packaged by RBPs, they need to be kept in the nucleus for degradation. If these mRNPs are export-competent, they need to bypass the disrupted mRNA export pathway, likely by adjusting the amount of mRNA export factors.

It has to be taken into account, that Nup60 interacts with the structural proteins Mlp1 and Mlp2 and anchors them together with the nucleoporin Nup2 to the NPC. Deletion of *NUP60* causes delocalization of Mlp1 and Nup2 from the nuclear rim. In Δ*nup60* cells Mlp1 is mislocalized in foci in the nucleus, while Nup2 is distributed all over the nucleus (Cibulka et al., 2022). Importantly, Mlp1 is involved in mRNA export via direct interaction with Nab2 (Fasken et al., 2008). Therefore, observed change in nuclear mRNP composition in Δ*nup60* strain (Fig. 30) could be a secondary effect caused by loss of interaction with Mlp1. To check this, mRNA export and nuclear mRNP composition in Δ*mlp1* cells should be investigated. It is also important to see if Nab2 or Yra1 overexpression can suppress mRNA export defect in Δ*nup60* cells similarly to Δ*hpr1* strain.

If increased Nab2, Yra1 and Mex67 are the hallmarks of the aberrant mRNPs in Δ*hpr1* and Δ*nup60* cells, it is important to find an interconnection between Hpr1 and Nup60. Deletion of *MLP1* or *NUP60* have been reported to cause leakage of un-spliced pre-mRNAs to the cytoplasm (Galy et al., 2004). Therefore, it is important to find out if Δ*hpr1* strain also has such a leakage of un-spliced pre-mRNAs. If yes, then both, Hpr1 and Nup60, might be involved in surveillance and quality control of pre-mRNAs. Hpr1 might be responsible for a check-up at the transcription site, while Nup60 is active at the NPC. In case of Hpr1, the nuclear exosome could be

associated with this quality control to degrade defective mRNPs. Therefore, absence of the nuclear exosome protein Rrp6 in Δ*hpr1* strain would lead to a release of defective mRNAs from the transcription site and their mRNA export to the cytoplasm. Further investigation should be done to assess the role of Nab2 as potential surveillance factor. Nab2 was shown to directly interact with Rrp6, and Rrp6, in turn, was able to displace Nab2 from nuclear poly(A) tails (Schmid et al., 2012). In our study, overexpression of Nab2 in Δ*hpr1* cells leads to its increase in nuclear mRNPs and restored mRNA export (Fig. 23, Fig. 25B). Therefore, role of Nab2 in the recruitment of the nuclear exosome for degradation of potentially aberrant mRNPs in Δ*hpr1* cells is another interesting point to investigate.

If Nup60 functions as a checkpoint for quality control, its interaction with the protein Swt1 should be examined. Swt1 is an RNA endonuclease that can be associated with the NPC and plays a role in mRNA quality control (Skružný et al., 2009). Moreover, Swt1 was shown to have genetic interaction with some proteins, among them Hpr1, Nup60 and Mlp1 (Röther et al., 2006; Skružný et al., 2009). This is an additional hint to explore link between Hpr1 and Nup60 and their role in mRNA quality control. On the contrary to Nup60, Swt1 did not show genetic interaction with Nup1, another nucleoporin located on the nucleoplasmic side of the NPC. Interestingly, in our study the Δ*nup1* strain also did not show changes in nuclear mRNPs (Fig. 30). It suggests that Nup1 may have a distinct role in mRNA export. Nup1 was shown to anchor TREX-2 complex to the NPC (Jani et al., 2014). Remarkably, the protein Sac3 of the TREX-2 complex was not co-enriched in Nab2-TAP purification, while Mlp1 was (Batisse et al., 2009). Likely, Nup60, Mlp1 and Nab2 functionally work together to perform mRNA export, while Nup1 might represent structural support by tethering TREX-2 to the NPC. Possibly, Nup60 might even compensate the absence of Nup1, because acetylation of Nup60 is also reported to recruit TREX-2 via Sac3 (Gomar-Alba et al., 2022). However, this requires additional studies.

7.3. Conclusions and outlook

Studying the structure of transcript-specific mRNPs requires an efficient and specific method of their isolation. In this study, RNA-centric approaches were established and optimized to purify the transcript-specific *CCW12* mRNP. The ASO-based method represents a good tool to purify RNAs of interest solely, but not within the endogenous mRNP complex. The ASOs have strong non-specific binding to RBPs and, likely, disrupt the mRNP structure. The aptamer-based approach via Mango or MS2 aptamers ensures the purification of *CCW12* mRNPs in good amount and purity. Detection of *CCW12* mRNPs by electron microscopy revealed particles of 28 nm in size. For further investigation, it will be important to verify the particles by immunogold labeling. To preserve the integrity of the mRNPs, cross-linking before electron microscopy or during the isolation will be applied. Moreover, advanced visualization techniques, such as cryo-EM and cryo-ET, will be implemented to obtain a detailed structure of transcript-specific mRNPs.

As the second part of this study, role of the protein Hpr1 in mRNP assembly was investigated. Deletion of *HPR1* leads to increased levels of mRNA exporter Mex67 and its adaptor proteins Nab2 and Yra1 in nuclear mRNPs. Overexpression of Nab2 or Yra1 suppresses mRNA export defect in Δ*hpr1* cells. These cases of restored mRNA export are associated with similar changes in mRNPs: further increase of Nab2 and reduction of Mex67 to the WT level. Overexpression of Yra1 in Δ*hpr1* cells leads to higher occupancy of Yra1 and also Nab2 at transcribing genes. This suggests that Yra1 could assists loading of Nab2 onto mRNP. Restored mRNA export is independent from poly(A) tail length control, R-loop resolution or transcription termination. Disrupting the mRNA export pathway either at transcription site by deletion of *HPR1* or at the nuclear pore complex by deletion of *NUP60* results in similar mRNP composition changes: an increase of Nab2, Yra1 and Mex67. Remarkably, higher levels of mRNA export factor Mex67 are associated with mRNA retention. Further investigations are needed to assess if increased amounts of Nab2, Yra1 and Mex67 represent the hallmarks of aberrant RNPs or a disrupted mRNA export pathway. For this purpose, leakage of unspliced pre-mRNAs in Δ*hpr1* strain, as well as role of NPC proteins Mlp1 and Mlp2 will be assessed. Taken together, Nab2, Yra1 and Mex67 are proposed to be involved in regulation of mRNA export and retention (Fig. 31).

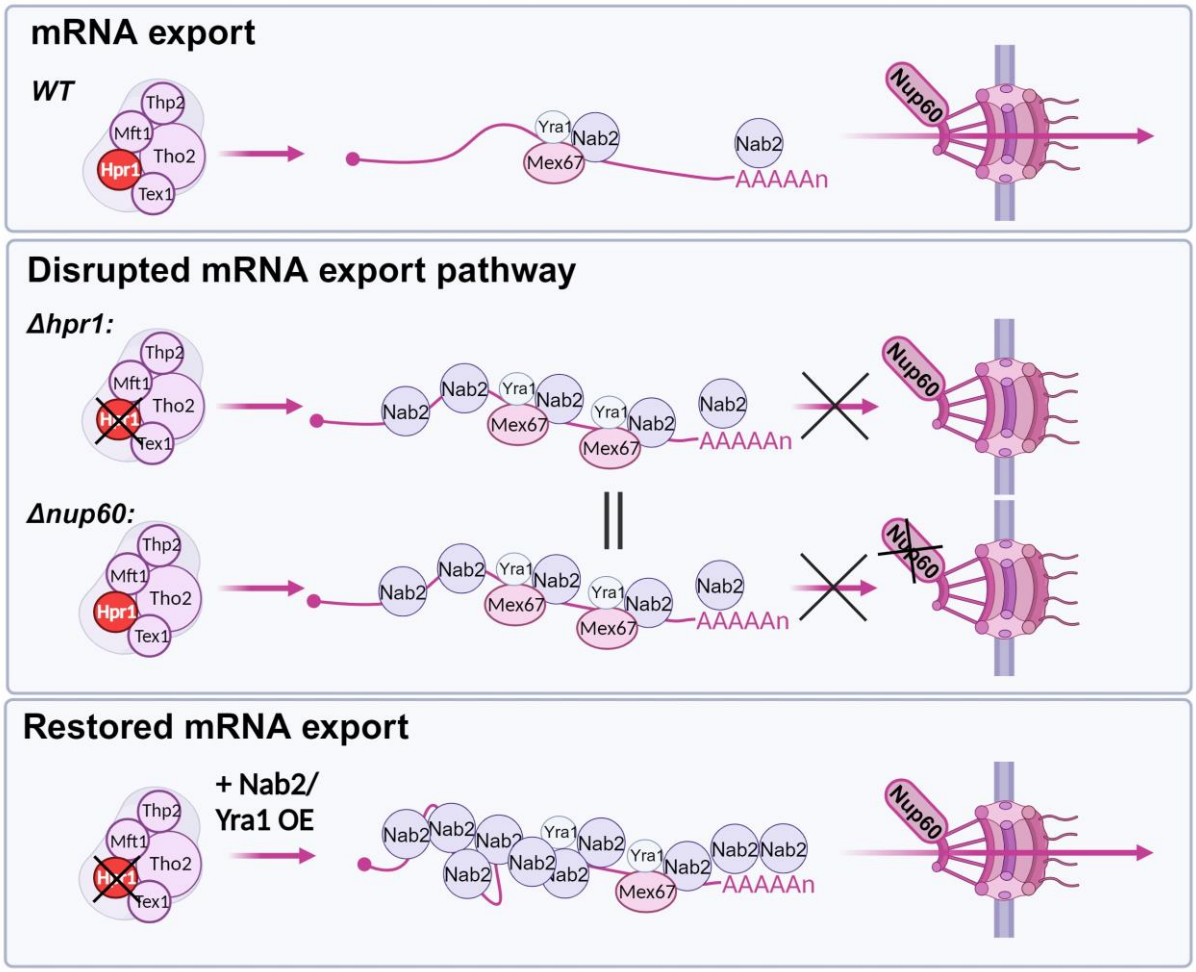

Figure 31. Levels of Nab2, Yra1 and Mex67 in nuclear mRNPs are proposed to regulate mRNA export and retention. In a WT strain, Nab2 and Yra1 act as adaptors for Mex67-Mtr2 to mediate mRNA export to the cytoplasm. Deletion of *HPR1*, a component of the THO complex, causes nuclear mRNA retention and increased amounts of Nab2, Yra1 and Mex67 in nuclear mRNPs. Downstream disruption of mRNA export at the nuclear pore by deletion of *NUP60* results in similar changes in mRNP composition. Increased levels of Nab2, Yra1 and Mex67 within the mRNPs in Δ*hpr1* or Δ*nup60* cells could be a hallmarks of nuclear mRNA retention. Overexpression of Nab2 or Yra1 in Δ*hpr1* strain changes mRNP composition. These changes are associated with restored mRNA export. In this case, further increase of Nab2 and decrease of Mex67 to the WT level are observed in nuclear mRNPs. Overexpression of Yra1 can assist the Nab2 loading onto the mRNP, and increased Nab2 promotes the mRNA export. Level of Mex67 can work as a switch between retention and export of mRNA.

8. References

Adams, R. L., Terry, L. J., & Wente, S. R. (2014). Nucleoporin FG domains facilitate mRNP remodeling at the cytoplasmic face of the nuclear pore complex. *Genetics*, *197*(4), 1213–1224. https://doi.org/10.1534/GENETICS.114.164012

Aibara, S., Gordon, J. M. B., Riesterer, A. S., McLaughlin, S. H., & Stewart, M. (2017). Structural basis for the dimerization of Nab2 generated by RNA binding provides insight into its contribution to both poly(A) tail length determination and transcript compaction in Saccharomyces cerevisiae. *Nucleic Acids Research*, *45*(3), 1529–1538. https://doi.org/10.1093/NAR/GKW1224

Alpert, T., Straube, K., Carrillo Oesterreich, F., & Neugebauer, K. M. (2020). Widespread Transcriptional Readthrough Caused by Nab2 Depletion Leads to Chimeric Transcripts with Retained Introns. *Cell Reports*, *33*(4), 108324. https://doi.org/10.1016/J.CELREP.2020.108324

Amberg, D. C., Goldstein, A. L., & Cole, C. N. (1992). Isolation and characterization of RATI: an essential gene of *Saccharomyces cerevisiae* required for the efficient nucleocytoplasmic trafficking of mRNA. *Genes Dev*; 6(7):1173-89. doi: 10.1101/gad.6.7.1173.

Amrani, N., Miche`, M., Minet, M., Le Gouar, M., Lacroute, O., & Wyers, O. (1997). Yeast Pab1 interacts with Rna15 and participates in the control of the poly(A) tail length in vitro. *Molecular and Cellular Biology*, *17*(7), 3694. https://doi.org/10.1128/MCB.17.7.3694

Ansari, S. A., & Morse, R. H. (2012). Selective role of mediator tail module in the transcription of highly regulated genes in yeast. *Transcription*, *3*(3), 110–114. https://doi.org/10.4161/TRNS.19840

Ares M., J., Grate, L., & Pauling, M. H. (1999). A handful of intron-containing genes produces the lion's share of yeast mRNA. *RNA (New York, N.Y.)*, *5*(9), 1138–1139. https://doi.org/10.1017/S1355838299991379

Autour, A., Jeng, S. C. Y., Cawte, A. D., Abdolahzadeh, A., Galli, A., Panchapakesan, S. S. S., Rueda, D., Ryckelynck, M., & Unrau, P. J. (2018). *Fluorogenic RNA Mango aptamers for imaging small non-coding RNAs in mammalian cells*. https://doi.org/10.1038/s41467-018-02993-8

Badjatia, N., Rossi, M. J., Bataille, A. R., Mittal, C., Lai, W. K. M., & Pugh, B. F. (2021). Acute stress drives global repression through two independent RNA polymerase II stalling events in Saccharomyces. *Cell Reports*, *34*(3). https://doi.org/10.1016/J.CELREP.2020.108640

Baejen, C., Andreani, J., Torkler, P., Battaglia, S., Schwalb, B., Lidschreiber, M., Maier, K. C., Boltendahl, A., Rus, P., Esslinger, S., Söding, J., & Cramer, P. (2017). Genome-wide Analysis of RNA Polymerase II Termination at Protein-Coding Genes. *Molecular Cell*, *66*(1), 38-49.e6. https://doi.org/10.1016/J.MOLCEL.2017.02.009

Baejen, C., Torkler, P., Gressel, S., Essig, K., Söding, J., & Cramer, P. (2014). Transcriptome Maps of mRNP Biogenesis Factors Define Pre-mRNA Recognition. *Molecular Cell*, *55*(5), 745–757. https://doi.org/10.1016/j.molcel.2014.08.005

Bai, R., Yan, C., Wan, R., Lei, J., & Shi, Y. (2017). Structure of the Post-catalytic Spliceosome from Saccharomyces cerevisiae. *Cell*, *171*(7), 1589-1598.e8. https://doi.org/10.1016/J.CELL.2017.10.038

Balbo, P. B., & Bohm, A. (2007). Mechanism of poly(A) polymerase: structure of the enzyme-MgATP-RNA ternary complex and kinetic analysis. *Structure (London, England : 1993)*, *15*(9), 1117–1131. https://doi.org/10.1016/J.STR.2007.07.010

Batisse, J., Batisse, C., Budd, A., Böttcher, B., & Hurt, E. (2009). Purification of Nuclear Poly(A)-binding Protein Nab2 Reveals Association with the Yeast Transcriptome and a Messenger Ribonucleoprotein Core Structure. *The Journal of Biological Chemistry*, *284*(50), 34911. https://doi.org/10.1074/JBC.M109.062034

Beilharz, T. H., & Preiss, T. (2009). Transcriptome-wide measurement of mRNA polyadenylation state. *Methods (San Diego, Calif.)*, *48*(3), 294–300. https://doi.org/10.1016/J.YMETH.2009.02.003

Bensidoun, P., Zenklusen, D., & Oeffinger, M. (2021). Choosing the right exit: How functional plasticity of the nuclear pore drives selective and efficient mRNA export. *Wiley Interdisciplinary Reviews: RNA*, *12*(6), e1660. https://doi.org/10.1002/WRNA.1660

Berglund, J. A., Chua, K., Abovich, N., Reed, R., & Rosbash, M. (1997). The splicing factor BBP interacts specifically with the pre-mRNA branchpoint sequence UACUAAC. *Cell*, *89*(5), 781–787. https://doi.org/10.1016/S0092-8674(00)80261-5

Betz, J. L., Chang, M., Washburn, T. M., Porter, S. E., Mueller, C. L., & Jaehning, J. A. (2002). Phenotypic analysis of Paf1/RNA polymerase II complex mutations reveals connections to cell cycle regulation, protein synthesis, and lipid and nucleic acid metabolism. *Molecular Genetics and Genomics : MGG*, *268*(2), 272–285. https://doi.org/10.1007/S00438-002-0752-8

Bharati, A. P., Singh, N., Kumar, V., Kashif, M., Singh, A. K., Singh, P., Singh, S. K., Siddiqi, M. I., Tripathi, T., & Akhtar, M. S. (2016). The mRNA capping enzyme of Saccharomyces cerevisiae has dual specificity to interact with CTD of RNA Polymerase II. *Scientific Reports*, *6*. https://doi.org/10.1038/SREP31294

Blancett, C. D., Fetterer, D. P., Koistinen, K. A., Morazzani, E. M., Monninger, M. K., Piper, A. E., Kuehl, K. A., Kearney, B. J., Norris, S. L., Rossi, C. A., Glass, P. J., & Sun, M. G. (2017). Accurate virus quantitation using a Scanning Transmission Electron Microscopy (STEM) detector in a scanning electron microscope. *Journal of Virological Methods*, *248*, 136–144. https://doi.org/10.1016/J.JVIROMET.2017.06.014

Blobel, G. (1985). Gene gating: a hypothesis. *Proceedings of the National Academy of Sciences of the United States of America*, *82*(24), 8527. https://doi.org/10.1073/PNAS.82.24.8527

Blythe, A. J., Yazar-Klosinski, B., Webster, M. W., Chen, E., Ne Vandevenne, M., Bendak, K., Mackay, J. P., Hartzog, G. A., & Vrielink, A. (2016). *The yeast transcription elongation factor Spt4/5 is a sequence-specific RNA binding protein*. https://doi.org/10.1002/pro.2976

Boesler, C., Rigo, N., Anokhina, M. M., Tauchert, M. J., Agafonov, D. E., Kastner, B., Urlaub, H., Ficner, R., Will, C. L., & Lührmann, R. (2016). A spliceosome intermediate with loosely associated tri-snRNP accumulates in the absence of Prp28 ATPase activity. *Nature Communications 2016 7:1*, *7*(1), 1–12. https://doi.org/10.1038/ncomms11997

Bonneau, F., Basquin, J., Steigenberger, B., Schäfer, T., Schäfer, I. B., & Conti, E. (2023). Nuclear mRNPs are compact particles packaged with a network of proteins promoting RNA–RNA interactions. *Genes and Development*, *37*(11–12), 505–517. https://doi.org/10.1101/GAD.350630.123/-/DC1

Boreikaitė, V., & Passmore, L. A. (2023). 3'-End Processing of Eukaryotic mRNA: Machinery, Regulation, and Impact on Gene Expression. *Annual Review of Biochemistry*, *92*, 199–225. https://doi.org/10.1146/ANNUREV-BIOCHEM-052521-012445

Bucheli, M. E., He, X., Kaplan, C. D., Moore, C. L., & Buratowski, S. (2007). Polyadenylation site choice in yeast is affected by competition between Npl3 and polyadenylation factor CFI. *RNA (New York, N.Y.)*, *13*(10), 1756–1764. https://doi.org/10.1261/RNA.607207

Casañal, A., Kumar, A., Hill, C. H., Easter, A. D., Emsley, P., Degliesposti, G., Gordiyenko, Y., Santhanam, B., Wolf, J., Wiederhold, K., Dornan, G. L., Skehel, M., Robinson, C. V., & Passmore, L. A. (2017). Architecture of eukaryotic mRNA 3'-end processing machinery. *Science (New York, N.Y.)*, *358*(6366), 1056–1059. https://doi.org/10.1126/SCIENCE.AAO6535

Castello, A., Fischer, B., Eichelbaum, K., Horos, R., Beckmann, B. M., Strein, C., Davey, N. E., Humphreys, D. T., Preiss, T., Steinmetz, L. M., Krijgsveld, J., & Hentze, M. W. (2012). Insights into RNA biology from an atlas of mammalian mRNA-binding proteins. *Cell*, *149*(6), 1393–1406. https://doi.org/10.1016/J.CELL.2012.04.031

Cawte, A. D., Unrau, P. J., & Rueda, D. S. (2020). Live cell imaging of single RNA molecules with fluorogenic Mango II arrays. *Nature Communications*, *11*(1). https://doi.org/10.1038/s41467-020-14932-7

Chan, S., Choi, E. A., & Shi, Y. (2011). Pre-mRNA 3'-end processing complex assembly and function. *Wiley Interdisciplinary Reviews. RNA*, *2*(3), 321–335. https://doi.org/10.1002/WRNA.54

Chan, S. P., & Cheng, S. C. (2005). The Prp19-associated complex is required for specifying interactions of U5 and U6 with pre-mRNA during spliceosome activation. *The Journal of Biological Chemistry*, *280*(35), 31190–31199. https://doi.org/10.1074/JBC.M505060200

Chang, M., French-Cornay, D., Fan, H., Klein, H., Denis, C. L., & Jaehning, J. A. (1999). A complex containing RNA polymerase II, Paf1p, Cdc73p, Hpr1p, and Ccr4p plays a role in protein kinase C signaling. *Molecular and Cellular Biology*, *19*(2), 1056–1067. https://doi.org/10.1128/MCB.19.2.1056

Changela, A., Ho, C. K., Martins, A., Shuman, S., & Mondragón, A. (2001). Structure and mechanism of the RNA triphosphatase component of mammalian mRNA capping enzyme. *The EMBO Journal*, *20*(10), 2575. https://doi.org/10.1093/EMBOJ/20.10.2575

Charenton, C., Wilkinson, M. E., & Nagai, K. (2019). Mechanism of 5' splice site transfer for human spliceosome activation. *Science (New York, N.Y.)*, *364*(6438), 362–367. https://doi.org/10.1126/SCIENCE.AAX3289

Chávez, S., Beilharz, T., Rondón, A. G., Erdjument-Bromage, H., Tempst, P., Svejstrup, J. Q., Lithgow, T., & Aguilera, A. (2000). A protein complex containing Tho2, Hpr1, Mft1 and a novel protein, Thp2, connects transcription elongation with mitotic recombination in *Saccharomyces cerevisiae*. *The EMBO Journal*, *19*(21), 5824–5834. https://doi.org/10.1093/EMBOJ/19.21.5824

Chávez, S., García-Rubio, M., Prado, F., & Aguilera, A. (2001). Hpr1 is preferentially required for transcription of either long or G+C-rich DNA sequences in Saccharomyces cerevisiae. *Molecular and Cellular Biology*, *21*(20), 7054–7064. https://doi.org/10.1128/MCB.21.20.7054-7064.2001

Chen, W., & Moore, M. J. (2015). Spliceosomes. *Current Biology : CB*, *25*(5), R181–R183. https://doi.org/10.1016/J.CUB.2014.11.059

Chu, C., Zhang, Q. C., Da Rocha, S. T., Flynn, R. A., Bharadwaj, M., Calabrese, J. M., Magnuson, T., Heard, E., & Chang, H. Y. (2015). Systematic discovery of Xist RNA binding proteins. *Cell*, *161*(2), 404–416. https://doi.org/10.1016/J.CELL.2015.03.025

Chu, C., Zhang, Q. C., Teixeira Da Rocha, S., Flynn, R. A., Bharadwaj, M., Calabrese, J. M., Magnuson, T., Heard, E., & Chang, H. Y. (2015). *Systematic discovery of Xist RNA binding proteins*. https://doi.org/10.1016/j.cell.2015.03.025

Cibulka, J., Bisaccia, F., Radisavljević, K., Carrillo, R. M. G., & Köhler, A. (2022). Assembly principle of a membrane-anchored nuclear pore basket scaffold. *Science Advances*, *8*(6). https://doi.org/10.1126/SCIADV.ABL6863

Company, M., Arenas, J., & Abelson, J. (1991). Requirement of the RNA helicase-like protein PRP22 for release of messenger RNA from spliceosomes. *Nature*, *349*(6309), 487–493. https://doi.org/10.1038/349487A0

Deckert, J., Hartmuth, K., Boehringer, D., Behzadnia, N., Will, C. L., Kastner, B., Stark, H., Urlaub, H., & Lührmann, R. (2006). Protein Composition and Electron Microscopy Structure of Affinity-Purified Human Spliceosomal B Complexes Isolated under Physiological Conditions. *MOLECULAR AND CELLULAR BIOLOGY*, *26*(14), 5528–5543. https://doi.org/10.1128/MCB.00582-06

Deka, P., Bucheli, M. E., Moore, C., Buratowski, S., & Varani, G. (2008). *Structure of the Yeast SR protein Npl3 and Interaction with mRNA 3'-End Processing Signals*. www.ebi.ac.uk/dali/

Dermody, J. L., Dreyfuss, J. M., Villé, J., Ogundipe, B., Gygi, S. P., Park, P. J., Ponticelli, A. S., Moore, C. L., Buratowski, S., Bucheli, M. E., & Kane, C. M. (2008). *Unphosphorylated SR-Like Protein Npl3 Stimulates RNA Polymerase II Elongation*. https://doi.org/10.1371/journal.pone.0003273

Dhuri, K., Bechtold, C., Quijano, E., Pham, H., Gupta, A., Vikram, A., & Bahal, R. (2020). Clinical Medicine Antisense Oligonucleotides: An Emerging Area in Drug Discovery and Development. *J Clin Med*, 9(6):2004. https://doi.org/10.3390/jcm9062004

Dimitrova, L., Valkov, E., Aibara, S., Flemming, D., McLaughlin, S. H., Hurt, E., & Stewart, M. (2015). Structural Characterization of the Chaetomium thermophilum TREX-2 Complex and its Interaction with the mRNA Nuclear Export Factor Mex67:Mtr2. *Structure(London, England:1993)*, *23*(7), 1246. https://doi.org/10.1016/J.STR.2015.05.002

Dolgosheina, E. V., Jeng, S. C. Y., Panchapakesan, S. S. S., Cojocaru, R., Chen, P. S. K., Wilson, P. D., Hawkins, N., Wiggins, P. A., & Unrau, P. J. (2014). RNA Mango aptamer-fluorophore: A bright, high-affinity complex for RNA labeling and tracking. *ACS Chemical Biology*, *9*(10), 2412–2420. https://doi.org/10.1021/cb500499x

Duncan, K., Umen, J. G., & Guthrie, C. (2000). A putative ubiquitin ligase required for efficient mRNA export differentially affects hnRNP transport. *Current Biology : CB*, *10*(12), 687–696. https://doi.org/10.1016/S0960-9822(00)00527-3

Dunn, E. F., Hammell, C. M., Hodge, C. A., & Cole, C. N. (2005). Yeast poly(A)-binding protein, Pab1, and PAN, a poly(A) nuclease complex recruited by Pab1, connect mRNA biogenesis to export. *Genes & Development*, *19*(1), 90–103. https://doi.org/10.1101/GAD.1267005

Eick, D., & Geyer, M. (2013). The RNA polymerase II carboxy-terminal domain (CTD) code. *Chemical Reviews*, *113*(11), 8456–8490. https://doi.org/10.1021/CR400071F

Estruch, F., Hodge, C., Gómez-Navarro, N., Peiró-Chova, L., Heath, C. V., & Cole, C. N. (2012). Insights into mRNP biogenesis provided by new genetic interactions among export and transcription factors. *BMC Genetics*, *13*. https://doi.org/10.1186/1471-2156-13-80

Fabrizio, P., Dannenberg, J., Dube, P., Kastner, B., Stark, H., Urlaub, H., & Lührmann, R. (2009). The evolutionarily conserved core design of the catalytic activation step of the yeast spliceosome. *Molecular Cell*, *36*(4), 593–608. https://doi.org/10.1016/J.MOLCEL.2009.09.040

Fan, X., Lamarre-Vincent, N., Wang, Q., & Struhl, K. (2008). Extensive chromatin fragmentation improves enrichment of protein binding sites in chromatin immunoprecipitation experiments. *Nucleic Acids Research*, *36*(19). https://doi.org/10.1093/nar/gkn535

Fasken, M. B., Stewart, M., & Corbett, A. H. (2008). Functional significance of the interaction between the mRNA-binding protein, Nab2, and the nuclear pore-associated protein, Mlp1, in mRNA export. *The Journal of Biological Chemistry*, *283*(40), 27130–27143. https://doi.org/10.1074/JBC.M803649200

Fischer, T., Sträßer, K., Rácz, A., Rodriguez-Navarro, S., Oppizzi, M., Ihrig, P., Lechner, J., & Hurt, E. (2002). The mRNA export machinery requires the novel Sac3p–Thp1p complex to dock at the nucleoplasmic entrance of the nuclear pores. *The EMBO Journal*, *21*(21), 5843. https://doi.org/10.1093/EMBOJ/CDF590

Flaherty, S. M., Fortes, P., Izaurralde, E., Mattaj, I. W., & Gilmartin, G. M. (1997). Participation of the nuclear cap binding complex in pre-mRNA 3' processing. *Proceedings of the National Academy of Sciences of the United States of America*, *94*(22), 11893–11898. https://doi.org/10.1073/PNAS.94.22.11893

Fortes, P., Inada, T., Preiss, T., Hentze, M. W., Mattaj, I. W., & Sachs, A. B. (2000). The yeast nuclear cap binding complex can interact with translation factor eIF4G and mediate translation initiation. *Molecular Cell*, *6*(1), 191–196. https://doi.org/10.1016/S1097-2765(05)00003-1

Fribourg, S., Braun, I. C., Izaurralde, E., & Conti, E. (2001). Structural basis for the recognition of a nucleoporin FG repeat by the NTF2-like domain of the TAP/p15 mRNA nuclear export factor. *Molecular Cell*, *8*(3), 645–656. https://doi.org/10.1016/S1097-2765(01)00348-3

Galej, W. P., Wilkinson, M. E., Fica, S. M., Oubridge, C., Newman, A. J., & Nagai, K. (2016). Cryo-EM structure of the spliceosome immediately after branching. *Nature*, *537*(7619), 197–201. https://doi.org/10.1038/NATURE19316

Galy, V., Gadal, O., Fromont-Racine, M., Romano, A., Jacquier, A., & Nehrbass, U. (2004). Nuclear Retention of Unspliced mRNAs in Yeast Is Mediated by Perinuclear Mlp1. *Cell*, *116*(1), 63–73. https://doi.org/10.1016/S0092-8674(03)01026-2

García-Oliver, E., García-Molinero, V., & Rodríguez-Navarro, S. (2012). mRNA export and gene expression: The SAGA–TREX-2 connection. *Biochimica et Biophysica Acta (BBA) - Gene Regulatory Mechanisms*, *1819*(6), 555–565. https://doi.org/10.1016/J.BBAGRM.2011.11.011

Gatfield, D., & Izaurralde, E. (2002). REF1/Aly and the additional exon junction complex proteins are dispensable for nuclear mRNA export. *The Journal of Cell Biology*, *159*(4), 579–588. https://doi.org/10.1083/JCB.200207128

Gavaldá, S., Santos-Pereira, J. M., García-Rubio, M. L., Luna, R., & Aguilera, A. (2016). Excess of Yra1 RNA-Binding Factor Causes Transcription-Dependent Genome Instability, Replication Impairment and Telomere Shortening. *PLoS Genetics*, *12*(4). https://doi.org/10.1371/JOURNAL.PGEN.1005966

Geisberg, J. V., Moqtaderi, Z., & Struhl, K. (2020). The transcriptional elongation rate regulates alternative polyadenylation in yeast. *ELife*, *9*, 1–55. https://doi.org/10.7554/ELIFE.59810

Gemmill, D., D'souza, S., Meier-Stephenson, V., & Patel, T. R. (n.d.). *REVIEW Current approaches for RNA-labelling to identify RNA-binding proteins 1*. https://doi.org/10.1139/bcb-2019-0041

Gerber, A. P. (2021). Rna-centric approaches to profile the rna–protein interaction landscape on selected RNAs. In *Non-coding RNA* (Vol. 7, Issue 1, pp. 1–15). MDPI AG. https://doi.org/10.3390/ncrna7010011

Gibson, D. G., Young, L., Chuang, R.-Y., Craig Venter, J., Hutchison III, C. A., & Smith, H. O. (2009). Enzymatic assembly of DNA molecules up to several hundred kilobases *NATURE METHODS*, *6*(5). https://doi.org/10.1038/NMETH.1318

Gilbert, W., & Guthrie, C. (2004). The Glc7p Nuclear Phosphatase Promotes mRNA Export by Facilitating Association of Mex67p with mRNA. *Molecular Cell*, *13*(2), 201–212. https://doi.org/10.1016/S1097-2765(04)00030-9

Gó Mez-Gonzá Lez, B. N., García-Rubio, M., Bermejo, R., Lè Ne Gaillard, H., Shirahige, K., Marín, A., Foiani, M., & Aguilera, A. S. (2011). Genome-wide function of THO/TREX in active genes prevents R-loop-dependent replication obstacles. *The EMBO Journal*, *30*, 3106–3119. https://doi.org/10.1038/emboj.2011.206

Gomar-Alba, M., Pozharskaia, V., Cichocki, B., Schaal, C., Kumar, A., Jacquel, B., Charvin, G., Igual, J. C., & Mendoza, M. (2022). Nuclear pore complex acetylation regulates mRNA export and cell cycle commitment in budding yeast. *The EMBO Journal*, *41*(15). https://doi.org/10.15252/EMBJ.2021110271

Gómez-González, B., & Aguilera, A. (2009). R-loops do not accumulate in transcription-defective hpr1-101 mutants: implications for the functional role of THO/TREX. *Nucleic Acids Research*, *37*(13), 4315–4321. https://doi.org/10.1093/NAR/GKP385

González-Aguilera, C., Tous, C., Babiano, R., De La Cruz, J., Luna, R., & Aguilera, A. (2011). Nab2 functions in the metabolism of RNA driven by polymerases II and III. *Molecular Biology of the Cell*, *22*(15), 2729. https://doi.org/10.1091/MBC.E11-01-0055

Görnemann, J., Kotovic, K. M., Hujer, K., & Neugebauer, K. M. (2005). Cotranscriptional spliceosome assembly occurs in a stepwise fashion and requires the cap binding complex. *Molecular Cell*, *19*(1), 53–63. https://doi.org/10.1016/J.MOLCEL.2005.05.007

Graber, J. H., Nazeer, F. I., Yeh, P. C., Kuehner, J. N., Borikar, S., Hoskinson, D., & Moore, C. L. (2013). DNA damage induces targeted, genome-wide variation of poly(A) sites in budding yeast. *Genome Research*, *23*(10), 1690–1703. https://doi.org/10.1101/GR.144964.112

Grant, R. P., Hurt, E., Neuhaus, D., & Stewart, M. (2002). Structure of the C-terminal FG-nucleoporin binding domain of Tap/NXF1. *Nat Struct Biol*; 9(4):247-51. doi: 10.1038/nsb773.https://doi.org/10.1038/nsb773

Greber, B. J., & Nogales, E. (2019). The Structures of Eukaryotic Transcription Pre-initiation Complexes and Their Functional Implications. *Sub-Cellular Biochemistry*, *93*, 143–192. https://doi.org/10.1007/978-3-030-28151-9_5

Grund, S. E., Fischer, T., Cabal, G. G., Antúnez, O., Pérez-Ortín, J. E., & Hurt, E. (2008). The inner nuclear membrane protein Src1 associates with subtelomeric genes and alters their regulated gene expression. *The Journal of Cell Biology*, *182*(5), 897–910. https://doi.org/10.1083/JCB.200803098

Gu, M., Rajashankar, K. R., & Lima, C. D. (2010). Structure of the Saccharomyces cerevisiae Cet1-Ceg1 mRNA capping apparatus. *Structure (London, England : 1993)*, *18*(2), 216. https://doi.org/10.1016/J.STR.2009.12.009

Guisbert, K. K., Duncan, K., Li, H., & Guthrie, C. (2005). Functional specificity of shuttling hnRNPs revealed by genome-wide analysis of their RNA binding profiles. *RNA*; 11(4):383-93. https://doi.org/10.1261/rna.7234205

Gwizdek, C., Iglesias, N., Rodriguez, M. S., Ossareh-Nazari, B., Hobeika, M., Divita, G., Stutz, F., & Dargemont, C. (2006). Ubiquitin-associated domain of Mex67 synchronizes recruitment of the mRNA export machinery with transcription. *Proceedings of the National Academy of Sciences of the United States of America*, *103*(44), 16376–16381. https://doi.org/10.1073/PNAS.0607941103

Hackmann, A., Wu, H., Schneider, U. M., Meyer, K., Jung, K., & Krebber, H. (2014). Quality control of spliced mRNAs requires the shuttling SR proteins Gbp2 and Hrb1. *Nature Communications*, *5*, 3123. https://doi.org/10.1038/NCOMMS4123

Hantsche, M., & Cramer, P. (2017). Conserved RNA polymerase II initiation complex structure. *Current Opinion in Structural Biology*, *47*, 17–22. https://doi.org/10.1016/J.SBI.2017.03.013

Harlen, K. M., & Churchman, L. S. (2017). The code and beyond: transcription regulation by the RNA polymerase II carboxy-terminal domain. *Nature Reviews. Molecular Cell Biology*, *18*(4), 263–273. https://doi.org/10.1038/NRM.2017.10

Hassan, T., Smith, S. G. J., Gaughan, K., Oglesby, I. K., O'neill, S., Mcelvaney, N. G., & Greene, C. M. (2013). Isolation and identification of cell-specific microRNAs targeting a messenger RNA using a biotinylated anti-sense oligonucleotide capture affinity technique. *Nucleic Acids Res*; 41(6):e71.https://doi.org/10.1093/nar/gks1466

Haurwitz, R. E., Jinek, M., Wiedenheft, B., Zhou, K., & Doudna, J. A. (2010). Sequence-and structure-specific RNA processing by a CRISPR endonuclease. *Science* 10; 329(5997):1355-8. doi: 10.1126/science.1192272.

He, X., & Moore, C. (2005). Regulation of yeast mRNA 3' end processing by phosphorylation. *Molecular Cell*, *19*(5), 619–629. https://doi.org/10.1016/J.MOLCEL.2005.07.016

Hector, R. E., Nykamp, K. R., Dheur, S., Anderson, J. T., Non, P. J., Urbinati, C. R., Wilson, S. M., Minvielle-Sebastia, L., & Swanson, M. S. (2002). Dual requirement for yeast hnRNP Nab2p in mRNA poly(A) tail length control and nuclear export. *The EMBO Journal*, *21*(7), 1800–1810. https://doi.org/10.1093/EMBOJ/21.7.1800

Hieronymus, H., & Silver, P. A. (2003). Genome-wide analysis of RNA-protein interactions illustrates specificity of the mRNA export machinery. *Nature Genetics*, *33*(2), 155–161. https://doi.org/10.1038/NG1080

Hobeika, M., Brockmann, C., Iglesias, N., Gwizdek, C., Neuhaus, D., Stutz, F., Stewart, M., Divita, G., & Dargemont, C. (2007). Coordination of Hpr1 and ubiquitin binding by the UBA domain of the mRNA export factor Mex67. *Molecular Biology of the Cell*, *18*(7), 2561–2568. https://doi.org/10.1091/MBC.E07-02-0153

Holmes, R. K., Tuck, A. C., Zhu, C., Dunn-Davies, H. R., Kudla, G., Clauder-Munster, S., Granneman, S., Steinmetz, L. M., Guthrie, C., & Tollervey, D. (2015). Loss of the Yeast SR Protein Npl3 Alters Gene Expression Due to Transcription Readthrough. *PLoS Genetics*, *11*(12). https://doi.org/10.1371/JOURNAL.PGEN.1005735

Huang, Y., Wan, Z., Tang, Y., Xu, J., Laboret, B., Nallamothu, S., Yang, C., Liu, B., Lu, R. O., Lu, B., Feng, J., Cao, J., Hayflick, S., Wu, Z., & Zhou, B. (2022). Pantothenate kinase 2 interacts with PINK1 to regulate mitochondrial quality control via acetyl-CoA metabolism. *Nature Communications 2022 13:1*, *13*(1), 1–16. https://doi.org/10.1038/s41467-022-30178-x

Huertas, P., & Aguilera, A. (2003). Cotranscriptionally formed DNA:RNA hybrids mediate transcription elongation impairment and transcription-associated recombination. *Molecular Cell*, *12*(3), 711–721. https://doi.org/10.1016/J.MOLCEL.2003.08.010

Huertas, P., García-Rubio, M. L., Wellinger, R. E., Luna, R., & Aguilera, A. (2006). An hpr1 Point Mutation That Impairs Transcription and mRNP Biogenesis without Increasing Recombination. *Molecular and Cellular Biology*, *26*(20), 7451. https://doi.org/10.1128/MCB.00684-06

Hurt, E., Luo, M.-J., Rö Ther §, S., Reed, R., & Strä, K. (2004). *Cotranscriptional recruitment of the serine-arginine-rich (SR)-like proteins Gbp2 and Hrb1 to nascent mRNA via the TREX complex*. www.pnas.orgcgidoi10.1073pnas.0308663100

Hyjek-Składanowska, M., Anderson, B. A., Mykhaylyk, V., Orr, C., Wagner, A., Poznański, J. T., Skowronek, K., Seth, P., & Nowotny, M. (2023). Structures of annexin A2-PS DNA complexes show dominance of hydrophobic interactions in phosphorothioate binding. *Nucleic Acids Research*, *51*(3), 1409–1423. https://doi.org/10.1093/NAR/GKAC774

Iadevaia, V., Matia-González, A. M., & Gerber, A. P. (2018). An Oligonucleotide-based Tandem RNA Isolation Procedure to Recover Eukaryotic mRNA-Protein Complexes. *J. Vis. Exp*, *138*, 58223. https://doi.org/10.3791/58223

Iglesias, N., Tutucci, E., Gwizdek, C., Vinciguerra, P., Dach, E., Corbett, A. H., Dargemont, C., & Xoise Stutz, F. (2010). Ubiquitin-mediated mRNP dynamics and surveillance prior to budding yeast mRNA export. *Genes Dev* 1;24(17):1927-38. doi: 10.1101/gad.583310.

Iii, R. J. T., Demeshkina, N. A., Lau, M. W. L., Shyam, S., Panchapakesan, S., Jeng, S. C. Y., Unrau, P. J., Ferré-D'amaré, A. R., Chem, N., & Author, B. (2017). Structural basis for high-affinity fluorophore binding and activation by RNA Mango HHS Public Access Author manuscript. *Nat Chem Biol*, *13*(7), 807–813. https://doi.org/10.1038/nchembio.2392

Jani, D., Valkov, E., & Stewart, M. (2014). Structural basis for binding the TREX2 complex to nuclear pores, GAL1 localisation and mRNA export. *Nucleic Acids Research*, *42*(10), 6686–6697. https://doi.org/10.1093/nar/gku252

Jänicke, A., Vancuylenberg, J., Boag, P. R., Traven, A., & Beilharz, T. H. (2012). ePAT: a simple method to tag adenylated RNA to measure poly(A)-tail length and other 3' RACE applications. *RNA (New York, N.Y.)*, *18*(6), 1289–1295. https://doi.org/10.1261/RNA.031898.111

Jeong, K., Ryu, I., Park, J., Hwang, H. J., Ha, H., Park, Y., Oh, S. T., & Kim, Y. K. (2019). Staufen1 and UPF1 exert opposite actions on the replacement of the nuclear cap-binding complex by eIF4E at the 5 end of mRNAs. *Nucleic Acids Research*, *47*(17), 9313–9328. https://doi.org/10.1093/nar/gkz643

Jiang, L., & Patel, D. J. (1998). Solution structure of the tobramycin–RNA aptamer complex. *Nature Structural Biology 1998 5:9*, *5*(9), 769–774. https://doi.org/10.1038/1804

Jimeno, S., Luna, R., García-Rubio, M., & Aguilera, A. (2006). Tho1, a Novel hnRNP, and Sub2 Provide Alternative Pathways for mRNP Biogenesis in Yeast THO Mutants. *Molecular and Cellular Biology*, *26*(12), 4387. https://doi.org/10.1128/MCB.00234-06

Jimeno, S., Rondón, A. G., Luna, R., & Aguilera, A. (2002). The yeast THO complex and mRNA export factors link RNA metabolism with transcription and genome instability. *The EMBO Journal*, *21*(13), 3526–3535. https://doi.org/10.1093/EMBOJ/CDF335

Johnson, S. A., Cubberley, G., & Bentley, D. L. (2009). Co-transcriptional recruitment of the mRNA export factor Yra1 by direct interaction with the 3′-end processing factor Pcf11. *Mol Cell* 30; 33(2):215-26. doi: 10.1016/j.molcel.2008.12.007.

Juliano, R. L. (2016). SURVEY AND SUMMARY The delivery of therapeutic oligonucleotides. *Nucleic Acids Research*, *44*(14), 6518–6548. https://doi.org/10.1093/nar/gkw236

Juneau, K., Nislow, C., & Davis, R. W. (2009). Alternative Splicing of PTC7 in Saccharomyces cerevisiae Determines Protein Localization. *Genetics*, *183*(1), 185–194. https://doi.org/10.1534/GENETICS.109.105155

Karaki, S., Paris, C., Rocchi, P., Karaki, S., Paris, C., & Rocchi, P. (2019). Antisense Oligonucleotides, A Novel Developing Targeting Therapy. *Antisense Therapy*. https://doi.org/10.5772/INTECHOPEN.82105

Kastner, B., Will, C. L., Stark, H., & Lührmann, R. (2019). Structural Insights into Nuclear pre-mRNA Splicing in Higher Eukaryotes. *Cold Spring Harbor Perspectives in Biology*, *11*(11). https://doi.org/10.1101/CSHPERSPECT.A032417

Keil, P., Wulf, A., Kachariya, N., Reuscher, S., Hühn, K., Silbern, I., Altmüller, J., Keller, M., Stehle, R., Zarnack, K., Sattler, M., Urlaub, H., & Sträßer, K. (2023). Npl3 functions in mRNP assembly by recruitment of mRNP components to the transcription site and their transfer onto the mRNA. *Nucleic Acids Research*, *51*(2), 831–851. https://doi.org/10.1093/NAR/GKAC1206

Kelly, S. M., Pabit, S. A., Kitchen, C. M., Guo, P., Marfatia, K. A., Murphy, T. J., Corbett, A. H., & Berland, K. M. (2007). Recognition of polyadenosine RNA by zinc finger proteins. *Proceedings of the National Academy of Sciences of the United States of America*, *104*(30), 12306. https://doi.org/10.1073/PNAS.0701244104

Kim, M., Ahn, S. H., Krogan, N. J., Greenblatt, J. F., & Buratowski, S. (2004). Transitions in RNA polymerase II elongation complexes at the 3′ ends of genes. *EMBO Journal*, *23*(2), 354–364. https://doi.org/10.1038/SJ.EMBOJ.7600053

Kim, M., Krogan, N. J., Vasiljeva, L., Rando, O. J., Nedea, E., Greenblatt, J. F., & Buratowski, S. (2004). The yeast Rat1 exonuclease promotes transcription termination by RNA polymerase II. *Nature*, *432*(7016), 517–522. https://doi.org/10.1038/NATURE03041

Kim, S. J., Fernandez-Martinez, J., Sampathkumar, P., Martel, A., Matsui, T., Tsuruta, H., Weiss, T. M., Shi, Y., Markina-Inarrairaegui, A., Bonanno, J. B., Sauder, J. M., Burley, S. K., Chait, B. T., Almo, S. C., Rout, M. P., & Sali, A. (2014). Integrative structure-function mapping of the nucleoporin Nup133 suggests a conserved mechanism for membrane anchoring of the nuclear pore complex. *Molecular and Cellular Proteomics*, *13*(11), 2911–2926. https://doi.org/10.1074/MCP.M114.040915

Klass, D. M., Scheibe, M., Butter, F., Hogan, G. J., Mann, M., & Brown, P. O. (2013). Quantitative proteomic analysis reveals concurrent RNA-protein interactions and identifies new RNA-binding proteins in Saccharomyces cerevisiae. *Genome Research*, *23*(6), 1028–1038. https://doi.org/10.1101/GR.153031.11

Knoener, R. A., Becker, J. T., Scalf, M., Sherer, N. M., & Smith, L. M. (2017). Elucidating the in vivo interactome of HIV-1 RNA by hybridization capture and mass spectrometry. *Sci Rep ;*7(1):16965. doi: 10.1038/s41598-017-16793-5.

Knop, M., Finger, A., Braun, T., Hellmuth, K., & Wolf, D. H. (1996). Der1, a novel protein specifically required for endoplasmic reticulum degradation in yeast. *EMBO Journal*, *15*(4), 753–763. https://doi.org/10.1002/j.1460-2075.1996.tb00411.x

Köhler, A., & Hurt, E. (2007). Exporting RNA from the nucleus to the cytoplasm. *Nature Reviews. Molecular Cell Biology*, *8*(10), 761–773. https://doi.org/10.1038/NRM2255

Komili, S., & Silver, P. A. (2008). Coupling and coordination in gene expression processes: a systems biology view. *Nature Reviews. Genetics*, *9*(1), 38–48. https://doi.org/10.1038/NRG222

Kress, T. L., Krogan, N. J., & Guthrie, C. (2008). A single SR-like protein, Npl3, promotes pre-mRNA splicing in budding yeast. *Mol Cell* 5; 32(5):727-34. doi: 10.1016/j.molcel.2008.11.013.

Krishnamurthy, S., He, X., Reyes-Reyes, M., Moore, C., & Hampsey, M. (2004). Ssu72 Is an RNA Polymerase II CTD Phosphatase. *Molecular Cell*, *14*(3), 387–394. https://doi.org/10.1016/S1097-2765(04)00235-7

Kühn, U., Gündel, M., Knoth, A., Kerwitz, Y., Rüdel, S., & Wahle, E. (2009). Poly(A) tail length is controlled by the nuclear poly(A)-binding protein regulating the interaction between poly(A) polymerase and the cleavage and polyadenylation specificity factor. *The Journal of Biological Chemistry*, *284*(34), 22803–22814. https://doi.org/10.1074/JBC.M109.018226

Kumar, A., Clerici, M., Muckenfuss, L. M., Passmore, L. A., & Jinek, M. (2019). Mechanistic insights into mRNA 3′-end processing. *Current Opinion in Structural Biology*, *59*, 143–150. https://doi.org/10.1016/J.SBI.2019.08.001

Kumar, A., Yu, C. W. H., Rodríguez-Molina, J. B., Li, X. H., Freund, S. M. V., & Passmore, L. A. (2021). Dynamics in Fip1 regulate eukaryotic mRNA 3′ end processing. *Genes and Development*, *35*(21–22), 1510–1526. https://doi.org/10.1101/GAD.348671.121/-/DC1

Laemmli, U. K. (1970). Cleavage of structural proteins during the assembly of the head of bacteriophage T4. *Nature* 15; 227(5259):680-5. doi: 10.1038/227680a0.

Lee, H. Y., Haurwitz, R. E., Apffel, A., Zhou, K., Smart, B., Wenger, C. D., Laderman, S., Bruhn, L., & Doudna, J. A. (2013). RNA-protein analysis using a conditional CRISPR nuclease. *Proc Natl Acad Sci U S A*, 2;110(14):5416-21. doi: 10.1073/pnas.1302807110.

Lee, M. S., Henry, M., & Silver, P. A. (1996). A protein that shuttles between the nucleus and the cytoplasm is an important mediator of RNA export. *Genes & Development*, *10*(10), 1233–1246. https://doi.org/10.1101/GAD.10.10.1233

Lei, E. P., Krebber, H., & Silver, P. A. (2001). Messenger RNAs are recruited for nuclear export during transcription. *Genes & Development*, *15*(14), 1771–1782. https://doi.org/10.1101/GAD.892401

Leppek, K., & Stoecklin, G. (2014). An optimized streptavidin-binding RNA aptamer for purification of ribonucleoprotein complexes identifies novel ARE-binding proteins. *Nucleic Acids Research*, *42*(2). https://doi.org/10.1093/nar/gkt956

Li, W., Giles, C., & Li, S. (2014). Insights into how Spt5 functions in transcription elongation and repressing transcription coupled DNA repair. *Nucleic Acids Research*, *42*(11), 7069–7083. https://doi.org/10.1093/NAR/GKU333

Li, Y., Wang, X., Zhang, X., & Goodrich, D. W. (2005). Human hHpr1/p84/Thoc1 regulates transcriptional elongation and physically links RNA polymerase II and RNA processing factors. *Molecular and Cellular Biology*, *25*(10), 4023–4033. https://doi.org/10.1128/MCB.25.10.4023-4033.2005

Liang, X.-H., Shen, W., Sun, H., Prakash, T. P., & Crooke, S. T. (2014). TCP1 complex proteins interact with phosphorothioate oligonucleotides and can co-localize in oligonucleotide-induced nuclear bodies in mammalian cells. *Nucleic Acids Research*, *42*(12), 7819–7832. https://doi.org/10.1093/nar/gku484

Libri, D., Graziani, N., Saguez, C., & Boulay, J. (2001). Multiple roles for the yeast SUB2/yUAP56 gene in splicing. *Genes & Development*, *15*(1), 36. https://doi.org/10.1101/GAD.852101

Lidschreiber, M., Leike, K., & Cramer, P. (2013). Cap Completion and C-Terminal Repeat Domain Kinase Recruitment Underlie the Initiation-Elongation Transition of RNA Polymerase II. *Molecular and Cellular Biology*, *33*(19), 3805. https://doi.org/10.1128/MCB.00361-13

Lim, F., Downey, T. P., & Peabody, D. S. (2001). Translational Repression and Specific RNA Binding by the Coat Protein of the Pseudomonas Phage PP7. *Journal of Biological Chemistry*, *276*(25), 22507–22513. https://doi.org/10.1074/jbc.M102411200

Liu, Y., Warfield, L., Zhang, C., Luo, J., Allen, J., Lang, W. H., Ranish, J., Shokat, K. M., & Hahn, S. (2009). Phosphorylation of the Transcription Elongation Factor Spt5 by Yeast Bur1 Kinase Stimulates Recruitment of the PAF Complex. *MOLECULAR AND CELLULAR BIOLOGY*, *29*(17), 4852–4863. https://doi.org/10.1128/MCB.00609-09

Livak, K. J., & Schmittgen, T. D. (2001). Analysis of Relative Gene Expression Data Using Real-Time Quantitative PCR and the 2 C T Method. *METHODS*, *25*, 402–408. https://doi.org/10.1006/meth.2001.1262

Longman, D., Johnstone, I. L., & Cáceres, J. F. (2003). The Ref/Aly proteins are dispensable for mRNA export and development in Caenorhabditis elegans. *RNA (New York, N.Y.)*, *9*(7), 881–891. https://doi.org/10.1261/RNA.5420503

Lu, Y. Y., & Krebber, H. (2021). Nuclear mRNA Quality Control and Cytoplasmic NMD Are Linked by the Guard Proteins Gbp2 and Hrb1. *International Journal of Molecular Sciences*, *22*(20). https://doi.org/10.3390/IJMS22201127

Luna, R., Rondón, A. G., Pérez-Calero, C., Salas-Armenteros, I., & Aguilera, A. (2019). The THO Complex as a Paradigm for the Prevention of Cotranscriptional R-Loops. *Cold Spring Harb Symp Quant Biol*, 84:105-114. doi: 10.1101/sqb.2019.84.039594.

Lund, M. K., & Guthrie, C. (2005). The DEAD-box protein Dbp5p is required to dissociate Mex67p from exported mRNPs at the nuclear rim. *Molecular Cell*, *20*(4), 645–651. https://doi.org/10.1016/j.molcel.2005.10.005

Lunde, B. M., Moore, C., & Varani, G. (2007). RNA-binding proteins: modular design for efficient function. *Nature Reviews Molecular Cell Biology 2007 8:6*, *8*(6), 479–490. https://doi.org/10.1038/nrm217

Lusetti, S. L., Wood, E. A., Fleming, C. D., Modica, M. J., Korth, J., Abbott, L., Dwyer, D. W., Roca, A. I., Inman, R. B., & Cox, M. M. (2003). C-terminal deletions of the Escherichia coli RecA protein. Characterization of in vivo and in vitro effects. *J Biol Chem* 2; 278(18):16372-80. doi: 10.1074/jbc.M212917200.

Lyons, D. E., McMahon, S., & Ott, M. (2020). A combinatorial view of old and new RNA polymerase II modifications. *Transcription*, *11*(2), 66–82. https://doi.org/10.1080/21541264.2020.1762468

Mallikaratchy, P. (2017). Evolution of Complex Target SELEX to Identify Aptamers against Mammalian Cell-Surface Antigens. *Molecules : A Journal of Synthetic Chemistry and Natural Product Chemistry*, *22*(2). https://doi.org/10.3390/MOLECULES22020215

Maranon, D. G., & Wilusz, J. (2020). Mind the Gapmer: Implications of Co-transcriptional Cleavage by Antisense Oligonucleotides. *Molecular Cell*, *77*(5), 932–933. https://doi.org/10.1016/J.MOLCEL.2020.02.010

Marfatia, K. A., Crafton, E. B., Green, D. M., & Corbett, A. H. (2003). Domain analysis of the Saccharomyces cerevisiae heterogeneous nuclear ribonucleoprotein, Nab2p. Dissecting the requirements for Nab2p-facilitated poly(A) RNA export. *The Journal of Biological Chemistry*, *278*(9), 6731–6740. https://doi.org/10.1074/JBC.M207571200

Martinez-Rucobo, F. W., Kohler, R., van de Waterbeemd, M., Heck, A. J. R., Hemann, M., Herzog, F., Stark, H., & Cramer, P. (2015). Molecular Basis of Transcription-Coupled Pre-mRNA Capping. *Molecular Cell*, *58*(6), 1079–1089. https://doi.org/10.1016/J.MOLCEL.2015.04.004

Mason, P. B., & Struhl, K. (2005). Distinction and relationship between elongation rate and processivity of RNA polymerase II in vivo. *Molecular Cell*, *17*(6), 831–840. https://doi.org/10.1016/J.MOLCEL.2005.02.017

Masuda, S., Das, R., Cheng, H., Hurt, E., Dorman, N., & Reed, R. (2005). Recruitment of the human TREX complex to mRNA during splicing. *Genes & Development*, *19*(13), 1512–1517. https://doi.org/10.1101/GAD.1302205

Matia-González, A. M., Iadevaia, V., & Gerber, A. P. (2017). A versatile tandem RNA isolation procedure to capture in vivo formed mRNA-protein complexes. *Methods*, 15:118-119:93-100. doi: 10.1016/j.ymeth.2016.10.005.

Mayer, A., Heidemann, M., Lidschreiber, M., Schreieck, A., Sun, M., Hintermair, C., Kremmer, E., Eick, D., & Cramer, P. (2012). CTD tyrosine phosphorylation impairs termination factor recruitment to RNA polymerase II. *Science (New York, N.Y.)*, *336*(6089), 1723–1725. https://doi.org/10.1126/SCIENCE.1219651

Mayer, A., Lidschreiber, M., Siebert, M., Leike, K., Söding, J., & Cramer, P. (2010). Uniform transitions of the general RNA polymerase II transcription complex. *Nature Structural and Molecular Biology*, *17*(10), 1272–1278. https://doi.org/10.1038/nsmb.1903

Mayer, A., Schreieck, A., Lidschreiber, M., Leike, K., Martin, D. E., & Cramer, P. (2012). The spt5 C-terminal region recruits yeast 3' RNA cleavage factor I. *Molecular and Cellular Biology*, *32*(7), 1321–1331. https://doi.org/10.1128/MCB.06310-11

McCracken, S., Fong, N., Rosonina, E., Yankulov, K., Brothers, G., Siderovski, D., Hessel, A., Foster, S., Shuman, S., & Bentley, D. L. (1997). 5'-Capping enzymes are targeted to pre-mRNA by binding to the phosphorylated carboxy-terminal domain of RNA polymerase II. *Genes & Development*, *11*(24), 3306–3318. https://doi.org/10.1101/GAD.11.24.3306

Mchugh, C. A., Chen, C.-K., Chow, A., Surka, C. F., Tran, C., Mcdonel, P., Pandya-Jones, A., Blanco, M., Burghard, C., Moradian, A., Sweredoski, M. J., Shishkin, A. A., Su, J., Lander, E. S., Hess, S., Plath, K., & Guttman, M. (2015). The Xist lncRNA directly interacts with SHARP to silence transcription through HDAC3 HHS Public Access. *Nature*, *521*(7551), 232–236. https://doi.org/10.1038/nature14443

McHugh, C. A., Russell, P., & Guttman, M. (2014). Methods for comprehensive experimental identification of RNA-protein interactions. *Genome Biology*, *15*(1). https://doi.org/10.1186/GB4152

Meinel, D. M., Burkert-Kautzsch, C., Kieser, A., O'duibhir, E., & Siebert, M. (2013). Recruitment of TREX to the Transcription Machinery by Its Direct Binding to the Phospho-CTD of RNA Polymerase II) Recruitment of TREX to the Transcription Machinery by Its Direct Binding to the Phospho-CTD of RNA Polymerase II. *PLoS Genet*, *9*(11), 1003914. https://doi.org/10.1371/journal.pgen.1003914

Meinel, D. M., & Sträßer, K. (2015). Co-transcriptional mRNP formation is coordinated within a molecular mRNP packaging station in S. cerevisiae. *BioEssays*, *37*(6), 666–677. https://doi.org/10.1002/BIES.201400220

Merz, C., Urlaub, H., Will, C. L., & Lührmann, R. (2007). Protein composition of human mRNPs spliced in vitro and differential requirements for mRNP protein recruitment. *RNA*;13(1):116-28. doi: 10.1261/rna.336807.

Millevoi, S., & Vagner, S. (2010). Molecular mechanisms of eukaryotic pre-mRNA 3' end processing regulation. *Nucleic Acids Research*, *38*(9), 2757–2774. https://doi.org/10.1093/NAR/GKP1176

Minvielle-Sebastia, L., Preker, P. J., Wiederkehr, T., Strahm, Y., & Keller, W. (1997). The major yeast poly(A)-binding protein is associated with cleavage factor IA and functions in premessenger RNA 3′-end formation. *Proceedings of the National Academy of Sciences of the United States of America*, *94*(15), 7897. https://doi.org/10.1073/PNAS.94.15.7897

Minvielle-Sebastia, L., Winsor, B., Bonneaud,' And, N., & Lacroute1, F. (1991). Mutations in the Yeast RNA14 and RNAJ5 Genes Result in an Abnormal mRNA Decay Rate; Sequence Analysis Reveals an RNA-Binding Domain in the RNA15 Protein. *MOLECULAR AND CELLULAR BIOLOGY*, 3075–3087.

Miosga, M. (2022). Function of the RNA helicase Sub2 from Saccharomyces cerevisiae and its regulation by Tho1. https://jlupub.ub.uni-giessen.de/handle/jlupub/3279

Mischo, H. E., & Proudfoot, N. J. (2013). Disengaging polymerase: terminating RNA polymerase II transcription in budding yeast. *Biochimica et Biophysica Acta*, *1829*(1), 174–185. https://doi.org/10.1016/J.BBAGRM.2012.10.003

Mishra, P. K., Chakraborty, A., Yeh, E., Feng, W., Bloom, K. S., & Basrai, M. A. (2021). R-loops at centromeric chromatin contribute to defects in kinetochore integrity and chromosomal instability in budding yeast. *Molecular Biology of the Cell*, *32*(1), 74–89. https://doi.org/10.1091/MBC.E20-06-0379

Mitchell, S. F., Jain, S., She, M., & Parker, R. (2013). Global analysis of yeast mRNPs. *Nature Structural & Molecular Biology*, *20*(1), 127–133. https://doi.org/10.1038/NSMB.2468

Murakami, K.. (2015). Structure of an RNA polymerase II preinitiation complex. *Proc Natl Acad Sci U S A* 3;112(44):13543-8. doi: 10.1073/pnas.1518255112.*112*. https://doi.org/10.1073/pnas.1518255112

Nishimura, K., Fukagawa, T., Takisawa, H., Kakimoto, T., & Kanemaki, M. (2009). An auxin-based degron system for the rapid depletion of proteins in nonplant cells. *Nature Methods*, *6*(12), 917–922. https://doi.org/10.1038/NMETH.1401

Nousch, M., Techritz, N., Hampel, D., Millonigg, S., & Eckmann, C. R. (2013). The Ccr4-Not deadenylase complex constitutes the main poly(A) removal activity in C. elegans. *Journal of Cell Science*, *126*(Pt 18), 4274–4285. https://doi.org/10.1242/JCS.132936

Oeffinger, M., Wei, K. E., Rogers, R., DeGrasse, J. A., Chait, B. T., Aitchison, J. D., & Rout, M. P. (2007). Comprehensive analysis of diverse ribonucleoprotein complexes. *Nature Methods*, *4*(11), 951–956. https://doi.org/10.1038/NMETH1101

Pacheco-Fiallos, B., Vorländer, M. K., Riabov-Bassat, D., Fin, L., O'Reilly, F. J., Ayala, F. I., Schellhaas, U., Rappsilber, J., & Plaschka, C. (2023). mRNA recognition and packaging by the human transcription–export complex. *Nature 2023*, 1–8. https://doi.org/10.1038/s41586-023-05904-0

Parenteau, J., Durand, M., Véronneau, S., Lacombe, A. A., Morin, G., Guérin, V., Cecez, B., Gervais-Bird, J., Koh, C. S., Brunelle, D., Wellinger, R. J., Chabot, B., & Abou Elela, S. (2008). Deletion of Many Yeast Introns Reveals a Minority of Genes that Require Splicing for Function. *Molecular Biology of the Cell*, *19*(5), 1932. https://doi.org/10.1091/MBC.E07-12-1254

Passmore, L. A., & Coller, J. (2022). Roles of mRNA poly(A) tails in regulation of eukaryotic gene expression. *Nat Rev Mol Cell Biol*; 23(2):93-106. https://doi: 10.1038/s41580-021-00417-y

Patrizia Derrer, C., Mancini, R., Vallotton, P., Huet, S., Weis, K., & Dultz, E. (2019). The RNA export factor Mex67 functions as a mobile nucleoporin. *J Cell Biol* 2; 218(12):3967-3976. https://doi: 10.1083/jcb.201909028

Petrenko, N., & Struhl, K. (2021). Comparison of transcriptional initiation by RNA polymerase II across eukaryotic species. *Elife*, 13:10:e67964. https://doi.org/10.7554/eLife

Phillips, S. L., Soderblom, E. J., Bradrick, S. S., & Garcia-Blanco, M. A. (2016). Identification of proteins bound to dengue viral RNA In Vivo reveals new host proteins important for virus replication. *MBio*, *7*(1). https://doi.org/10.1128/MBIO.01865-15/FORMAT/EPUB

Plaschka, C., Larivière, L., Wenzeck, L., Seizl, M., Hemann, M., Tegunov, D., Petrotchenko, E. V, Borchers, C. H., Baumeister, W., Herzog, F., Villa, E., & Cramer, P. (2015). Architecture of the RNA polymerase II-Mediator core initiation complex. *Nature*, 518(7539):376-80. https://doi.org/10.1038/nature14229

Plaschka, C., Lin, P. C., Charenton, C., & Nagai, K. (2018). Prespliceosome structure provides insights into spliceosome assembly and regulation. *Nature*, *559*(7714), 419–422. https://doi.org/10.1038/S41586-018-0323-8

Plaschka, C., Newman, A. J., & Nagai, K. (2019). Structural Basis of Nuclear pre-mRNA Splicing: Lessons from Yeast. *Cold Spring Harbor Perspectives in Biology*, *11*(5), a032391. https://doi.org/10.1101/CSHPERSPECT.A032391

Pollak, A. J., Hickman, J. H., Liang, X. H., & Crooke, S. T. (2020). Gapmer Antisense Oligonucleotides Targeting 5S Ribosomal RNA Can Reduce Mature 5S Ribosomal RNA by Two Mechanisms. *Nucleic Acid Therapeutics*, *30*(5), 312–324. https://doi.org/10.1089/NAT.2020.0864

Portman, D. S., O'Connor, J. P., & Dreyfuss, G. (1997). YRA1, an essential Saccharomyces cerevisiae gene, encodes a novel nuclear protein with RNA annealing activity. *RNA*, *3*(5), 527-37.

Pühringer, T., Hohmann, U., Fin, L., Pacheco-Fiallos, B., Schellhaas, U., Brennecke, J., & Plaschka, C. (2020). Structure of the human core transcription-export complex reveals a hub for multivalent interactions. *ELife*, *9*, 1–65. https://doi.org/10.7554/ELIFE.61503

Puig, O., Caspary, F., Rigaut, G., Rutz, B., Bouveret, E., Bragado-Nilsson, E., Wilm, M., & Séraphin, B. (2001). The tandem affinity purification (TAP) method: A general procedure of protein complex purification. *Methods*, *24*(3), 218–229. https://doi.org/10.1006/METH.2001.1183

Quemener, A. M., Bachelot, L., Forestier, A., Donnou-Fournet, E., Gilot, D., & Galibert, M. D. (2020). The powerful world of antisense oligonucleotides: From bench to bedside. *Wiley Interdisciplinary Reviews. RNA*, *11*(5). https://doi.org/10.1002/WRNA.1594

Rajoo, S., Vallotton, P., Onischenko, E., & Weis, K. (2018). Stoichiometry and compositional plasticity of the yeast nuclear pore complex revealed by quantitative fluorescence microscopy. *Proceedings of the National Academy of Sciences of the United States of America*, *115*(17), E3969–E3977. https://doi.org/10.1073/PNAS.1719398115/-/DCSUPPLEMENTAL

Ramanathan, A., Robb, G. B., & Chan, S. H. (2016). mRNA capping: biological functions and applications. *Nucleic Acids Research*, *44*(16), 7511–7526. https://doi.org/10.1093/NAR/GKW551

Ren, Y., Schmiege, P., & Blobel, G. (2017). Structural and biochemical analyses of the DEAD-box ATPase Sub2 in association with THO or Yra1. *ELife*, *6*. https://doi.org/10.7554/ELIFE.20070

Reuter, L. M., Meinel, D. M., & Sträßer, K. (2015). The poly(A)-binding protein Nab2 functions in RNA polymerase III transcription. *Genes & Development*, *29*(14), 1565–1575. https://doi.org/10.1101/GAD.266205.115

Rodríguez-Molina, J. B., & Turtola, M. (2023). Birth of a poly(A) tail: mechanisms and control of mRNA polyadenylation. *FEBS Open Bio*, *13*(7). https://doi.org/10.1002/2211-5463.13528

Rodríguez-Molina, J. B., West, S., & Passmore, L. A. (2023). Knowing when to stop: Transcription termination on protein-coding genes by eukaryotic RNAPII. *Molecular Cell*, *83*(3), 404–415. https://doi.org/10.1016/J.MOLCEL.2022.12.021

Rogell, B., Fischer, B., Rettel, M., Krijgsveld, J., Castello, A., & Hentze, M. W. (2017). Specific RNP capture with antisense LNA/DNA mixmers. *RNA*; 23(8):1290-1302. https://doi.org/10.1261/rna

Rondón, A. G., Jimeno, S., García-Rubio, M., & Aguilera, A. (2003). Molecular evidence that the eukaryotic THO/TREX complex is required for efficient transcription elongation. *Journal of Biological Chemistry*, *278*(40), 39037–39043. https://doi.org/10.1074/jbc.M305718200

Röther, S., Clausing, E., Kieser, A., & Strässer, K. (2006). Swt1, a novel yeast protein, functions in transcription. *The Journal of Biological Chemistry*, *281*(48), 36518–36525. https://doi.org/10.1074/JBC.M607510200

Rougemaille, M., Dieppois, G., Kisseleva-Romanova, E., Gudipati, R. K., Lemoine, S., Blugeon, C., Boulay, J., Jensen, T. H., Stutz, F., Devaux, F., & Libri, D. (2008). THO/Sub2p functions to coordinate 3'-end processing with gene-nuclear pore association. *Cell*, *135*(2), 308–321. https://doi.org/10.1016/J.CELL.2008.08.005

Saguez, C., Gonzales, F. A., Schmid, M., Bøggild, A., Latrick, C. M., Malagon, F., Putnam, A., Sanderson, L., Jankowsky, E., Brodersen, D. E., & Jensen, T. H. (2013). Mutational analysis of the yeast RNA helicase Sub2p reveals conserved domains required for growth, mRNA export, and genomic stability. *RNA*, *19*(10), 1363. https://doi.org/10.1261/RNA.040048.113

Saguez, C., Schmid, M., Olesen, J. R., Ghazy, M. A. E. H., Qu, X., Poulsen, M. B., Nasser, T., Moore, C., & Jensen, T. H. (2008). Nuclear mRNA Surveillance in THO/sub2 Mutants Is Triggered by Inefficient Polyadenylation. *Molecular Cell*, *31*(1), 91–103. https://doi.org/10.1016/J.MOLCEL.2008.04.030

Sainsbury, S., Bernecky, C., & Cramer, P. (2015). Structural basis of transcription initiation by RNA polymerase II. *NATURE REVIEWS | MOLECULAR CELL BIOLOGY*, *16*, 129. https://doi.org/10.1038/nrm395

San Martin-Alonso, M., Soler-Oliva, M. E., García-Rubio, M., García-Muse, T., & Aguilera, A. (2021). Harmful R-loops are prevented via different cell cycle-specific mechanisms. *Nat Commun* 22; 12(1):4451. https://doi.org/10.1038/s41467-021-24737-x

Santos-Pereira, J. M., Herrero, A. B., García-Rubio, M. L., Marín, A., Moreno, S., & Aguilera, A. (2013). The Npl3 hnRNP prevents R-loop-mediated transcription-replication conflicts and genome instability. *Genes & Development*, *27*(22), 2445–2458. https://doi.org/10.1101/GAD.229880.113

Santos-Rosa, H., Moreno, H., Simos, G., Segref, A., Fahrenkrog, B., Panté, N., & Hurt, E. (1998). Nuclear mRNA export requires complex formation between Mex67p and Mtr2p at the nuclear pores. *Molecular and Cellular Biology*, *18*(11), 6826–6838. https://doi.org/10.1128/MCB.18.11.6826

Scarff, C. A., Fuller, M. J., Thompson, R. F., & Iadaza, M. G. (2018). Variations on Negative Stain Electron Microscopy Methods: Tools for Tackling Challenging Systems. *J. Vis. Exp*, *132*, 57199. https://doi.org/10.3791/57199

Schmid, M., Poulsen, M. B., Olszewski, P., Pelechano, V., Saguez, C., Gupta, I., Steinmetz, L. M., Moore, C., & Jensen, T. H. (2012). Rrp6p controls mRNA poly(A) tail length and its decoration with poly(A) binding proteins. *Molecular Cell*, *47*(2), 267–280. https://doi.org/10.1016/J.MOLCEL.2012.05.005

Schroeder, S. C., Schwer, B., Shuman, S., & Bentley, D. (2000). Dynamic association of capping enzymes with transcribing RNA polymerase II. *Genes Dev*; 14(19):2435-40.https://doi.org/10.1101/gad.836300

Schuller, S. K., Schuller, J. M., Prabu, J. R., Baumgärtner, M., Bonneau, F., Basquin, J., & Conti, E. (2020). Structural insights into the nucleic acid remodeling mechanisms of the yeast tho-SUB2 complex. *ELife*, *9*, 1–51. https://doi.org/10.7554/ELIFE.61467

Schwer, B., & Shuman, S. (2011). Deciphering the RNA polymerase II CTD code in fission yeast. *Molecular Cell*, *43*(2), 311–318. https://doi.org/10.1016/J.MOLCEL.2011.05.02

Selth, L. A., Gilbert, C., & Svejstrup, J. Q. (2009). RNA Immunoprecipitation to Determine RNA-Protein Associations In Vivo. *Cold Spring Harb Protoc*; (6):pdb.prot5234. https://doi.org/10.1101/pdb.prot5234

Sen, R., Barman, P., Kaja, A., Ferdoush, J., Lahudkar, S., Roy, A., & Bhaumik, S. R. (2019). Distinct Functions of the Cap-Binding Complex in Stimulation of Nuclear mRNA Export. *Molecular and Cellular Biology*, *39*(8). https://doi.org/10.1128/MCB.00540-18

Shyam Panchapakesan, S. S., Ferguson, M. L., Hayden, E. J., Chen, X., Hoskins, A. A., & Unrau, P. J. (2017). Ribonucleoprotein purification and characterization using RNA Mango. *RNA*; 23(10):1592-1599. https://doi: 10.1261/rna.062166.117

Sikorski, R. S., & Hieter, P. (1989). A System of Shuttle Vectors and Yeast Host Strains Designed for Efficient Manipulation of DNA in Saccharomyces ceratisiae. Genetics; 122(1):19-27. doi: 10.1093/genetics/122.1.19.

Singh, N., Asalam, M., Ansari, M. O., Gerasimova, N. S., Studitsky, V. M., & Akhtar, M. S. (2022). Transcription by RNA polymerase II and the CTD-chromatin crosstalk. *Biochemical and Biophysical Research Communications*, *599*, 81–86. https://doi.org/10.1016/J.BBRC.2022.02.039

Skružný, M., Schneider, C., Rácz, A., Weng, J., Tollervey, D., & Hurt, E. (2009). An endoribonuclease functionally linked to perinuclear mRNP quality control associates with the nuclear pore complexes. *PLoS Biology*, *7*(1). https://doi.org/10.1371/JOURNAL.PBIO.1000008

Slobodin, B., & Gerst, J. E. (2010). A novel mRNA affinity purification technique for the identification of interacting proteins and transcripts in ribonucleoprotein complexes. *RNA*; 16(11):2277-90. doi: 10.1261/rna.2091710

Smith, J. E., & Baker, K. E. (2017). Purification of Transcript-Specific mRNP Complexes Formed In Vivo from Saccharomyces cerevisiae. *Methods in Molecular Biology (Clifton, N.J.)*, *1648*, 201. https://doi.org/10.1007/978-1-4939-7204-3_15

Soucek, S., Zeng, Y., Bellur, D. L., Bergkessel, M., Morris, K. J., Deng, Q., Duong, D., Seyfried, N. T., Guthrie, C., Staley, J. P., Fasken, M. B., & Corbett, A. H. (2016). The Evolutionarily-conserved Polyadenosine RNA Binding Protein, Nab2, Cooperates with Splicing Machinery to Regulate the Fate of pre-mRNA. *Molecular and Cellular Biology*, *36*(21), 2697–2714. https://doi.org/10.1128/MCB.00402-16

Soutourina, J., Wydau, S., Ambroise, Y., Boschiero, C., & Werner, M. (2011). Direct interaction of RNA polymerase II and mediator required for transcription in vivo. *Science (New York, N.Y.)*, *331*(6023), 1451–1454. https://doi.org/10.1126/SCIENCE.1200188

Spiniello, M., Steinbrink, M. I., Cesnik, A. J., Miller, R. M., Scalf, M., Shortreed, M. R., & Smith, L. M. (2019). Comprehensive in vivo identification of the c-Myc mRNA protein interactome using HyPR-MS. *RNA*, *25*(10), 1337–1352. https://doi.org/10.1261/RNA.072157.119/-/DC1

Squazzo, S. L., Costa, P. J., Lindstrom, D. L., Kumer, K. E., Simic, R., Jennings, J. L., Link, A. J., Arndt, K. M., & Hartzog, G. A. (2002). The Paf1 complex physically and functionally associates with transcription elongation factors in vivo. *EMBO Journal*, *21*(7), 1764–1774. https://doi.org/10.1093/EMBOJ/21.7.176

Srisawat, C., & Engelke, D. R. (2002). RNA affinity tags for purification of RNAs and ribonucleoprotein complexes. Methods, 26(2):156-61. https://doi: 10.1016/S1046-2023(02)00018-X

Srisawat, C., Goldstein, I. J., & Engelke, D. R. (2001). Sephadex-binding RNA ligands: rapid affinity purification of RNA from complex RNA mixtures. *Nucleic Acids Research*, *29*(2). https://doi.org/10.1093/NAR/29.2.E4

Strambio-De-Castillia, C., Niepel, M., & Rout, M. P. (2010). The nuclear pore complex: bridging nuclear transport and gene regulation. *Nature Reviews. Molecular Cell Biology*, *11*(7), 490–501. https://doi.org/10.1038/NRM2928

Sträßer, K., Masuda, S., Mason, P., Pfannstiel, J., Oppizzi, M., Rodriguez-Navarro, S., Rondón, A. G., Aguilera, A., Struhl, K., Reed, R., & Hurt, E. (2002). TREX is a conserved complex coupling transcription with messenger RNA export. *Nature 2002 417:6886*, *417*(6886), 304–308. https://doi.org/10.1038/nature746

Sträßer, K., & Hurt, E. (2000). Yra1p, a conserved nuclear RNA-binding protein, interacts directly with Mex67p and is required for mRNA export. *The EMBO Journal*, *19*(3), 410–420.

Sträßer, K., Baßler, J., & Hurt, E. (2000). Binding of the Mex67p/Mtr2p Heterodimer to FXFG, GLFG, and FG Repeat Nucleoporins Is Essential for Nuclear mRNA Export. *The Journal of Cell Biology*, *150*(4), 695–706. http://www.jcb.org

Sträßer, K., & Hurt, E. (2001). Splicing factor Sub2p is required for nuclear mRNA export through its interaction with Yra1p. *Nature 2001 413:6856*, *413*(6856), 648–652. https://doi.org/10.1038/35098113

Takase, Y., Takagi, T., Komarnitsky, P. B., & Buratowski, S. (2000). The Essential Interaction between Yeast mRNA Capping Enzyme Subunits Is Not Required for Triphosphatase Function In Vivo. *Mol Cell Biol*; 20(24):9307-16. https://doi: 10.1128/MCB.20.24.9307-9316.2000

Tallet-Lopez, B., Aldaz-Carroll, L., Chabas, S., Dausse, E., Staedel, C., & Toulme, J. J. (2003). Antisense oligonucleotides targeted to the domain IIId of the hepatitis C virus IRES compete with 40S ribosomal subunit binding and prevent in vitro translation. *Nucleic Acids Research*, *31*(2), 734–742. https://doi.org/10.1093/NAR/GKG139

Tanaka, N., Aronova, A., & Schwer, B. (2007). Ntr1 activates the Prp43 helicase to trigger release of lariat-intron from the spliceosome. *Genes & Development*, *21*(18), 2312. https://doi.org/10.1101/GAD.1580507

Taylor, R. G., Walker, D. C., & Mclnnes, R. R. (1993). E.coli host strains significantly affect the quality of small scale plasmid DNA preparations used for sequencing. *Nucleic Acids Research*, *21*(7), 1677–1678. https://academic.oup.com/nar/article/21/7/1677/2386065

Terry, L. J., & Wente, S. R. (2009). Flexible Gates: Dynamic Topologies and Functions for FG Nucleoporins in Nucleocytoplasmic Transport. *Eukaryotic Cell*, *8*(12), 1814. https://doi.org/10.1128/EC.00225-09

Theil, K., Imami, K., & Rajewsky, N. (2019). Identification of proteins and miRNAs that specifically bind an mRNA in vivo. *Nature Communications 2019 10:1*, *10*(1), 1–13. https://doi.org/10.1038/s41467-019-12050-7

Thomas, B. J., & Rothstein, R. (1989). Elevated recombination rates in transcriptionally active DNA. *Cell*, *56*(4), 619–630. https://doi.org/10.1016/0092-8674(89)90584-9

Towbin, H., Staehelint, T., & Gordon, J. (1979). Electrophoretic transfer of proteins from polyacrylamide gels to nitrocellulose sheets: Procedure and some applications (ribosomal proteins/radioimmunoassay/fluorescent antibody assay/peroxidase-conjugated antibody/autoradiography). *Biochemistry*, *76*(9), 4350–4354. https://www.pnas.org

Turtola, M., Manav, C. M., Kumar, A., Tudek, A., Mroczek, S., Krawczyk, P. S., Dziembowski, A., Schmid, M., Passmore, L. A., Casanal, A., & Jensen, T. H. (2021). Three-layered control of mRNA poly(A) tail synthesis in Saccharomyces cerevisiae. *Genes and Development*, *35*(17–18), 1290–1303. https://doi.org/10.1101/GAD.348634.121/-/DC1

Tutucci, E., Vera, M., Biswas, J., Garcia, J., Parker, R., & Singer, R. H. (2018). An improved MS2 system for accurate reporting of the mRNA life cycle. *Nature Methods*, *15*(1), 81–89. https://doi.org/10.1038/NMETH.4502

Upadhyay, A., Dixit, U., Manvar, D., Chaturvedi, N., & Pandey, V. N. (2013). Affinity Capture and Identification of Host Cell Factors Associated with Hepatitis C Virus (+) Strand Subgenomic RNA. *Molecular & Cellular Proteomics : MCP*, *12*(6), 1539. https://doi.org/10.1074/MCP.M112.017020

Vinciguerra, P., Iglesias, N., Camblong, J., Zenklusen, D., & Stutz, F. (2005). Perinuclear Mlp proteins downregulate gene expression in response to a defect in mRNA export. *The EMBO Journal*, *24*(4), 813. https://doi.org/10.1038/SJ.EMBOJ.7600527

Voynov, V., Verstrepen, K. J., Jansen, A., Runner, V. M., Buratowski, S., & Fink, G. R. (2006). Genes with internal repeats require the THO complex for transcription. *Proceedings of the National Academy of Sciences of the United States of America*, *103*(39), 14423–14428. https://doi.org/10.1073/PNAS.0606546103

Wallace, S. T., & Schroede, R. (1998). In vitro selection and characterization of streptomycin-binding RNAs: recognition discrimination between antibiotics. *RNA*, 4(1):112-23.

Wan, R., Bai, R., Yan, C., Lei, J., & Shi, Y. (2019). Structures of the Catalytically Activated Yeast Spliceosome Reveal the Mechanism of Branching. *Cell*, *177*(2), 339-351.e13. https://doi.org/10.1016/J.CELL.2019.02.006

Wan, R., Yan, C., Bai, R., Lei, J., & Shi, Y. (2017). Structure of an Intron Lariat Spliceosome from Saccharomyces cerevisiae. *Cell*, *171*(1), 120-132.e12. https://doi.org/10.1016/j.cell.2017.08.029

Wang, Q., Zhang, L., Lynn, B., & Rymond, B. C. (2008). A BBP-Mud2p heterodimer mediates branchpoint recognition and influences splicing substrate abundance in budding yeast. *Nucleic Acids Research*, *36*(8), 2787–2798. https://doi.org/10.1093/NAR/GKN144

Wellinger, R. E., Prado, F., & Aguilera, A. (2006). Replication fork progression is impaired by transcription in hyperrecombinant yeast cells lacking a functional THO complex. *Molecular and Cellular Biology*, *26*(8), 3327–3334. https://doi.org/10.1128/MCB.26.8.3327-3334.2006

West, J. A., Davis, C. P., Sunwoo, H., Simon, M. D., Sadreyev, R. I., Wang, P. I., Tolstorukov, M. Y., & Kingston, R. E. (2014). The long noncoding RNAs NEAT1 and MALAT1 bind active chromatin sites. *Molecular Cell*, *55*(5), 791–802. https://doi.org/10.1016/J.MOLCEL.2014.07.012

Wier, A. D., Mayekar, M. K., Héroux, A., Arndt, K. M., & Vandemark, A. P. (2013). Structural basis for Spt5-mediated recruitment of the Paf1 complex to chromatin. *Proc Natl Acad Sci U S A*; 110(43):17290-5. https://doi: 10.1073/pnas.1314754110.

Wierschem, C. (2020). A twostep affinity purification of nuclear mRNPs. https://jlupub.ub.uni-giessen.de/handle/jlupub/120

Wilkinson, M. E., Charenton, C., & Nagai, K. (2020). RNA Splicing by the Spliceosome. *Annual Review of Biochemistry*, *89*, 359–388. https://doi.org/10.1146/ANNUREV-BIOCHEM-091719-064225

Wilkinson, M. E., Fica, S. M., Galej, W. P., Norman, C. M., Newman, A. J., & Nagai, K. (2017). Postcatalytic spliceosome structure reveals mechanism of 3'-splice site selection. *Science (New York, N.Y.)*, *358*(6368), 1283–1288. https://doi.org/10.1126/SCIENCE.AAR3729

Windbichler, N., & Schroeder, R. (2006). Isolation of specific RNA-binding proteins using the streptomycin-binding RNA aptamer. *Nature Protocols*, *1*(2), 637–640. https://doi.org/10.1038/NPROT.2006.95

Wong, C., Sridhara, S., Bardwell, J. C. A., & Jakob, U. (2000). Heating greatly speeds coomassie blue staining and destaining. *BioTechniques*, *28*(3), 426–432. https://doi.org/10.2144/00283BM07

Xie, Y., Clarke, B. P., Kim, Y. J., Ivey, A. L., Hill, P. S., Shi, Y., & Ren, Y. (2021). Cryo-EM structure of the yeast TREX complex and coordination with the SR-like protein Gbp2. *ELife*, *10*. https://doi.org/10.7554/ELIFE.65699

Xie, Y., Gao, S., Zhang, K., Bhat, P., Clarke, B. P., Batten, K., Mei, M., Gazzara, M., Shay, J. W., Lynch, K. W., Angelos, A. E., Hill, P. S., Ivey, A. L., Fontoura, B., & Ren, Y. (2023). Structural basis for high-order complex of SARNP and DDX39B to facilitate mRNP assembly. *Cell Reports*, *42*(8). https://doi.org/10.1016/J.CELREP.2023.112988

Xie, Y., Lord, C. L., Clarke, B. P., Ivey, A. L., Hill, P. S., Hayes McDonald, W., Wente, S. R., & Ren, Y. (2021). Structure and activation mechanism of the yeast RNA Pol II CTD kinase CTDK-1 complex. *Proceedings of the National Academy of Sciences of the United States of America*, *118*(3). https://doi: 10.1073/pnas.2019163118.

Xie, Y., & Ren, Y. (2019). Mechanisms of nuclear mRNA export: a structural perspective HHS Public Access. *Traffic*; 20(11):829-840. https://doi.org/10.1111/tra.12691

Yan, C., Wan, R., & Shi, Y. (2019). Molecular Mechanisms of pre-mRNA Splicing through Structural Biology of the Spliceosome. *Cold Spring Harbor Perspectives in Biology*, *11*(1). https://doi.org/10.1101/CSHPERSPECT.A032409

Yeh, F. L., Chang, S. L., Ahmed, G. R., Liu, H. I., Tung, L., Yeh, C. S., Lanier, L. S., Maeder, C., Lin, C. M., Tsai, S. C., Hsiao, W. Y., Chang, W. H., & Chang, T. H. (2021). Activation of Prp28 ATPase by phosphorylated Npl3 at a critical step of spliceosome remodeling. *Nature Communications 2021 12:1*, *12*(1), 1–9. https://doi.org/10.1038/s41467-021-23459-

Yoon, J.-H., & Gorospe, M. (2016). Identification of mRNA-interacting factors by MS2-TRAP (MS2-tagged RNA affinity purification). *Methods Mol Biol* 1421:15-22. https://doi.org/10.1007/978-1-4939-3591-8_2

Zenklusen, D., Vinciguerra, P., Strahm, Y., & Stutz, F. (2001). The yeast hnRNP-Like proteins Yra1p and Yra2p participate in mRNA export through interaction with Mex67p. *Molecular and Cellular Biology*, *21*(13), 4219–4232. https://doi.org/10.1128/MCB.21.13.4219-4232.2001

Zenklusen, D., Vinciguerra, P., Wyss, J.-C., & Stutz, F. (2002). Stable mRNP formation and export require cotranscriptional recruitment of the mRNA export factors Yra1p and Sub2p by Hpr1p. *Molecular and Cellular Biology*, *22*(23), 8241–8253. https://doi.org/10.1128/MCB.22.23.8241-8253.2002

Zhang, L., Vickers, T. A., Sun, H., Liang, X.-H., & Crooke, S. T. (2021). Binding of phosphorothioate oligonucleotides with RNase H1 can cause conformational changes in the protein and alter the interactions of RNase H1 with other proteins. *Nucleic Acids Research*, *49*(5), 2721–2739. https://doi.org/10.1093/nar/gkab078

Zhang, M., & Green, M. R. (2001). Identification and characterization of yUAP/Sub2p, a yeast homolog of the essential human pre-mRNA splicing factor hUAP56. *Genes & Development*, *15*(1), 30–35. https://doi.org/10.1101/GAD.851701

Zhou, Z., Licklider, L. J., Gygi, S. P., & Reed, R. (2002). Comprehensive proteomic analysis of the human spliceosome. *Nature*, *419*(6903), 182–185.

Zhou, Z., Sim, J., Griffith, J., & Reed, R. (2002). Purification and electron microscopic visualization of functional human spliceosomes. *Proc Natl Acad Sci U S A*; 99(19):12203-7. https://doi: 10.1073/pnas.182427099.

9. List of figures

10. List of tables

11. Abbreviations

Abbreviation	Description
°C	degree Celsius
µL	microlitre
nm	nanometer
2’-MOE	2’-O-methoxyethyl
2’-OMe	2’-O-methyl
7mG	7-methyl-guanosine
A	adenine
AID	Auxin-inducible degron
ASO	Antisence oligonucleotide
bp	basepaires
BP	branch point
BBP	branch point binding protein
C	cytosine
CBC	cap-binding complex
CF	cleavage factor
ChIP	Chromatin immunoprecipitation
Cryo-EM	Cryo-electron microscopy
Cryo-ET	Cryo-electron tomography
CPF	cleavage and polyadenylation factor
CTD	C-terminal domain
CTR	C-terminal region
DEPC	Diethyl pyrocarbonate
DNA	desoxyribonucleic acid
Dtb	desthiobiotin
E. coli	*Escherichia coli*
EJC	exon junction complex
ePAT	Extension poly(A) test
EtOH	ethanol
FG	phenylalanine glycine
FISH	Fluorescence *in situ* hybridization

G	guanine
GAP	GTPase activating protein
GDP	guanosindiphosphat
GEF	GDF exchange factor
GMP	guanosinmonophosphat
GraFIX	gradient centrifuation with cross-linking
GTF	general transcription factor
GTP	guanosintriphosphat
IAA	indole-3-acetic acid
ILS	intron lariat spliceosome
KH	K homology domain
LNA	locked nucleic acids
lncRNA	Long non-coding RNA
MBP	Maltose binding protein
MCP	MS2-coat protein
MDa	Megadalton
mRNA	messenger ribonucleic acid
mRNP	messenger ribonucleoprotein particle
MS2-TRAP	MS2-tagged RNA affinity purification
NAA	1-naphtaleneacetic acid
NPC	Nuclear pore complex
nt	nucleotide
Nup	nucleoporin
OD600	optical density at 600 nanometres
OE	overexpression
P	phosphorylation
PAGE	polyacrylamide gel electrophoresis
PAS	polyadenylation signal
PIC	pre-initiator complex
PMO	phosphorodiamidate morpholino oligomers
PNA	peptide nucleic acid
Poly(A)	polyadenosine
PS	Phosphorothioate
PCR	Polymerase chain reaction

RaPID	RNA binding protein purification and identification
RBP	RNA-binding protein
RIP	RNA-immunoprecipitation
RNA	ribonucleic acid
RNAPII	RNA polymerase II
RRM	RNA-recognition motif
RT	Room temperature
RT-qPCR	Reverse transcription - quantitative polymerase chain reaction
S. cerevisiae	*Saccharomyces cerevisiae*
SBP	streptavidin-binding protein
SELEX	systematic evolution of ligands by exponential enrichment
SD	standard deviation
snRNA	small nuclear RNAs
snRNP	small nuclear ribonucleoprotein particles
SR	serine-arginine
SS	splicing site
ssRNA	Single stranded RNA
T	thymine
TAF	TBP associated factors
TAP	Tandem affinity purification
TBP	TATA-box binding protein
TO	thiazole orange
TO1-Dtb	thiazole orange 1 desthiobiotin
TREX	transport export complex
TRIP	tandem RNA isolation procedure
U	Uracil
UTR	Untranslated region
qPCR	quantitative polymerase chain reaction
Ub	ubiquitin
UBA	ubiquitin associated domain
WT	Wild type
YPD	Yeast extract, peptone, dextrose
ZnF	zinc finger domain

12. Acknowledgements

First of all, I want to thank Prof. Dr. Katja Sträßer for the opportunity to work on the fascinating projects in the lab and for scientific support. Secondly, I want to acknowledge my second assessor Prof. Dr. Elena Evguenieva-Hackenberg and examiners Prof. Dr. Reinhard Dammann and Prof. Dr. Kai Thormann for being the part of my disputation committee: I appreciate your time and expertise. I also want to thank people who contributed to this study: Johanna Seidler and Christoph Wierschem for working together on mRNP project, collaborators Dr. Ulrich Gärtner (Institute for Anatomy and Cell Biology, JLU) and Janett Piesker (Max Plank Institute for Heart and Lung Research) for electron microscopy, my Master student Salome Barbakadze for contribution to Hpr1 project. Many thanks to all former and current lab members with whom I had pleasure to work together: thank you for support and help in the lab.

For the private thanks, I want to say thank you to my family for endless support with all my decisions. Thank you my father, mother and my little sister for always being there for me, in moments of happiness and moments of sorrow and for your unconditional love. I also want to thank my partner Matthias for all the support as well as proofreading my thesis – so nice to have scientist Dr. rer. nat. at home ☺. I want to thank my friend Olya who advertised this PhD position to me and, more importantly, made my first years in Germany easier and joyful. I want to thank Carina and Fabienne and all other people who became my friends during this time: I appreciate to know all of you, thank you. Being Ukrainian, I also want to say words of gratitude to all Ukrainians who are fighting for our freedom and independency. ДЯКУЮ!

13. Eidesstattliche Erklärung

Ich erkläre: Ich habe die vorgelegte Dissertation selbstständig und ohne unerlaubte fremde Hilfe und nur mit den Hilfen angefertigt, die ich in der Dissertation angegeben habe. Alle Textstellen, die wörtlich oder sinngemäß aus veröffentlichten Schriften entnommen sind, und alle Angaben, die auf mündlichen Auskünften beruhen, sind als solche kenntlich gemacht. Ich stimme einer evtl. Überprüfung meiner Dissertation durch eine Antiplagiat-Software zu. Bei den von mir durchgeführten und in der Dissertation erwähnten Untersuchungen habe ich die Grundsätze guter wissenschaftlicher Praxis, wie sie in der „Satzung der Justus-Liebig-Universität Gießen zur Sicherung guter wissenschaftlicher Praxis“ niedergelegt sind, eingehalten.

Gießen, den: ..... Unterschrift: .....

(Vorname, Nachname)

14. Appendix

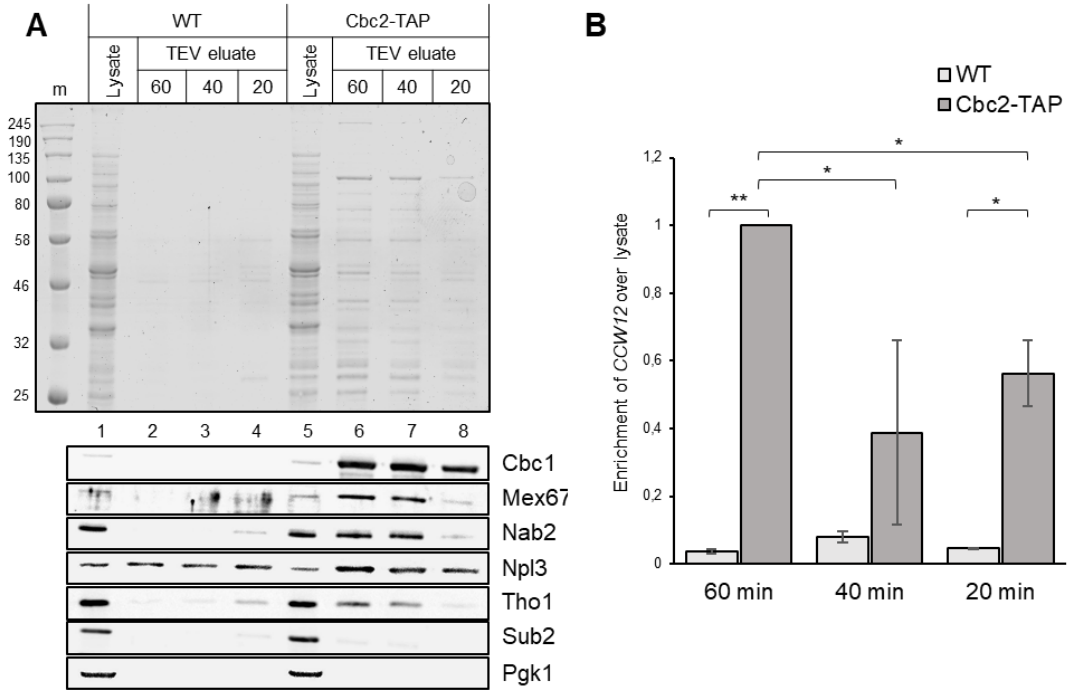

Appendix figure 1. Further reduction of binding time leads to decreased yield of nuclear mRNPs. (A) Coomassie stained SDS-PAGE of lysates and purified TEV eluates (top) ("m" – protein ladder with noted kDa sizes). Western blot (bottom) with antibodies against RBPs of mRNPs. Cytosolic protein Pgk1 was used to assess purity of the sample. **(B)** RNA level of *CCW12* mRNA in TEV eluate determined by RT-qPCR. Fold enrichment of *CCW12* was calculated over *CCW12* level in lysate and set to 1 for the first comparative condition (Cbc2-TAP 60 min) (bars represent mean ± SD; Student's t-test, ** p≤0.01; * p≤0.05).

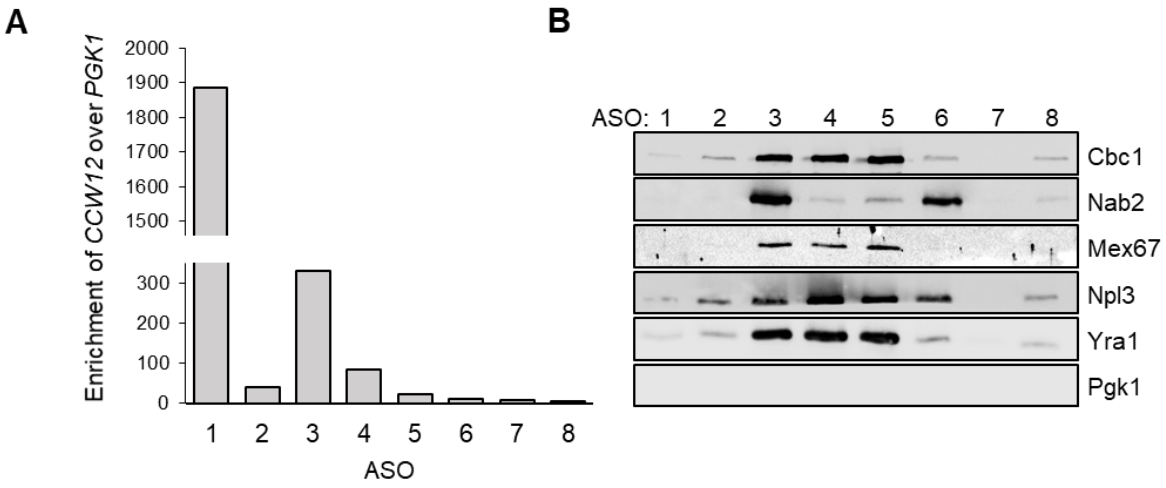

Appendix figure 2. Pre-selection of ASOs for *CCW12* purification. (A) The RNA level of *CCW12* mRNA in final eluate was calculated as fold enrichment over unrelated *PGK1* mRNA. **(B)** Western blot against co-purified proteins. Protein Pgk1 was used as a control of cytoplasmic contamination.

Appendix table 1. Optimization of the ASO-based purification of *CCW12* mRNA. Summary of main tested conditions, their explanation and conclusions.

Test	Aim	Conclusion
ASO amount	Titration of ASO amount for optimal purification of *CCW12*	ASO amount is critical for *CCW12* purification. 100 pmol ASO provides the highest RNA yield
ASO type	Compare 2'-OMe RNA, LNA RNA, or DNA ASOs for purification	2'-OMe ASO is the most optimal for *CCW12* purification
Competitive binding	To reduce non-specific protein binding to ASOs or beads	No specific effect of BSA or tRNA on protein background is observed
Combining of ASOs	To increase a chance to purify target *CCW12* using few ASO-„anchores" for pull down	Leads to more unspecific purification and more of unrelated *PGK1* mRNA in eluate
ASO binding time	To find out which ASO binding time provides the highest yield of *CCW12* (5, 10, 15 and 30 min)	The highest *CCW12* level is observed after 30 min of binding
Glycerol in buffer	To check if glycerol in buffer (5, 10, 20, 30, 40%) provides better conditions for mRNP stability and purification	Glycerol in buffer leads to increased background level of both, protein and target RNA
Tween-20 in buffer	To test if detergent affect the yield and purity	0.05% Tween-20 improves purification yield and purity, but seems to interfere with electron microscopy imaging
Mild cross-linking of TEV eluate	Cross-linking with glutaraldehyde (0.01%, 0.1%, 0.25%, 0.5%) to stabilize particles and prevent their potential disruption by ASO binding	Cross-linking largely decreases purification yield of *CCW12* (approx. 8 times less *CCW12*). Non-specific protein binding remains observed in Δ*ccw12* control

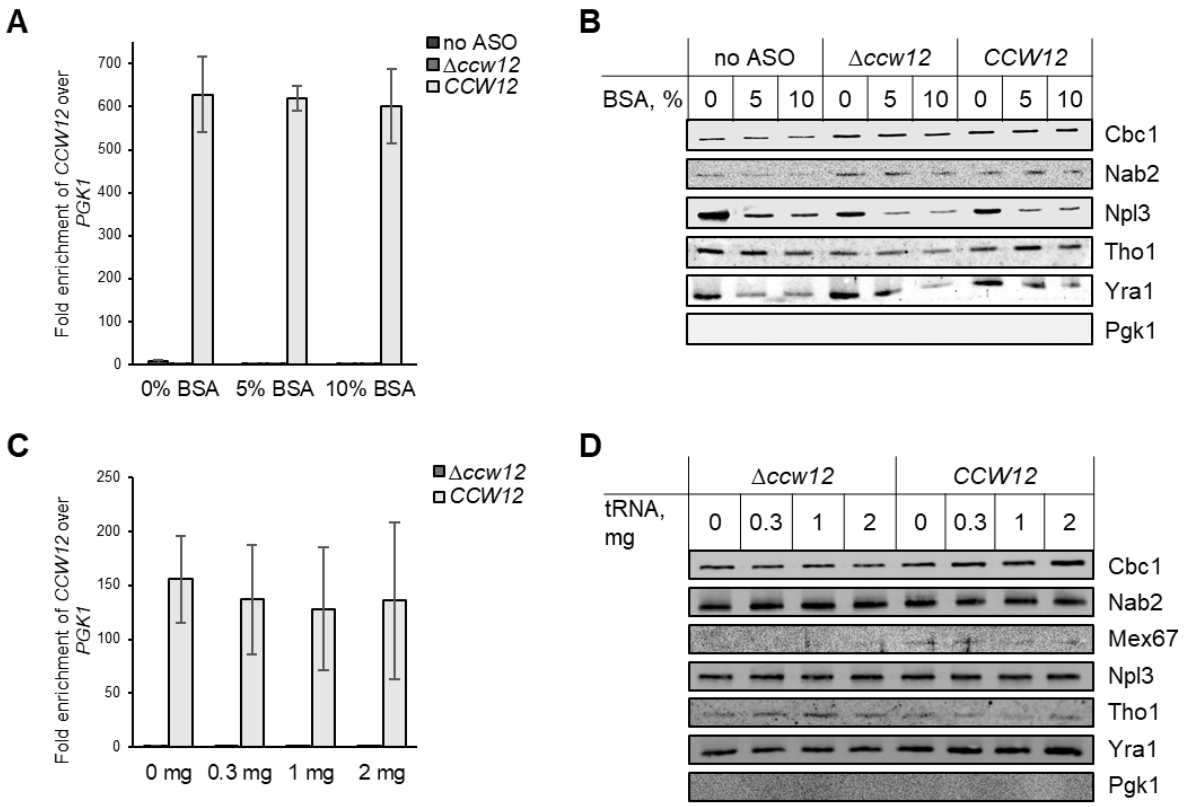

Appendix figure 3. Non-specific protein level is not reduced by competitive binding with BSA or tRNA. (A) Fold enrichment of purified *CCW12* mRNA over unrelated *PGK1*. M280 streptavidin beads incubated for 1 h with 0, 5 or 10% BSA before the binding. **(B)** Detected by Western blot RBPs co-purified with *CCW12*. **(C)** Using tRNA (0, 0.3, 1 and 2 mg) as a competitor during the ASO binding. Fold enrichment of purified *CCW12* mRNA over unrelated *PGK1*. **(D)** Western blot of co-purified RBPs.

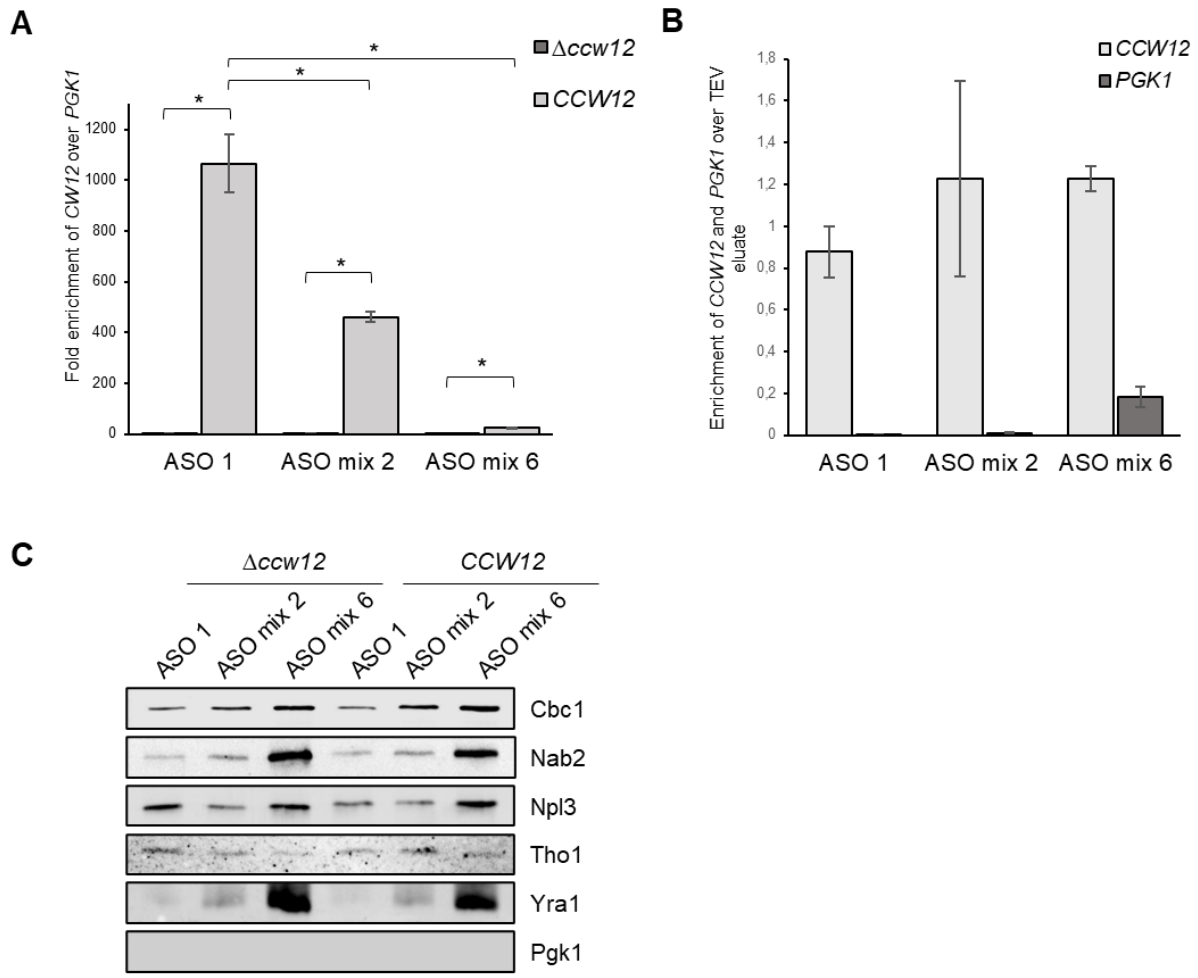

Appendix figure 4. Combining ASOs for *CCW12* purification. (A) *CCW12* mRNA purified via 100 pmol ASO1, or 100 pmol of ASO mix 2 or ASO mix 6. ASO mix 2 consists of ASO1 and ASO8, and ASO mix 6 consist of ASO 1, 3, 4, 6, 7, 8. Choice of ASOs for mix was based on results of RNase H assay. Fold enrichment of *CCW12* calculated over unrelated *PGK1*. Bars represent mean ± SD; Student's t-test, * p≤0.05. **(B)** The same purification via ASO mix 2 and ASO mix 6, but represented as amount of target *CCW12* and unrelated *PGK1* control. This visualizes unspecific enrichment of *PGK1*, that leads to decreased fold enrichment observed in A. Levels of *CCW12* and *PGK1* mRNA in final eluate were calculated over TEV eluate. Bars represent mean ± SD. **(C)** Proteins co-purified via ASO1 or ASO mix 2 or mix 6 were detected by Western blot.

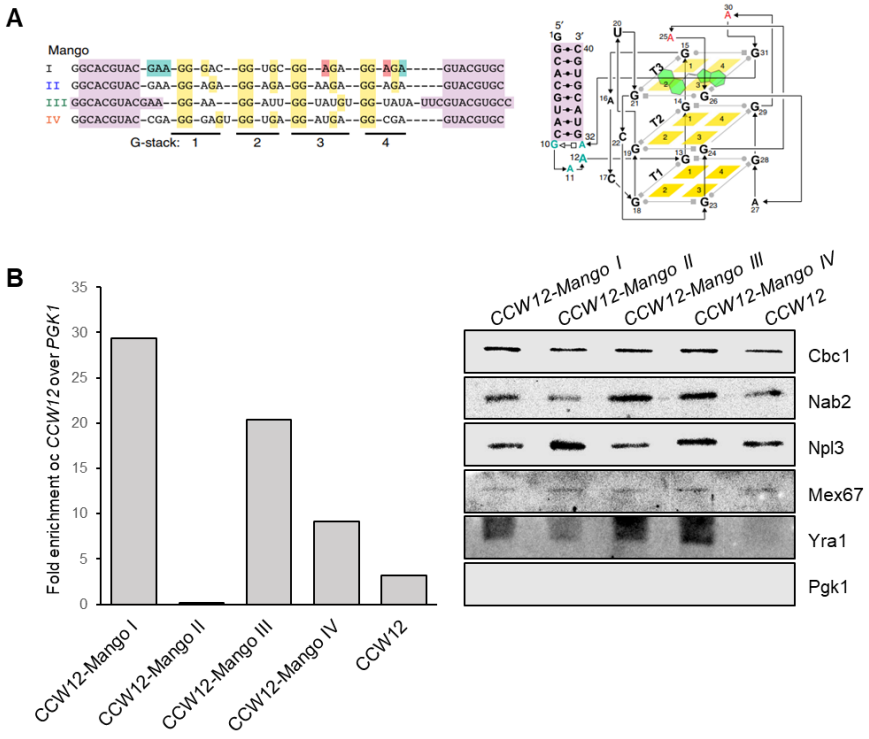

Appendix figure 5. Mango aptamer type for *CCW12-Mango* purification. (A) Aligned core sequences of Mango aptamer types (I, II, III and IV) and schematic representation of tertiary structure of Mango I aptamer. Color shading represents folding pattern of the aptamer. Ligand TO1-Dtb is depicted in the aptamer structure in light green (Autour, 2018). **(B)** mRNA (left) and protein (right) levels of *CCW12* mRNP purified via different Mango aptamer types.

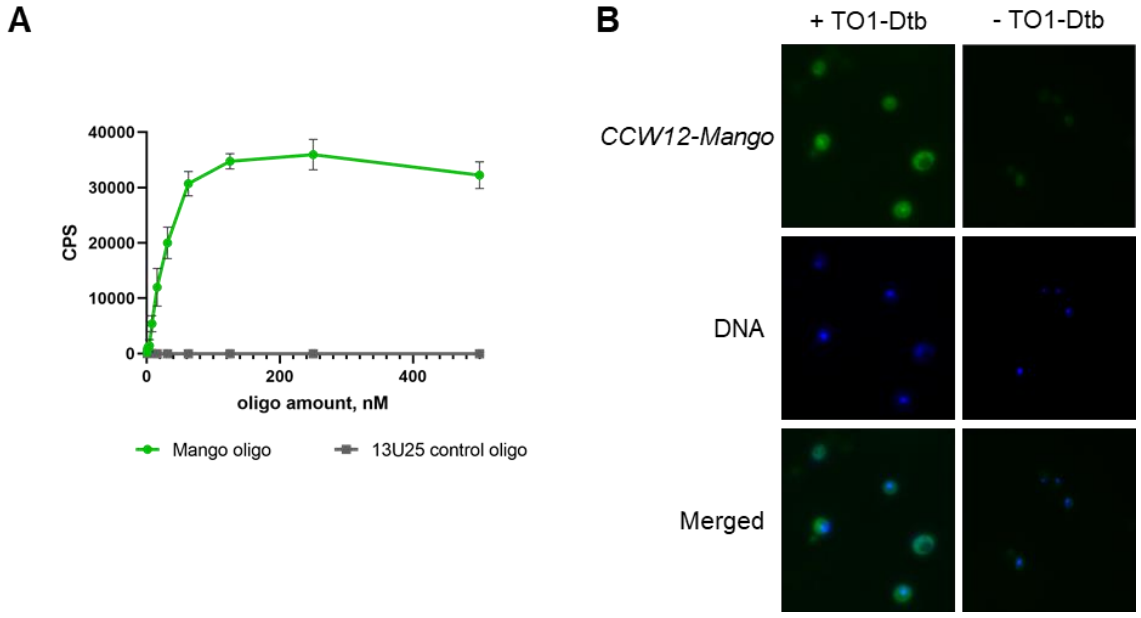

Appendix figure 6. Mango aptamer fluorescence upon binding its ligand TO1-Desthiobiotin. (A) *In vitro* fluorescence of TO1-Dtb bound to Mango RNA oligo. **(B)** *In vivo* fluorescence of TO1-Dtb bound to *CCW12-Mango* in yeast cells. The cells were incubated with TO1-Dtb for 15 min, mounted with DAPI and visualized with fluorescence microscopy.

Appendix table 2. Optimization of the Mango aptamer-based purification of *CCW12* mRNA. Summary of main tested conditions and their conclusions.

Condition	Test	Conclusion
Insertion position of the Mango aptamer	How integration of Mango I in 3 different position (P1, P2, P3) in 3‘ UTR of *CCW12* affects purification	Position 1 (P1) provides the best purification result
Type of Mango aptamer	To compare Mango I, II, II and IV for *CCW12* purification	Mango I provides the highest enrichment of mRNA and proteins
Beads type	To compare agarose or magnetic streptavidin beads	High-capacity streptavidin agarose can be used for purification. No enrichment with magnetic beads
Beads amount	To determine optimal beads amount	The 25, 50 and 100 ul beads does not affect purification, but 12.5 ul decreases enrichment of *CCW12*
Ligand amount	To titrate TO1-Dtb amount (6, 2, 1, 0.5 nmol)	The 1 nmol TO1-Dtb provides the highest mRNA yield
TO1-Dtb alone or pre-coupled to the beads	To use pre-coupled TO1-Dtb beads, or first TO1-Dtb and then beads	Step-wise usage – first incubation with TO1-Dtb and then with beads – results in higher purification yield
Binding order	Cbc2-TAP with following Mango-binding or *vice versa*	First Cbc2-TAP, then Mango step. Opposite order fails to efficiently enrich *CCW12*
Purification from the strains with nuclear mRNA retention	To check if Δ*sac3* and Δ*nup133* strains with more of nuclear mRNAs provide higher yield of *CCW12*	Does not lead to higher yield of purification
Salt concentration in the wash buffer	To test 100, 150 and 200 mM KCl	The 150 mM KCl for 2 L culture sample and 200 mM for 24 L sample improve the sample purity
Upscaling purification	To check if increase amount of culture from 2 L to 24 L increase the purification yield	12x upscale (24 L culture) leads to increased enrichment of *CCW12* without increase of background *PGK1*

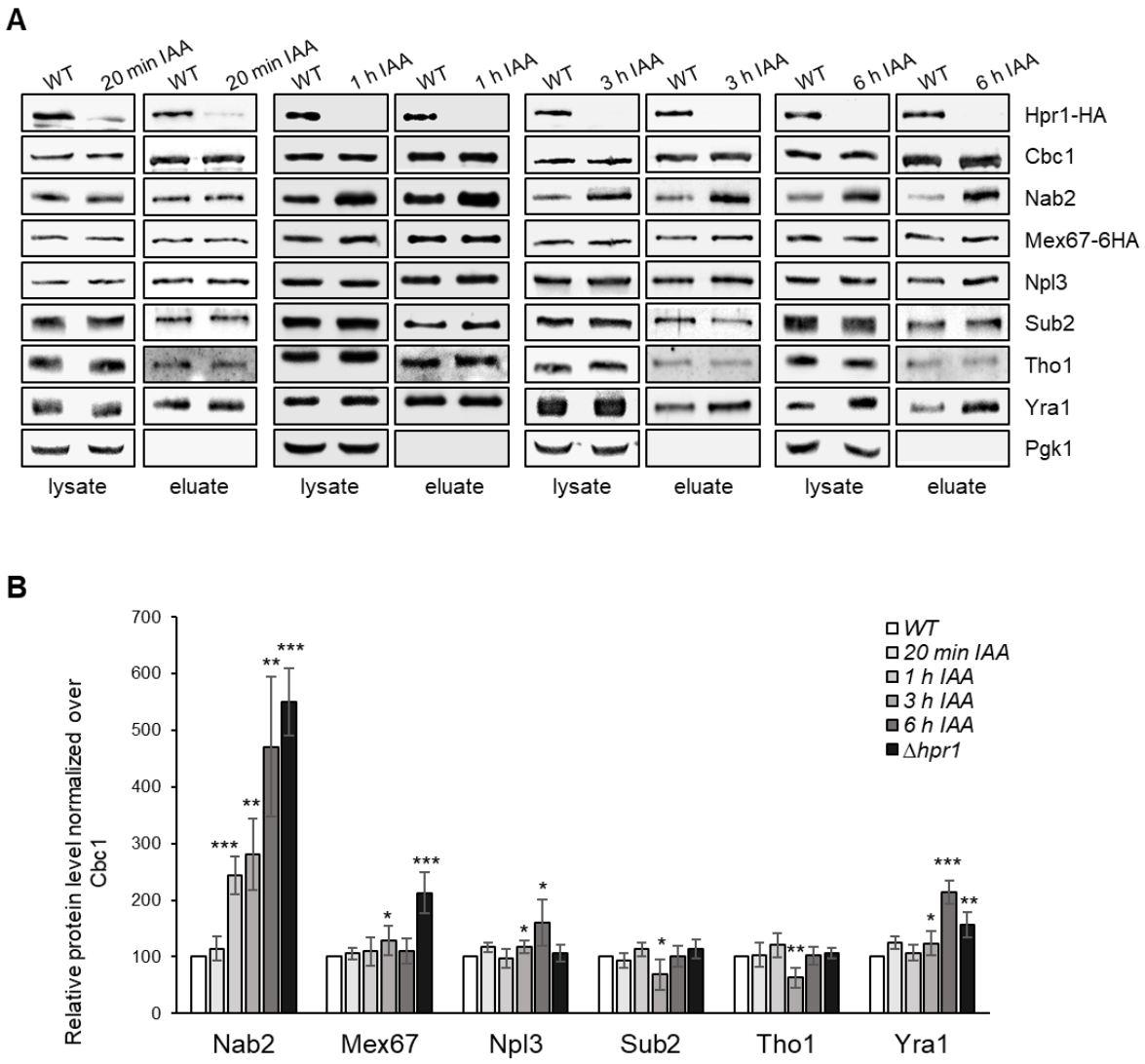

Appendix figure 7. Changes in mRNP composition after 20 min, 1 h, 3 h and 6 h of Hpr1 depletion. Nuclear mRNPs purified via Cbc2-TAP from WT and Hpr1-depleted cells after 20 min, 1 h, 3 h or 6 h of treatment with auxin (IAA). **(A)** Western blot of lysate and TEV eluate with antibodies against the indicated RBPs. **(B)** Protein levels in TEV eluates, quantified with ImageJ, normalized to the signal of the CBC subunit Cbc1 and set to 1 for WT cells (n=6; bars represent mean ± SD; Student's t-test, ***p<0.001, ** p≤0.01, * p≤0.05).

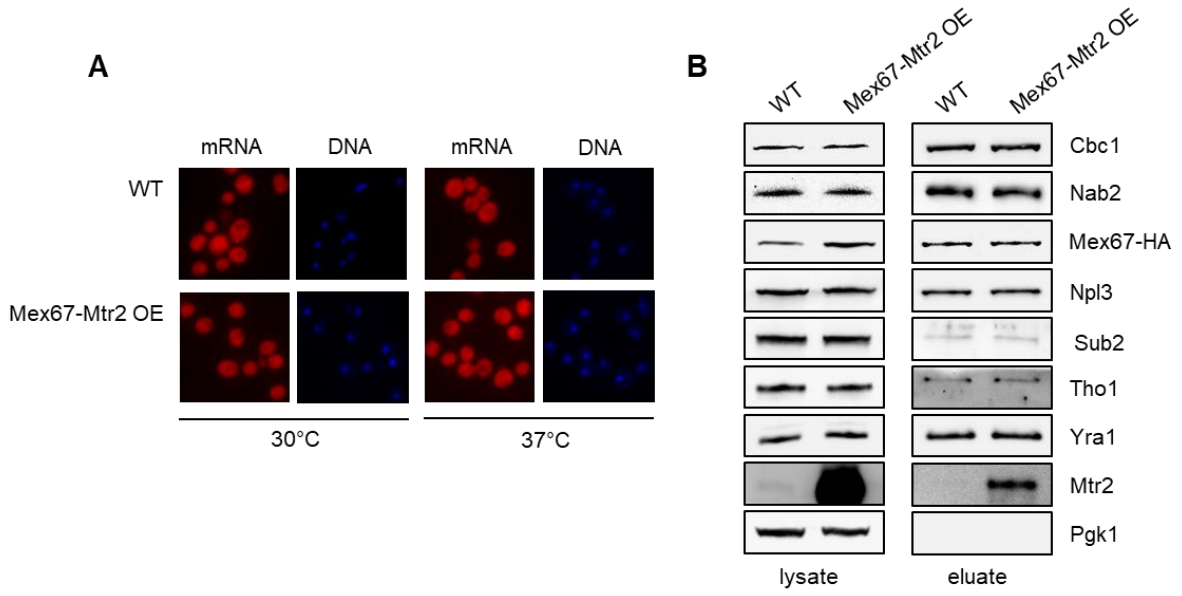

Appendix figure 8. Overexpression of Mex67-Mtr2 in WT does not lead to more Mex67 in mRNPs or mRNA export defect. (A) mRNA export is visualized with fluorescence *in situ* hybridization (FISH) at 30 and 37°C. mRNA was detected by oligo(dT)50 coupled to a Cy3-fluorecent dye. DNA was stained with DAPI. **(B)** Nuclear mRNPs purified via Cbc2-TAP from WT strain and cells overexpressing Mex67 and Mtr2. Visualized by Western blot of lysate and TEV eluate with antibodies against the indicated RBPs.

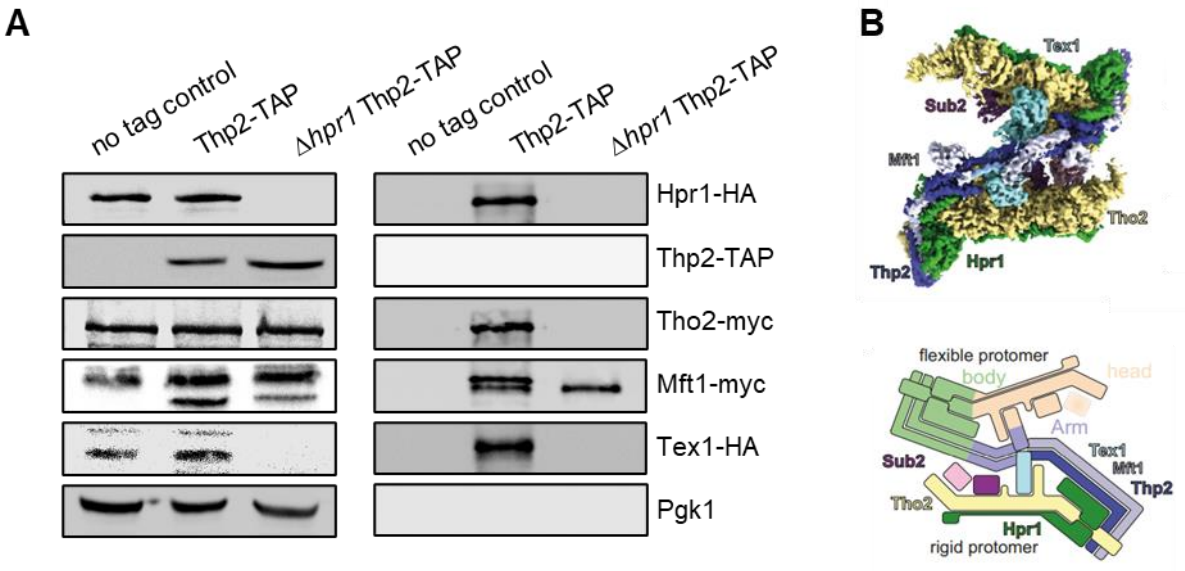

Appendix figure 9. THO complex is no longer formed upon deletion of *HPR1*. (A) Pull down of THO complex via Thp2-TAP in WT and Δ*hpr1* cells. Western blot of lysate and TEV eluate with antibodies against the components of THO complex. **(B)** Published (Schuller, 2020) cryo-EM reconstruction of THO-Sub2 complex (upper panel) and its scheme (lower).